

DNA-Based Conducting Polymer Nanowires for Biosensor Applications

By Joseph H. Hedley

A Thesis Submitted to Newcastle University
In Partial fulfilment of the Requirements for the Degree of
Doctor of Philosophy

Supervisors: Prof. B. A. Connolly, Prof. A. Houlton and Dr. B. R. Horrocks

November 2013

List of Abbreviations and Symbols

Å	Angstrom
AFM	atomic force microscopy
Au	gold
°C	degrees Celsius
CT-DNA	calf thymus DNA
Cu	copper
CP c	Conducting polymer
1D	one dimension
3D	three dimensions
dc	direct current
D	diameter
DMF	dimethylformamide
DNA	Deoxyribonucleic acid
eV	electron volt
FeCl ₃	ferric chloride
FTIR	Fourier Transform Infrared
G	conductance
HOMO	highest occupied molecular orbital
<i>I-V</i>	current-voltage
IC	Integrated Circuit
K	Kelvin
LUMO	lowest unoccupied molecular orbital
TMS	chlorotrimethylsilane
min	minutes
mM	milli molar
N ₂	nitrogen
nm	nanometre
pA	pico amperes
PIn	polyIndole
Py	pyrrole
PPy	polypyrrole

RT	room temperature
s	second
SCM	scanning capacitance microscopy
μm	micrometre
UV	ultraviolet
R	resistance
S	Siemens (conductance unit)
G	conductivity
VRH	variable-range hopping
UV-Vis	ultraviolet-visible
Ω	ohm (resistance unit)
Si	silicon
SiO ₂	silicon dioxide

Acknowledgments

Firstly, I would like to express my sincere gratitude to my supervisors, Prof. Bernard Connolly, Prof. Andrew Houlton and Dr. Ben Horrocks, for their valuable guidance, scientific support and assistance, which made the completion of this work possible. I would like also to thank Dr. Andrew Pike, Dr. David Fulton and Dr. Eimer Tuite for their encouragement and support during my research. I am also grateful to my fellow postgraduates; past and present. In particular, I must express thanks to Dr. Jennifer Hannant, Dr. Miguel Galindo and Dr. Scott Watson for their motivation, insights and inspiration. I could never have completed my PhD without the support of other academic and administrative staff at Newcastle University without their help and friendship. Special thanks go to the school of electrical engineering for fabricating the bespoke microelectrodes. I would also like to thank EPSRC for the financial support without which this work could never have happened. Special thank you goes to my work colleagues for picking me up when I thought all was lost. Finally, a huge thank you goes to my family, who have helped me through thick and thin, especially my mother, Moira Cunningham, for simply being there when I have always needed her. My brother, Jonathan, who is a constant source of inspiration and grounding-point in all of my escapades. And finally and most importantly, my late grandmother, 'Granny', who from teaching me to read when my school teachers could not, continued to support me throughout my entire education both in academia and in life.

"I will persist until I succeed. Always will I take another step, If that is of no avail I will take another, and yet another. In truth, one step at a time is not too difficult. I know the small attempts repeated will complete any undertaking."

Og Mandino

Abstract

Novel DNA-based conductive polymer nanowires formed from thienyl-pyrrole derivatives have been synthesized and characterised by high-resolution ES-MS, ^1H and ^{13}C NMR spectroscopy. Bulk DNA-templating of these materials is demonstrated by FTIR, while relative control over nanowire dimensions and deposition is shown by AFM.

The electronic properties of these materials were investigated by Scanned Conductance Microscopy (SCM) and two-point I - V measurements. The resistance of the DNA/polymer nanowires, determined from variable temperature I - V measurements, was found to be in the range of 10^{12} - $10^{14}\Omega$. Nanowire conductivity values were calculated to be in the range of 1.9×10^{-7} - $3.75 \times 10^{-4} \text{ S cm}^{-1}$ at 303K.

FTIR data demonstrates the availability of the alkyne group in bulk DNA-templated materials for subsequent nanowire functionalisation using ‘click’ chemistry. Efforts to couple 3-azido propanol and ssDNA probe DNA is also presented.

List of Figures

Figure 1.1. The basic mechanism of a biological sensor	2
Figure 1.2. SPR imaging. A light source projects light onto a gold surface, on which a biomolecular interaction is occurring, and the reflected light is imaged onto a CCD detector	4
Figure 1.3. The chemical structure of trans-polyacetylene	7
Figure 1.4. The chemical structure of thiophene (left) and the repeating unit of polythiophene (right)	8
Figure 1.5. The chemical structure of pyrrole (left) and the repeating unit of polypyrrole (right)	9
Figure 1.6. Polymerisation of pyrrole can proceed through the α -position forming a conjugated polymer. Where n represents the number of repeating units and M^+ indicates the cationic nature of the material produced	10
Figure 1.7. A positively charged polaron in polypyrrole	12
Figure 1.8. Removal of a second electron leads to bipolaron formation in polypyrrole	13
Figure 1.9. Polarons and bipolarons produced upon oxidation are the principle charge carriers in conducting polymers. Neutral polymer, (a), polarons, (b), and bipolarons, (c), are symmetrically located within the band gap of polypyrrole	13
Figure 1.10. Structure of <i>N</i> -substituted -pyrrole and β -substituted pyrrole, illustrating the alternative sites for coupling functional groups	15
Figure 1.11. Attack at the 2-position forms a linear conjugated system which is more slightly more stable than the 'cross conjugated' intermediate formed by upon attack at the 3-position	16

Figure 1.12. . Substituted pyrrole derivatives that have been prepared as conducting polymers	17
Figure 1.13. An illustration of the electrochemical entrapment of an enzyme with a polymer (yellow) immobilized on an electrode surface. Entrapment of biomolecules in polymer films during their electrogeneration on an electrode surface is easily applicable to a wide variety of biological macromolecules and the monomers are often commercially available	20
Figure 1.14. Avidin (a) is a tetrameric glycoprotein (4 biotin molecules may bind) produced in the oviducts of birds, reptiles and amphibians, the monomeric version is shown; (b) biotin, also known as vitamin H or coenzyme R has a well-known, high-affinity for avidin	21
Figure 1.15. Conducting polymers such as polypyrrole can be surface functionalised with a bi-functional linker molecule such as glutaraldehyde (a) electrosynthesis of polypyrrole, (b) activation by glutaraldehyde, and (c) covalent binding of a DNA/enzyme	25
Figure 1.16. . The three alternative dimensions of nano-scale materials	27
Figure 1.17. . Scanning electron micrograph of the surface of a nanopore alumina template membrane prepared in the Martin lab	28
Figure 1.18. The four bases that make up DNA	31
Figure 1.19. The chemical structure of dsDNA	31
Figure 1.20. Hydrogen bonding between the base-pairs of DNA	33
Figure 1.21. Top row, folding paths. a, square; b, rectangle; c, star; d, disk with three holes; e, triangle with rectangular domains; f, sharp triangle with trapezoidal domains and bridges between them (red lines in inset). Second row, diagrams showing the bend of helices at crossovers (where helices touch). Colour indicates the base-pair index along the folding path; red is the 1st base, purple the 7,000th. Bottom rows, AFM images. Scale bars: b, 1µm; c–f, 100 nm.	35

Figure 1.22. Aniline modified nucleoside, X, represented in a structural model of a hexameric aniline oligomer conjoined to a DNA strand	36
Figure 1.23. The chemical structure of poly(p-phenylene vinylene)	38
Figure 1.24. AFM height images of DNA-templated growth of CdS on mica. (a) Large area image of DNA-templated CdS nanoparticles; height scale is 3 nm, and the white bar indicates 200 nm. (b) enlargement of a region indicated by the white arrow in the left figure; height scale is 5 nm, (white bar indicates 25 nm)	39
Figure 1.25. An AFM image of DNA/PAni synthesized by the HRP/H ₂ O ₂ method in solution and stretched on a mica substrate	41
Figure 1.26. An AFM image of part of an actual two-terminal electrical measurement device indicates one DNA/PPy nanowire (black arrow) ~5 nm diameter, bridging the 7 μm gap	43
Figure 1.27. AFM image of DNA/PPy nanoropes after 48 hours on SiO ₂ /Si surface. Scale bar, 500 nm, height scale is 8 nm	43
Figure 2.1. A basic illustration showing the method of function of an atomic force microscope (AFM). a) The tip attached to a flexible cantilever driven by piezoelectric motor; b) the tip oscillates at its resonant frequency across the surface	64
Figure 2.2. AFM schematic representation	65
Figure 2.3. A basic representation outlining the principles of SCM operation, used to evaluate the electronic properties of one-dimensional nanostructure	67
Figure 2.4. Schematic diagram of the attractive and repulsive forces in the SCM experiment	68
Figure 2.5. Resonance curve. The resonance frequency shifted $\Delta\omega$ from ω_0 to $\omega=\omega_0+\Delta\omega$, and phase shift $\Delta\phi$ occurs at the frequency ω_0 motor; b) the tip oscillates at its resonant	70

frequency across the surface	
Figure 2.6. A typical cross-section of a conducting DNA/polymer nanowire, illustrating the negative-positive-negative phase shifts is characteristic of semi-conducting materials	72
Figure 2.7. Experimental set-up for cAFM measurements carried out upon DNA-based polymer nanowires. Measurements are recorded upon individual nanowires located at the periphery of a dense network of nanowires	74
Figure 2.8. Optical images of Au electrode pairs, micro-fabricated using photolithography, embedded in a thermally grown insulating SiO ₂ layer, on a silicon substrate. The Au electrodes were typically separated by a gap of 2–8 μm	76
Figure 2.9. A screen shot taken from the CAM 101 used for contact angle measurements in this study. A droplet of water is deposited onto the appropriately functionalized surface and the static contact angle is measured by the camera	77
Figure 2.10. The theoretical description of contact arises from the consideration of a thermodynamic equilibrium between the three phases: the liquid phase (L), the solid phase (S), and the gas/vapor phase (G)	78
Figure 2.11. An illustration of showing the procedure by which molecular combing was carried out during this project	80
Figure 3.1. Polymerisation of pyrrole can proceed through the β-position	85
Figure 3.2. Structure of poly 2-(2-thienyl)-pyrrole, polyTP	86
Figure 3.3. The three possible configurations of poly-TP formation, a) ‘head-to-tail’, b) ‘tail-to-tail’, c) ‘head-to-head’	87
Figure 3.4. Structure of 2,5-(di-2-thienyl)-pyrrole, polyTPT	87
Figure 3.5. Structures of <i>N</i> -alkylated alkynyl units	88

Figure 3.6. Molecular structure of 2-(2-thienyl)-pyrrole, TP , recrystallized from dichloromethane and obtained by a single crystal X-ray study	91
Figure 3.7. CV of C5-P . 10 mM of sample, 100 mM LiClO ₄ in MeCN, working electrode Pt, counter electrode Au and quasi-reference electrode Ag. Scan rate 0.2 V/s	94
Figure 3.8. CV of C5-TP . 10 mM of sample, 100 mM LiClO ₄ in MeCN, working electrode Pt, counter electrode Au and quasi-reference electrode Ag. Scan rate 0.2 V/s	95
Figure 3.9. CV of C5-TPT . 10 mM of sample, 100 mM LiClO ₄ in MeCN, working electrode Pt, counter electrode Au and quasi-reference electrode Ag. Scan rate 0.2 V/s	96
Figure 3.10. FTIR spectra (3500 – 2000 cm ⁻¹ region) of C5-P (blue) and poly C5-P (red)	97
Figure 3.11. FTIR spectra (1300 – 900 cm ⁻¹ region) of C5-P (blue) and poly C5-P (red) showing the disappearance of narrow plane vibrations bands of C-H deformation and appearance of weak bands attributed to C-H bending, ring breathing and ring deformation from polymer formation	98
Figure 3.12. FTIR spectra (1800 – 800 cm ⁻¹ region) of C5-TP (blue) and poly C5-TP (red). Bands attributed to the monomer species are shown to diminish and shift in conjunction with the appearance of new bands	100
Figure 3.13. FTIR spectra (1800 – 600 cm ⁻¹ region) of C5-TPT (blue) and poly C5-TPT (red). Bands attributed to the monomer species are shown to recede in conjunction with the appearance of new bands attributed to polymer formation	101
Figure 4.1. Recognition groups in the major and minor grooves of dsDNA	113
Figure 4.2. Hydrogen bonding sites available in a) polypyrrole; b) poly C5-P ; c) poly C5-TP and d) poly C5-TPT . These have quite different hydrogen bonding capabilities, the red circle indicates strong (NH) hydrogen-bond donor sites while blue circle denotes relatively weak acceptor sites (-S-)	114
Figure 4.3. FTIR spectra of (blue) C5-P , (red) poly C5-P and (green) poly C5-P /DNA	119

Figure 4.4. FTIR spectra of CT-DNA	120
Figure 4.5. FTIR spectra of C5-TP (blue), polyC5-TP (red) and DNA/polyC5-TP (green)	121
Figure 4.6. FTIR spectra of C5-TPT (blue), polyC5-TPT (red) and DNA/polyC5-TPT (green)	122
Figure 4.7. Contact angle variation with exposure of Si/SiO ₂ surfaces to TMS vapour	123
Figure 4.8. DNA/polyC5-P on silanised silicon <111> surface, scale bar = 4 μm, height scale is 20 nm, (0.5 mM C5-P, DNA ~80 μg mL ⁻¹ , 0.5 mM MgCl ₂ , 1 mM FeCl ₃ , incubated for 1.5 hours	125
Figure 4.9. DNA/polyC5-P nanowires aligned on silanised silicon <111> surface, scale bar = 3 μm, height scale is 20 nm, DNA ~80 μg mL ⁻¹ , 0.5 mM MgCl ₂ , 1 mM FeCl ₃ , incubated for 2 hours	126
Figure 4.10. An AFM image of DNA/polyC5-P drop cast onto Si/SiO ₂ , height average 65.2 nm, the scale bar = 2 μm and the height scale is 10 nm, 500 μg mL ⁻¹ , 1.5 hour incubation, 0.5 mM MgCl ₂ , 1 mM FeCl ₃ . Demonstrating the ability of this approach to deposit large wires/ropes and the effect of DNA concentration on rope formation	127
Figure 4.11. DNA/polyC5-P stretched on silanised silicon <111> surface, scale bar = 1 μm, height scale is 10 nm. 300 μM C5-P, DNA ~80 μg mL ⁻¹ , 1.5 hour incubation, 0.5 mM MgCl ₂ , 1 mM FeCl ₃	128
Figure 4.12. A histogram displaying the mean diameters of 100 DNA/polyC5-P nanowires	128
Figure 4.13. DNA/C5-TP stretched on silanised silicon <111> surface, scale bar = 3 μm, height scale 10 nm. 30 μM C5-TP, ~80 μg mL ⁻¹ CT-DNA, 2 hour incubation, 0.5 mM MgCl ₂ and 1 mM FeCl ₃	130
Figure 4.14. DNA/C5-TP stretched on silanised silicon <111> surface, scale bar = 4 μm, height scale 20 nm left, 10 nm right. Left; demonstrates the effect of increasing monomer concentration (500 μM C5-TP, DNA ~80 μg mL ⁻¹ , 2 hour incubation). Right; indicates	131

the formation of ropes at incubation times of 3 hours with reduced monomer concentrations (30 μM C5- TP , DNA $\sim 80 \mu\text{g mL}^{-1}$, 3 hour incubation)	
Figure 4.15. DNA/polyC5- TPT stretched on silanised silicon <111> surface, scale bar = 1 μm , height scale is 20 nm	132
Figure 4.16. DNA/polyC5- TPT drop cast on silanised silicon (111) surface, scale bar = 3 μm , height scale is 20 nm. 10 nm. 300 μM $\sim 80 \mu\text{g mL}^{-1}$, 1.5 hour incubation, 0.5 mM MgCl_2 and 1 mM FeCl_3 . Typical height $\sim 30\text{-}40$ nm	133
Figure 4.17. A typical AFM image of DNA/polyC5- P ~ 9.08 nm in height aligned on Si/SiO ₂ using molecular combing, the scale bar = 2 μm and the height scale is 10 nm.	135
Figure 4.18. UV-Vis spectrum (400-500 nm) of C5- P incubated with FeCl_3 over 0-2 hours	136
Figure 4.19. UV-Vis spectrum (400-500 nm) of C5- P in pH 5 media over 0-2 hours	137
Figure 4.20. UV-Vis studies of the addition of C5- P to CT-DNA at pH 5, the increase in absorbance indicates polymer systems through an extended conjugated system	138
Figure 4.21. UV-Vis studies of the addition of C5- P to CT-DNA at pH 5 when all solutions were degassed prior to mixing	139
Figure 5.1. A UHV NANOPROBE equipped with four SEM's capable of <4 nm resolution	152
Figure 5.2. Optical images of Au electrode pairs, micro-fabricated using photolithography, embedded in a thermally grown insulating SiO ₂ layer, on a silicon substrate. The Au electrodes were typically separated by a gap of 2–8 μm	153
Figure 5.3. (a) Colorized topographic image of SWNT bundles and single tubes, colored red, and λ -DNA molecules, colored green. (c) Scanned conductance image of the region shown in part (a)	153

<p>Figure 5.4. ES-state PANi nanofibres. Left; tapping mode AFM height image of the structures, right; the corresponding SCM phase image. The negative-positive-negative phase shifts in the scanned conductance image is characteristic of semi-conducting materials; this corresponds to a negative phase shift as the tip crosses the nanowire and demonstrates the existence of charge conduction in the wire</p>	155
<p>Figure 5.5. AFM and scanned conductance (SCM phase) images of PIn/DNA nanowires on SiO₂/Si surface with a SiO₂ thickness of 220 nm. (a) AFM image of a nanowire with a diameter of 5 nm (grayscale 10 nm). (b) Phase image of the same nanowire</p>	155
<p>Figure 5.6. A typical cross-section of a conducting DNA/C5-P nanowire, illustrating the negative-positive-negative phase shifts is characteristic of semi-conducting materials</p>	157
<p>Figure 5.7. SCM phase images of a) DNA/polyC5-P; b) DNA/polyC5-TP; c) DNA/polyC5-TPT nanowires stretched on silanised silicon <111> surface, scale bar = 3 μm, height scale 10 nm when a -7 mV bias was applied. The negative-positive-negative phase shifts characteristic of semi-conducting materials was observed in each case (Figure 5.2 and Appendix)</p>	158
<p>Figure 5.8. DNA/polyC5-TPT nanowires stretched on silanised silicon <111> surface, scale bar = 3 μm, height scale 10 nm when different tip/sample biases. a) 0 bias; b) -2 mV; c) -3 mV</p>	159
<p>Figure 5.9. A plot of the (tangent) phase shift against the dc bias applied to the substrate for DNA/polyC5-P (10.80 nm in diameter)</p>	159
<p>Figure 5.10. Left, a representation of a polymer nanowire with a terminal alkyne group aligned between two gold micro-electrodes using molecular combing; right, bespoke micro-fabricated Au electrodes for <i>I-V</i> measurements. The Au electrodes were typically separated by a gap of 2–8 μm while the chip was ~1 cm²</p>	161
<p>Figure 5.11. An AFM image of DNA/polyC5-TP 8 nm in height stretched between two Au micro-electrodes, the scale bar = 2 μm and the height scale is 20 nm. The Au electrodes are embedded in a thermally grown, 200 nm thick insulating SiO₂ layer on a Si substrate</p>	163

Figure 5.12. A 3-D image of the same wire illustrating the connection between the Au electrodes and the DNA/polyC5- TP nanowire	164
Figure 5.13. A typical current-voltage plot for a DNA/polyC5- TP nanowire obtained from the Agilent B1500 probe station	165
Figure 5.14. Variable temperature <i>I-V</i> measurements carried out upon a DNA/polyC5- TP nanowire aligned across two Au electrodes	168
Figure 5.15. Arrhenius plot for the conductance of a DNA/polyC5- TP nanowire	169
Figure 5.16. An AFM image of DNA/poly TPT nanowire (25 nm diameter) aligned across a 2.5 μm gap between two Au micro-electrodes, the scale bar = 2 μm and the height scale is 20 nm	170
Figure 5.17. Variable temperature <i>I-V</i> measurements carried out upon a DNA/poly TPT nanowire aligned across two Au electrodes	171
Figure 5.18. Arrhenius plot for the conductance of a DNA/poly TPT nanowire	172
Figure 5.19. An AFM image of DNA/polyC5- P ~9 nm in diameter stretched between two Au micro-electrodes, the scale bar = 5 μm and the height scale is 40 nm. The Au electrodes are embedded in a thermally grown, 200nm thick insulating SiO ₂ layer on a Si substrate	173
Figure 5.20. A 3-D image of DNA/polyC5- P ~9 nm in diameter stretched between two gold microelectrodes indicating the connection between the gold electrodes and the nanowire	173
Figure 5.21. Variable temperature <i>I-V</i> measurements carried out upon a DNA/polyC5- P nanowire prepared in the absence of a chemical oxidant, aligned across two Au micro-electrodes	174
Figure 6.1. The chemical structure of maleimide, formed through over oxidation of	186

pyrrole	
Figure 6.2. The structure of pyrrolidine units implicated in the acid initiated polymerisation of pyrrole	187
Figure 6.3. The chemical hydrolysis of ferric chloride yielding HCl	187
Figure 6.4. A typical current-voltage plot for bulk polypyrrole samples obtained from the Agilent B1500 Agilent probe station	189
Figure 6.5. Conductivity measurements of polypyrrole against varied oxidant ratio (1:1 to 3:1) after 1 hour incubation	192
Figure 6.6 Conductivity measurements of polypyrrole against varied oxidant ratio (1:1 to 3:1) after 3 hour incubation	193
Figure 6.7. Conductivity measurements of polypyrrole against varied oxidant ratio (1:1 to 3:1) after 24 hour incubation	194
Figure 7.1. A range of silane compounds have been used in the modification on SiO ₂ coated NWs	203
Figure 7.2. Some commercially available oligonucleotide modifications	205
Figure 7.3 Possible modification sites at C-5, 3'-OH and 5'-OH prevents disruption of possible hydrogen bonding	206
Figure 7.4. The phosphoramidite oligonucleotide synthesis cycle	207
Figure 7.5. Structures of <i>N</i> -alkylated alkynyl units	209
Figure 7.6. The chemical structure of 3-azido propan-1-ol	210
Figure 7.7. FTIR spectra (3500-500 cm ⁻¹) of DNA/polyC5-P (blue) and DNA/ polyC5-P	212

'clicked' (red)	
Figure 7.8. FTIR spectra (1800-500 cm^{-1}) of DNA/polyC5-P (blue) and DNA/ polyC5-P 'clicked' (red)	213
Figure 7.9. FTIR spectra of polyC5-TP, blue; DNA/polyC5-TP 'clicked', red and the subtraction of polyC5-TP 'clicked' from DNA/polyC5-TP, green	214
Figure 7.10. FTIR spectra of C5-TPT (red), DNA/polyC5-TPT (blue) and 'clicked' result (red)	215
Figure 7.11. An illustration of ssDNA probe attachment to an alkyne terminated DNA-templated CP. The azide terminated DNA reacts with the alkyne group to form a highly stable triazole linkage	216
Figure 7.12. Denaturation of 5'azido-hexyl-25mer duplex with increased temperature shown by an increase in absorbance in the UV-Vis spectra (260 nm)	219
Figure 7.13. Left; contact mode AFM height image of a DNA/polyC5-P nanowire, 25 μm scan size, 100 nm height scale. Right; a zoomed cAFM current image of the same wire acquired at a dc bias of +10 V, 5 μm scan size	221
Figure 7.14. AFM images of DNA/polyC5-TP nanowires before (A, 4 μm scan size, 15 nm height scale) and after modification with dansyl azide (B, 7 μm scan size, 50 nm height scale). EFM image of the DNA/polyC5-TP nanowire (C, 4 μm scan size, grey scale corresponds to negative-positive-negative phase shift). Fluorescence image of a DNA/polyC5-TP nanowire after click reaction with dansyl azide	123

List of Tables

Table 1.1. A list of the most commonly studied conducting polymers and their conductivities	8
Table 3.1. CV oxidation peaks of C5-P, C5-TP and C5-TPT. 10 mM of sample, 100 mM LiClO ₄ , acetonitrile, working electrode Pt, counter electrode Au and Ag quasi-reference electrode. Scan rate 0.2 V/s	93
Table 6.1. Bulk conductivity values of polyP, polyTP, polyTPT and polyC5-P, polyC5-TP and polyC5-TPT	190
Table 6.2. Oxidant to Py ratio 1:1, 2:1, 3:1, 1 hour incubation, pH 5 (Tris-HCl)	194
Table 6.3. Oxidant to Py ratio 1:1, 2:1, 3:1, 1 hour incubation, pH 7 (Tris-HCl buffer)	195
Table 6.4. Bulk conductivity data for co-polymer systems of Py/polyC5-P, polyC5-TP and polyC5-TPT prepared	196

List of Schemes

Scheme 1.1. When functionalized with appropriate ‘capture probes’ (left), nanowires can act as transducers for label-free electrical detection of chemical and biological species (right)	6
Scheme 1.2. The mechanism for the polymerisation of pyrrole. (i) the one electron oxidation of the respective monomer unit to a radical cation; (ii) the combination of two radical cation monomers to produce a 2,2'-bipyrrole dimer; (iii) the polymer chain continues to grow through the re-oxidation of the bipyrrole and further addition of radical cation monomers	11
Scheme 1.3. . Schematic of the conduction pathways in a conducting polymer a) intra-chain; b) interchain and c) inter-particle where the blues lines represent polymer chains and the red circles represent particles	14
Scheme 1.4. The reaction scheme for A) reaction with electrophiles in the 2-position of pyrrole; B) reaction with electrophiles in the 3-position of pyrrole	15
Scheme 1.5. A common method to avoiding the chemical ambiguity associated with 3-derived compounds is to block the desired site with a preferential leaving group	16
Scheme 1.6. <i>N</i> -alkylation of pyrrole is commonly achieved using a strong base such as butyl lithium or sodium hydride and an alkylhalide, where X can be I, Br or Cl	17
Scheme 1.7. Key steps in the preparation of the DNA hybridization sensor probe: (1) MgCl ₂ aqueous, 5 mM, 10 min; (2) aqueous ssDNA(a), 10 min, then rinsed with TRIS buffer	19
Scheme 1.8. Schematic of a sensor design based on electrocopolymerization of biotinylated pyrrole and the use of biotin–avidin interactions	22
Scheme 1.9. Synthesis of the phosphoramidite building block through modification of pyrrole at the <i>N</i> -position.	23

Scheme 1.10. Alternative capture probe addressing by electrodirected co-polymerization: Py ODN 1 is first copolymerized on the electrode 1; following washing of the cell, copolymerization of the Py-ODN 2 is carried out by activation of electrode 2	24
Scheme 1.11. Schematic of the preparation of a electrochemical DNA sensor based on a poly(pyrrole-co-4-(3-pyrrolyl) butanoic acid) conducting polymer	25
Scheme. 1.12. Electropolymerization to form a co-polymer film consisting of functionalized polypyrrole, poly(3-acetic acid pyrrole-co-3- <i>N</i> -hydroxyphthalimide pyrrole)	26
Scheme 1.13. A schematic diagram for a DNA-templated self-assembly of a conductive silver wire connecting two electrodes	37
Scheme 1.14. Generalized reaction sequence for the growth of nanoscale binary materials and conducting polymers at a DNA-template	38
Scheme 1.15. Fabrication of a polyaniline nanowire immobilized on a Si surface with stretched double-stranded DNA as a guiding template	40
Scheme 1.16. Cartoon scheme highlighting the templating effect of DNA in directing the growth of the polymers towards forming 1-D nano structures. The red species represent monomers and subsequent cationic oligomer formation in solution	42
Scheme 1.17. An illustration representing the key stages towards device construction within this project. A) functional conducting polymer nanowire alignment between two gold micro-electrodes; B) modified ssDNA probe attachment; C) Introduction of the probe complement; D) detection of a binding event through a measured change in conductance	47
Scheme 2.1. An illustration of DNA alignment across Si/SiO ₂ surfaces using molecular combing	79
Scheme 3.1. A general scheme for the formation of 1,4-triazoles via ‘click’ chemistry	88
Scheme 3.2. Synthetic route for the <i>N</i> -alkylation of pyrrole derivatives. a) NaH, b) 5-chloro-	90

1-pentyne, DMF. R ₁ = R ₂ = H (P), R ₁ = H, R ₂ = thiophene (TP), R ₁ and R ₂ = thiophene (TPT)	
Scheme 3.3. Reaction scheme for 2-(2-thienyl)-pyrrole, TP. i) allylamine, pyridine ii) thionyl chloride, toluene/DMF iii) KO ^t Bu, DMF	91
Scheme 3.4. Reaction scheme for 2, 5-di (2-thienyl)-pyrrole, TPT. i) succinyl chloride, AlCl ₃ , dry CH ₂ Cl ₂ ii) acetic anhydride, HOAc. NH ₄ OAc	92
Scheme 4.1. Surface modification of Si/SiO ₂ surfaces with TMS in order to facilitate molecular combing	116
Scheme 4.2. An illustration of DNA alignment across Si/SiO ₂ surfaces using molecular combing	116
Scheme 6.1. Chemical co-polymerization of pyrrole and C5-P. The resulting product retains the alkyne functionality with the improved conductivity afforded by the additional unmodified pyrrole moieties	185
Scheme 7.1. The Lieber group demonstrated the capability for multiplexed real-time monitoring of analytes present in femtomolar concentrations by firstly developing an integrated nanowire array of distinct nanowires so surface bound capture probes	204
Scheme 7.2. A general scheme for the formation of 1,4-triazoles via ‘click’ chemistry	209
Scheme 7.3. Reaction scheme for coupling 3-azido propanol, C5-P, when R ₁ and R are H, C5-TP, when R ₁ is H and R is thiophene, and C5-TPT when R ₁ and R are thiophene	211
Scheme 7.4. The synthetic pathway to 5’azido-modified oligonucleotides	217

Table of Contents

List of Abbreviations.....	ii
Acknowledgments.....	iv
Abstract.....	v
List of Figures.....	vi
List of Tables.....	xvii
List of Schemes.....	xviii
Chapter 1 – DNA-Bases Conducting Polymer Nanowires for Biosensing Applications.....	1
Introduction	2
Label-Free Biosensors	2
Conducting Polymers	7
Synthesis of Polypyrrole.....	10
Conduction Mechanism.....	12
Derivatisation of Pyrrole Compounds	15
Bio-functionalisation of Conducting Polymers	18
1-D Conducting Polymer Nanostructures	27
Deoxyribonucleic Acid.....	31
DNA as a Construction Tool	35
Project Overview	45
Thesis Outline.....	48
References	49
Chapter 2 – Characterisation Techniques	62
Overview	63
Atomic Force Microscopy (AFM)	64
Scanned Conductance Microscopy (SCM)	67
Conductive Atomic Force Microscopy (cAFM)	74
Two-Probe <i>I-V</i> Measurements	76
Contact Angle Measurements	77
Nanowire Alignment	79
References	81

Chapter 3 – Synthesis and Characterisation of Monomer Building Blocks and Conversion to Conducting Polymers	82
Chapter Overview	83
Introduction	84
Results and Discussion	90
Monomer Synthesis	90
Alkylation of <i>N</i> -pyrrolyl Units	92
Electrochemical Characterisation	92
Chemical Polymerisation.....	95
Conclusions	102
Experimental.....	103
Thiophene <i>N</i> -allylcarboxamide	103
Imidoyl Chloride	103
2-(2-Thienyl)-pyrrole from Imidoyl Chloride	103
Preparation of 1, 4-Bis(2-thienyl)-1, 4-butanedione	104
Preparation of 2,5-Di(thiophen-2-yl)-pyrrole.....	104
General procedure for Alkylation of Monomer Units using 5-Chloro-1-pentyne	105
General Procedure for Electrochemical Polymerisation	105
General Procedure for Chemical Polymerisation	106
Preparation of Si/SiO ₂ Wafers for FTIR.....	106
Fourier Transform Infrared Spectroscopy (FTIR).....	106
References	107
Chapter 4 – DNA-Based Nanowires	110
Chapter Overview	111
Introduction	112
Results and Discussion	118
Large Scale DNA-Templating.....	118
Si/SiO ₂ Surface Modification	122
Nanowire Formation and Deposition	124
Iron-free DNA Catalysed Nanowire Formation	134
Conclusions	140
Experimental.....	141

Preparation of SiO ₂ wafers for AFM/FTIR	140
Fourier Transform Infrared (FTIR)	140
General Procedure for DNA-templated Synthesis for FTIR Studies	141
General Procedure for DNA-templated Synthesis for SPM Studies	141
Atomic Force Microscopy (AFM).....	141
General Procedure for DNA-Catalyzed Nanowire Formation	142
General Procedure for UV-Vis Studies	142
References	143
Chapter 5 – Electrical Characterisation of DNA-Templated Polymer Nanowires	148
Chapter Overview	149
Introduction	150
Results and Discussion	157
SCM Studies of Conductive Polymer Nanowires	157
Nanowire Two-Probe <i>I-V</i> Measurements	161
Conclusions	177
Experimental.....	179
Scanned Conductance Microscopy (SCM)	179
Two-Point probe Current-Voltage Measurements	179
References	180
Chapter 6 – Conductivity Studies of Pyrrole-Thiophene Co-Polymer Films	183
Chapter Overview	184
Introduction	184
Results and Discussion	187
Bulk Conductivity Measurements	187
Optimised Preparation of Polypyrrole.....	190
Co-Polymer Systems	194
Conclusions	196
Experimental.....	197
General Procedure for Bulk Polymerisation and Conductivity Measurements.....	197
General Procedure for Bulk Two-Probe <i>I-V</i> Measurements	197
References	198

Chapter 7 –DNA-Based Nanowire Modification	201
Chapter Overview	202
Introduction	203
Results and Discussion	210
Functionalization of Bulk DNA/Polymer Hybrid Materials	210
Modified Oligonucleotide Synthesis	216
Hybridization Studies	218
Nanowire Modification	220
Conclusions	224
Experimental.....	225
Preparation of 3-Azido Propanol from 3-Bromo Propanol	225
General Procedure for ‘Click’ Chemistry of 3-Azido Propanol with Monomer Units	225
General Procedure for ‘Click’ Chemistry of DNA Hybrid Polymers on Si/SiO ₂	226
Oligonucleotide Synthesis	226
UV-Vis Oligonucleotide Hybridisation Studies	226
Electrical Characterisation by c-AFM General Procedure	227
Azide Modified Duplex Coupling Method 1.....	227
Azide Modified Oligonucleotide Coupling Method 2.....	227
Fluorescence Microscopy	228
References	229
Chapter 8 – Summary and Further Work	232
Achievements	233
Further Work	234

Appendix

Published Work

Chapter 1

DNA-Based Conducting Polymer Nanowires for Biosensor Applications

1.1 Introduction

1.1.1 Label-Free Biosensors

Current technologies for complex molecular diagnostics require large, multiple and expensive bench top devices, operated by highly-trained and high salaried scientists.¹⁻³ Due to the limitations of these devices, vital results can take days and in some cases weeks, impacting on the spread of disease and accurate cost effective treatment. In order to allow medical clinicians to deliver tailored medicine at the point of care within minutes, the most sort after attributes for diagnostic devices/biosensors are high sensitivity, portability, low cost and a quick turnaround time.^{4, 5}

The basic mechanism of a biological sensor makes use of a highly selective and specific capture probe linked to a transduction pathway which produces a signal relative to the quantity measured (Figure 1.1).⁶⁻⁸ Transduction mechanisms can be broadly classified as electrochemical, optical, mass or thermal.

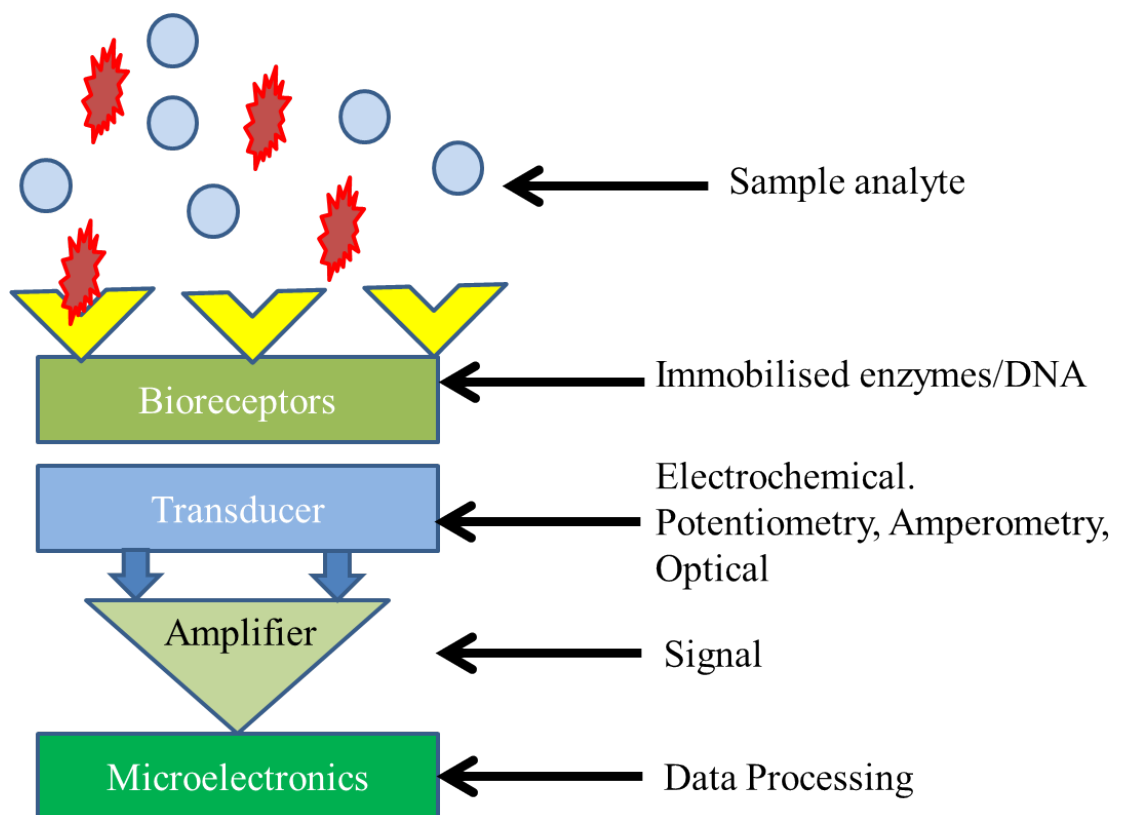


Figure 1.1. An illustration of the basic mechanism of a biological sensor

Sensors can be roughly grouped into two major categories: those that identify molecules spectroscopically^{9, 10} or those that use a direct or indirect means of sensing a specific molecule.^{8, 11, 12} The detection of small molecules is readily achieved with the first category, many of which are now being scaled down in efforts to meet many of the desired attributes listed earlier. This has resulted in development of a number of new spectroscopic approaches such as miniaturized Fourier transform infrared spectrometers.¹⁰ However, many of these techniques face lower limits of size due to scaling limitations and lower limits on power dissipation because of fundamental physical phenomenon by which they operate.¹³ Furthermore, they are incapable of sensing large molecular species such as proteins and viruses.^{5, 7, 14}

In contrast, the macromolecular sensing required for biological research and clinical applications is predominately achieved by specific molecule detection methods because these molecules are often too complex for spectroscopic recognition.^{3, 5, 13-15} Many existing specific molecule detection techniques require the capture probes or their target biomolecules to 'labeled', typically through the attachment of a fluorescent dye.¹⁶ Indirect detection methods of this nature, while useful, have a number of drawbacks. For example, attaching the dyes is not a trivial exercise and detection of fluorescence often requires expensive lab-based equipment.¹⁵

Label-free detection of molecular interactions presents an attractive alternative to traditional techniques such as fluorescence, largely through a desire to avoid the necessity of molecular labels, especially where labels can compromise the nature of the interaction under investigation.¹⁷⁻²¹

Electrochemical detection methods offer an ideal route to providing real-time monitoring of interactions between an immobilized ligand (such as a receptor) to an analyte in solution without the need for complex preparation.^{22, 23} Electrochemical sensors are devices that extract information about a sample by measurement of an electrical parameter.²⁴ Changes to the electronic structure of the chosen transduction element induced through the presence of charged species, such as DNA, result in altered electrical properties.^{20, 25} When measured, these permutations can provide a signal for the presence of a target analyte molecule and can be quantified as a change in current at a fixed applied potential (amperometry), a change in conductivity (conductometry), impedance (impedimetry) or potential

(potentiometry).^{22, 26, 27} While useful for small molecule and ion detection, few of the approaches presently employed are particularly sensitive, with detection limits are generally in parts per million.^{28, 29}

Surface Plasmon Resonance (SPR) overcomes the sensitivity barrier and currently serves as the standard for label-free sensing.^{30, 31} In this approach, an antibody of the protein is attached to a gold film (Figure 1.2). The angular reflection of the laser beam off the back-side of the gold is dependent on the local di-electric constant; binding the protein changes the dielectric constant and thus modulates the deflection of the laser beam. However, this technique has not met with success outside research environments due to its price, size and mechanical alignment issues.

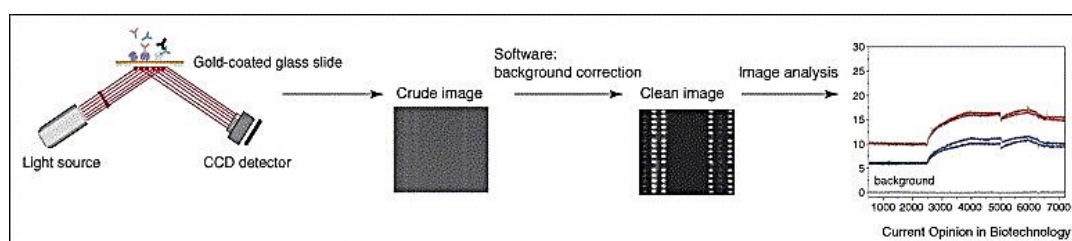


Figure 1.2. SPR imaging. A light source projects light onto a gold surface, on which a biomolecular interaction is occurring, and the reflected light is imaged onto a CCD detector. This process is performed over a period of time and a collection of images obtained. Reproduced from reference³¹

As a result, a number of label-free detection strategies are presently under development. Cantilever sensors, which sense the binding of the desired molecule to a thin cantilever by measuring the deflection of the beam with a laser on piezo resistive elements;³² fiber optic sensors, which sense the binding of nanoparticles linker antibodies to a protein after binding to a fiber-optic strand;³³ and waveguide sensors, which sense the presence of a specifically bound protein to an antibody film on a chip between two waveguides.³⁴ While each of these technologies have shown promise, none meet the needs of sensitivity, versatility and power consumption required to take biosensing from the bench to the bedside.

Due to these shortcomings, much research is focused around solid state conductance sensors, with a drive to increase sensitivity and versatility by reducing the dimensions of the devices in order to maximize the effect of surface charge on charge transport. Progress in the development of nanoscale materials is fundamental to this approach in order to achieve the level sensitivity required for quantitative analysis of samples containing a minimal amount of matter.^{35, 36} Consequently, one-

dimensional (1-D) nanostructures, or nanowires (NW), have attracted great interest in biological sensing research.^{24, 25, 37, 38} When functionalized with appropriate ‘capture probes’ and integrated into electronic devices, these materials can act as transducers for label-free electrical detection of chemical and biological species.^{27, 39} Moreover, and perhaps the dominant driving force towards miniaturization, is that the high surface-to-volume ratio of these structures has been proposed to increase sensitivity due to the higher free energy or reduced conformational entropy of surface atoms.^{40, 41}

The most commonly supplied rationale is that as the cross sectional area of a device decreases, the ratio of surface to volume increases. the geometry of the NW restricts current flow to a much thinner region than in the bulk and thus the absorbed molecules impose a stronger influence on charge-carrier transport.⁴² The explanation usually proceeds as follows:⁴³

A cylindrical NW of diameter, d , with uniform doping density, N_D , and length, L , has conductance, G_0 :

$$G_0 = q\mu N_D \pi d^2 / 4L$$

Where, q , is the elementary charge and μ , is charge carrier mobility (assumed to be uniform).

Introduction of surface charge density, σ , to approximate the charge due to molecular conjugation, the NW will be accumulated or depleted by an equal amount of charge, ΔQ :

$$\Delta Q = \sigma \pi d L$$

Therefore, change in conductance, ΔG , is given by:

$$\Delta G = \pi d \mu \sigma / L$$

Where, d , is the diameter of the nanowire.

Therefore sensitivity, S ,

$$S = \frac{\Delta G}{G_0} = \frac{4\sigma}{qdN_D}$$

Sensitivity is inversely proportional to diameter, d , and doping density, N_D .

The one-dimensional geometries of these structures have also been shown to enhance response times by virtue of their two-dimensional mass transfer profile.⁴⁴ Furthermore, continued device miniaturization facilitates the construction of sensor arrays, enabling duplicate elements to reduce false positives/negatives and provide a fingerprint type response that increases sensitivity and selectivity.

In a practical sense, the use of nanowires in sensing applications allows a single architecture to act as both the capture layer and transducer to directly convert chemical information into an electronic signal, as such these materials can act as transducers for label-free electrical detection of chemical and biological species as illustrated in Scheme 1.1.^{27, 39}



Scheme 1.1. When functionalized with appropriate ‘capture probes’ (left), nanowires can act as transducers for label-free electrical detection of chemical and biological species (right). Reproduced from reference⁴⁵

In light of the benefits afforded by one-dimensional (1-D) nanostructures, recent research has been devoted to the development of 1-D metallic and semiconductor based nanomaterials for sensor applications.⁴⁶⁻⁴⁸ The synthesis, assembly and device integration of these materials have progressed at an impressive rate typically using what is known as the ‘top down approach’, with silicon a well-established material of choice.

At the same time, 1-D nanostructures of organic semi-conductors such as conducting polymers (CPs) have attracted growing interest due to the potential advantages of combining these materials with low dimensionality.⁴⁹⁻⁵² CPs possess highly desirable characteristics such as an readily tunable conductivity, high mechanical flexibility and greater biocompatibility than many inorganic materials. As a special subclass of conducting polymers, conducting polymer nanostructures not only retain their unique properties but also have the characteristics of

nanomaterials e.g. large surface area, miniaturized dimensions, which further increases the merit of conducting polymers in designing and making novel sensors.

1.1.2 Conducting Polymers

Conducting polymers (CPs) are polymers that possess electrical and optical properties similar to those of metals and inorganic semiconductors.^{53, 54} Significantly, these materials also possess the attractive properties associated with conventional polymers, such as ease of synthesis, functionalisation and flexibility in processing.

The potential for organic materials to pass a current was demonstrated as early as the 1950s, when polycyclic aromatic compounds were shown to form charge-transfer complex salts with halogens which exhibited resistivities as low as 8 ohms cm^{-1} .⁵⁵ Largely influenced by the prediction of superconductivity,⁵⁶ research into organic polymer compounds intensified in the early 1960s, with multiple reports since of conductivity observed in oxidised polyacetylene (Figure 1.3).⁵⁷⁻⁵⁹

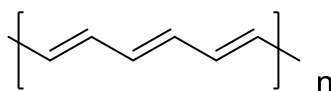


Figure 1.3. The chemical structure of trans-polyacetylene

Significantly, in 1977, Shirakawa *et.al.* made the observation of remarkably high electrical conductivity of halogen-treated polyacetylene.⁶⁰ The group found that partial oxidation of acetylene with chlorine, bromine or iodine vapour produced a ‘doped’ polymeric material 10^8 times more conductive than originally reported,⁶¹ with conductivity levels similar to that of silver observed (10^5 S cm^{-1} compared to 10^8 S cm^{-1} for silver). In the context of CPs ‘doping’ refers to the introduction of charge carriers by partial oxidation and this discovery transformed many insulating polymers into highly conductive materials, making such materials the focus of much research ever since. Table 1.1 lists the repeat units and conductivities for some commonly studied conducting polymers.⁶²

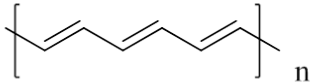
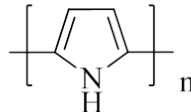
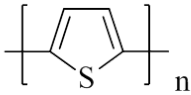
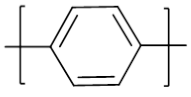
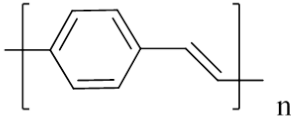
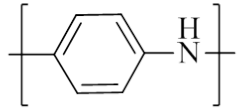
Polymer (date conductivity discovered)	Structure	Conductivity (S/cm)
Polyacetylene (1977)		$10^3 - 1.7 \times 10^5$
Polypyrrole (1979)		$10^2 - 7.5 \times 10^3$
Polythiophene (1981)		$10 - 10^3$
Poly(paraphenylene) (1979)		$10^2 - 10^3$
Poly(p-phenylenevinylene) (1979)		$3 - 5 \times 10^3$
Polyaniline (1980)		$30 - 200$

Table 1.1. A list of the most commonly studied conducting polymers and their conductivities. Reproduced from reference⁶²

Although polyacetylene is one of the most studied polymers, limitations in its use due to instability in air and poor processability has led to particular emphasis being placed upon more stable aromatic compounds.⁵⁴ In particular, pyrrole and thiophene-based materials have attracted significant interest as these compounds find an agreeable balance between stability, ease of functionalisation and high conductivity when polymerized (10^{-12} - 10^5 S cm⁻¹).^{54, 63-70}

Polythiophene (Figure 1.4) is an aromatic-based polymer that has shown to exhibit high electrical conductivity (up to 10^3 S cm⁻¹), good environmental stability and structural versatility.⁵⁴ First discovered in 1882 by Victor Meyers,⁷¹ the polymeric form of thiophene has attracted considerable attention largely due to its especially wide range of unique electronic and optical applications.^{67, 68}

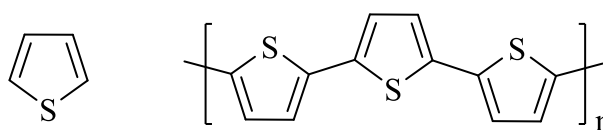


Figure 1.4. The chemical structure of thiophene (left) and the repeating unit of polythiophene (right)

Bolto *et. al* in 1963, were the first to report low levels of resistance in partially iodine oxidized polypyrrole (1 ohm cm^{-1} , Figure 1.5), another heterocyclic material.⁷²⁻⁷⁴ Since then, research examining a range of preparation methods and dopants has been performed, with a varying levels of conductivity observed.⁷⁵⁻⁸¹ For example, in 1981 Kanazawa *et. al.* reported conductivities up to 100 S cm^{-1} ,⁸² while conductivity of over 1000 S cm^{-1} has also been reported for 2-D films of polypyrrole.⁸³

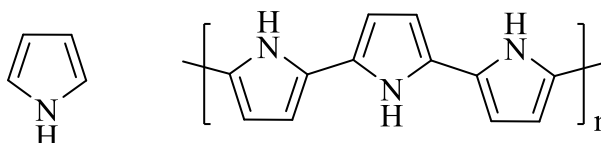


Figure 1.5. The chemical structure of pyrrole (left) and the repeating unit of polypyrrole (right)

1.1.3 Synthesis of Polypyrrole

The formation of polypyrrole is typically achieved via the one electron oxidation of the corresponding monomer unit to the radical cation using one of two approaches: (i) electrochemical or (ii) chemical oxidation. In each case, the resulting polymerisation has been shown to proceed predominantly through the α -positions (2- and 5-positions) of the heterocyclic ring (Figure 1.6) to form a conjugated polymer chain.⁸⁴

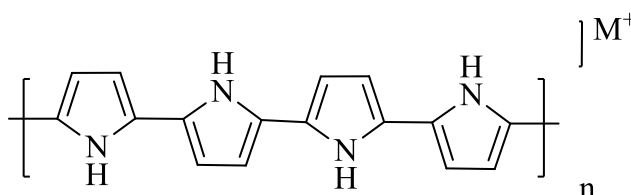
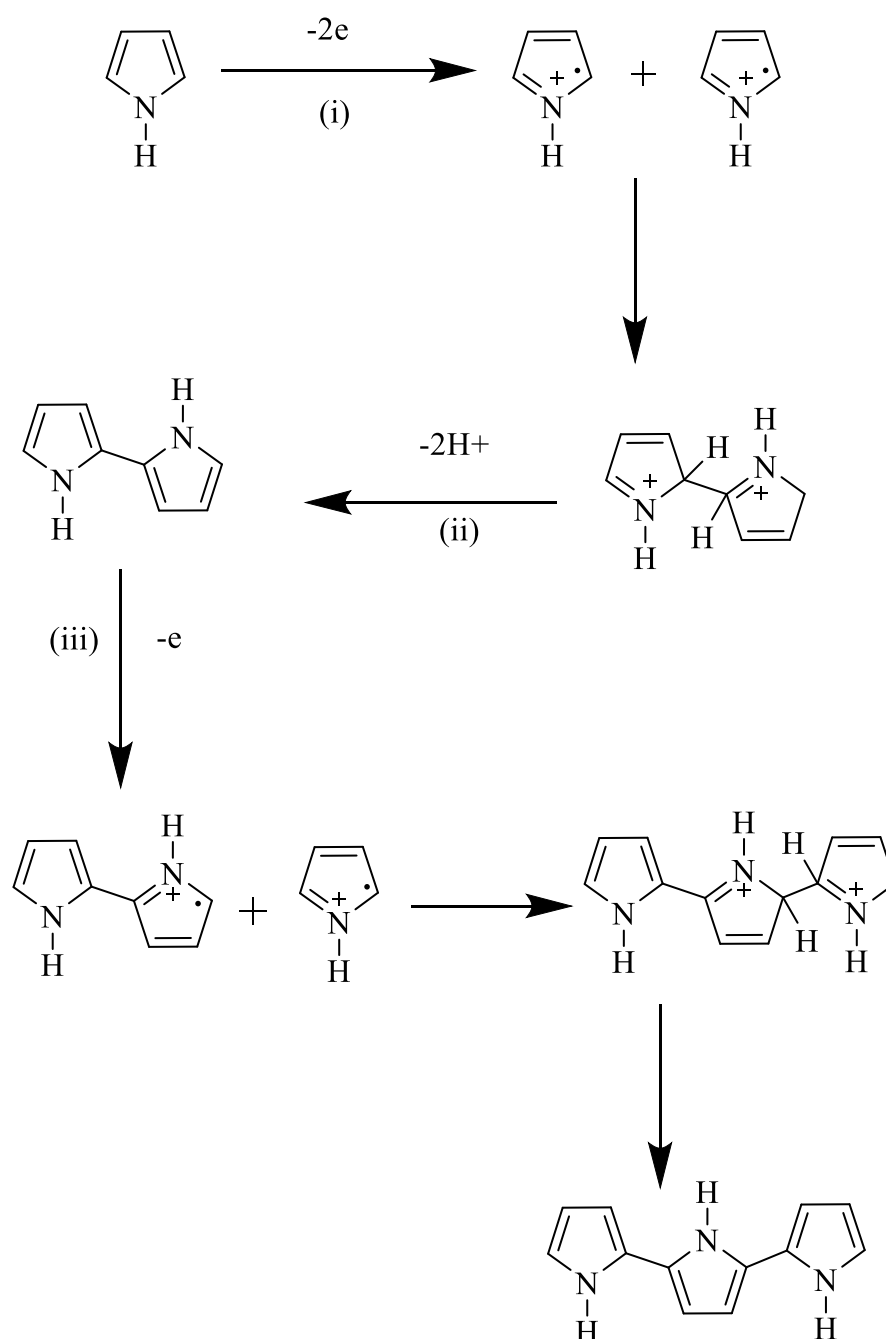


Figure 1.6. Polymerisation of pyrrole can proceed through the α -position forming a conjugated polymer. Where n represents the number of repeating units and M^+ indicates the cationic nature of the material produced

In the case of electrochemical polymerisation,^{85, 86} polymer formation is achieved by subjecting the monomer unit to an oxidizing voltage (+0.8 V) in an electrochemical cell. Chemical polymerisation requires the addition of a chemical oxidant, such as $FeCl_3$.^{85, 87} In both cases, a cationic polymer is formed with charge neutrality maintained by incorporation of the counter ion from the electrolyte solution or oxidizing agent respectively.

The mechanism of polymer formation by either method is very similar and is illustrated in Scheme 1.2. The process is initiated via the one electron oxidation of the pyrrole monomer unit to a radical cation (i). The combination of two radical cation monomers through the formation of a carbon-carbon linkage at the 2-position of each pyrrole ring produces a 2,2'-bipyrrole dimer (after the loss of two protons, (ii)). The dimer has a lower oxidation potential so is preferentially oxidised; as such the polymer chain continues to grow through the re-oxidation of the bipyrrole and further addition of radical cation monomers (iii). Termination only occurs when no more monomer is present.



Scheme 1.2. The mechanism for the polymerisation of pyrrole. (i) the one electron oxidation of the respective monomer unit to a radical cation; (ii) the combination of two radical cation monomers to produce a 2,2'-bipyrrrole dimer; (iii) the polymer chain continues to grow through the re-oxidation of the bipyrrrole and further addition of radical cation monomers

Many similar materials such as thiophene and poly(3,4-ethylenedioxythiophene) (PEDOT) are formed by an analogous mechanism.

1.1.4 Conduction Mechanism

All the main conducting polymers (CPs) have conjugated π -systems. While conjugation is not enough to make the polymer material conductive it is however key to the formation of the principal charge carriers in conducting polymers. As discussed earlier, CPs are required to be doped in order to reach levels of high conductivity. Doping is the process of oxidizing (*p*-doping) or reducing (*n*-doping) a neutral polymer and providing a counter anion or cation (i.e. dopant). In 1984, Brédès *et. al.*⁸⁸ researched the conduction mechanisms of polypyrrole and found conduction took the form of a *p*-type semiconductor.⁵⁴

The π -electrons in conjugated polymers such as polypyrrole are delocalized along the polymer chain making the system essentially electronically one dimensional and the elastic energy required to distort the polymer chain is small. As a result, the electrons are strongly coupled to vibrations of the polymer chain and the removal of electrons during oxidation (oxidative doping) has a significant effect on the electronic properties of the system. The resulting half-filled π system gives rise to symmetry distortion of the polymer chain (known as Peierls distortion) causing the formation of self-localized electronic states known as polarons and bipolarons which underpin the electrical conduction in CPs.

A polaron (Figure 1.7) is essentially a free radical and a positive charge. The charge is typically localised over ~3-4 pyrrole units with charge neutrality maintained through incorporation of the counter ion (A^-) from the electrolyte solution or oxidizing agent.

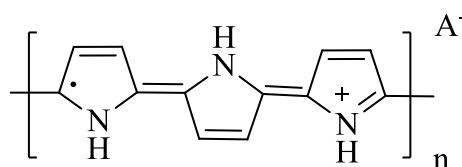


Figure 1.7. A positively charged polaron in polypyrrole

Removal of a second electron results in bipolaron formation (defined as a pair of like charges associated with a strong local lattice distortion (Figure 1.8)). This is due to the localised nature of the polaron states. One bipolaron is thermodynamically more stable than two polarons.

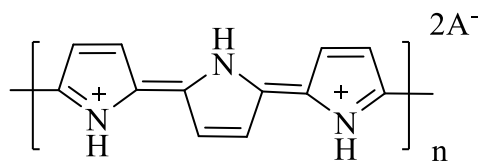


Figure 1.8. Removal of a second electron leads to bipolaron formation in polypyrrole

Stabilization of Peierls distortion and an increase in elastic energy from the polymer's newly formed partially oxidised state results in the molecule adopting a new equilibrium geometry. This is brought about by an upward shift of the highest occupied molecular orbital (HOMO) and a downward shift of the lowest unoccupied molecular orbital (LUMO), creating an energy gap, known as the band gap (E_g , <3 eV), thus making the system a semiconductor.

Polaron and bipolaron formation introduces two localised electronic levels within the band gap. It is the location of polarons/bipolarons within the band gap which allows them to act as charge carriers. The polaron state of polypyrrole is symmetrically located at 0.5 eV from the band edges (Figure 1.9, b)), with bipolarons found at 0.75 eV (Figure 1.9, c)).

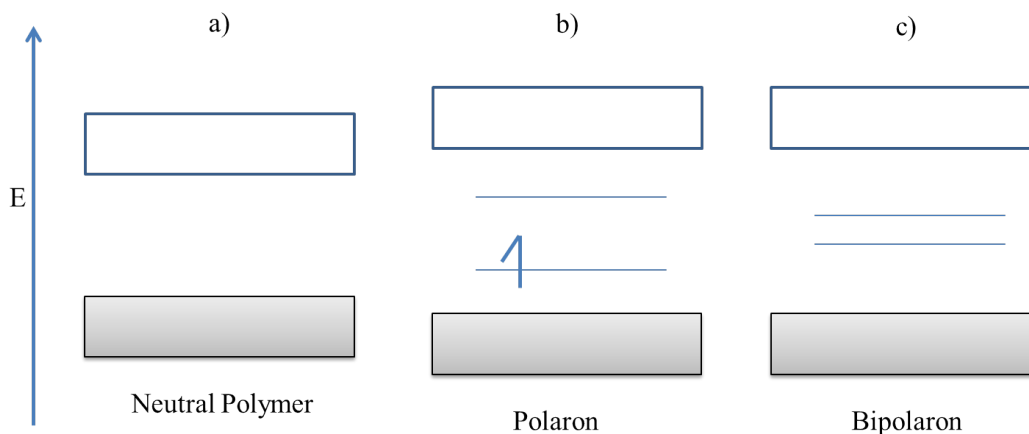
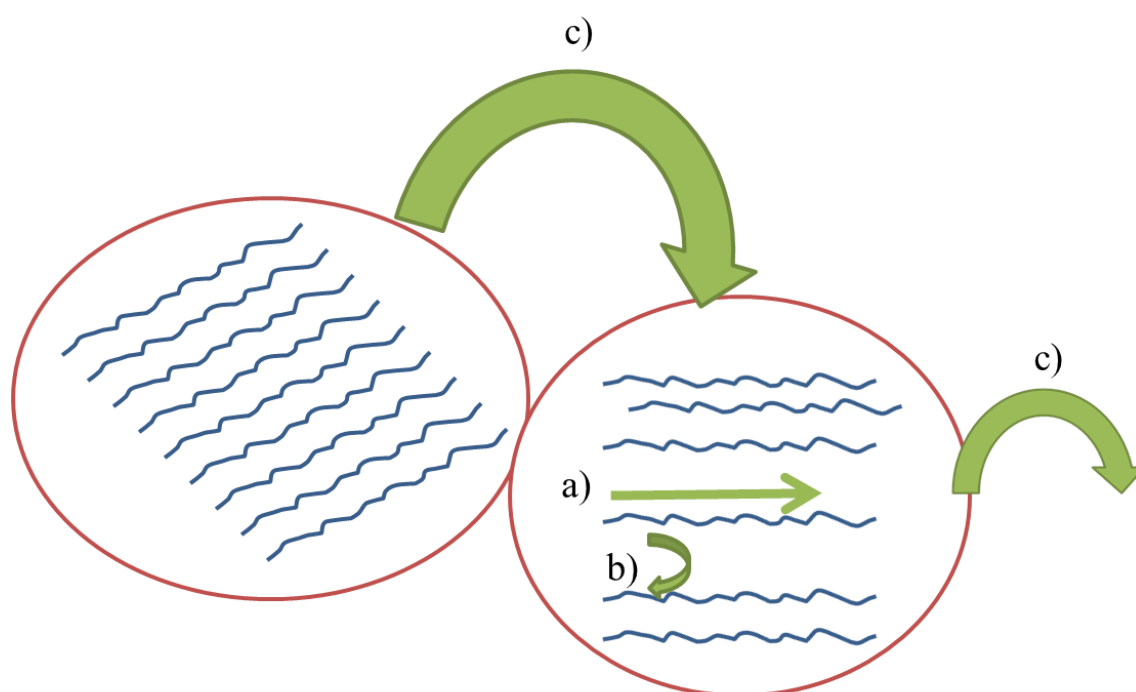


Figure 1.9. Polarons and bipolarons produced upon oxidation are the principle charge carriers in conducting polymers. Neutral polymer, (a), polarons, (b), and bipolarons, (c), are symmetrically located within the band gap of polypyrrole

In contrast to conventional semiconductors where the conduction mechanism is largely dependent on the size of the band gap and promotion of electrons into the conduction band, conductivity in conducting polymers, such as polypyrrole, is dependent on the number, density and mobility of polaron/bipolarons in the material. The attraction of electrons in one repeat-unit to the nuclei in neighboring

units yields charge mobility along the conjugated chain (Scheme 1.3, a)), between chains (Scheme 1.3, b)) and between particles (Scheme 1.3, c)) which is often referred to as ‘electron hopping’. Polarons and bipolarons normally have low mobility largely due to Columbic attraction to the relative counter-ion and do not delocalize along a polymer chain completely. The introduction of a high concentration of counter-ions (‘doping’) is required so that the polaron/bipolarons can move freely between the localised sites in the electric field created. Bulk conductivity in the polymer material is limited by the need for electrons to jump from one chain to the next i.e. charge transfer. The rate of hops depends on the electric field, contacts between different domains in the material, temperature and the product of concentrations of neighbouring empty and filled sites.



Scheme 1.3. Schematic of the conduction pathways in a conducting polymer a) intra-chain; b) interchain and c) inter-particle where the blues lines represent polymer chains and the red circles represent particles

1.1.5 Derivatisation of Pyrrole Compounds

The organic nature of materials such as pyrrole offers the opportunity to tailor the electronic and optical properties in conjunction with functionality, using relatively straightforward molecular chemistry. As a result, conducting polymers continue to be the focus of much research for a variety of applications such as solar cells⁸⁹, organic light emitting diodes^{90, 91}, transistors⁹² and bio/chemical sensors.^{37, 93, 94} The synthetic flexibility, ease of preparation and stability of polypyrrole in particular, make it an attractive starting point for the design of new materials.

Synthetic modifications can be made on the ring system or through the central nitrogen (Figure 1.10) to introduce new functionality and/or tune the electronic properties.

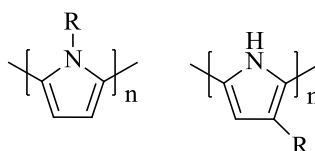
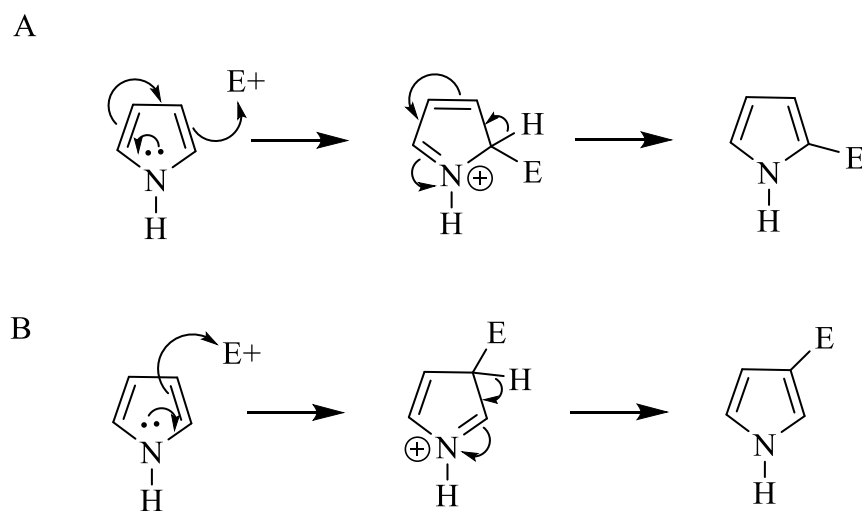


Figure 1.10. Structure of *N*-substituted -pyrrole and β -substituted pyrrole, illustrating the alternative sites for coupling functional groups

Pyrrole readily undergoes electrophilic aromatic substitution predominantly at the 2- and 5- positions. This preferential reactivity can be explained by the considering the resonance forms of each, shown in Scheme 1.4.⁹⁵



Scheme 1.4. The reaction scheme for A) reaction with electrophiles in the 2-position of pyrrole; B) reaction with electrophiles in the 3-position of pyrrole

In both intermediates shown (better illustrated in Figure 1.11), the two double bonds are conjugated with each other but only in the intermediate formed from attack at the 2-position (Scheme 1.4, A)) are both double bonds conjugated with N⁺ making it a more stable linear conjugated system.

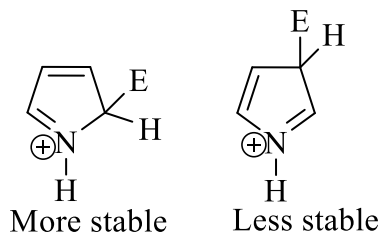
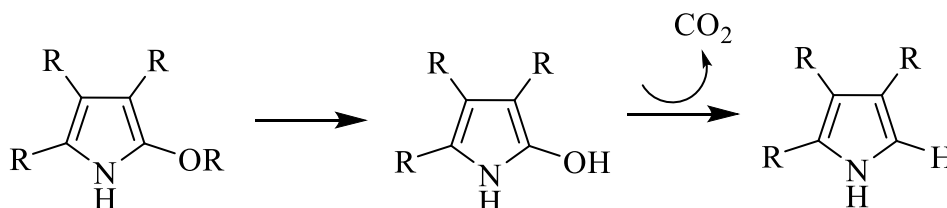


Figure 1.11. Attack at the 2-position forms a linear conjugated system which is more slightly more stable than the ‘cross conjugated’ intermediate formed by upon attack at the 3-position

However, modification of the 2-position as a route to introducing new functionality forces polymerisation to proceed through the 3- or 4-position of the pyrrole ring; resulting in unfavourable effects the conductive properties of the material produced (Chapter 3) and is therefore not viable route for this project.

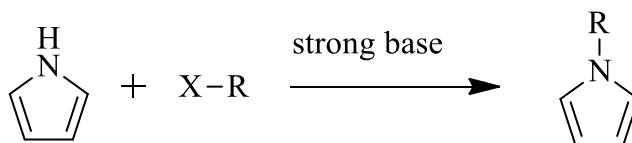
Despite the preferential reactivity of the 2-position, pyrrole also readily undergoes electrophilic aromatic substitution at each ring position, often producing a mixture of products. One method of controlling regioselectivity is to block a desired position prior to adding substituents to the ring system (Scheme 1.5).



Scheme 1.5. A common method to avoiding the chemical ambiguity associated with 3-derived compounds is to block the desired site with a preferential leaving group

An alternative strategy is to make synthetic modifications through the central nitrogen. Significant benefits of this approach are that it avoids the chemical ambiguity that can arise with the asymmetric 3-derived compounds and such compounds can be made through relatively straightforward synthetic chemistry. Materials modified in this manner still retain conductive nature and are particularly useful due to the relatively straightforward means of introducing new functionality.

The NH proton in pyrrole is moderately acidic with a pKa of 16.5.⁹⁵ Pyrrole can be deprotonated with strong bases such as butyl lithium and sodium hydride (Scheme 1.6). The resulting alkali pyrrolide is nucleophilic. Treating this conjugate base with an alkylhalide such as methyl iodide gives *N*-methylpyrrole in an SN2 reaction.



Scheme 1.6. *N*-alkylation of pyrrole is commonly achieved using a strong base such as butyl lithium or sodium hydride and an alkylhalide, where X can be I, Br or Cl

Utilizing the chemistry described above, a wide range of substituted pyrrole compounds have been prepared for a variety of applications.^{50, 54, 93} Figure 1.12 illustrates some substituted pyrrole compounds that have been prepared as conducting polymers.⁹⁶⁻⁹⁸

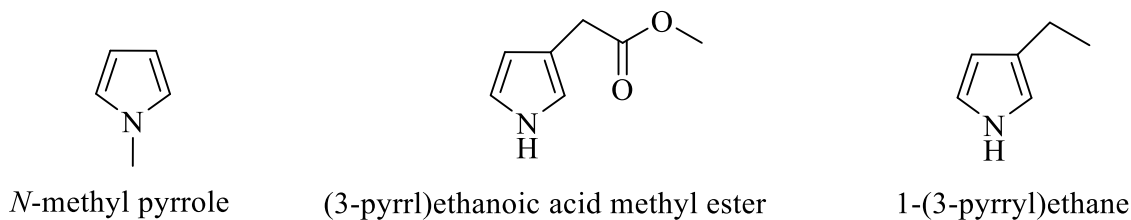


Figure 1.12. Substituted pyrrole derivatives that have been prepared as conducting polymers

1.1.6 Bio-functionalisation of Conducting Polymers

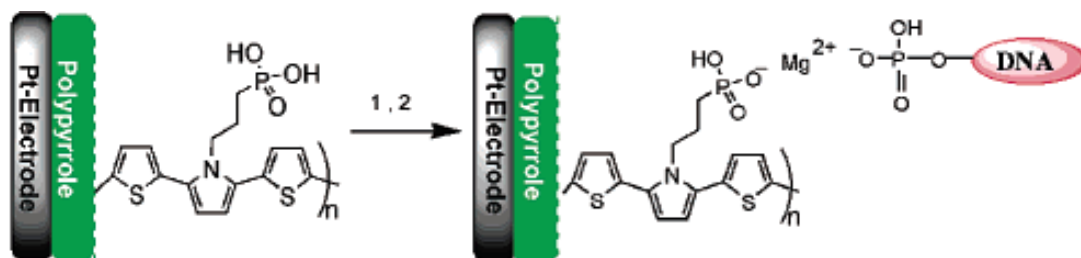
Functionalisation of conducting polymers for biomedical applications is an area where conducting polymers have shown significant potential. The simple means of fabrication, high sensitivity to changes in their surrounding environment and biological compatibility of these materials has meant conducting polymers have found application in tissue-engineering scaffolds, neural probes, drug-delivery devices, bio-actuators and in particular, biosensors.^{99, 100}

A CP by itself lacks the specificity/selectivity necessary to function as a biosensor. Biological recognition molecules, such as antibodies, enzymes or oligonucleotides, impart the desired selectivity and specificity to conducting polymers in order for these materials to be used in this manner. As such, the polymer is not only used as an immobilization matrix but also provides the electrical component of these two elements.

In this regard, the opportunity offered by the organic nature and bio-compatibility of conducting polymers to readily tune the electrical, chemical, physical properties to better suit the nature of the specific application is attractive. To this end, the immobilization of bioactive macromolecules in or on electrically conductive polymers has been explored and can be achieved through a number of techniques which are broadly classified as physical adsorption, entrapment, affinity and covalent attachment. Critical factors to be considered in biomolecule immobilization are the stability, accessibility and retention of biological activity of any immobilised molecules, it is these fundamental considerations that largely govern the route taken to achieve probe immobilization.⁹³

Physical adsorption is the simplest method of immobilization and one of the first approaches used for conducting polymer based biosensors. A number of pyrrole based biosensors have been realized utilizing this method which essentially makes electrostatic interactions for the immobilization of biomolecules. For example, the direct electrochemical detection of a DNA hybridization event has been demonstrated utilizing electrostatic modulation of ion-exchange kinetics of polypyrrole (PPy) film.¹⁰¹ This approach takes advantage of the reversible electrochemical behavior of PPy after its surface has been modified with a layer of electrochemically grafted poly(2,5-dithienylpyrrole) modified with a phosphonic

acid group (Scheme 1.7). An oligonucleotide was linked to the modified conducting polymer via Mg^{2+} by forming a bidentate complex between an alkyl phosphonic acid group at the *N*-position of the polymer and the phosphate group of the DNA. Ion exchange was controlled by the reaction of a surface immobilized, unlabeled, single-stranded DNA oligomer molecule, ssDNA, with its complementary DNA.



Scheme 1.7. Key steps in the preparation of the DNA hybridization sensor probe: (1) $MgCl_2$ aqueous, 5 mM, 10 min; (2) aqueous ssDNA(a), 10 min, then rinsed with TRIS buffer. Reproduced from reference¹⁰¹

The modified Pt electrode was placed in a solution of the non-complementary oligonucleotide and complementary oligonucleotide with the cyclic voltammogram (CV) recorded in each instance. In the case of the complementary oligonucleotide sequence there was a marked change of the shape of CV while the recognition layer showed no effect on CV when it was exposed to the solution containing a non-complementary oligonucleotide ssDNA.

Although physical adsorption is a relatively simple approach to probe immobilization, controlling the concentration of the immobilized compound is difficult and immobilization is not always stable due to the weak non-covalent forces involved. An alternative approach to physical adsorption is electrochemical entrapment. Now one of the most extensively used techniques for probe immobilisation, this method originates from work on enzyme sensors by Umana and Waller¹⁰² when investigating electrode immobilization of glucose oxidase through electropolymerization of pyrrole in the presence of the enzyme. The group demonstrated that polypyrrole-modified electrodes are relatively stable and applicable for the indirect determination of electrochemically active products of glucose oxidase catalyzed reactions that occur in a solution contacting the electrode.¹⁰²

The technique requires a monomer, dopant and capture probes to be mixed in a single solution used for electrochemical polymerization, resulting in the formation

hybrid polymer-probe material (Figure 1.13). This process is usually performed under mild conditions as to prevent any alteration to the activity of capture probes with a significant advantage of this technique being that only a single step for both polymerization and biomolecule immobilization required.

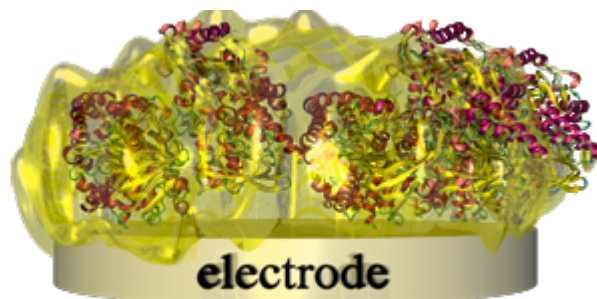


Figure 1.13. An illustration of the electrochemical entrapment of an enzyme with a polymer (yellow) immobilized on an electrode surface. Entrapment of biomolecules in polymer films during their electrogeneration on an electrode surface is easily applicable to a wide variety of biological macromolecules and the monomers are often commercially available. Reproduced from reference¹⁰³

CPs such as PPy, are frequently used in the entrapment of biomolecules, with the entrapment of glucose oxidase (GOx) in PPy films found historically to be the most common application.¹⁰⁴ Wang *et. al.*¹⁰⁵ were first to demonstrate the entrapment of oligonucleotides during the growth of polypyrrole films while maintaining their hybridization activity. Here, ssDNA probes were effectively doped within electropolymerized polypyrrole (PPy) films using an upside-down two-electrode electrolytic cell. Subsequent monitoring of current changes induced by a hybridization event demonstrated that the oligonucleotide probes can serve as the sole counter anion during the growth of conducting PPy films and still maintain their hybridization activity within the host polymer network.

Subsequently, entrapment of biomolecules in CP films has been used to construct biosensors using DNA and a wide range of enzymes such as horseradish peroxidase, cholesterol oxidase/esterase and dopamine.^{37, 106} While entrapment is a popular immobilization technique, it has some important limitations. The high potentials employed during polymerization and poor target accessibility to the incorporated probe in the bulk films afforded are significant drawbacks to this approach.

An alternative method for capture probe immobilization is high affinity binding. Here, the extremely specific, high-affinity, strong non-covalent interactions are utilized for the immobilization of biomolecules onto the surface of CPs. As the

strongest known non-covalent interaction, biotin-avidin complexes find particular use in this category of immobilization ($K_D \sim 10^{-15}$ M, Figure 1.14).¹⁰⁷

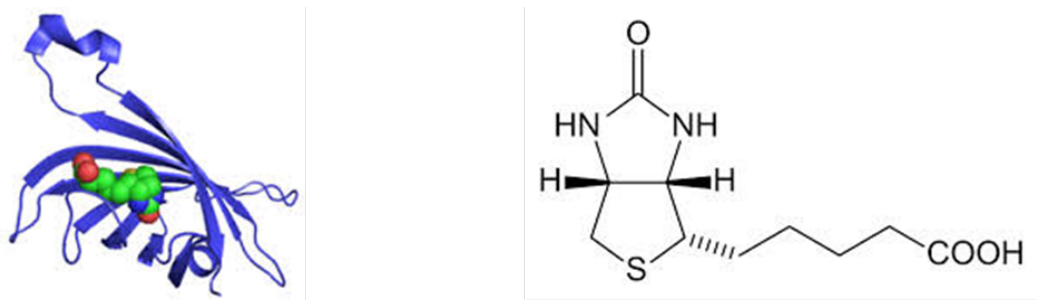
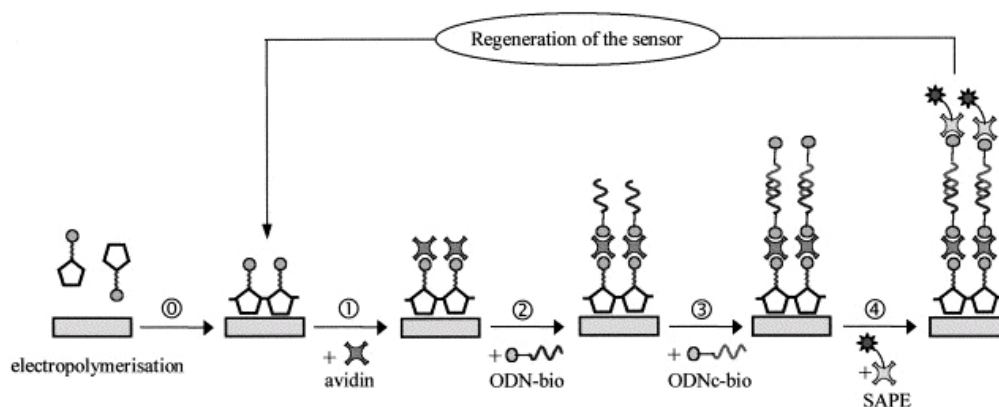


Figure 1.14. Avidin (a) is a tetrameric glycoprotein (4 biotin molecules may bind) produced in the oviducts of birds, reptiles and amphibians, the monomeric version is shown; (b) biotin, also known as vitamin H or coenzyme R has a well-known, high-affinity for avidin. Reproduced from reference¹⁰³

The binding between biotin and avidin is rapid and once formed, is unaffected by extremes of pH, temperature, organic solvents and other denaturing agents.

Interestingly, using this avidin-biotin linkage, the sensor can be regenerated by treatment with a detergent solution at high temperature (*ca.* 70 °C) that breaks the avidin-biotin bridge but does not affect the support matrix. This principle was first demonstrated by Dupont-Filliard *et. al.*¹⁰⁸ to reversibly immobilize oligonucleotide probes. Here, a biotinylated polypyrrole film was synthesized (Scheme 1.8, 0), followed by immobilization of avidin units through the highly specific biotin-avidin interaction (Scheme 1.8, 1 and 2), the film was subsequently exposed to biotinylated oligonucleotide probes for immobilization to take place (Scheme 1.8, 3). Reversibility was achieved by treatment in aqueous solution of sodium dodecylsulfate to cleave the avidin-biotin connection.

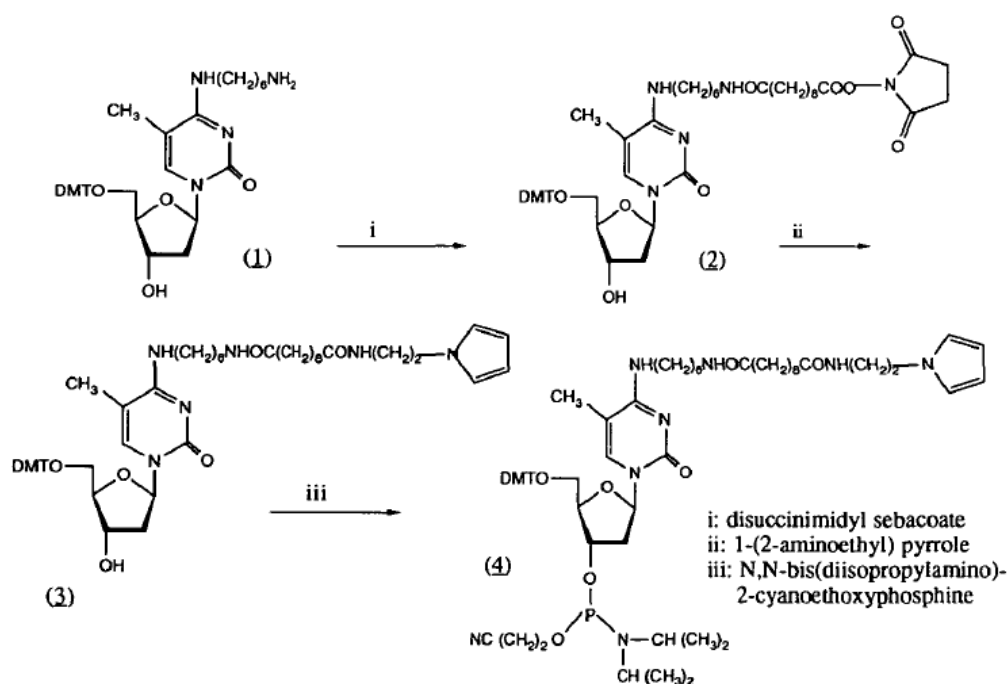


Scheme 1.8. Schematic of a sensor design based on electrocopolymerization of biotinylated pyrrole and the use of biotin–avidin interactions. Reproduced from reference¹⁰⁸

Conducting polymers containing covalently substituted monomers have also been synthesized as a means to facilitate the immobilization of biomolecules. Generally, capture probes functionalised with $-\text{NH}_2$, $-\text{COOH}$ are covalently attached to either a functionalised monomer or functionalised polymer. Pyrrole has been extensively investigated in this regard, largely owing to its synthetic flexibility, stability, ease and variety of preparation.

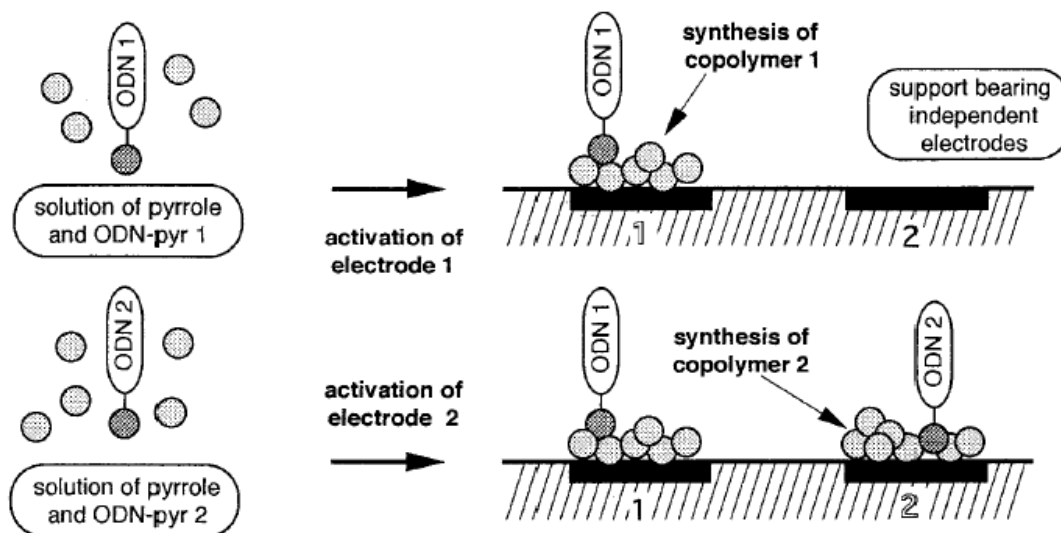
Livarche *et al.* developed a process that utilizes pyrrole bearing oligonucleotides (ODN) for the direct immobilization of multiple probes on electrode arrays through co-polymerisation with unmodified pyrrole.¹⁰⁹⁻¹¹¹ The group used this approach to prepare an oligonucleotide array consisting of a matrix of 48 addressable $50\ \mu\text{m}$ microelectrodes that was applied to detect hepatitis C virus in blood samples.¹¹¹

Here, the synthesis of the pyrrole bearing oligonucleotides involved the preparation of a phosphoramidite building block (Scheme 1.9) from 5'-O-(4,4'-dimethoxytrityl)-4-N-(6-aminohexyl)-5-methyl-2'-deoxycytidine (1) and 1-*N*-aminoethylpyrrole. A series of modified oligonucleotides were subsequently prepared using phosphoramidite building block in a standard DNA synthesizer.



Scheme 1.9. Synthesis of the phosphoramidite building block through modification of pyrrole at the *N*-position. Reproduced from reference¹¹¹

Oligonucleotide modified PPy films were synthesized on each working micro electrode by electro-co-polymerization by a cyclic voltamperometric method. Each electrode was covered by a conducting co-polymer comprising of covalently modified pyrrole (Py-ODN) and un-substituted pyrrole. A series of capture probes were immobilized on alternative electrodes by depositing different solutions of pyrrole modified with ssDNA and selectively switching on the working electrodes located to initiate polymerisation (Scheme 1.10).



Scheme 1.10. Alternative capture probe addressing by electrodirected co-polymerization: Py-ODN 1 is first copolymerized on the electrode 1; following washing of the cell, copolymerization of the Py-ODN 2 is carried out by activation of electrode 2. Reproduced from reference¹¹¹

A more common approach for covalent biomolecule attachment is for modifications to be made post-polymerization. Here, typically, a CP film is first polymerized from a solution containing functionalized monomer units followed by covalent attachment of the desired capture probe onto the surface of the functional CP. A significant advantage to this method is that the conducting polymer films can be prepared under conditions that are potentially incompatible with the capture probe, such as organic solvents or high electropolymerization potentials; while probe attachment can be performed under mild conditions to ensure probe integrity.

Glutaraldehyde crosslinking techniques have been extensively used in this regard, particularly in the immobilization of enzymes such as glucose oxidase and chloramphenicol onto PPy films (Figure 1.15, a).¹¹²⁻¹¹⁴ Here, the conducting polymer is functionalized with a linker molecule (glutaraldehyde) to present an aldehyde functional group on the surface of the polymer which can be subsequently used for covalent attachment. Glutaraldehyde is a bi-functional linker molecule with aldehyde groups at both ends. One aldehyde group can be used to attach primary or secondary amine group of the polymer (Figure 1.15, b) while the other can be attached to the amine group of the recognition molecule i.e. an enzyme (Figure 1.15, c).

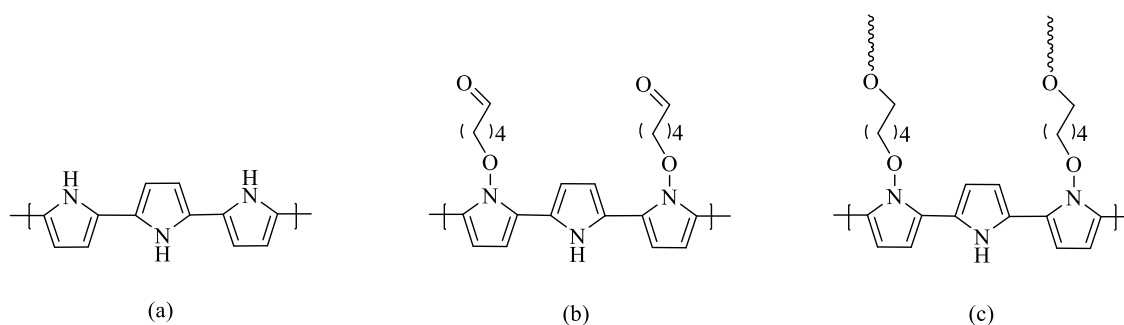
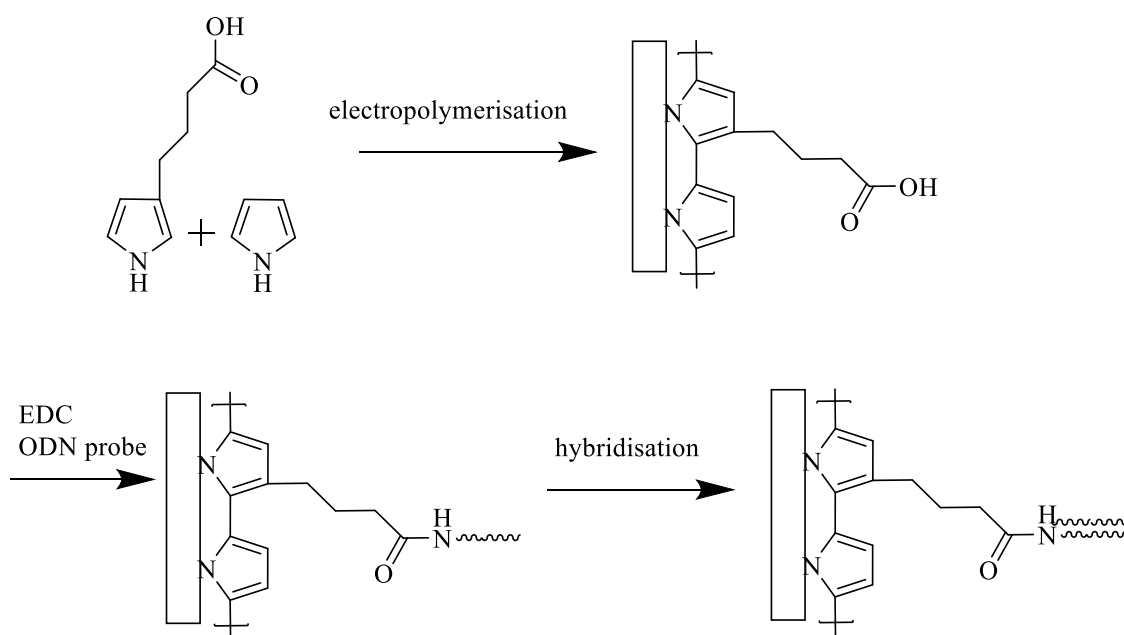


Figure 1.15. Conducting polymers such as polypyrrole can be surface functionalised with a bi-functional linker molecule such as glutaraldehyde (a) electrosynthesis of polypyrrole, (b) activation by glutaraldehyde, and (c) covalent binding of a DNA/enzyme. Redrawn from reference¹¹⁴

The immobilization of DNA has also been demonstrated post-polymerisation. For example, Peng *et al.*⁹⁷ reported the acid functionalized polypyrrole, poly(pyrrole-co-4-(3-pyrrolyl) butanoic acid) to enable covalent attachment of amino-functionalized oligonucleotides via amide coupling (Scheme 1.11).

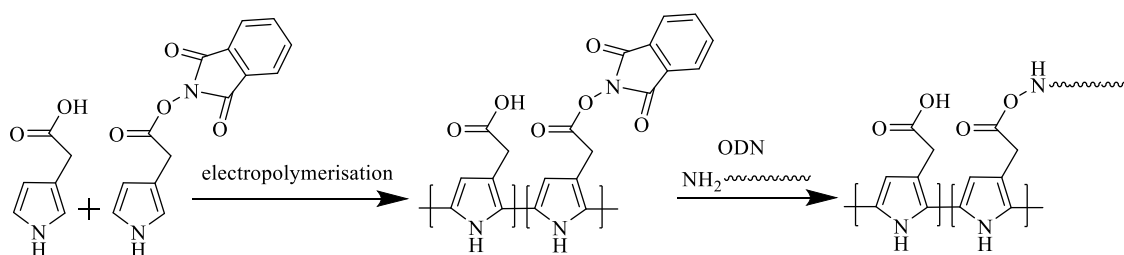


Scheme 1.11. Schematic of the preparation of an electrochemical DNA sensor based on a poly(pyrrole-co-4-(3-pyrrolyl) butanoic acid) conducting polymer. Redrawn from reference⁹⁷

Here, the precursor monomer, pyrrole-4-(3-pyrrolyl) butanoic acid, was synthesised by Friedel-Crafts acylation of pyrrole using succinic anhydride in the presence of AlCl_3 , followed by Clemmensen reduction and deprotection. After electro-co-polymerisation with pyrrole to form a co-polymer at the electrode surface, an amino-substituted oligonucleotide (ODN) probe was coupled to the polymer (using 1-ethyl-3-(3-dimethylaminopropyl)carbodiimide (EDC) as a coupling agent) in a

one-step procedure and tested for hybridization with complementary ODN segments.

Using a similar approach, Garnier *et. al.*⁹⁸ prepared a co-polymer film consisting of functionalized polypyrrole, poly(3-acetic acid pyrrole-co-3-*N*-hydroxyphthalimide pyrrole) (Scheme 1.12.). Here, pyrrole was first substituted at the 3-position with NHS and further electrochemically co-polymerized into a film of poly [3-NHS pyrrole] and 3-acetic acid pyrrole. The *N*-hydroxyphthalimide termination provides a good leaving group for amide coupling with amino substituted oligonucleotides.



Scheme 1.12. Electropolymerization to form a co-polymer film consisting of functionalized polypyrrole, poly(3-acetic acid pyrrole-co-3-*N*-hydroxyphthalimide pyrrole). Redrawn from reference⁹⁸

Significantly, the examples described above cite the necessity for probe attachment at the 3-position, using relatively long side chains and co-polymerisation with the principle monomer unit i.e. pyrrole in order to achieve a working DNA sensor by which hybridization of a complementary ODN can be detected electrochemically.

1.1.7 1-D Conducting Polymer | Nanostructures

1-D nanostructures of organic semi-conductors such as conducting polymers have attracted growing interest due to the potential advantages of combining these materials with low dimensionality.⁴⁹⁻⁵² As described earlier, CPs possess highly desirable characteristics such as an readily tunable band gap, high mechanical flexibility and greater biocompatibility than many inorganic materials.

Nanoscale materials by definition are when one dimension is between 1 – 100 nm (Figure 1.16) and provide an ideal platform for the marriage of electronics and biology to produce nano-scale sensors.

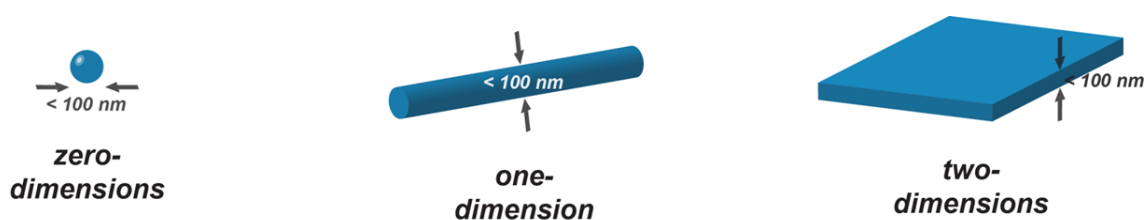


Figure 1.16. The three alternative dimensions of nano-scale materials¹¹⁵

When bulk polymer is used to construct a sensor, the response time is relatively long due to slow penetration of the target molecules into the conducting polymer, a process which is often accompanied by a hysteretic effect.¹¹⁶ In contrast, for a sensor constructed of conducting polymer nanostructures, the response time is expected to be significantly faster due to the smaller more porous structure. For example, a nano-fiber film of polyaniline has been shown to respond more rapidly than conventional polyaniline films.¹¹⁷ Conducting polymer nanostructures with large specific surface area and porous structure are therefore predicted to be excellent sensing materials.¹¹⁸ As such, the field of nano-scale electrochemical sensors has continued to mature with a large number of studies demonstrating the superior device performance of 1-D conducting polymer nanostructures over that of conventional bulk conducting polymers.^{40, 117, 119}

Despite recent progress, the search for simple and efficient synthetic methods to prepare conducting polymers on a large scale with deliberate control of morphologies and sizes is still a major challenge.

Template-directed growth is the most frequently used approach for preparing such 1-D nanostructured materials with several different methods shown to be effective.

Here, an external ‘membrane’ is used to direct the growth of the polymer into the desired architecture. A variety of alternative materials have been used to facilitate this process which can be broadly split into two categories; ‘hard’ or ‘soft’ templates.

The use of ‘hard’ templates was pioneered by Martin *et. al.*. This method entails using nanoscopic pores as a host membrane (Figure 1.17) and follows a rather simplistic 3-step approach, 1) fill the nanoscale pores of a membrane with a monomer, 2) polymerize the monomer inside the pores, and 3) remove the template in order to obtain the pure polymer. The diameter and morphology of the structures created are determined by the pores or channels of the template employed. In recent years, the most commonly used hard-templates have been an alumina film containing anodically etched pores. These membranes can be prepared from aluminium metal with pores arranged in a regular hexagonal lattice of relatively high densities. A range of pore sizes have been synthesized and some as small as 5 nm have been reported.¹²⁰⁻¹²²

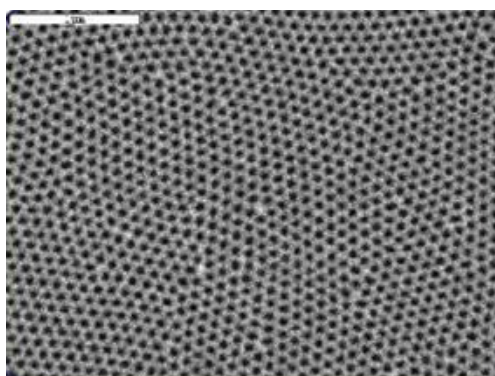


Figure 1.17. Scanning electron micrograph of the surface of a nanopore alumina template membrane prepared in the Martin lab

Using this approach, the Martin group in particular have synthesised a number of nanostructures of polyaniline (PAni), polypyrrole (PPy), poly(pyrrolepropylic acid)¹²³, polyaniline and polythiophene (PTh)¹²⁴ using anodized aluminium oxide (AAO) and track-etched polycarbonate (PC) membranes as templates. The only prerequisite for creating nanostructures of conducting polymers in this fashion is to be able to load the pores with the precursor materials.

This can vary in difficulty depending on the monomer of interest and the membrane used. The different methods used to load the pores include negative pressure, liquid

phase injection, vapour phase deposition or submerging the template into a solution of the monomer. The latter method allows good control over the length of the structure produced by controlling the amount of monomer passed through the pores. Polymerization of monomer-filled pores can be achieved by the addition of a chemical oxidizing agent or, more commonly, through electrochemical polymerization.

The soft-template method is another relatively simple, cheap and powerful approach for fabricating conducting polymer nanostructures. This method is based on selective control of non-covalent interactions, such as hydrogen bonds, van der Waals forces, π - π stacking, co-ordination and dispersive forces to direct the self-assembly of nanoscale polymeric materials. To date, colloidal particles, oligomers, soap bubbles and colloids have all been implemented as soft templates to prepare wire, ribbons and sphere like nanostructures.¹²⁵⁻¹²⁸ For example, PPy nanotubes (~94 nm in diameter and ~2 μ m in length) have been synthesized using sodium bis(2-ethylhexyl) sulfosuccinate (AOT) reverse cylindrical micelles as a soft-templates.¹²⁷

A common drawback to many 'hard' and 'soft' templates is the need to remove the template post polymerisation, which can vary greatly with difficulty depending on the template used. In some cases, template removal can be quite straightforward e.g. bulky dopant acids and certain types of surfactants can usually be washed away with an appropriate solvent. However, template removal can be quite cumbersome for other types of hard-templates such as anodic aluminum oxide (AAO) that typically requires harsh conditions for template dissolution.

Pre-existing 1-D nanostructures such as naturally occurring biopolymers can also serve as useful soft-templates or seeds in order to direct the growth of conducting polymer nanowires.¹²⁹ Conducting polymer nanostructures produced in this manner are often composite core-sheath materials consisting of a biopolymer core and a conducting polymer sheath, eliminating the need to remove the template post-synthesis. In contrast to templating in porous media, this approach yields hybrid supramolecular polymers,^{130, 131, 132, 133,134} a relatively recent class of material. Largely owing to their ability to self-assemble and form highly complex supramolecular structures, biological molecules provide an impressive arsenal for

use in the construction of supramolecular nanoscale structures with a number of strategies explored.

For example, Niu *et. al.*¹³⁵ developed a procedure for producing conducting polymer nanowires using the tobacco mosaic virus (TMV). Native TMV particles possess a tube like structure that measures 300 nm in length and 18 nm in diameter with a 4 nm cylindrical cavity along the central core. The negatively charged surface residues of TMV can ‘bind’ monomers such as pyrrole through electrostatic interactions or hydrogen-bonding. When pyrrole is mixed with TMV, the monomers accumulate on the surface of the TMV. Subsequent polymerization of the adsorbed monomers produces a thin layer of polymer on the surface of the TMV to produce a TMV core and a conducting polymer sheath. Moreover, the TMV particles can also be stitched together by a head-to-tail ordered assembly which allows for the production of conducting polymer nanowires that exceed the length of individual TMV particles.

In addition to TMV, a variety of other biological templates¹³⁶ have also been used to produce 1-D nanostructures, such as amino acid residues¹³⁷ and proteins.¹³⁸ Most applicable to this project is the use of DNA as a soft template to direct the formation of 1-D conducting polymer nanostructures.^{130-133, 139-146}

1.1.8 Deoxyribonucleic Acid (DNA)

DNA is a long anionic polymer consisting of subunits called nucleotides, which together form molecules called nucleic acids. DNA was first identified and isolated by Friedrich Miescher in 1871.¹⁴⁷ The double helix structure of DNA was deduced by James Watson and Francis Crick 1953.¹⁴⁸

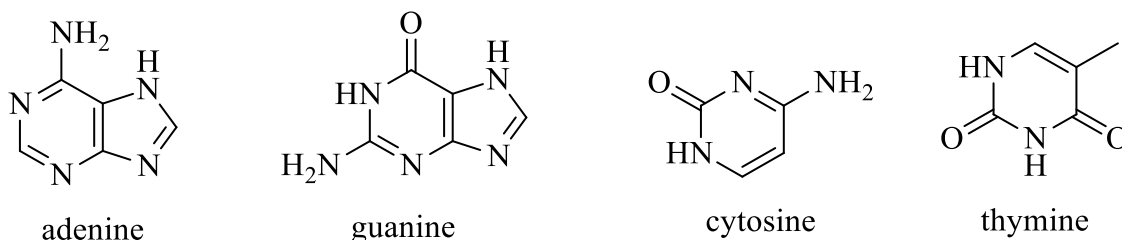


Figure 1.18. The four bases that make up DNA

Natural nucleobases can be one of four subunits adenine (A), cytosine (C), guanine (G) & thymine (T) (Figure 1.18). Double stranded DNA (dsDNA) comprises two long chains of nucleotides comprising the different nucleotide bases (e.g. AGTCATCGTAGCT) with a backbone of alternating phosphate and sugar residues joined by phosphodiester bonds (Figure 1.19). The nucleobases are classified into two types: the purines, A and G, being fused five- and six-membered heterocyclic compounds and the pyrimidines, the six-membered rings C and T.

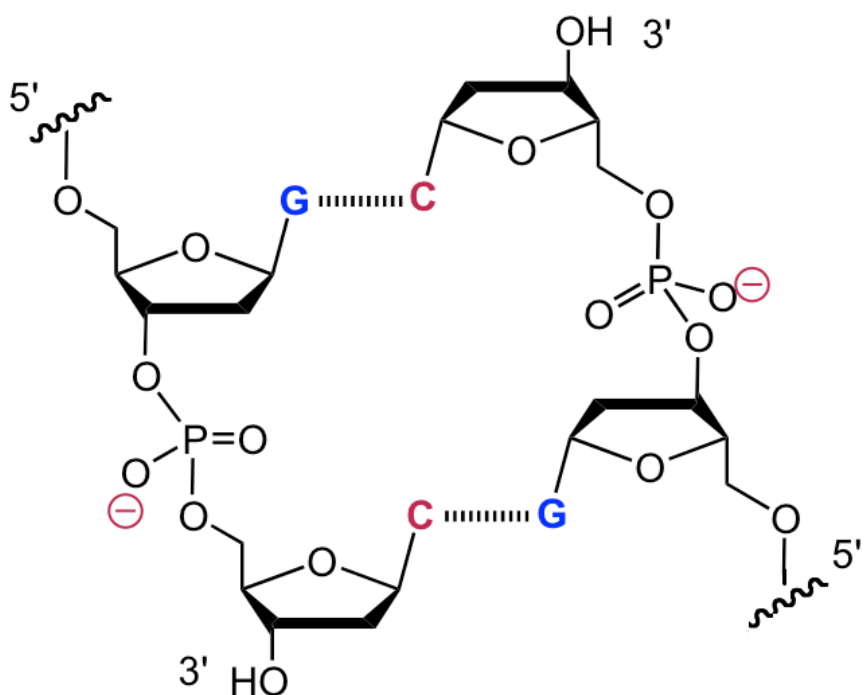


Figure 1.19. The chemical structure of dsDNA

In a DNA double helix, each type of nucleobase on one strand hydrogen bonds with just one type of nucleobase on the other strand. This is called complementary base pairing. Here, purines form hydrogen bonds to pyrimidines, with adenine preferentially bonding only to thymine via two hydrogen bonds and cytosine bonding to guanine by three hydrogen bonds. This double stranded antiparallel structure (dsDNA) is maintained largely by the intra-strand base stacking interactions, which are strongest for G,C sequences. The stability of the dsDNA form depends not only on the GC-content (% G,C base pairs) but also on sequence (since stacking is sequence specific) and also length (longer molecules are more stable). The stability can be measured in various ways; a common way is the 'melting temperature', which is the temperature at which 50% of the double stranded molecules are converted to single stranded molecules. Melting temperature is dependent on ionic strength and the concentration of DNA. As a result, it is both the percentage of GC base pairs and the overall length of a DNA double helix that determines the strength of the association between the two strands of DNA. Long DNA helices with a high GC-content have stronger-interacting strands, while short helices with high AT content have weaker-interacting strands. This reversible and specific interaction between complementary base pairs is critical for all the functions of DNA in living organisms.

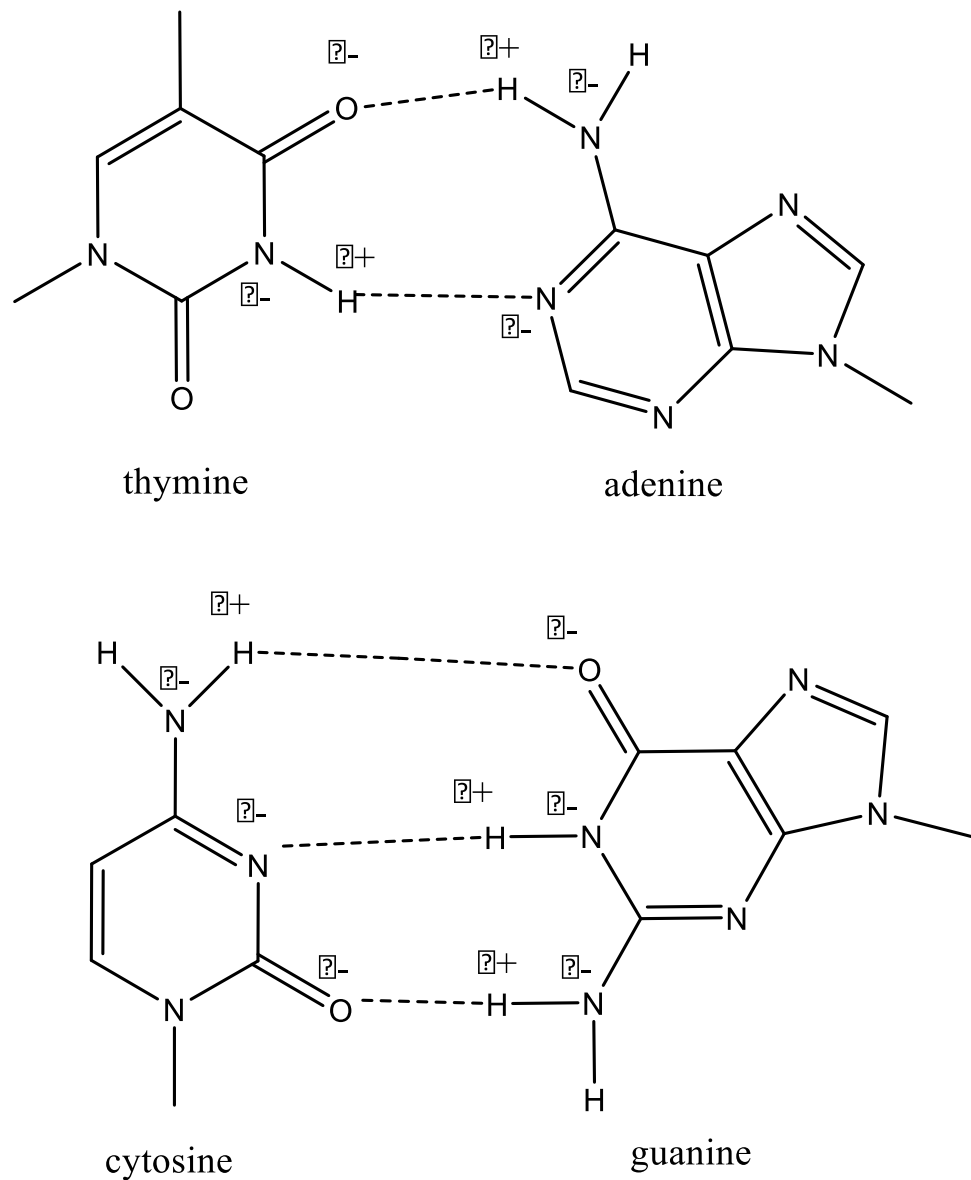


Figure 1.20. Hydrogen bonding between the base-pairs of DNA

The two strands of a DNA double helix run in opposite directions to each other (anti-parallel), one backbone being 3' (three prime) and the other 5' (five prime) with the 5' end having a terminal phosphate group and the 3' end a terminal hydroxyl group (Figure 1.19). It is the sequence of these four nucleobases along the backbone that encodes genetic information which specifies the sequence of the amino acids within proteins.

The structure of DNA of all species comprises two helical chains each coiled round the same axis, each with a pitch of 34 ångströms (3.4 nanometres) and a radius of 22 ångströms (2.2 nanometres).

As the strands are not symmetrically located with respect to each other, two grooves of unequal size can be found in the structure. One groove, the major groove, is 22 Å wide and the other, the minor groove, is 12 Å wide. The narrowness of the minor groove means that the edges of the bases are more accessible in the major groove. As a result, proteins like transcription factors that can bind to specific sequences in double-stranded DNA usually make contacts to the sides of the bases exposed in the major groove.

1.1.9 DNA as a Construction Tool

The unique molecular recognition properties, chemical stability, ease of manipulation and ‘wire-like’ structure of DNA (*ca.* 2 nm in diameter) allow it to be incorporated into nanostructured materials via covalent, non-covalent and coordinate binding methods which has resulted in an increasing number of DNA based nanomaterials presented in the literature.^{63, 139, 141, 144, 149-152} Pioneering research by Seeman and co-workers^{151, 153} to characterize four-arm branched DNA molecules, known as Holliday junctions, laid the foundation for construction of nanoscale structures from DNA, an area of research known as DNA nanotechnology.

The invention of scaffolded DNA origami was a milestone in the advancement of nucleic acid nanotechnology. Developed by Paul Rothemund¹⁵⁴, DNA origami is the use of DNA to construct 2-D nanoscale lattices by folding of singular stranded DNA. Two or more nonadjacent segments of the scaffold strand are brought together and held in place by hybridization to different portions of the same staple oligonucleotide in aggregate, enabling the creation of arbitrary shapes based solely on the staple sequences (Figure 1.21). The staples may be extended at their 5’ ends to make them addressable for patterning with a resolution of 6 nm on the assembled origami, imposed by the interstaple distance on the assembled DNA duplexes of the origami.

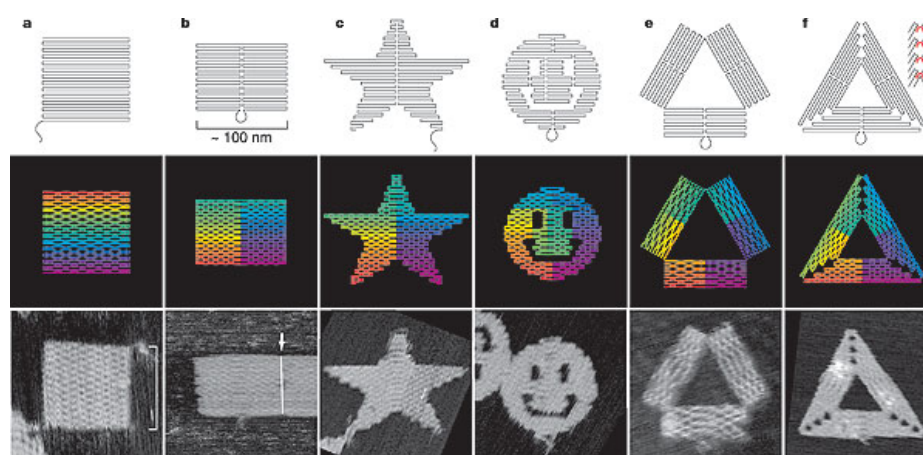


Figure 1.21. Top row, folding paths. a, square; b, rectangle; c, star; d, disk with three holes; e, triangle with rectangular domains; f, sharp triangle with trapezoidal domains and bridges between them (red lines in inset). Second row, diagrams showing the bend of helices at crossovers (where helices touch). Colour indicates the base-pair index along the folding path; red is the 1st base, purple the 7,000th. Bottom rows, AFM images. Scale bars: b, 1 μ m; c–f, 100 nm. Reproduced from reference¹⁵⁴

The DNA origami method has so far provided a scaffold for many applications including forming the track for molecular nanorobots,¹⁵⁵ constructing ordered molecular assembly lines¹⁵⁶ and assembling components for nanoelectronic circuits.¹⁵⁷

An alternative approach to using DNA as a construction tool is the scaffold approach which involves the covalent modification of nucleotides to enable specific binding of metals and organic molecules in the form of artificial ligand-like nucleobases.^{158, 159} By substituting the nucleobases of natural nucleotides with analogues capable of metal binding, DNA-like double helices containing precise numbers of metal ions have been prepared.

For example, work by Schuster *et. al.*¹⁶⁰ employed DNA as a scaffold to prepare polymer chains of polyaniline by modifying the cytosine nucleoside. In this work the exocyclic N4-amino group of cytidine was modified with a tethered aniline group (Figure 1.22). 22-mer oligonucleotide strands with central contiguous regions of 5-6 aniline-modified nucleosides formed duplexes that show UV absorption bands characteristic of oligoaniline after treatment with H₂O₂ and horseradish peroxidase.

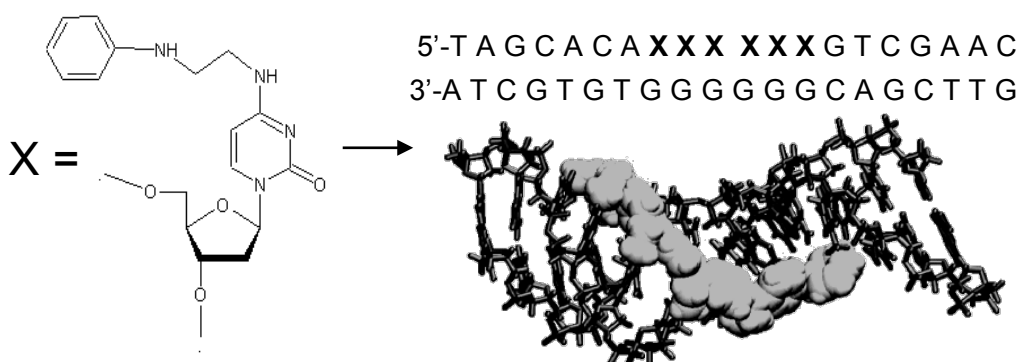
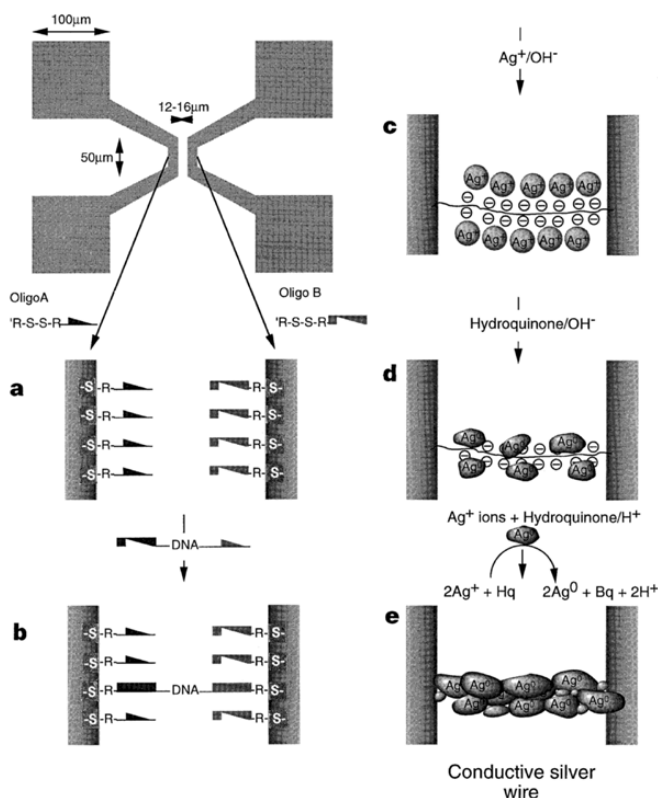


Figure 1.22. Aniline modified nucleoside, X, represented in a structural model of a hexameric aniline oligomer conjoined to a DNA strand. Adapted from reference¹⁶⁰

DNA has also been used to prepare semiconducting nanomaterials, including wires and particle arrays, through templating reactions. Here, DNA is used as a ‘soft’ template to direct the growth of the given material into the desired architecture.

The feasibility of this approach was first demonstrated by Braun *et. al.*¹³⁹ through the DNA-templated self-assembly of conductive silver nanowires. Here, a two-step

procedure was used which involved the hybridization of DNA molecules with surface bound nucleotides stretched between two gold electrodes (Scheme 1.13. a) and b)). Positively charged silver was absorbed onto the negatively charged DNA molecules and reduced to form silver coated DNA nanowire with the width of *ca.* 100 nm and length on the order of micrometer. Importantly, the current-voltage (*I-V*) characteristic of the silver nanowire showed the silver nanowire became conductive at a very high bias voltage.



Scheme. 1.13. A schematic diagram for a DNA-templated self-assembly of a conductive silver wire connecting two electrodes. Reproduced from reference¹³⁹

In the same work, this method was extended to the self-assembly of an ultrathin poly(p-phenylene vinylene), PPV (Figure 1.23), to afford a highly luminescent polymer wire along the DNA molecule. Significantly, this indicated the use of DNA templates for the assembly of electronically active materials was not limited to metallic species. Since, DNA-templating methods have been used to prepare nanowires from a number of materials such as silver¹⁶¹, copper^{162, 163}, palladium¹⁶⁴, cadmium¹⁴⁵, polyaniline¹⁵⁰, polypyrrole^{63, 66} and polyindole.⁶⁴

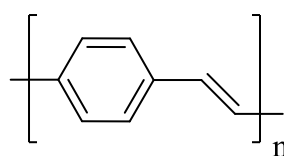
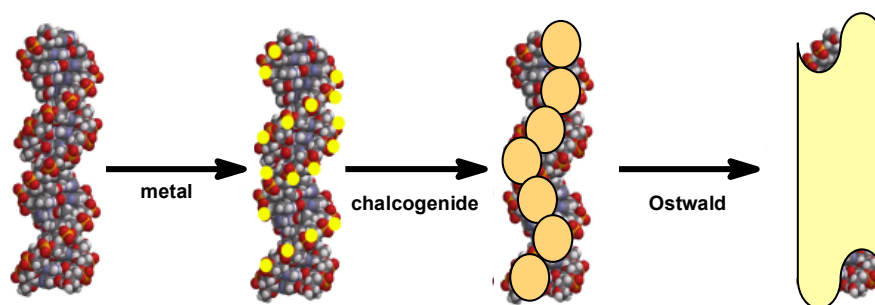


Figure 1.23. The chemical structure of poly(p-phenylene vinylene)

In case of binary materials, the intrinsic metal ion binding capabilities of DNA allows the template strands to be seeded with the metal component of the binary material (Scheme 1.14). Subsequent treatment of the metal-ion seeded DNA with the appropriate chalcogenide anion allows the desired material to nucleate and grow along the template. Different modes of growth can be achieved depending on whether stoichiometric quantities of metal are used (particles),¹⁶⁵ or if a small concentration of metal and chalcogenide is present in the bulk solution (wires).¹⁴⁵



Scheme 1.14. Generalized reaction sequence for the growth of nanoscale binary materials and conducting polymers at a DNA-temple. Reproduced from reference¹⁴⁵

The most widely studied binary compound with regards to DNA-templating reactions is CdS. Reports by Coffey¹⁶⁵ first illustrated the ability of DNA to stabilize nanocrystalline CdS. Calf thymus DNA was shown to give nanocrystals with a range of diameter 2.3-12 nm with a zinc blende lattice structure. At these dimensions the material is quantum-confined and exhibits the expected blue-shifted luminescence.

Houlton *et. al.*¹⁴⁵ demonstrated that by carefully optimizing the reaction conditions CdS can be prepared as either 1-D nanoparticle arrays or as continuous nanowires. In the former case, templating reactions were performed at immobilized λ -DNA. On mica, DNA molecules can be effectively anchored via interactions between the metal ions, the surface oxygen functionalities and the phosphate groups of the DNA. Stepwise templating reactions were performed on DNA-modified surfaces where,

after an initial addition of $\text{Cd}(\text{NO}_3)_2$, the substrates are treated with Na_2S solution. Nanoparticles are seen along individual DNA strands resulting in a beads-on-a-string appearance (Figure 1.24, a and b). The particles are highly mono-disperse, ($\sim 10\text{-}15$ nm in width and ~ 3 nm height as measured by AFM) and show notable registry along some of the DNA strands.

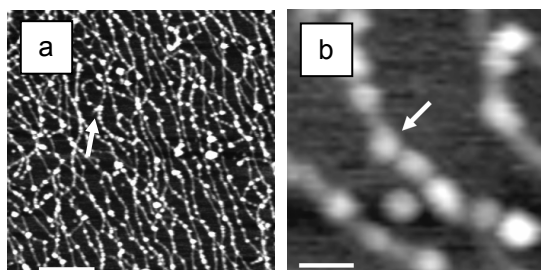


Figure 1.24. AFM height images of DNA-templated growth of CdS on mica. (a) Large area image of DNA-templated CdS nanoparticles; height scale is 3 nm, and the white bar indicates 200 nm. (b) enlargement of a region indicated by the white arrow in the left figure; height scale is 5 nm, (white bar indicates 25 nm). Reproduced from reference¹⁴⁵

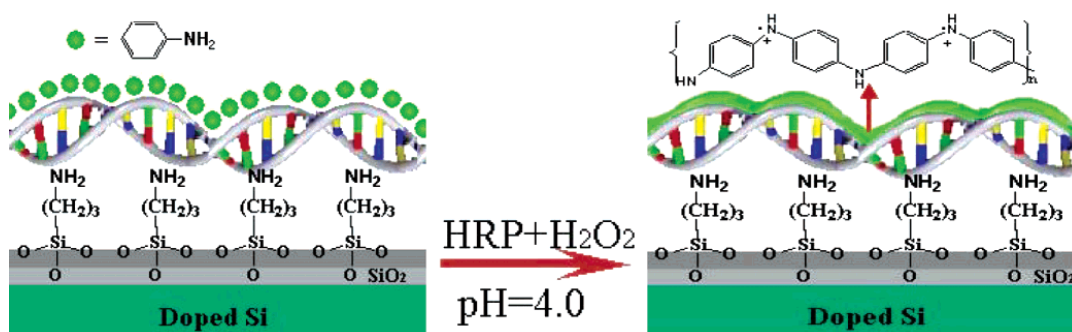
The formation of conducting polymers as nanowires on DNA templates has also been reported by several groups.^{129, 153, 161, 166, 167} As discussed earlier, CPs are interesting materials for new types of ultra-miniature electronic applications as they are flexible, their conductivity can be chemically controlled and they are readily functionalised. The resulting materials considered as supramolecular polymers, as they comprise of anionic DNA and cationic conducting polymer strands held together via supramolecular interactions.

The ability of DNA to act as a template for CP growth arises for a combination of two principal factors. Firstly, the high anionic charge from the negatively charged phosphodiester backbone and hydrogen bonding sites from the aromatic nucleobases. Secondly, the general class of CP derived from aromatic heterocyclic systems, such as pyrrole, are formed in their cationically charged, conducting, form through oxidative polymerization. Hence electrostatic attraction between the growing, cationic, CP and the anionic DNA template, allied with additional supramolecular interactions provide an effective means by which the CP growth is affected.

Horseradish peroxidase (HRP) was employed as an oxidant in the first DNA template guided synthesis of DNA-PAni complexes in 2001 by Samuleson *et. al.*^{168,}

¹⁶⁹ Here, polyaniline was synthesized enzymatically in order to preserve the integrity of the DNA template. Polyaniline is typically synthesized by oxidizing aniline monomer either electrochemically or chemically in a strong acid environment which precludes the use of delicate biological based materials as templates such as DNA.

The mild reaction conditions involved and the relatively inert nature of the HRP allowed Ma *et. al.*¹⁴² to apply a similar method in the fabrication of the first DNA-templated conducting polymer nanowires using aniline. Here, DNA was aligned onto a silicon substrate via ‘molecule combing’. Subsequent incubation and polymerisation (H_2O_2 , pH 4) with a protonated aniline solution formed the polyaniline nanowires (Scheme 1.15).



Scheme 1.15. Fabrication of a polyaniline nanowire immobilized on a Si surface with stretched double-stranded DNA as a guiding template. Reproduced from reference¹⁵⁰

Since the pK_a of aniline monomer is 4.6, a pH of 4 was sufficient to protonate the aniline monomers for the electrostatic interaction between the positively charged aniline monomers and the negatively charged phosphate groups in the DNA.

In 2004, Simmel *et. al.*¹⁷⁰ demonstrated the formation of polyaniline (PAni) nanowires in solution. Here, three different methods were employed to synthesize polyaniline on DNA. A mild oxidative method using horseradish peroxidase (HRP) and hydrogen peroxide, a photo-oxidation method using ruthenium tris(bipyridinium) ($\text{Ru}(\text{bpy})^{2+}$) complexes and a harsh method using ammonium persulfate (APS) as an oxidizing agent. The resulting DNA/PAni hybrids were stretched on mica/silicon substrates and characterized using atomic force microscopy (AFM). DC transport measurements performed on un-doped DNA/PAni wires yield conductance values of $40 \times 10^{-7} \text{ S cm}^{-1}$ which are consistent with those obtained for weakly conducting polyaniline films. This poor level of conductivity is thought to be due to the lack of continuity (a ‘beads-on-a-string’ morphology) of the

polyaniline wire, doping and the influence of contact resistance on between the gold electrodes and the hybrid material (Figure 1.25).

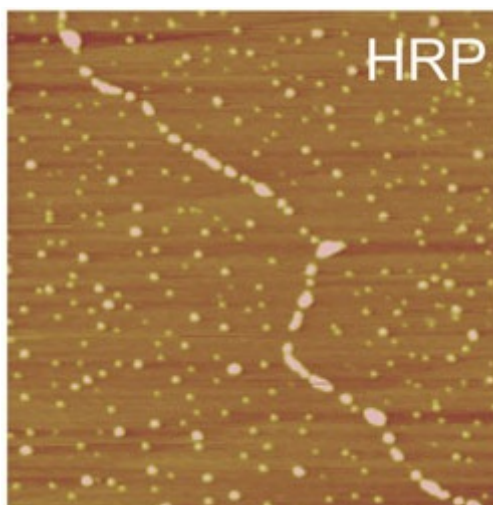
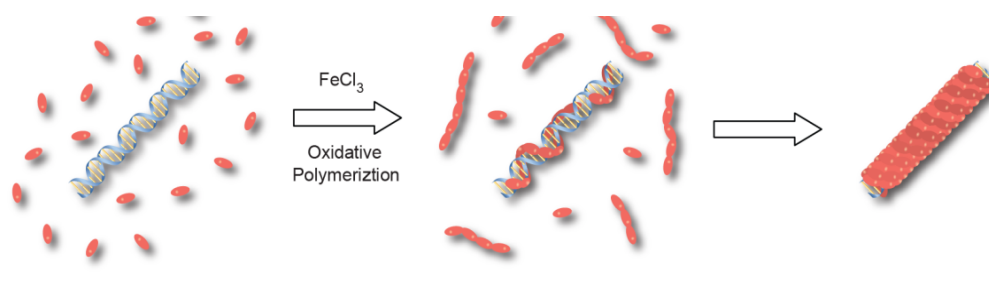


Figure 1.25. An AFM image of DNA/PAni synthesized by the HRP/H₂O₂ method in solution and stretched on a mica substrate. Reproduced from reference¹⁷⁰

The Houlton group have also demonstrated the utility of this solution based approach for the formation of hybrid supramolecular DNA/polymer nanowires from various monomers such as pyrrole,^{130, 131} (alkyne)thiophene-pyrrole,^{132, 133} and indole¹³⁴ using FeCl₃ as a chemical oxidant.

Similar to previous work described, initial studies focused on using DNA strands immobilized on solid support (mica) and showed the surface bound DNA to be an effective template for pyrrole, with clear evidence of preferential growth along individual biopolymer strands. However, the resulting DNA/PPy hybrid material exhibited a 'beads-on-a-string' morphology.

Templating reactions carried out in solution were shown to cause a significant effect on the morphology of the nanowires. Here, polymerization is initiated by oxidation of the monomer unit using Fe³⁺, forming cationic oligomers throughout the solution (Scheme 1.16). The oligomers bind to the DNA helix through both electrostatics and groove binding interactions which in turn seed polymer growth along the template.⁶³ Additionally, a significant advantage of pyrrole in this regard and in contrast to aniline, oxidation to initiate polymer formation can be performed at neutral pH, negating concerns of depurination.



Scheme 1.16. Cartoon scheme highlighting the templating effect of DNA in directing the growth of the polymers towards forming 1-D nano structures. The red species represent monomers and subsequent cationic oligomer formation in solution. Reproduced from reference¹⁷¹

Nanowires produced using this approach were of a continuous coverage and typically 5 nm in height compared to ~1.5 nm for bare DNA, as measured by AFM. Some height variation along individual nanowires was observed. However, compared to DNA-templated metallic wires, nanowires produced in this fashion are highly regular and smooth.

In some cases, confirmation that the resulting structures were in fact nanowires i.e. electrically conducting, was been made by fabricating 2-terminal nanowire devices. Successful alignment of DNA/PPy nanowires between two bespoke microelectrodes facilitated the construction of a two-terminal electrical device (Figure 1.26). Upon assessing the electrical conductance the electrically conducting nature of the DNA/PPy nanowires was confirmed and found to be $\sim 4 \text{ Scm}^{-1}$ at room temperature which is of the same order as the conductivity of bulk polypyrrole powder (1.7 Scm^{-1}) prepared in the same manner (FeCl_3).⁶³

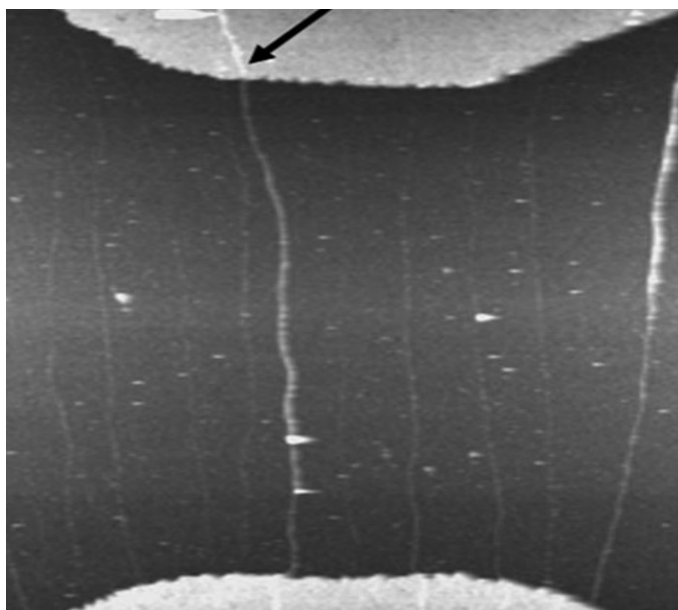


Figure 1.26. An AFM image of part of an actual two-terminal electrical measurement device indicates one DNA/PPy nanowire (black arrow) ~ 5 nm diameter, bridging the $7 \mu\text{m}$ gap. Reproduced from reference⁶³

An extension of this work has demonstrated that DNA-templated polypyrrole (DNA/PPy) nanowires spontaneously assemble to form rope-like structures (Figure 1.27).⁶⁶ Microscopy studies suggest that the assembly process involves braiding of individual strands (where strands are 1–3 nm nanowires) and is quite regular.

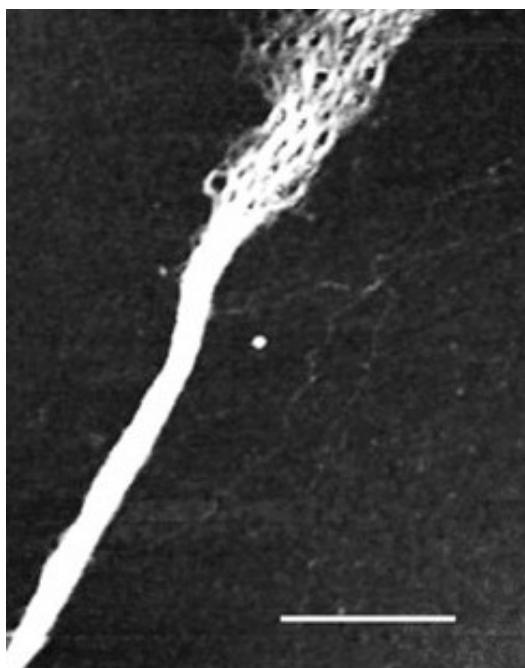


Figure 1.27. AFM image of DNA/PPy nanoropes after 48 hours on SiO_2/Si surface. Scale bar, 500 nm, height scale is 8 nm. Reproduced from reference⁶⁶

The driving force for this process is considered to be similar to the condensation of DNA by multivalent cations and cationic polymers. Two-terminal I - V measurements and conducting AFM (cAFM) demonstrated the nanoropes were conducting.

1.2 Project Overview

Lieber *et. al.* amongst others, has extensively demonstrated the use of silicon nanowire based FETs for label-free, electrical detection of a variety of species, such as antibodies, DNA and cancer markers.^{25, 172-175} Conducting polymers have also shown significant promise for such applications.^{99, 100}

Largely due to difficulties in nanowire fabrication, conducting polymers have typically found application as electrochemical sensors in their 2-D form, with many examples of polypyrrole based sensors in particular found in the literature.^{50, 93, 176, 177}

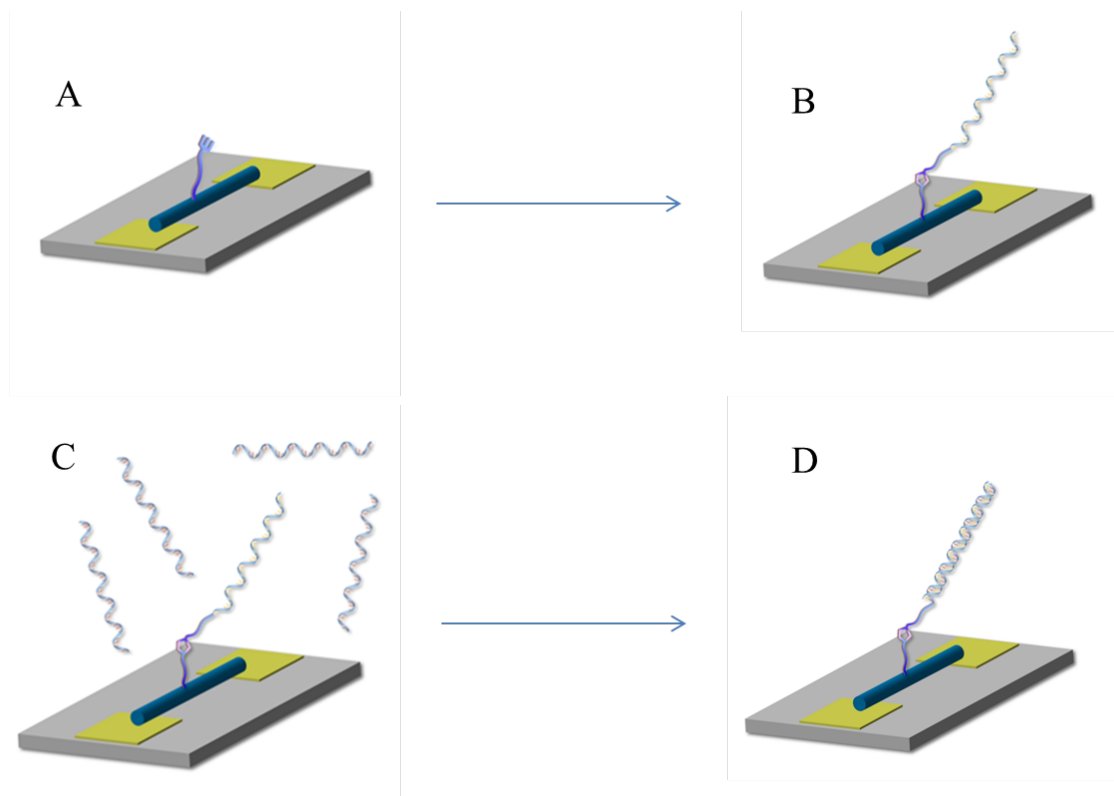
Nevertheless, polypyrrole based nanowires synthesized by electrochemical polymerization have been used to make a single-nanowire chemoresistive sensor for CA 125 biomarker detection and rapid detection of human serum albumin.^{178 123} While direct formation of biologically functionalized polypyrrole has been demonstrated through electropolymerization of pyrrole and avidin- or streptavidin-conjugated ZnSe/CdSe quantum dots with sensitivity to biotin–DNA reported to be as low as 1 nM.¹⁷⁹ Polyaniline nanowire-modified electrodes have also been used in the detection of DNA hybridization events.¹⁸⁰

The formation of nanowires using a variety of materials is now becoming relatively common; the functionalisation of these types of materials beyond their conductive nature is not. In order to realize the huge potential of conducting polymers in biosensing applications, it is necessary to impart the desired functionality and specificity to these materials. As discussed, one approach is the introduction of functional groups directly into the monomer units prior to polymerisation to facilitate further chemistries after the formation of the desired architecture.

Moreover, developing reliable and scalable strategies for the controlled synthesis of 1-D conductive polymer nanostructures in order to further unlock the potential of further miniaturization is the principal challenge facing the next generation of nano device development. Promising approaches have been advanced that exploit the properties of certain biomolecules. DNA-templating is a proven reproducible and facile route to such architectures and has been shown to be compatible with a number of conducting polymers. Furthermore, this approach also lends itself well to

the synthesis of highly desired single nanowire arrays for application in multiplexed detection presently being employed using silicon nanowires. As such, to achieve single nanowire-based device configuration, very precise control of the alignment, placement and number of nanostructures between two metal contacts is highly desirable.

In an effort to further explore these challenges and the application of conducting polymer nanowires in biological sensing, this project investigates the DNA-templating of functional pyrrole and thiophene oligomers to prepare supramolecular polymer nanowires for potential application in biological sensing. The main goal of this project was to construct such a system consisting of a DNA-templated conducting polymer nanowire aligned between two gold micro-electrodes, the surface of which is functional (Scheme 1.17, A). The functionality of the nanowire facilitates the binding of specific capture probes, in this case ssDNA (Scheme 1.17, B, the probe). As the target molecules (probe complement) diffuse through the solution (Scheme 1.17, C) they bind to their complement close to the surface (Scheme 1.17, D). The electrostatic charge of DNA results in a columbic interaction effecting a change in conductivity of the nanowire. These binding events are recorded as an analogue electrical measurement that may be digitized and processed accordingly to give an immediate diagnosis according to the sequence of the probe attached.



Scheme 1.17. An illustration representing the key stages towards device construction within this project. A) functional conducting polymer nanowire alignment between two gold micro-electrodes; B) modified ssDNA probe attachment; C) Introduction of the probe complement; D) detection of a binding event through a measured change in conductance¹¹⁵

1.3 Thesis Outline

The structure of this thesis is as follows; Chapter 1, the introduction, presents the motivation and background for the work presented. Chapter 2 outlines the main techniques used in this research project while Chapter 3 describes the motivation, synthesis and polymerisation of the functionalised monomer units for application in DNA-based nanowire formation. Chapter 4 discusses the suitability of each system for DNA-templating through comparison of FTIR spectra of bulk polymeric and DNA-templated materials. Also presented in this chapter is Si/SiO₂ surface chemistry studies and the characterisation of DNA templated polymer nanowires by atomic force microscopy (AFM). Chapter 5 describes the electrical properties of DNA polymer nanowires of each system using scanned conductance microscopy (SCM) and two-terminal I - V measurements. Chapter 6 presents bulk conductivity studies of the relevant alkylated and none alkylated monomer units in addition to co-polymers with pyrrole. The seventh and the final results chapter of this thesis is concerned with DNA probe attachment to each DNA/polymer system via ‘click’ chemistry. Studies using UV-Vis, conductive AFM and fluorescence microscopy are also presented. Chapter 8 summarises the findings of this project, presents the conclusions and suggests future work.

1.4 References

1. F. S. Ligler and J. S. Erickson, *Nature*, 2006, **440**, 159-160.
2. L. A. P. Mickey Urdea, Stuart S. Olmsted, Maria Y. Giovanni, Peter Kaspar, Andrew Shepherd, Penny Wilson, Carol A. Dahl, Steven Buchsbaum, Gerry Moeller and Deborah C. Hay Burgess, *Nature*, 2006, **444**, 73-79.
3. J. Kling, *Nature Biotechnology*, 2006, **24**, 891-893.
4. M. Cretich, F. Damin, G. Pirri and M. Chiari, *Biomolecular Engineering*, 2006, **23**, 77-88.
5. D. Janasek, J. Franzke and A. Manz, *Nature*, 2006, **442**, 374-380.
6. F.-G. Bănică, in *Chemical Sensors and Biosensors*, John Wiley & Sons, Ltd, 2012, pp. 1-20.
7. F.-G. Bănică, in *Chemical Sensors and Biosensors*, John Wiley & Sons, Ltd, 2012, pp. 28-49.
8. F.-G. Bănică, in *Chemical Sensors and Biosensors*, John Wiley & Sons, Ltd, 2012, pp. 118-134.
9. D. H. Williams, Fleming, Ian, *Spectroscopic Methods in Organic Chemistry*, 5th edn., McGraw-Hall, 1995.
10. R. Beer, *Remote Sensing by Fourier Transform Spectroscopy*, Wiley-Interscience, London, 1992.
11. W. J. Benett, J. B. Richards, P. Stratton, D. R. Hadley, B. H. Bodtker, S. L. Nasarabadi, F. P. Milanovich, J. R. P. Mariella, R. P. Koopman and P. Belgrader, *Proceedings of SPIE: Biochemical and Biomolecular Sensing*, 2000, 55-63.
12. C. J. Bruckner-Lea, J. N. C. Anheier, D. A. Holman, T. Tsukuda, M. T. Kingsley, F. J. Brockman, J. M. Price, J. W. Grate and D. P. Chandler, *Proceedings of SPIE: Biochemical and Biomolecular Sensing*, 2000, 74-81.
13. M. J. Madou and R. Cubicciotti, *Proceedings of the IEEE*, 2003, **91**, 830-838.

14. S. S. Iqbal, M. W. Mayo, J. G. Bruno, B. V. Bronk, C. A. Batt and J. P. Chambers, *Biosensors and Bioelectronics*, 2000, **15**, 549-578.
15. J. V. Frangioni, *Nature Biotechnology*, 2006, **24**, 909-913.
16. F. Progatzy, M. J. Dallman and C. Lo Celso, *Interface Focus*, 2013, **3**.
17. X. Duan, Y. Li, N. K. Rajan, D. A. Routenberg, Y. Modis and M. A. Reed, *Nature Nanotechnology*, 2012, **7**, 401-407.
18. G.-J. Zhang and Y. Ning, *Analytica Chimica Acta*, 2012, **749**, 1-15.
19. R. L. Rich and D. G. Myszka, *Drug Discovery Today: Technologies*, 2004, **1**, 301-308.
20. N. Ramachandran, D. N. Larson, P. R. H. Stark, E. Hainsworth and J. LaBaer, *FEBS Journal*, 2005, **272**, 5412-5425.
21. M. M.-C. Cheng, G. Cuda, Y. L. Bunimovich, M. Gaspari, J. R. Heath, H. D. Hill, C. A. Mirkin, A. J. Nijdam, R. Terracciano, T. Thundat and M. Ferrari, *Current Opinion in Chemical Biology*, 2006, **10**, 11-19.
22. D. Wei, M. J. A. Bailey, P. Andrew and T. Ryhanen, *Lab on a Chip*, 2009, **9**, 2123-2131.
23. T. G. Drummond, M. G. Hill and J. K. Barton, *Nature Biotechnology*, 2003, **21**, 1192-1199.
24. A. K. Wanekaya, *Electroanalysis*, 2006, **18**, 533-550.
25. Y. Cui, Q. Wei, H. Park and C. M. Lieber, *Science*, 2001, **293**, 1289-1292.
26. M. Gerard, A. Chaubey and B. D. Malhotra, *Biosensors and Bioelectronics*, 2002, **17**, 345-359.
27. U. Yogeswaran and S.-M. Chen, *Sensors*, 2008, **8**, 290-313.
28. M. Situmorang, D. Brynn Hibbert, J. Justin Gooding and D. Barnett, *Analyst*, 1999, **124**, 1775-1779.

29. N. K. Rajan, K. Brower, X. Duan and M. A. Reed, *Applied Physics Letters*, 2014, **104**, -.
30. E. Petryayeva and U. J. Krull, *Analytica Chimica Acta*, 2011, **706**, 8-24.
31. C. Boozer, G. Kim, S. Cong, H. Guan and T. Londergan, *Current Opinion in Biotechnology*, 2006, **17**, 400-405.
32. K. M. Hansen and T. Thundat, *Methods*, 2005, **37**, 57-64.
33. T. Konry, A. Novoa, S. Cosnier and R. S. Marks, *Analytical chemistry*, 2003, **75**, 2633-2639.
34. D. V. Lim, *Proceedings of the IEEE*, 2003, **91**, 902-907.
35. H. Ju, X. Zhang and J. Wang, Springer New York, 2011, pp. 535-567.
36. H. Ju, *SCIENCE CHINA Chemistry*, 2011, **54**, 1202-1217.
37. J. Janata and M. Josowicz, *Nature Materials*, 2003, **2**, 19-24.
38. F. Patolsky, *Analytical chemistry*, 2006, **78**, 4260-4269.
39. U. Lange, N. V. Roznyatovskaya and V. M. Mirsky, *Analytica Chimica Acta*, 2008, **614**, 1-26.
40. H. Liu, J. Kameoka, D. A. Czaplewski and H. G. Craighead, *Nano Letters*, 2004, **4**, 671-675.
41. I. Heller, A. M. Janssens, J. Mannik, E. D. Minot, S. G. Lemay and C. Dekker, *Nano Letters*, 2007, **8**, 591-595.
42. J.-F. Lutz and H. G. Börner, *Progress in Polymer Science*, 2008, **33**, 1-39.
43. P. R. Nair and M. A. Alam, *Electron Devices, IEEE Transactions on*, 2007, **54**, 3400-3408.
44. P. R. Nair and M. A. Alam, *Applied Physics Letters*, 2006, **88**, 233120.
45. L. Xia, Z. Wei and M. Wan, *Journal of Colloid and Interface Science*, 2010, **341**, 1-11.

46. K.-I. Chen, B.-R. Li and Y.-T. Chen, *Nano Today*, 2011, **6**, 131-154.
47. R. M. Penner, *Annual Review of Analytical Chemistry*, 2012, **5**, 461-485.
48. U. Hashim, S. F. A. Rahman and M. E. A. Shohini, *Design and Fabrication of Nanowire-Based Conductance Biosensor Using Spacer Patterning Techniq*, 2010.
49. Y. Xia, P. Yang, Y. Sun, Y. Wu, B. Mayers, B. Gates, T. Yin, F. Kim and H. Yan, *Advanced Materials*, 2003, **15**, 353-387.
50. H. D. Tran, D. Li and R. B. Kaner, *Advanced Materials*, 2009, **21**, 1487-1499.
51. M. Hasegawa and M. Iyoda, *Chemical Society Reviews*, 2010, **39**, 2420-2427.
52. D. Eder, *Chemical Reviews*, 2010, **110**, 1348-1385.
53. R. Kiebooms, R. Menon and K. Lee, in *Handbook of Advanced Electronic and Photonic Materials and Devices*, eds. N. Hari Singh, M.Sc and M. S. P. D. Ph.D.A2 - Hari Singh Nalwa, Academic Press, Burlington, 2001, pp. 1-102.
54. T. A. Skotheim, R. L. Elsenbaumer and J. R. Reynolds, eds., , *Handbook of Conducting Polymers*, New York, 1998.
55. H. Akamatu, H. Inokuchi and Y. Matsunaga, *Nature*, 1954, **173**, 168-169.
56. W. A. Little, *Physical Review*, 1964, **134**, A1416-A1424.
57. J. Tsukamoto, *Advances in Physics*, 1992, **41**, 509-546.
58. Z.-X. L. N. Basescu, D. Moses, A. J. Heeger, H. Naarmann & N. Theophilou, *Nature*, 1987, **327**, 403-405.
59. C. K. Chiang, C. R. Fincher, Jr., Y. W. Park, A. J. Heeger, H. Shirakawa, E. J. Louis, S. C. Gau and A. G. MacDiarmid, *Physical Review Letters*, 1977, **39**, 1098-1101.
60. H. Shirakawa, E. J. Louis, A. G. MacDiarmid, C. K. Chiang and A. J. Heeger, *Journal of the Chemical Society, Chemical Communications*, 1977, **0**, 578-580.
61. W. B. Yoshikuko Okamoto, Reinhold, *Organic Semiconductors*, 1964.
62. L. Dai, *Journal of Macromolecular Science, Part C*, 1999, **39**, 273-387.

63. L. Dong, T. Hollis, S. Fishwick, B. A. Connolly, N. G. Wright, B. R. Horrocks and A. Houlton, *Chemistry – A European Journal*, 2007, **13**, 822-828.
64. R. Hassanien, M. Al-Hinai, S. A. Farha Al-Said, R. Little, L. Šiller, N. G. Wright, A. Houlton and B. R. Horrocks, *ACS Nano*, 2010, **4**, 2149-2159.
65. F. S. Kim, G. Ren and S. A. Jenekhe, *Chemistry of Materials*, 2010, **23**, 682-732.
66. S. Pruneanu, S. A. F. Al-Said, L. Dong, T. A. Hollis, M. A. Galindo, N. G. Wright, A. Houlton and B. R. Horrocks, *Advanced Functional Materials*, 2008, **18**, 2444-2454.
67. E. Rodlovskaia, N. Frolova, E. Savin and V. Nedel'kin, *Polymer Science Series C*, 2006, **48**, 58-84.
68. J. Roncali, *Chemical Reviews*, 1992, **92**, 711-738.
69. C. Li, H. Bai and G. Shi, *ChemInform*, 2009, **40**, no-no.
70. R. Ansari, *E-Journal of Chemistry*, 2006, **3**, 186-201.
71. S. Gronowitz, *The Chemistry of Heterocyclic Compounds, Thiophene and Its Derivatives*, Wiley, 2009.
72. R. McNeill, R. Siudak, J. Wardlaw and D. Weiss, *Australian Journal of Chemistry*, 1963, **16**, 1056-1075.
73. B. Bolto and D. Weiss, *Australian Journal of Chemistry*, 1963, **16**, 1076-1089.
74. B. Bolto, R. McNeill and D. Weiss, *Australian Journal of Chemistry*, 1963, **16**, 1090-1103.
75. P. M. George, D. A. LaVan, J. A. Burdick, C. Y. Chen, E. Liang and R. Langer, *Advanced Materials*, 2006, **18**, 577-581.
76. J. Serra Moreno, S. Panero, M. Artico and P. Filippini, *Bioelectrochemistry*, 2008, **72**, 3-9.
77. K. J. Wynne and G. B. Street, *Macromolecules*, 1985, **18**, 2361-2368.

78. S. Meng, M. Rouabhia, G. Shi and Z. Zhang, *Journal of Biomedical Materials Research Part A*, 2008, **87A**, 332-344.
79. P. Pfluger, M. Krounbi, G. B. Street and G. Weiser, *The Journal of Chemical Physics*, 1983, **78**, 3212-3218.
80. J. H. Collier, J. P. Camp, T. W. Hudson and C. E. Schmidt, *Journal of Biomedical Materials Research*, 2000, **50**, 574-584.
81. S. A. Jenekhe, *Nature*, 1986, **322**, 345-347.
82. K. K. Kanazawa, A. F. Diaz, M. T. Krounbi and G. B. Street, *Synthetic Metals*, 1981, **4**, 119-130.
83. C. C. Bof Bufon, T. Heinzl, P. Espindola and J. Heinze, *The Journal of Physical Chemistry B*, 2009, **114**, 714-718.
84. T. C. C. G.B. Street, R.H. Geiss, V. Y. Lee, A. Nazzal, P. Pfluger and J.C. Scott, *Journal De Physique*, 1983, **6**, 599.
85. J. A. Walker, L. F. Warren and E. F. Witucki, *Journal of Polymer Science Part A: Polymer Chemistry*, 1988, **26**, 1285-1294.
86. R. Qian, J. Qiu and B. Yan, *Synthetic Metals*, 1986, **14**, 81-87.
87. P. Audebert and G. Bidan, *Synthetic Metals*, 1986, **14**, 71-80.
88. J. L. Brédas, J. C. Scott, K. Yakushi and G. B. Street, *Physical Review B*, 1984, **30**, 1023-1025.
89. S. Fabiano, Z. Chen, S. Vahedi, A. Facchetti, B. Pignataro and M. A. Loi, *Journal of Materials Chemistry*, 2011, **21**, 5891-5896.
90. S. Kirchmeyer and K. Reuter, *Journal of Materials Chemistry*, 2005, **15**, 2077-2088.
91. H. Sasabe and J. Kido, *Chemistry of Materials*, 2010, **23**, 621-630.
92. T. K. Tam, M. Pita, M. Motornov, I. Tokarev, S. Minko and E. Katz, *Advanced Materials*, 2010, **22**, 1863-1866.

93. H. Peng, L. Zhang, C. Soeller and J. Travas-Sejdic, *Biomaterials*, 2009, **30**, 2132-2148.
94. A. Mulchandani and N. V. Myung, *Current Opinion in Biotechnology*, 2011, **22**, 502-508.
95. N. G. J. Clayden, S. Warren *Organic Chemistry*, 2nd edn., Oxford University Press, 2012.
96. J. Hegewald, L. Jakisch and J. Pionteck, *Synthetic Metals*, 2009, **159**, 103-112.
97. H. Peng, C. Soeller, N. Vigar, P. A. Kilmartin, M. B. Cannell, G. A. Bowmaker, R. P. Cooney and J. Travas-Sejdic, *Biosensors and Bioelectronics*, 2005, **20**, 1821-1828.
98. F. Garnier, H. Korri-Youssoufi, P. Srivastava, B. Mandrand and T. Delair, *Synthetic Metals*, 1999, **100**, 89-94.
99. C. M. Hangarter, M. Bangar, A. Mulchandani and N. V. Myung, *Journal of Materials Chemistry*, 2010, **20**, 3131-3140.
100. A. K. Wanekaya, W. Chen, N. V. Myung and A. Mulchandani, *Electroanalysis*, 2006, **18**, 533-550.
101. L. A. Thompson, J. Kowalik, M. Josowicz and J. Janata, *Journal of the American Chemical Society*, 2002, **125**, 324-325.
102. M. Umana and J. Waller, *Analytical chemistry*, 1986, **58**, 2979-2983.
103. D. d. C. Moléculaire, Access Date: 05/10/2013, http://dcm.ujf-grenoble.fr/site/site.php?id_rubrique=175&id_article=287&type=spip&langue=fr
104. J. Wang, D. Leech, M. Ozsoz, S. Martinez and M. R. Smyth, *Analytica Chimica Acta*, 1991, **245**, 139-143.
105. J. Wang, M. Jiang, A. Fortes and B. Mukherjee, *Analytica Chimica Acta*, 1999, **402**, 7-12.
106. *International Journal of Electrochemistry*, 2012, **2012**.
107. N. M. Green, *Biochemical Journal*, 1963, **89**, 599-590.

108. A. Dupont-Filliard, A. Roget, T. Livache and M. Billon, *Analytica Chimica Acta*, 2001, **449**, 45-50.
109. T. Livache, A. Roget, E. Dejean, C. Barthet, G. Bidan and R. Teoule, *Nucleic acids research*, 1994, **22**, 2915-2921.
110. N. Lassalle, A. Roget, T. Livache, P. Mailley and E. Vieil, *Talanta*, 2001, **55**, 993-1004.
111. T. Livache, B. Fouque, A. Roget, J. Marchand, G. Bidan, R. Téoule and G. Mathis, *Analytical Biochemistry*, 1998, **255**, 188-194.
112. N. Gupta Munishwar, in *Biocatalyst Design for Stability and Specificity*, American Chemical Society, 1993, vol. 516, pp. 307-324.
113. V. K. Gade, D. J. Shirale, P. D. Gaikwad, P. A. Savale, K. P. Kakde, H. J. Kharat and M. D. Shirsat, *Reactive and Functional Polymers*, 2006, **66**, 1420-1426.
114. N. A. Karaseva and T. N. Ermolaeva, *Talanta*, 2012, **93**, 44-48.
115. Image drawn by Dr. J. D. Watson, 2010.
116. W. Zheng, Y. Min, A. G. MacDiarmid, M. Angelopoulos, Y. H. Liao and A. J. Epstein, *Synthetic Metals*, 1997, **84**, 63-64.
117. J. Huang, S. Virji, B. H. Weiller and R. B. Kaner, *Journal of the American Chemical Society*, 2002, **125**, 314-315.
118. K. H. An, S. Y. Jeong, H. R. Hwang and Y. H. Lee, *Advanced Materials*, 2004, **16**, 1005-1009.
119. X. Zhang, W. J. Goux and S. K. Manohar, *Journal of the American Chemical Society*, 2004, **126**, 4502-4503.
120. Y. Berdichevsky and Y.-H. Lo, *Advanced Materials.*, 2006, **18**, 122-125.
121. M. G. Han and S. H. Foulger, *Chemical Communications*, 2005, 3092-3094.
122. A. Drury, S. Chaure, M. Kröll, V. Nicolosi, N. Chaure and W. J. Blau, *Chemistry of Materials.*, 2007, **19**, 4252-4258.

123. S. Tolani, M. Craig, R. DeLong, K. Ghosh and A. Wanekaya, *Analytical and Bioanalytical Chemistry*, 2009, **393**, 1225-1231.
124. C. R. Martin, R. Parthasarathy and V. Menon, *Synthetic Metals*, 1993, **55**, 1165-1170.
125. J. Jang and H. Yoon, *Chemical Communications*, 2003, 720-721.
126. X. Zhang, J. Zhang, Z. Liu and C. Robinson, *Chemical Communications*, 2004, 1852-1853.
127. J. Jang and H. Yoon, *Langmuir*, 2005, **21**, 11484-11489.
128. X. Zhang, J. Zhang, W. Song and Z. Liu, *J. Phys. Chem. B*, 2006, **110**, 1158-1165.
129. Y. Eichen, E. Braun, U. Sivan and G. Ben-Yoseph, *Acta Polymerica*, 1998, **49**, 663-670.
130. L. Dong, T. Hollis, S. Fishwick, B. A. Connolly, N. G. Wright, B. R. Horrocks and A. Houlton, *Chemistry a European Journal*, 2007, **13**, 822-828.
131. S. Pruneanu, S. A. F. Al-Said, L. Dong, T. A. Hollis, M. A. Galindo, N. G. Wright, A. Houlton and B. R. Horrocks, *Advanced Functional Materials*, 2008, **18**, 1-12.
132. S. A. F. Al-Said, R. Hassanien, J. Hannant, M. A. Galindo, S. Pruneanu, A. R. Pike, A. Houlton and B. R. Horrocks, *Electrochemistry Communications*, 2009, **11**, 550-553.
133. J. Hannant, J. H. Hedley, J. Pate, A. Walli, S. A. Farha Al-Said, M. A. Galindo, B. A. Connolly, B. R. Horrocks, A. Houlton and A. R. Pike, *Chemical Communications*, 2010, **46**, 5870-5872.
134. R. Hassanien, M. Al-Hinai, S. A. Farha Al-Said, R. Little, L. Siller, N. G. Wright, A. Houlton and B. R. Horrocks, *ACS Nano*, 2010, **4**, 2149-2159.
135. J. Rong, F. Oberbeck, X. Wang, X. Li, J. Oxsher, Z. Niu and Q. Wang, *Journal of Materials Chemistry*, 2009, **19**, 2841-2845.

136. S. Sotiropoulou, Y. Sierra-Sastre, S. S. Mark and C. A. Batt, *Chemistry of Materials*, 2008, **20**, 821-834.
137. S. Zhang, *Nature Biotechnology*, 2003, **21**, 1171-1178.
138. S. Behrens, J. Wu, W. Habicht and E. Unger, *Chemistry of Materials*, 2004, **16**, 3085-3090.
139. E. Braun, Y. Eichen, U. Sivan and G. Ben-Yoseph, *Nature*, 1998, **391**, 775-778.
140. J. Richter, M. Mertig, W. Pompe, I. Monch and H. K. Schackert, *Applied Physics Letters*, 2001, **78**, 536-538.
141. K. Keren, M. Krueger, R. Gilad, G. Ben-Yoseph, U. Sivan and E. Braun, *Science*, 2002, **297**, 72-75.
142. Y. Ma, J. Zhang, G. Zhang and H. He, *Journal of the American Chemical Society*, 2004, **126**, 7097-7101.
143. H. A. Becerril, R. M. Stoltenberg, D. R. Wheeler, R. C. Davis, J. N. Harb and A. T. Woolley, *Journal of the American Chemical Society*, 2005, **127**, 2828-2829.
144. H. A. Becerril, R. M. Stoltenberg, D. R. Wheeler, R. C. Davis, J. N. Harb and A. T. Woolley, *Journal of the American Chemical Society*, 2005, **127**, 2828-2829.
145. L. Dong, T. Hollis, B. A. Connolly, N. G. Wright, B. R. Horrocks and A. Houlton, *Advanced Materials*, 2007, **19**, 1748-1751.
146. S. M. D. Watson, N. G. Wright, B. R. Horrocks and A. Houlton, *Langmuir*, 2009, **26**, 2068-2075.
147. R. Dahm, *Developmental Biology*, 2005, **278**, 274-288.
148. J. D. Watson and F. H. C. Crick, *Nature*, 1953, **171**, 737-738.
149. A. Houlton, A. R. Pike, M. Angel Galindo and B. R. Horrocks, *Chemical Communications*, 2009, 1797-1806.
150. Y. Ma, J. Zhang, G. Zhang and H. He, *Journal of the American Chemical Society*, 2004, **126**, 7097-7101.

151. N. C. Seeman, *Nature*, 2003, **421**, 427-431.
152. C. S. S. R. Kumar, J. Hormes and C. Leuschner, *Nanofabrication Towards Biomedical Applications: Techniques, Tools, Applications, and Impact*, Wiley, 2006.
153. N. C. Seeman, *Molecular biotechnology*, 2007, **37**, 246-257.
154. P. W. K. Rothmund, *Nature*, 2006, **440**, 297-302.
155. K. Lund, A. J. Manzo, N. Dabby, N. Michelotti, A. Johnson-Buck, J. Nangreave, S. Taylor, R. Pei, M. N. Stojanovic, N. G. Walter, E. Winfree and H. Yan, *Nature*, 2010, **465**, 206-210.
156. H. Gu, J. Chao, S.-J. Xiao and N. C. Seeman, *Nature*, 2010, **465**, 202-205.
157. A.-P. Eskelinen, A. Kuzyk, T. K. Kaltiaisenaho, M. Y. Timmermans, A. G. Nasibulin, E. I. Kauppinen and P. Törmä, *Small*, 2011, **7**, 746-750.
158. A. R. Pike, L. C. Ryder, B. R. Horrocks, W. Clegg, M. R. Elsegood, B. A. Connolly and A. Houlton, *Chemistry -A European Journal*, 2002, **8**, 2891-2899.
159. A. R. Pike, L. C. Ryder, B. R. Horrocks, W. C. Clegg, B. A. Connolly and A. Houlton, Wiley-VCH, Weinheim, ALLEMAGNE, 2005.
160. B. Datta, G. B. Schuster, A. McCook, S. C. Harvey and K. Zakrzewska, *Journal of the American Chemical Society*, 2006, **128**, 14428-14429.
161. R. Stoltenberg and A. Woolley, *Biomedical Microdevices*, 2004, **6**, 105-111.
162. T. Nishinaka, A. Takano, Y. Doi, M. Hashimoto, A. Nakamura, Y. Matsushita, J. Kumaki and E. Yashima, *Journal of the American Chemical Society*, 2005, **127**, 8120-8125.
163. H. Reda, A. F. A.-S. Said, Š. Lidija, L. Ross, G. W. Nicholas, H. Andrew and R. H. Benjamin, *Nanotechnology*, 2012, **23**, 075601.
164. J. Richter, M. Mertig, W. Pompe, I. Mönch and H. K. Schackert, *Applied Physics Letters*, 2001, **78**, 536-538.

165. J. Coffey, R. Pinizzotto and Y. Rho, in *NanoBiotechnology Protocols*, eds. S. Rosenthal and D. Wright, Humana Press, 2005, vol. 303, pp. 167-178.
166. M. D. W. Scott, H. Andrew and R. H. Benjamin, *Nanotechnology*, 2012, **23**, 505603.
167. Houlton A., Horrocks B. R., Pike A., Galindo M. A., *Chemical Communications*, 2009, **14**, 1797.
168. W. Liu, J. Kumar, S. Tripathy, K. J. Senecal and L. Samuelson, *Journal of the American Chemical Society*, 1998, **121**, 71-78.
169. R. Nagarajan, W. Liu, J. Kumar, S. K. Tripathy, F. F. Bruno and L. A. Samuelson, *Macromolecules*, 2001, **34**, 3921-3927.
170. W. U. D. Patrick Nickels, Stefan Beyer, Jörg P Kotthaus and Friedrich C Simmel, *Nanotechnology*, 2004, **15**, 1524-1529.
171. S. M. D. Watson, J. H. Hedley, M. A. Galindo, S. A. F. Al-Said, N. G. Wright, B. A. Connolly, B. R. Horrocks and A. Houlton, *Chemistry – A European Journal*, 2012.
172. G. Zheng, F. Patolsky, Y. Cui, W. U. Wang and C. M. Lieber, *Nature Biotechnology*, 2005, **23**, 1294-1301.
173. C. M. Zheng, *Methods in molecular biology*, 2011, **790**, 223-237.
174. J.-i. Hahn and C. M. Lieber, *Nano Letters*, 2003, **4**, 51-54.
175. S. Su, Y. He, S. Song, D. Li, L. Wang, C. Fan and S.-T. Lee, *Nanoscale*, 2010, **2**, 1704-1707.
176. A. Ramanavičius, A. Ramanavičienė and A. Malinauskas, *Electrochimica Acta*, 2006, **51**, 6025-6037.
177. R. Salikhov, A. Lachinov, R. Rakhmiev, R. Gadiev, A. Yusupov and S. Salazkin, *Measurement Techniques*, 2009, **52**, 427-431.
178. M. A. Bangar, D. J. Shirale, W. Chen, N. V. Myung and A. Mulchandani, *Analytical chemistry*, 2009, **81**, 2168-2175.

179. K. Ramanathan, M. A. Bangar, M. Yun, W. Chen, N. V. Myung and A. Mulchandani, *Journal of the American Chemical Society*, 2004, **127**, 496-497.

180. N. Zhu, Z. Chang, P. He and Y. Fang, *Electrochimica Acta*, 2006, **51**, 3758-3762.

Chapter 2

Characterisation Techniques

2.1 Overview

The chemical composition of DNA-templated polymer hybrid materials was investigated by means of Fourier transform infrared (FTIR) spectroscopy and UV-Vis absorption spectroscopy. The morphology of DNA-templated polymer nanowires were investigated by atomic force microscopy (AFM); while electrical properties were investigated using scanned conductance microscopy (SCM) and two-terminal current-voltage (I - V) measurements using a probe station.

All chemicals were purchased from either Sigma Aldrich or Alfa Aesar and used as received unless otherwise stated. Where applicable, all the solutions were prepared in Ultrapure water supplied from a NANOpure® DIamond™ Life Science ultrapure water system equipped with a DIamond™ RO Reverse Osmosis System (Barnstead International); nominal resistivity 18.2 M Ω cm.

For FTIR, AFM and SCM studies Si<p-100> *ca.* 1 cm² chips (cut from 3 inch diameter wafers, boron doped, 525±50 μ m thickness, single side polished, 1-10 Ω cm resistance) and Si<n-100> *ca.* 1 cm² chips (cut from 3 inch diameter wafers, arsenic doped, 525±25 μ m thickness, double side polished, 0.005 Ω cm resistance, coated with a thermally grown SiO₂ layer, 200 nm±10% thick) were used and purchased from Compart Technology Ltd, Peterborough, Cambridgeshire, U.K.

Microelectrodes used to facilitate electrical testing of the nanowires using two-probe current voltage measurements were fabricated by the School of Electrical and Electronic Engineering, Newcastle University (dimensions given in the Appendix).

2.1.1 Atomic Force Microscopy (AFM)

Atomic Force Microscopy (AFM) is a form of Scanning Probe Microscopy (SPM) invented by Binnig, Gerber and Quate in 1986.¹ AFM has resolution near the atomic scale and produces high-resolution, 3-D images by scanning a sharp tip over the sample surface.

AFM operates by measuring attractive or repulsive forces between a tip and the sample. In its repulsive ‘contact’ mode, the instrument lightly touches a tip at the end of a leaf spring or ‘cantilever’ to the sample. As a raster-scan drags the tip over the sample, some sort of detection apparatus measures the vertical deflection of the cantilever, which indicates the local sample height. Thus, in contact mode the AFM measures hard-sphere repulsion forces between the tip and sample. In noncontact mode, the AFM derives topographic images from measurements of attractive forces; the tip does not touch the sample (Figure 2.1).

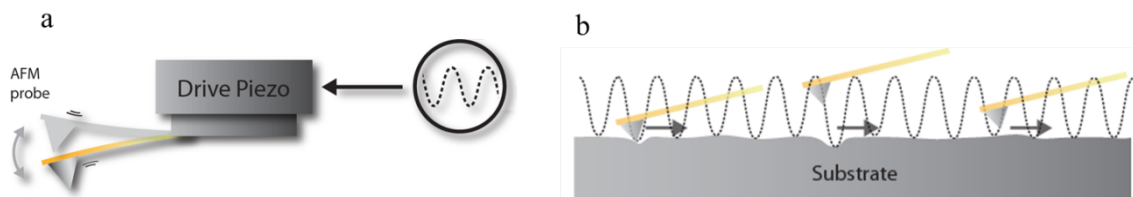


Figure 2.1. A basic illustration showing the method of function of an atomic force microscope (AFM). a) The tip attached to a flexible cantilever driven by piezoelectric motor; b) the tip oscillates at its resonant frequency across the surface²

AFMs can generally measure the vertical deflection of the cantilever with picometer resolution. The tip is attached to a flexible support known as the cantilever mounted on one end of a cylindrical piezoelectric tube mounted near the top of the microscope.

Unlike traditional microscopes, scanned-probe systems do not use lenses, so the size of the probe rather than diffraction effects generally limit. AFM cantilevers generally have spring constants of about 0.1 N/m and should have a high resonant frequency.

$$f_0 = \frac{1}{2\pi} \sqrt{\frac{\text{spring constant}}{\text{mass}}}$$

This equation shows that a cantilever can have both low spring constant and high resonant frequency if it has a small mass. Therefore AFM cantilevers tend to be very small. Commercial vendors manufacture almost all AFM cantilevers by microlithography processes similar to those used to make computer chips.

The piezo crystal attached to the cantilever is used to excite the tip vertically causing the cantilever itself to oscillate (Figure 2.2). The laser beam reflects from its back surface causing an electronic signal when patterned over the photodiode array consisting of two side-by-side photodiodes. Angular deflection of the cantilever causes a two-fold larger angular deflection of the laser beam. The difference between the two photodiode signals indicates the position of the laser spot on the detector and thus the angular deflection of the cantilever which combined reveals information (electrical and topographical information) about the sample surface under investigation.

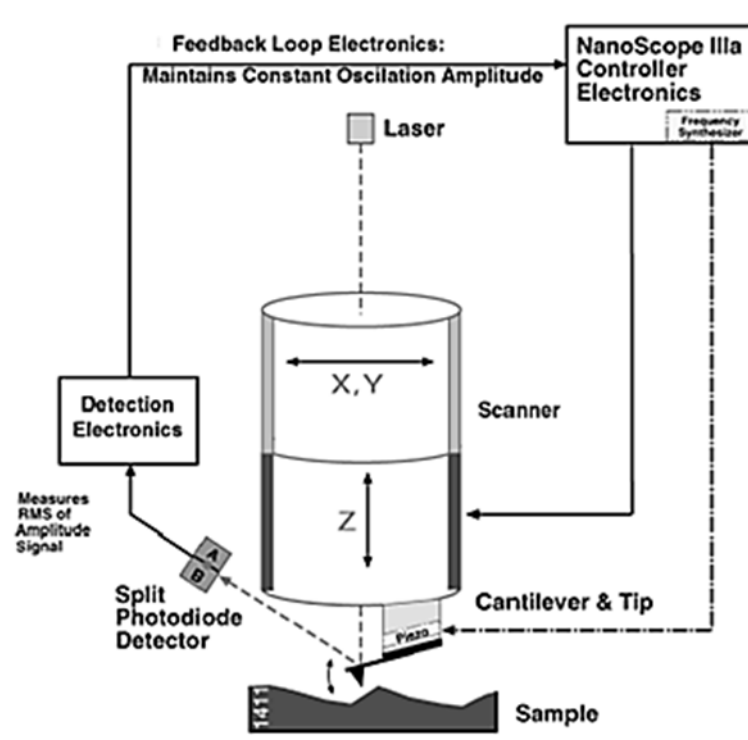


Figure 2.2. AFM schematic representation. Reproduced from Di Dimension Instruction manual, Veeco Instruments Inc. 2004 manual

The AFM not only measures the force on the sample but also regulates it through the feedback loop, allowing acquisition of images at very low forces. The feedback loop circuit attempts to keep the cantilever deflection constant by adjusting the voltage applied to the scanner. The faster the feedback loop can correct deviations of the cantilever deflection, the faster the AFM can acquire images.

In this work, surface topography images were obtained by TappingMode™ AFM performed in air AFM using a Dimension Nanoscope V system (Veeco Inc., Metrology group) using TESP7 probes (n-doped Si cantilevers, Veeco Instruments Inc., Metrology Group) with a resonant frequency of 234–287 kHz, and a spring constant of 20–80 Nm^{-1} . Tap300A1-G (Budget Sensors, Monolithic silicon cantilevers) with a resonance frequency of 100–400 kHz, and a spring constant of 20–75 Nm^{-1} (Windsor Scientific, Sloughm Berks., U.K.). Data acquisition was carried out using Nanoscope version 7.00b19 software (Veeco Instruments Inc., Digital Instruments). Vibrational noise was reduced with an isolation table/acoustic enclosure (Veeco Inc., Metrology Group).

2.1.2 Scanned Conductance Microscopy (SCM)

SCM provides a method for probing the electronic properties of one-dimensional nanomaterials in qualitative manner. The experiment set-up has a conductive tip and a nanowire sitting on an insulating oxide dielectric of about ~ 200 nm thickness, which in turn is grown on a conductive Si substrate. The electrical connection is between the tip and the substrate and this voltage (V) is held fixed at a value typically between $-10V$ and $+10V$. The height of the tip above the nanowire is about $50 - 70$ nm; too far for any tunneling current to pass so the tip and substrate behave like two metal plates separated by an insulating gap, i.e., a capacitor.

Figure 2.3 illustrates the principles of the method. The technique involves a ‘two-pass’ method in which the first pass of a metal-coated AFM probe over the sample surface is used to record the topography. In the second pass over the same scan line, the tip is then raised to a certain scan height (*ca.* $50-70$ nm) and a bias is applied above the sample.

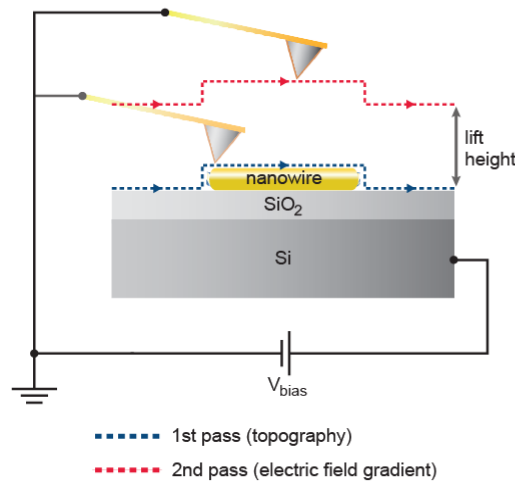


Figure 2.3. A basic representation outlining the principles of SCM operation, used to evaluate the electronic properties of one-dimensional nanostructures²

In general, SCM maps the attractive and repulsive forces between the tip and the sample, as shown in Figure 2.4. The tip-sample interaction changes the AFM cantilever resonance frequency. The resonant frequency is sensitive to any force

gradient. Attractive forces make the cantilever softer reducing its resonant frequency, while repulsive forces make it stiffer increasing its resonant frequency.

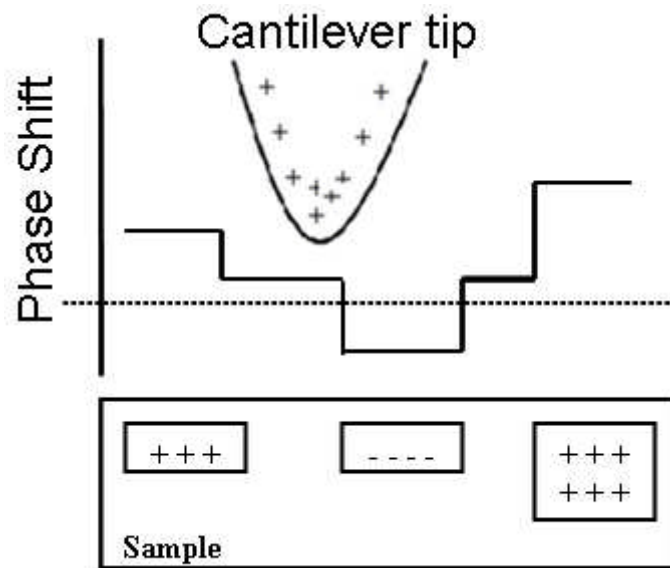


Figure 2.4. Schematic diagram of the attractive and repulsive forces in the SCM experiment

SCM Theory

The charge on the tip (Q) is balanced by an equal and opposite charge ($-Q$) on the substrate. The relation between the applied voltage and the amount of charge is:

$$Q = CV$$

C is the capacitance of the tip/substrate arrangement. Because there is an electric field between the tip and substrate, there is electrical energy (E) stored in the capacitor:

$$E = \frac{1}{2} CV^2$$

As discussed in Section 2.1.1, AFM works by monitoring the deflection of the tip (x) and uses Hooke's law to relate the deflection to a force, via the spring constant k :

$$F = kx$$

There is mechanical energy stored in the tip when it is deflected:

$$E = \frac{1}{2}kx^2$$

This energy exists independently of any applied voltage, however when a voltage is applied they are added together:

$$E = \frac{1}{2}kx^2 + \frac{1}{2}CV^2$$

It costs energy either to change x or to change C . In fact, the capacitance of two parallel plates is:

$$C = \frac{A\epsilon}{x}$$

Where, x is the distance between them. As far as the oscillation of the tip is concerned, anything that requires a supply of energy shifts the phase regardless of the source; electrical or mechanical.

As such, the spring constant of the cantilever is altered by an amount δk , it mimics the effect of the way the electrical energy changes with x :

$$\Delta E = \frac{1}{2}\delta kx^2$$

As long as the change in the spring constant is chosen so as to match the original electrical energy contribution:

$$\delta k = \frac{1}{2} \frac{\partial^2 C}{\partial x^2} V^2 = \frac{1}{2} C'' V^2$$

Where, C'' is just a convenient shorthand for the second derivative with respect to x . You can see this by writing the capacitance in terms of the value near the point of no deflection:

$$C = C_{x=0} + \frac{1}{2} C'' x^2$$

The effect of the tip/substrate capacitance is equivalent to a change in the spring constant of the cantilever. The capacitance acts just like an increase in the

stiffness of the cantilever. Changing the spring constant puts the tip out of resonance exhibiting a phase shift.

Phase shifts

The shift is known as the “phase lag” of the probe and is defined as the difference between the phase angle of the oscillating cantilever and the drive signal voltage used to generate the cantilever motion.

If we consider the cantilever as a harmonic oscillator, driven with frequency ω (damping coefficient γ) and resonant frequency, $\omega_0\sqrt{k/m}$, then the phase shift, ϕ , between the driving force and the cantilever resonance frequency ω_0 is given by:

$$\tan \phi = -\frac{\gamma\omega}{\omega_0^2 - \omega^2}$$

The phase shift is negative when $\omega < \omega_0$. Whereas, it is positive when $\omega > \omega_0$, as can be seen in Figure 2.5.

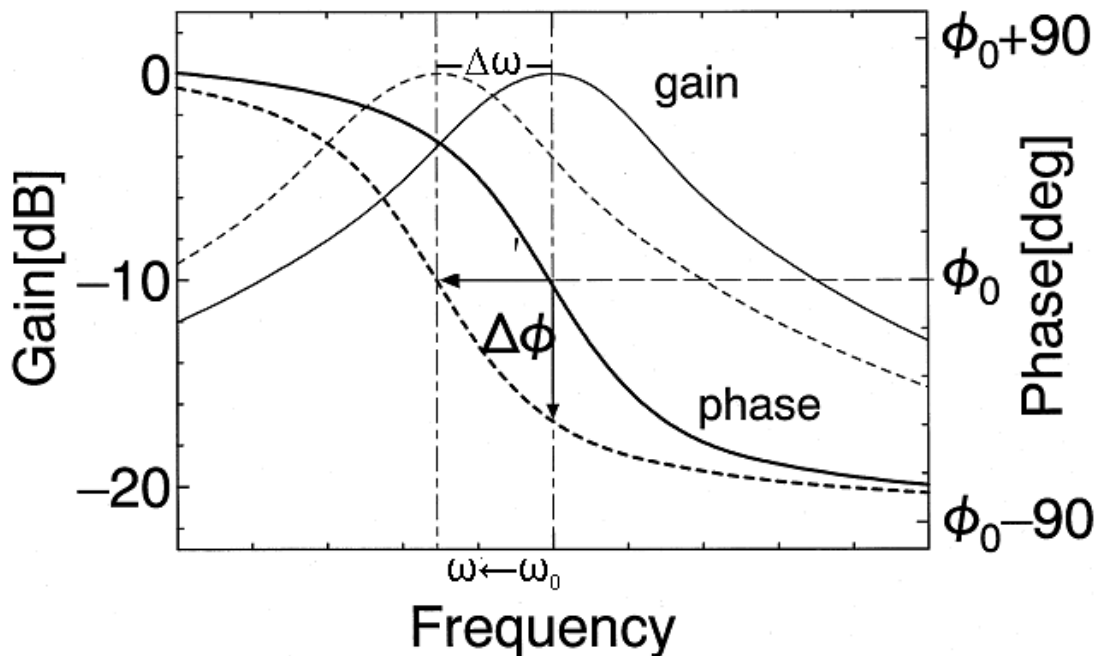


Figure 2.5. Resonance curve. The resonance frequency shifted $\Delta\omega$ from ω_0 to $\omega = \omega_0 + \Delta\omega$, and phase shift $\Delta\phi$ occurs at the frequency ω_0 . Reproduced from reference³

At resonance, the phase shift, $\phi = -\pi/2$. But, under usual SCM conventions, the bare substrate exhibits zero phase shift. This is because $\pi/2$ is subtracted from all measured phase shifts:

$$\Phi = \phi - \left(-\frac{\pi}{2}\right) = \phi + \pi/2$$

Since the total energy, as a function of h :

$$E_{tot} = 1/2 k h^2 + 1/2 C(h)V^2$$

Where $C(h)$ is the tip-substrate capacitance, k , is the spring constant of the cantilever, and V is the bias voltage applied between the tip and the substrate. Therefore,

$$1/2 C(h)V^2$$

is equivalent to a change in k ; Δk . For small forces, $F'(h) \ll k$, the frequency shift $\Delta\omega$ and the phase shift $\Delta\Phi$ are proportional to the force gradient $F'(h)$.

The Effect of the Nanowire

The sign of the phase shift ($\Delta\phi$, Figure 2.5) associated with the object under investigation, relative to the substrate background, indicates whether the wire is electrically conducting or insulating through the generation of a phase image. Figure 2.6 is a typical cross-sectional plot of a nanowire imaged by SCM. The negative-positive-negative phase shifts is characteristic of semi-conducting materials.⁴⁻⁶

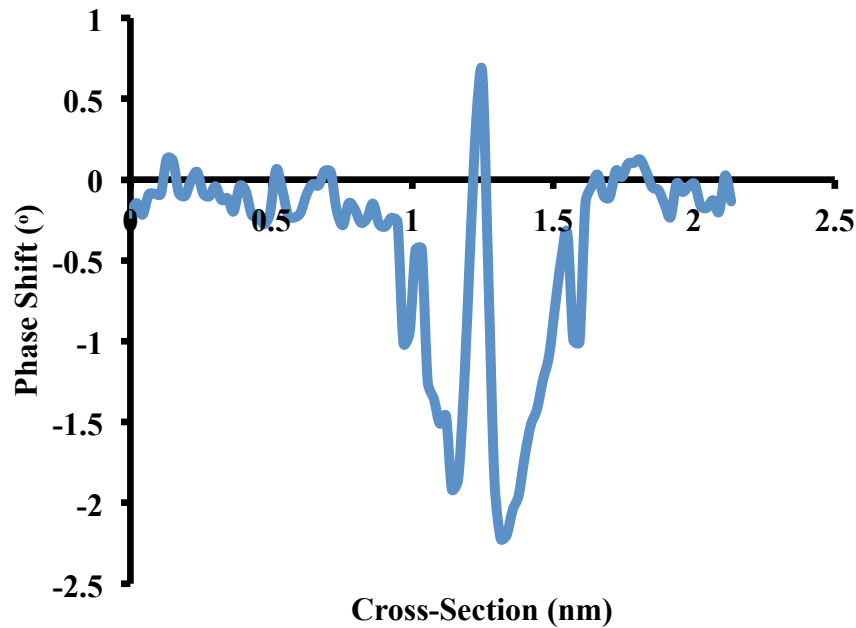


Figure 2.6. A typical cross-section of a conducting DNA/polymer nanowire, illustrating the negative-positive-negative phase shifts is characteristic of semi-conducting materials

The phase of the tip motion with respect to the driving force depends on the DC voltage applied and the capacitance between the tip and the underlying substrate. Negative phase shifts are only observed for conductive materials, whilst insulating materials exhibit positive phase shifts.⁷⁻⁹

The presence of the nanowire changes the tip/substrate capacitance because the electrons in the nanowire move in the electric field in the tip/substrate gap and affect the charge stored. There are two ways this happens; either the electrons are free to move along the whole length of the wire (it's conductive and is really a wire) or the electrons are just disturbed a bit from their equilibrium (it's a polarisable insulator and not a wire). Polarisation of the nanowire happens only directly beneath the tip because the electrons are not free to wander away in an insulator; a long boring calculation showed that the phase shift is either positive or tends to zero as the polarisability (responsiveness of electrons to the field) tends to infinity. Conduction has a bigger effect because electrons not tied to their nuclei can wander along the length of the whole wire - the whole wire not just the portion beneath the tip now affects the capacitance.

SCM studies were carried out upon DNA/polymer nanowires immobilized upon Si<n-100> substrates with a 200 nm thick, SiO₂ layer, modified with a TMS self-assembled monolayer, as described in Chapter 4. All experiments were performed in air with a Dimension Nanoscope V system (Veeco Instruments Inc., Metrology Group), using MESP probes (n-doped Si cantilevers, with a Co/Cr coating, Veeco Instruments Inc., Metrology Group) with a resonant frequency of *ca.* 70 kHz, a quality factor of 200–260, and a spring constant of 1–5 Nm⁻¹. Acquisition and processing of SCM data was carried out using Nanoscope version 7.00b19 software (Veeco Instruments Inc., Digital Instruments). During SCM experiments, an independently controlled bias, typically set between -7 V and +7 V, was applied to the sample whilst the tip was kept grounded and lift heights of 50–70nm were typically employed.

2.1.3 Conductive Atomic Force Microscopy (cAFM)

c-AFM techniques can provide direct electrical characterization, as well as the surface topography of individual nanowires through the use of a metal coated tip to contact the nanowire.

cAFM involves applying droplet of templating solution onto the Si/SiO₂ substrate with subsequent solvent evaporation leaving a dense network of nanowires on the surface, at the periphery of which individual nanowires can be found to extend out. The dense nanowire network can effectively be used as a macroscopic electrical contact to the nanowire under study. Electrical contact of the network to the metallic sample chuck can be made using a drop of Ga/In eutectic. The second electrical contact to the nanowire is made using the conductive metal-coated AFM probe itself. The main technical difficulty lies in making a second connection between the nanowire and the external circuit.

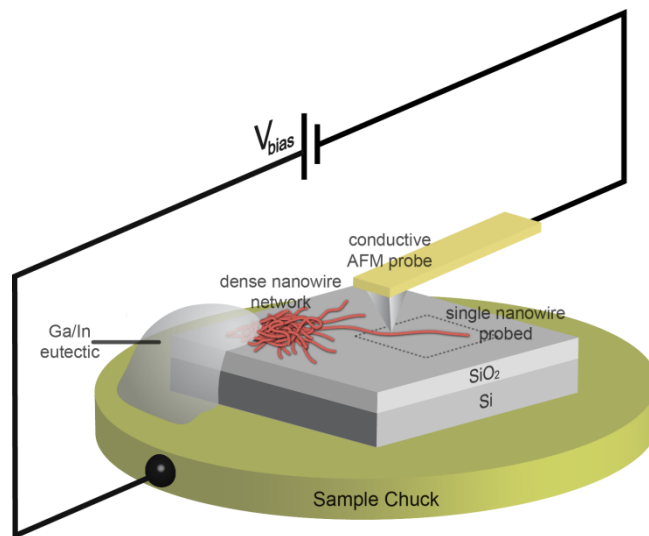


Figure 2.7 Experimental set-up for cAFM measurements carried out upon DNA-based polymer nanowires. Measurements are recorded upon individual nanowires located at the periphery of a dense network of nanowires²

c-AFM images are recorded with different biases applied between the cantilever and the metallic chuck. Essentially zero current is observed when the tip is above bare Si/SiO₂, but currents are observed when the tip was in contact with the nanowire.

After collecting an image, the closed loop positioning system of the NanoscopeV is used to touch the nanowire at defined points and an I - V curve is recorded over a range of bias voltages. We interpret the data in terms of a simple series circuit comprising three resistances; R_{tip} , R_{ext} and R_{wire} . Where R_{tip} , is the tip/nanowire contact resistance, R_{ext} is the resistance between the nanowire and the external circuit and R_{wire} is the resistance of the portion of the nanowire between the tip and the main drop deposit. The measured circuit resistance is clearly the sum of these, and we are assuming all the distance dependence lies in R_{wire} .

c-AFM studies were carried out upon DNA/polymer nanowires supported upon Si<n-100> wafers bearing a 200 nm thick, SiO_2 layer, modified with TMS self-assembled monolayer, as described in Chapter 4. All experiments were performed in air with a Dimension Nanoscope V system (Veeco Instruments Inc., Metrology Group), using MESP probes (n-doped Si cantilevers, with a Co/Cr coating, Veeco Instruments Inc., Metrology Group) with a spring constant of 1–5 Nm^{-1} , and SCM-PIC probes (n-doped Si cantilevers, with a PtIr/Cr coating, Veeco Instruments Inc., Metrology Group) with a spring constant of 0.2 Nm^{-1} . Acquisition and processing of SCM data was carried out using Nanoscope version 7.00b19 software (Veeco Instruments Inc., Digital Instruments). Ga/In eutectic was used to make an electrical contact between the DNA/ polyTPT material and the sample chuck.

2.1.4 Two-Probe I - V Measurements

Quantitative data on the electrical properties of individual DNA-based nanowire structures was gathered through two probe current-voltage (I - V) measurements; this required the fabrication of bespoke two-terminal devices (Figure 2.8 and Appendix). These devices were used as an interface between the nanowire and the probe station and were constructed using Au electrode pairs, micro-fabricated using photolithography, embedded in a thermally grown insulating SiO_2 layer, on a silicon substrate. The Au electrodes were typically separated by a gap of 2–8 μm , across which a DNA-based nanowire was be aligned using molecular combing.

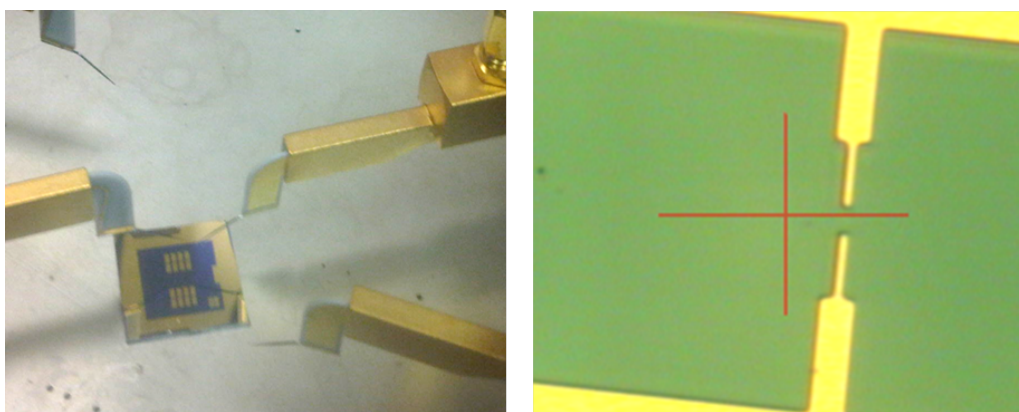


Figure 2.8. Optical images of Au electrode pairs, micro-fabricated using photolithography, embedded in a thermally grown insulating SiO_2 layer, on a silicon substrate. The Au electrodes were typically separated by a gap of 2–8 μm

Two-point probe current-voltage measurements were made using a Probe Station (Cascade Microtech, Inc., Oregon, USA) and B1500A Semiconductor analyzer (Agilent Technologies UK Ltd., Edinburgh, United Kingdom), equipped with Agilent EasyEXPERT software. Prior to electrical testing, the two-terminal devices underwent a heating/cooling cycle between 293–373K, using a heating/cooling chuck (Model ETC-200L, ESPEC Corp., Osaka, Japan), under a N_2 atmosphere, to drive off any water bound to the nanowire/bulk polymer. Subsequent I - V measurements were conducted under a N_2 atmosphere, in the dark and using a voltage range of -5 V to +5 V in steps of 0.05V. Variable temperature I - V measurements were carried out between a temperature range of 293–373K, at increments of 10K.

2.1.5 Contact Angle Measurements¹⁰

Surface hydrophobicity is estimated by measuring the angle a surface makes with the tangent of a drop of water at the contact point, known as the contact angle (Figure 2.9). The more hydrophilic a surface, the smaller the contact angle, as the solution maximizes its interaction with the surface. Larger contact angles indicate repulsion, as a result of an increasing hydrophobic surface.

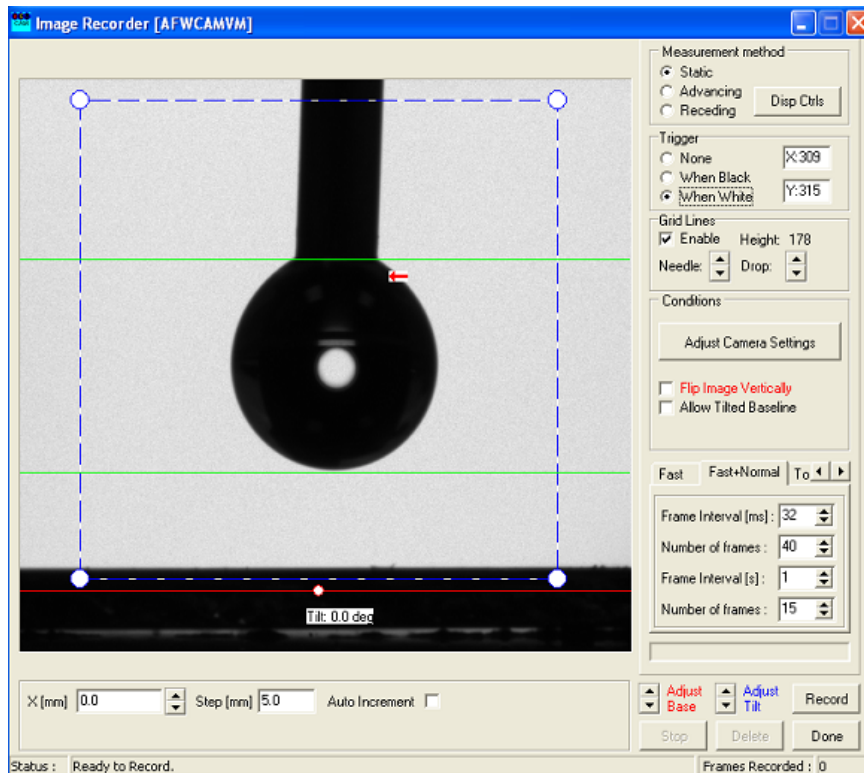


Figure 2.9. A screen shot taken from the CAM 101 used for contact angle measurements in this study. A droplet of water is deposited onto the appropriately functionalized surface and the static contact angle is measured by the camera

The theoretical description of contact arises from the consideration of a thermodynamic equilibrium between the three phases: the liquid phase (L), the solid phase (S), and the gas/vapor phase (G). If the solid–vapor interfacial energy is denoted by γ^{SG} , the solid–liquid interfacial energy by γ^{SL} , and the liquid–vapor interfacial energy (i.e. the surface tension) by γ^{LG} , then the equilibrium contact angle θ_C is determined from these quantities by Young's Equation:

$$0 = \gamma^{SG} - \gamma^{SL} - \gamma^{LG} \cos \theta_C$$

The contact angle can also be related to the work of adhesion via the Young-Dupré equation:

$$\gamma(1 + \cos \theta_c) = \Delta W_{SLV}$$

Where, ΔW_{SLV} is the solid - liquid adhesion energy per unit area when in the medium, V . Figure 2.10 summarizes the theoretical description of contact angles.

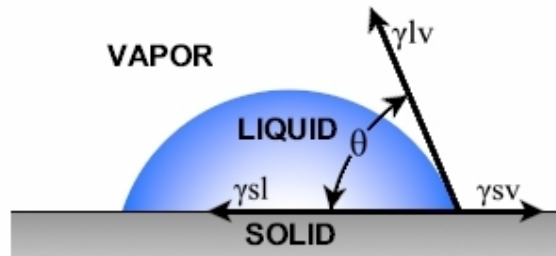


Figure 2.10. The theoretical description of contact arises from the consideration of a thermodynamic equilibrium between the three phases: the liquid phase (L), the solid phase (S), and the gas/vapor phase (G)

Where,

θ is the contact angle

γ^{sl} is the solid/liquid interfacial free energy

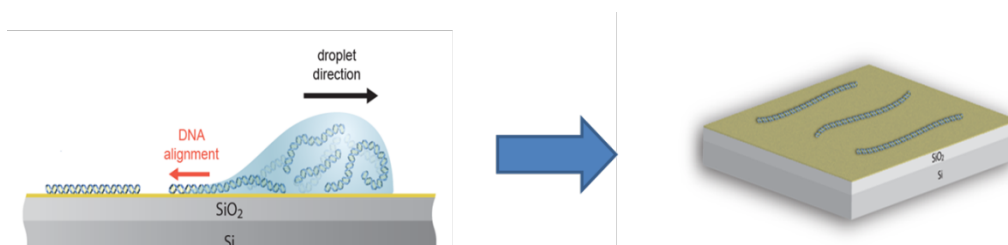
γ^{sv} is the solid surface free energy

γ^{lv} is the liquid surface free energy

2.1.6 Nanowire Alignment

A fundamental requirement for the characterization nanowires is reproducible methods for nanowire deposition/alignment. One approach is to essentially make use of the fluid and surface tension forces of the solution to elongate nanowires or DNA onto a surface.

Methods most applicable to this work are molecular combing and spin-coating, largely due to the simplicity and cost effectiveness. Molecular combing involves the direct manipulation of a drop of solution, with the alignment of the DNA/nanowires perpendicular to the receding meniscus of the solution through movement of the droplet (Scheme 2.1).¹¹



Scheme 2.1. An illustration of DNA alignment across Si/SiO₂ surfaces using molecular combing²

Spin-coating^{12, 13} involves the treatment of the surface with a liquid containing the desired material. Subsequent spinning of the sample provides an elongation force in the form of fluid flow, stretching, in this project the DNA/polymer nanowires across the surface.

In this work, molecular combing was the primary method for immobilization of DNA and DNA/polymer nanowires onto Si/SiO₂ surfaces, with spin-coating employed only when molecular combing proved unsuccessful.

In the case of molecular combing, 5 μ L of template reaction mixture was deposited applied to a modified Si/SiO₂ surface cut into 1 cm² portions (Chapter 4, Section 4.4.1). Using a micropipette tip, the templating solution was combed back and forth 20 times, using a wicking action by hand, at 1 second intervals (Figure 2.11), returning to the original point of deposition counting as 2 movements and taking 2 seconds to perform. All AFM images were taken from the alignment pathway.

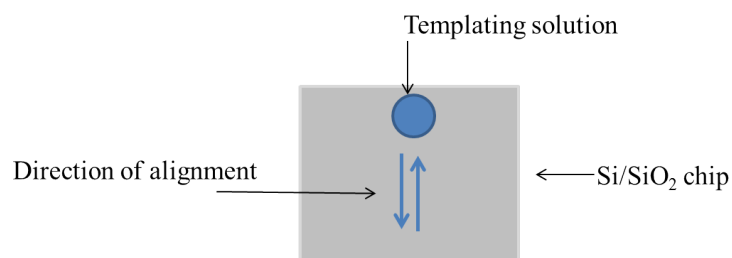


Figure 2.11. An illustration of showing the procedure by which molecular combing was carried out during this project

In the case of spin-coating, 5 μ L of template reaction mixture was deposited applied to the centre of a modified Si/SiO₂ surface cut into 1 cm² portions (Chapter 4, Section 4.4.1). Using centrifuge with a rotor radius of \sim 10 cm, the sample was spun for 30 seconds at 300 rpm with the droplet removed using a micropipette. All AFM images were taken from the periphery of a visible network of nanowires on the surface of which individual nanowires can be found to extend out.

2.2 References

1. G. Binnig, C. F. Quate and C. Gerber, *Physical Review Letters*, 1986, **56**, 930-933.
2. Image drawn by Dr. J. D. Watson, 2010.
3. R. Nishi, I. Houda, T. Aramata, Y. Sugawara and S. Morita, *Applied Surface Science*, 2000, **157**, 332-336.
4. R. Hassanien, M. Al-Hinai, S. A. Farha Al-Said, R. Little, L. Šiller, N. G. Wright, A. Houlton and B. R. Horrocks, *ACS Nano*, 2010, **4**, 2149-2159.
5. S. Pruneanu, S. A. F. Al-Said, L. Dong, T. A. Hollis, M. A. Galindo, N. G. Wright, A. Houlton and B. R. Horrocks, *Advanced Functional Materials*, 2008, **18**, 2444-2454.
6. J. Hannant, J. H. Hedley, J. Pate, A. Walli, S. A. Farha Al-Said, M. A. Galindo, B. A. Connolly, B. R. Horrocks, A. Houlton and A. R. Pike, *Chemical Communications*, 2010, **46**, 5870-5872.
7. C. Staii, A. T. Johnson and N. J. Pinto, *Nano Letters*, 2004, **4**, 859-862.
8. M. Bockrath, N. Markovic, A. Shepard, M. Tinkham, L. Gurevich, L. P. Kouwenhoven, M. W. Wu and L. L. Sohn, *Nano Letters*, 2002, **2**, 187-190.
9. J. Heo and M. Bockrath, *Nano Letters*, 2005, **5**, 853-857.
10. R. Tadmor, *Langmuir*, 2004, **20**, 7659-7664.
11. A. Bensimon, A. Simon, A. Chiffaudel, V. Croquette, F. Heslot and D. Bensimon, *Science*, 1994, **265**, 2096-2098.
12. J. Y. Ye, K. Umemura, M. Ishikawa and R. Kuroda, *Analytical Biochemistry*, 2000, **281**, 21-25.
13. H. Yokota, D. A. Nickerson, B. J. Trask, G. van den Engh, M. Hirst, I. Sadowski and R. Aebersold, *Analytical Biochemistry*, 1998, **264**, 158-164.

CHAPTER 3

Synthesis and Characterisation of Monomer Building Blocks and Conversion to Conducting Polymers

3.1 Chapter Overview

Overall Goal

To synthesis appropriate monomer units that when polymerized have the potential to both conduct and undergo further chemistries compatible with biomolecules.

Hypothesis

By synthesizing pyrrole-thiophene co-monomer units, a route to the formation of polymers with well-defined chemical structure with similar properties will be attained.

The introduction of functional groups directly into the monomer units prior to polymerisation will have little effect on the stability of these materials to polymerisation.

Objectives

To synthesis analogues of pyrrole and thiophene bearing functionality suitable for further chemistry with biomaterials.

To determine the redox potentials and assess the stability of each system as formed polymer.

3.2 Introduction

Organic polymers hold a great deal of potential for label-free detection of a variety of biological species.¹⁻³ In such applications, the polymer is not only used as a transduction element but also as an immobilization matrix for biological recognition molecules.⁴ One approach to achieving probe immobilization is through the synthetic modification of the chosen monomer unit i.e. pyrrole, to introduce further functionality; functionality that may be exploited post polymerisation for the introduction of a desired capture probe.^{5, 6} The role of the physical and chemical structure of these functional groups and the effect such modifications have on disorder, conformation and electronic characteristics are essential considerations to sensor design and performance.

In Chapter 1, pyrrole and thiophene were highlighted as compounds of significant interest due to the agreeable balance between stability, low cost and high conductivity when polymerized. Functionalisation of pyrrole is relatively straightforward in that synthetic modifications can be made on the ring system or through the central nitrogen.

Polymerisation of pyrrole proceeds predominantly through the α -positions of the heterocyclic ring. However, β -substituted (3- and 4- positions) polypyrrole formation is also possible (Figure 3.1). This has been shown to cause a loss of planarity to the polymer backbone by out of plane twisting of the ring system and has been observed to cause a reduction in conductivity; a process thought to be promoted by such synthetic modifications.⁷ For example, *N*-methylation of pyrrole has shown to result in a reduction in conductivity in comparison with unmodified polypyrrole, with *N*-methyl-polypyrrole reported to exhibit conductivities of $\sim 10^{-3}$ S cm^{-1} .⁸

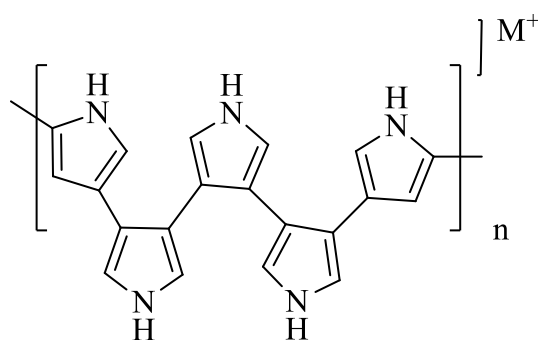


Figure 3.1. Polymerisation of pyrrole can proceed through the β -position

As such, two of the more fundamental goals in this field have been to optimize conductivity and maximize electrical performance and stability. Garnier *et. al.*⁵, amongst others^{8, 9}, noted that 3-substitution of pyrrole is more favourable than *N*-substitution with regard to maintaining the high intrinsic conductivity of the polymer. While studies have shown, by blocking the 3 and 4- positions on the pyrrole ring, unwanted β -substituted polypyrrole formation may be eliminated, with a higher levels of conductivity observed.⁹⁻¹¹

Despite the effect of reduced conductivity *N*-substitution has on polypyrrole, materials modified in this manner still retain a conductive nature and are particularly useful due to the relatively straightforward means of introducing new functionality. A significant benefit to this approach is that it avoids the stereo chemical ambiguity that can arise with the asymmetric 3-derived compounds and the necessity to block reactive sites in order to control regioselectivity (Chapter 1). The ease of modification and hence functionalisation via this chemistry, gives justification to pursue this route in the development of conducting polymers for sensory applications. Moreover, the organic nature of these materials allows for even further synthetic modifications to be made in order to attain an agreeable balance between ease of functionality and conductivity.

In this regard, a way of countering the adverse effect functionalisation at the *N*-position may have on conductivity is through the introduction of a second ring system covalently linked at the α -position of pyrrole, thus allowing for any functional groups attached to be spaced out; minimizing steric interactions which promote polymerization through the β -position. A suitable candidate for this second ring system is thiophene. As previously discussed, the high electrical conductivity, good environmental stability and structural versatility have made polythiophene the

focus of much research. These properties are also expected to be observed in a pyrrole-thiophene co-polymer material, making this class of compounds an attractive target.^{12, 13}

Co-polymerization of the corresponding mixtures of monomers to produce poly(2-(2-thienyl)-pyrrole) (polyTP, Figure 3.2) has previously been achieved through a variety of routes and the electronic properties of this polymer have subsequently been established.¹⁴⁻¹⁹ Conductivities up to 1 S cm^{-1} have been reported, in addition to good stability at ambient conditions. It was anticipated that by synthesizing a pyrrole-thiophene co-monomer unit, a route to the formation of polymers with well-defined chemical structure will be attained, which may not otherwise be easily synthesized through the equivalent co-polymerization of corresponding monomer mixtures.

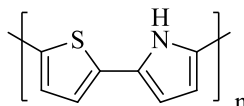


Figure 3.2. Structure of poly 2-(2-thienyl)-pyrrole, polyTP

Whilst this approach overcomes the random nature of monomer insertion afforded by co-polymerization, control over the orientation of each unit is still not straightforward. TP's chemical structure gives rise to three different configurations, "head-to-tail", "tail-to-tail", or "head-to-head" arrangement (Figure 3.3, a), b) and c) respectively) which could potentially result in a loss of planarity and reduced conductive properties.

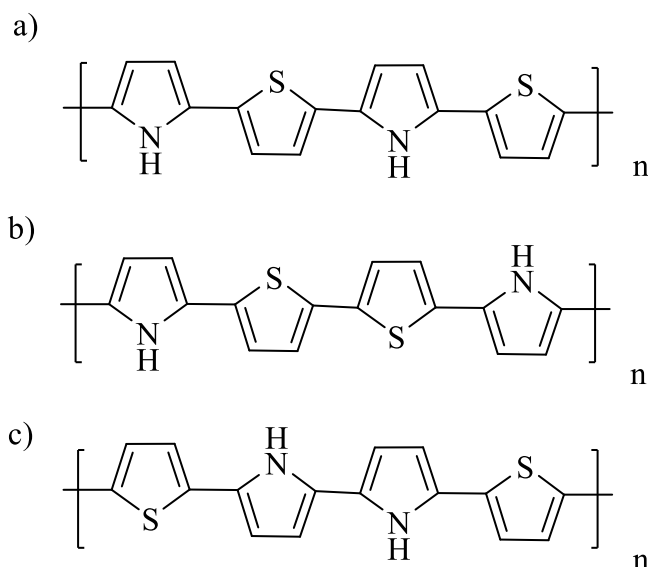


Figure 3.3. The three possible configurations of poly-**TP** formation, a) ‘head-to-tail’, b) ‘tail-to-tail’, c) ‘head-to-head’

A way to circumvent this concern is through the introduction of a second thiophene moiety adjacent to the pyrrole, affording a thiophene-pyrrole-thiophene structure, 2,5-(di-2-thienyl)-pyrrole (poly**TPT**, Figure 3.4). Previously reported in the literature,^{25, 27, 28} **TPT** provides the third monomer unit from this class of compounds and has been shown to possess similar properties to **TP**. It is anticipated that the symmetric nature of such an ‘oligomeric’ monomer unit will help ensure the formation of a well-defined, regular polymer structure. In this work it was decided to base the conducting polymers on **P**, **TP** and **TPT**.

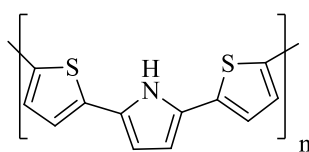


Figure 3.4. Structure of 2,5-(di-2-thienyl)-pyrrole, poly**TPT**

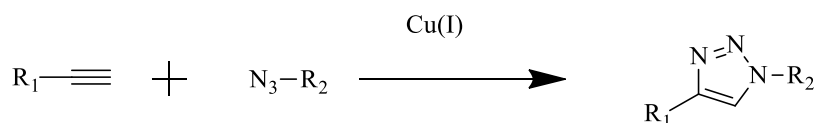
Introducing Further Functionality

As discussed in Chapter 1, the covalent modification of polymeric materials post polymerisation as a means to bio-probe attachment is well established route to functionalized conducting polymers.^{5, 6, 20} As discussed, *N*-substitution of pyrrole is a relatively straightforward means of introducing new functionality. A fundamental requirement in the covalent immobilisation of specific capture probes is the biological compatibility of the reaction and conditions. Mild, aqueous, conditions

and highly specific orthogonal bond formation to the groups present in the biomolecule are required in order to retain the functionality and specificity of the probe itself, post immobilisation. One such method is through the introduction of terminal alkyne group for 1,3-cyclo-addition.

The mechanism of 1,3-cyclo-addition of azides to terminal alkynes to form a triazole was pioneered by Rolf Husigen,²¹ with copper catalyzed 1,3-dipolar cycloaddition ('click' chemistry, Scheme 3.1) introduced by Sharpless in 2001.²² The highly specific nature, stability to a range of conditions, compatible with biological, aqueous conditions and tolerance of functional groups makes 'click' chemistry an ideal route to achieving the functionality envisaged.²³

Attachment of an alkyne group to each monomer unit described previously allows the use of 'click' chemistry to form a triazole linkage between an azide terminated capture probe and the CP nanowire of choice. By coupling 5-chloro-1-pentyne via the *N*-position of pyrrole the moiety for each of the three monomers units (**P**, **TP** and **TPT**); functionality is introduced to the polymer systems.



Scheme 3.1. A general scheme for the formation of 1,4-triazoles via 'click' chemistry

This approach gives rise to a range of compounds for application as functional conducting polymer nanowires (Figure 3.5), which will be referred to as C5-**P**, C5-**TP** and C5-**TPT**.

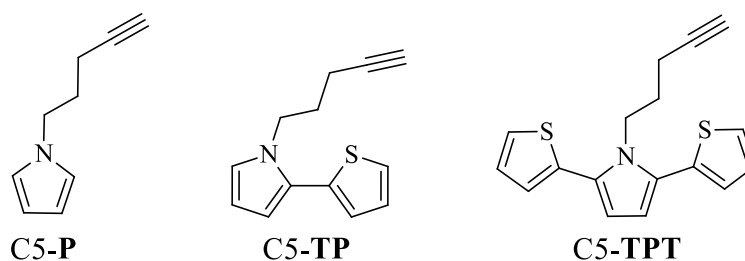


Figure 3.5. Structures of *N*-alkylated alkynyl units

Chapter Outline: *This chapter describes the initial synthesis characterization of **TP** and **TPT** monomer units. The alkylation of the relevant monomer units to afford **C5-P**, **C5-TP** and **C5-TPT** is also described. Polymerisation (chemically and electrochemically) and subsequent characterisation of **polyC5-P**, **polyC5-TP** and **polyC5-TPT** is also presented.*

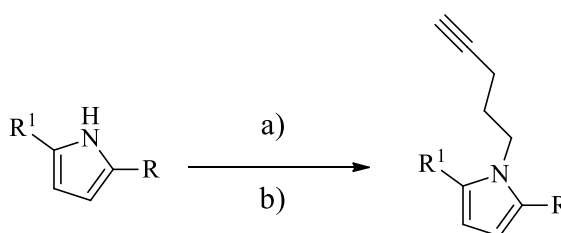
3.3 Results and Discussion

3.3.1 Monomer Synthesis

Goal: To synthesize pyrrole-thiophene co-monomer units.

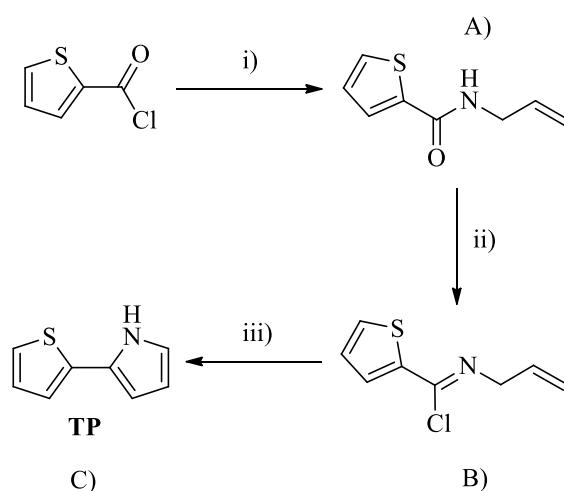
Monomer units, C5-**P**, C5-**TP** and C5-**TPT** were synthesised by using modified literature procedures.^{14, 15, 24-26} Characterisation was by high-resolution ES-MS, ¹H and ¹³C NMR spectroscopy to ascertain the reactions had yielded the desired products.

C5-**P** was synthesized directly in 89% yield by a one-step alkylation of pyrrole (sodium hydride, 5-bromo-1-pentyne in DMF, Scheme 3.2). **TP** and **TPT** analogues both involved a multi-step approaches in which the formation of the relevant ring system was required prior to alkylation of the pyrrole units.



Scheme 3.2. Synthetic route for the *N*-alkylation of pyrrole derivatives. a) NaH, b) 5-bromo-1-pentyne, DMF. R₁ and R₂ = H (**P**), R₁ = H, R₂ = thiophene (**TP**), R₁ and R₂ = thiophene (**TPT**)

TP synthesis began with thiophene carbonyl chloride; an addition-elimination reaction affords the amide, *N*-allylcarboxamide (Scheme 3.3 A)). This was a very clean reaction with no purification required and yields up to 87% were consistently observed. Conversion to imidoyl chloride (Scheme 3.3 B)) was achieved using thionyl chloride and subsequent elimination/ring-closing via the addition of strong base, potassium *tert*-butoxide affords 2-(2-thienyl)-pyrrole, **TP** (Scheme 3.3 C)). Typically yields of 61%, after purification by column chromatography, were obtained. Unequivocal confirmation of the compound synthesis was obtained by single crystal single X-ray diffraction; Figure 3.6 shows the molecular structure.



Scheme 3.3. Reaction scheme for 2-(2-thienyl)-pyrrole, **TP**. i) allylamine, pyridine ii) thionyl chloride, toluene/DMF iii) KO^tBu , DMF

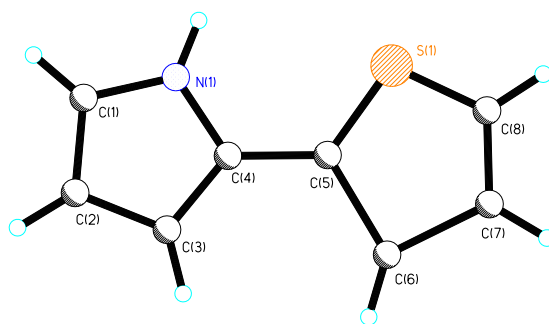
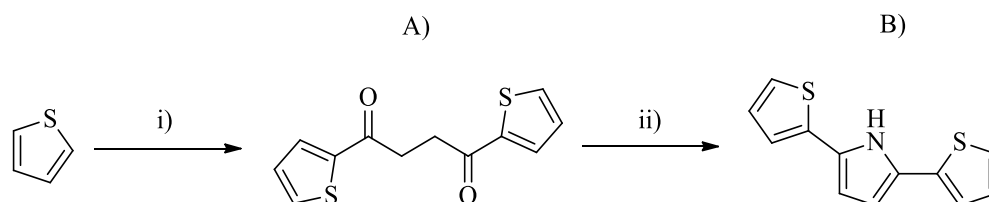


Figure 3.6. Molecular structure of 2-(2-thienyl)-pyrrole, **TP**, recrystallized from dichloromethane and obtained by a single crystal X-ray study. The data of which can be found in the Appendix, Section 9.1

The two step synthesis of **TPT** involves the formation of the central pyrrole moiety through ring closure of 1,4-bis(2thienyl)-1,4-butadione using the Paal-Knorr synthesis. The di-ketone precursor (Scheme 3.4 A)) was produced by Friedel-Crafts acylation of thiophene using succinyl chloride. The highly favoured 5-membered pyrrolyl ring unit was formed by cyclisation of an enamine intermediate produced by treatment with ammonium acetate and acetic anhydride. The final product, 2, 5-di (2-thienyl)-pyrrole, **TPT** (Scheme 3.4 B)), was formed typically in 70% yield.



Scheme 3.4. Reaction scheme for 2, 5-di (2-thienyl)-pyrrole, **TPT**. i) succinyl chloride, AlCl_3 , dry CH_2Cl_2 ii) acetic anhydride, HOAc . NH_4OAc

3.3.2 Alkylation of *N*-pyrrolyl Units

Goal: Modify pyrrole-thiophene co-monomer units produced in 3.3.1 to introduce chemical functionality suitable for reactions with biomaterials such as DNA.

5-chloro-1-pentyne was covalently attached at the *N*-position of each monomer unit via deprotonation of the NH group using a sodium hydride (Scheme 3.2). In each case, sodium hydride was suitable to deprotonate the relatively acidic proton to give a pyrrole anion. This facilitates nucleophilic attack of the alkylhalide and alkylation occurs via a concerted, $\text{S}_{\text{N}}2$, mechanism.

Again, these reactions were found to proceed relatively cleanly with purification of **C5-TP** and **C5-TPT** and **C5-P** achieved routinely by flash column chromatography. Yields of 89% were consistently observed for all monomer units.

3.3.3 Electrochemical Characterisation

Goal: To determine the redox potentials of **C5-TP** and **C5-TPT** and **C5-P** and their assess stability as formed polymer via electrochemical polymerization.

Each of the monomers was studied by cyclic voltammetry to determine the redox potentials and assess the stability of the formed polymer. Interpretation of the electrochemical data was aided by literature references.^{7, 16, 17, 27-31} Table 3.1 presents the redox potentials for the compounds.

Monomer	E/V (peak)
C5- P	>1.50
C5- TP	1.04
C5- TPT	0.99

Table 3.1. CV oxidation peaks of C5-**P**, C5-**TP** and C5-**TPT**. 10 mM of sample, 100 mM LiClO₄, acetonitrile, working electrode Pt, counter electrode Au and Ag quasi-reference electrode. Scan rate 0.2 V/s.³² The accuracy of these values is ± 10 mV based on the stability of the reference electrode

As shown in Table 3.1, decreasing oxidation potentials are observed in the sequence C5-**P**>C5-**TP**>C5-**TPT** which is in line with the increasing size of the ring system for each monomer unit. This is the net effect of continued stabilisation of the radical polymer system and a reduction in the band gap through formation of longer conjugated chains.³¹

Figure 3.7 shows the cyclic voltammogram for C5-**P**. The initial oxidation occurs at ~ 1.54 V with film deposited on the electrode, reduction of this film occurred at ~ 0.45 V upon reversal to a negative potential. Repeated cycles gave rise to the formation of oxidation peaks at lower potentials, this is in agreement with the expected stabilisation of the radical polymer system (Chapter 1) and a reduction in the band gap upon the formation of an extended conjugated system i.e. increased polymer chain length. Moreover, there was no evidence of monomer reduction on the return sweep, indicating irreversible polymerisation was taking place.

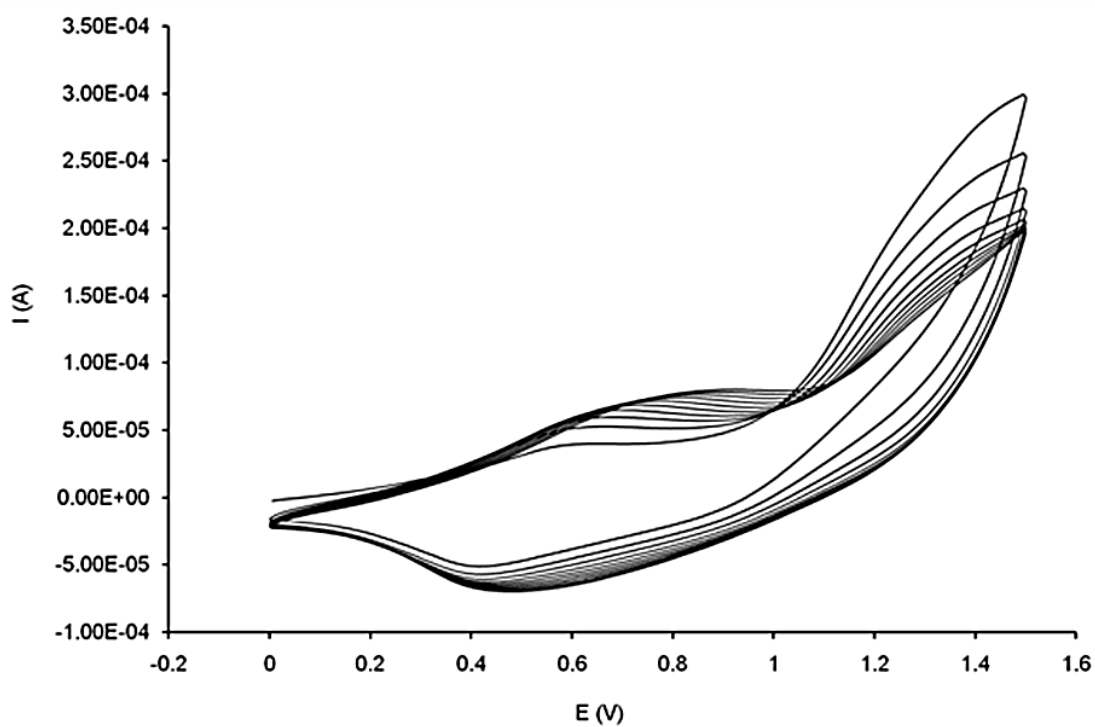


Figure 3.7. CV of C5-**P**. 10 mM of sample, 100 mM LiClO₄ in MeCN, working electrode Pt, counter electrode Au and quasi-reference electrode Ag. Scan rate 0.2 V/s³²

The behaviour of C5-**TP** (Figure 3.8) was similar to C5-**P**, though here oxidation took place at ~ 1.17 V and reduction observed at ~ 0.43 V. As with C5-**P**, repeated cycles gave rise to the formation of oxidation peaks at lower potentials, indicating polymer formation. This was found to be more pronounced in C5-**TP** than C5-**P**, where the oxidation potential of the polymer (~ 0.60 V) was considerably lower to that of the monomer (~ 1.19 V). Again, there was no evidence of monomer reduction on the return sweep, indicating irreversible polymerisation is taking place.

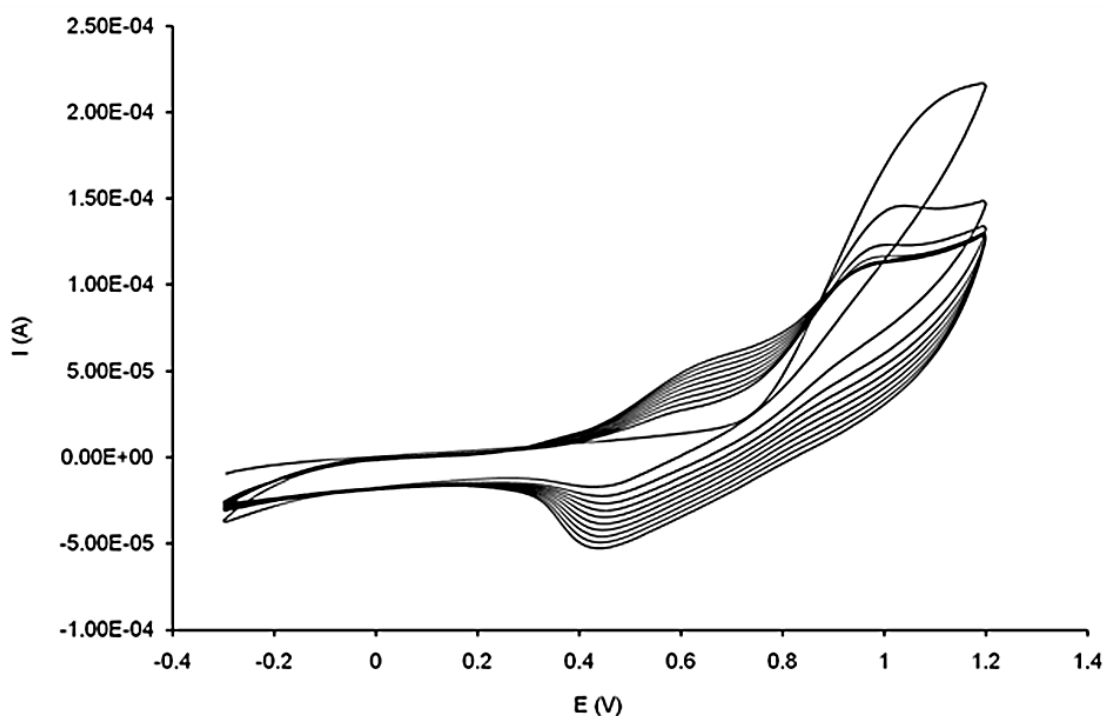


Figure 3.8. CV of C5-TP. 10 mM of sample, 100 mM LiClO₄ in MeCN, working electrode Pt, counter electrode Au and quasi-reference electrode Ag. Scan rate 0.2 V/s³²

In the case of C5-TPT, oxidation took place at ~ 1.17 V with a reduction peak observed at ~ 0.43 V (Figure 3.9). As expected, there was no evidence of monomer reduction on the return sweep. As with C5-P and C5-TP, the formation of oxidation peaks at lower potentials upon repeated cycles was observed. The oxidation potential of the polymer (~ 0.65 V) was considerably shifted to lower potential compared to that of the monomer (~ 1.17 V). It should be noted that in this work the E_p (anodic peak potential) is referred to as the oxidation potential of a given species.

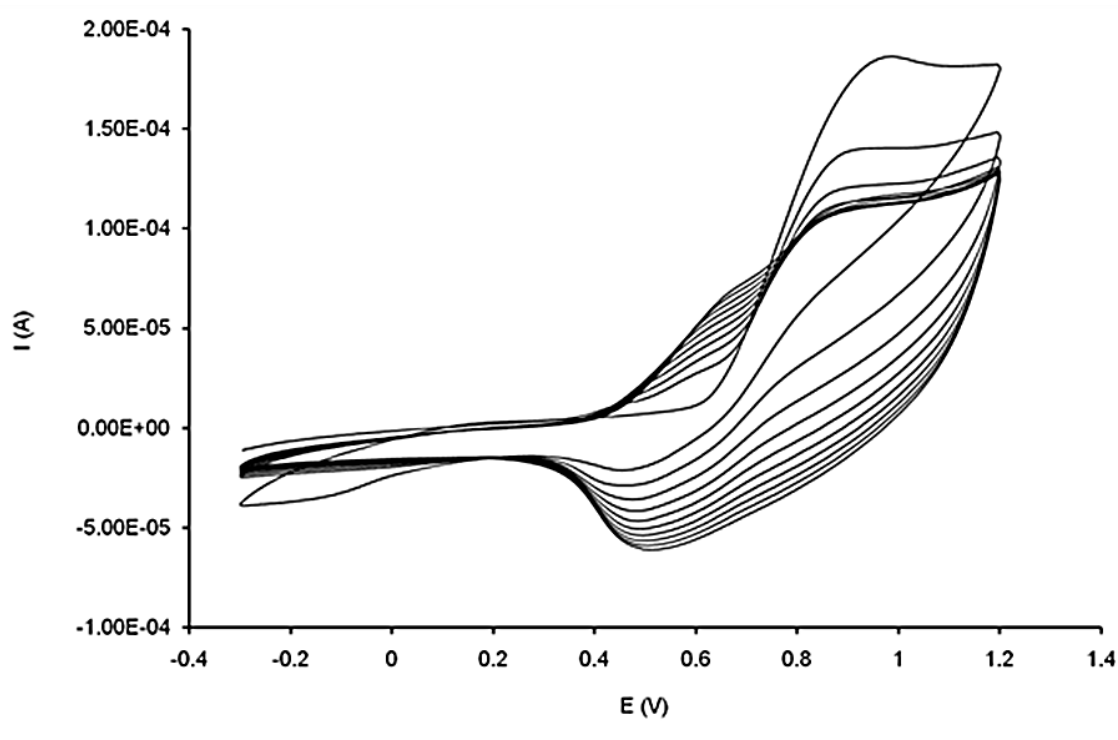


Figure 3.9. CV of C5-TPT. 10 mM of sample, 100 mM LiClO₄ in MeCN, working electrode Pt, counter electrode Au and quasi-reference electrode Ag. Scan rate 0.2 V/s³²

3.3.4 Chemical Polymerisation

Goal: To determine if C5-TP and C5-TPT and C5-P can be chemically polymerised using FeCl₃.

For each new monomer system, bulk polymerisation was achieved by adding FeCl₃ (in excess) to a water/DMF solution containing the monomer unit. The resulting precipitate was isolated from solution using a centrifuge, rinsed and dried prior to examination by FTIR. Evidence of the chemical polymerisation of each monomer unit was primarily observed through precipitate formation, which was in line with the electrochemical data presented in Section 3.3.3. This analysis was subsequently supported by key changes in the FTIR spectra. In particular, the retention of the alkynyl group was critically important for later conjugation of the probe sites.

In the case of polyC5-P, precipitate formation was slow (several hours) with no significant colour change in solution observed; any change may have been masked by the excess of FeCl₃ in solution. The isolated precipitate was found to be both brittle and foam-like. It is possible that polyC5-P forms a less densely packed structure and that slow precipitation was a result of the steric influence of the

pentynyl chain, perhaps inhibiting long polymer chain formation. When considering observations made in Section 3.3.3, precipitate formation alone indicates polymer formation via oxidative polymerisation using FeCl_3 . This visual observation was subsequently supported by FTIR analysis of the isolated precipitate. The following discussion is focused on bands observed in the FTIR spectra which indicate ring coupling and hence polymerisation, complete assignments can be found in the Appendix.

Figure 3.10 shows spectra of polyC5-P (3500 – 2000 cm^{-1} region). The restrictive effect that polymer formation has on vibration and therefore the vibrational modes of functional groups was evident in the spectra and resulted in a number of bands attributed to C-H vibrations shifting to lower wavenumbers.³³ For example, the alkyne C-H vibration observed 3309 cm^{-1} in the monomer, was shifted to 3263 cm^{-1} in the polymeric material. The aromatic C-H vibration was also observed to have shifted from 3066 cm^{-1} to 3028 cm^{-1} in conjunction with the appearance of weak bands at 3155 cm^{-1} and 3101 cm^{-1} , this was attributed to the formation of oligomers of different lengths.³⁴ The intensity of the polymer spectra was noted to be significantly reduced when compared to the monomer unit; this is a known issue with highly conductive materials which are inherently reflective.

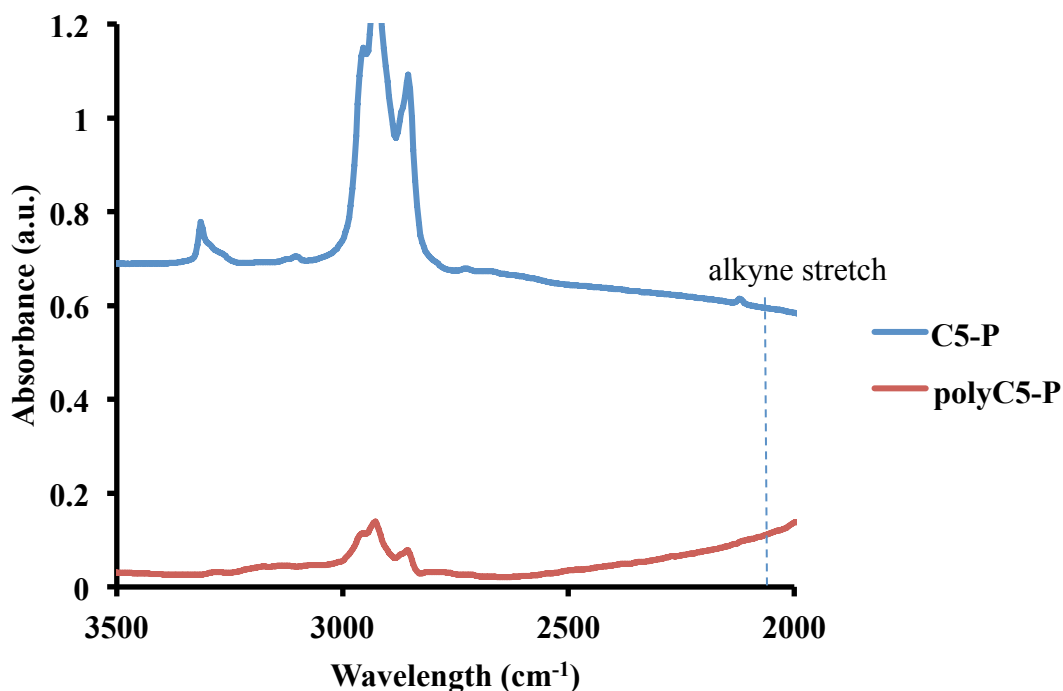


Figure 3.10. FTIR spectra (3500 – 2000 cm^{-1} region) of C5-P (blue) and polyC5-P (red). For clarity, 0.5 has been added to the absorbance values of C5-P

Importantly, the continued presence of the alkyne stretch (2152 cm^{-1} , Figure 3.10, dashed lines) indicates that this functional group remains intact throughout the polymerisation.

Inspection of spectral bands below 1300 cm^{-1} (Figure 3.11) gave further evidence of polymerisation. Narrow plane vibration bands of C-H deformation in the C5-P monomer unit are noted at 956 cm^{-1} , 968 cm^{-1} and 995 cm^{-1} . However, after incubation with FeCl_3 , these bands were no longer present and new weak absorbance bands were observed (1246 , 1122 cm^{-1} and 1056 cm^{-1}), these were attributed to C-H bending, ring breathing and ring deformation of shorter polymer chains, respectively.^{35,36}

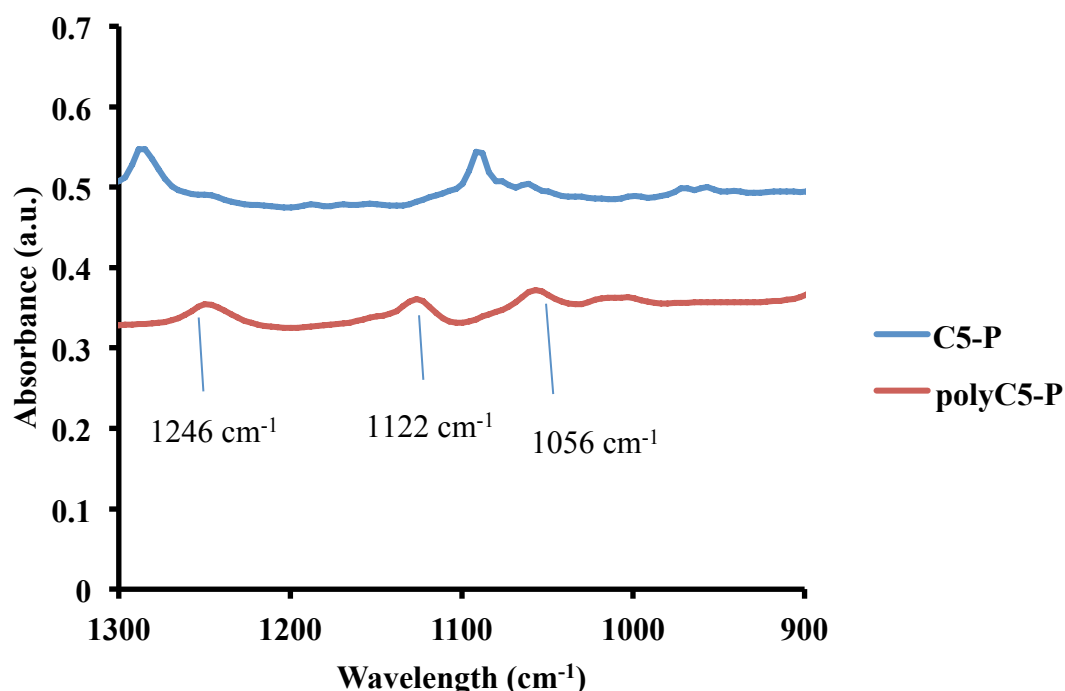


Figure 3.11. FTIR spectra ($1300 - 900\text{ cm}^{-1}$ region) of C5-P (blue) and polyC5-P (red) showing the disappearance of narrow plane vibrations bands of C-H deformation and appearance of weak bands attributed to C-H bending, ring breathing and ring deformation from polymer formation. For clarity, 0.2 has been added to the absorbance values of C5-P

The effect of the increasingly reflective nature of the polymer, often associated with mobile electrons or charge carriers in conductive materials, was clearly evident (broad band *ca.* 2000 cm^{-1}). The absorbance intensity of a number of bands clearly varies, with baseline response observed to be significantly less than when compared to the initial background spectra. Furthermore, after 24 hours incubation with FeCl_3 ,

no absorbance/bands related to the materials groups were observed, indicating the reflective polymer was the main constituent of the sample. This data supports electrochemical/visual observations that polymerisation of each monomer can be achieved both chemically and electrochemically.

In the case of polyC5-**TP**, precipitate formation was immediate, with a significant colour change from the ruby red of the C5-**TP** monomer to a very dark black/green solution observed. The isolated precipitate was found to be fairly robust and metallic-like in appearance. Furthermore, immediate precipitation upon the addition of FeCl₃ implies that the additional thiophene moiety present in C5-**TP** has the desired effect of reducing the steric hindrance posed by the pentynyl chain, thus allowing the formation of longer polymer chains more readily than poly-C5-**P**, mirrored by the lower observed oxidation potential. As with C5-**P**, precipitate formation from incubation with ferric chloride indicated polymer formation by oxidative polymerisation.

Further evidence supporting polyC5-**TP** formation was provided by FTIR analysis. Observed shifts in band positions, changes in relative intensities as well as an overall reduction in absorbance of a number of bands were again observed. Fewer new bands are observed to arise as polymerisation of the monomer takes place. The shifting and sharpening of bands is also more pronounced than observed in the monomer unit, specifically in the 1800 – 800 cm⁻¹ region (Figure 3.12), with bands attributed to the ring system significantly affected. A new band was observed at 1014 cm⁻¹, which can be assigned to the inter-ring C-C bond of longer poly-C5-**TP** oligomers, whilst the band arising from inter-ring bonding in the monomer unit is shifted to higher wavenumber (1649 cm⁻¹ to 1668 cm⁻¹) indicating the presence of short polymer chains, again signaling polymer formation had taken place.^{17, 35}

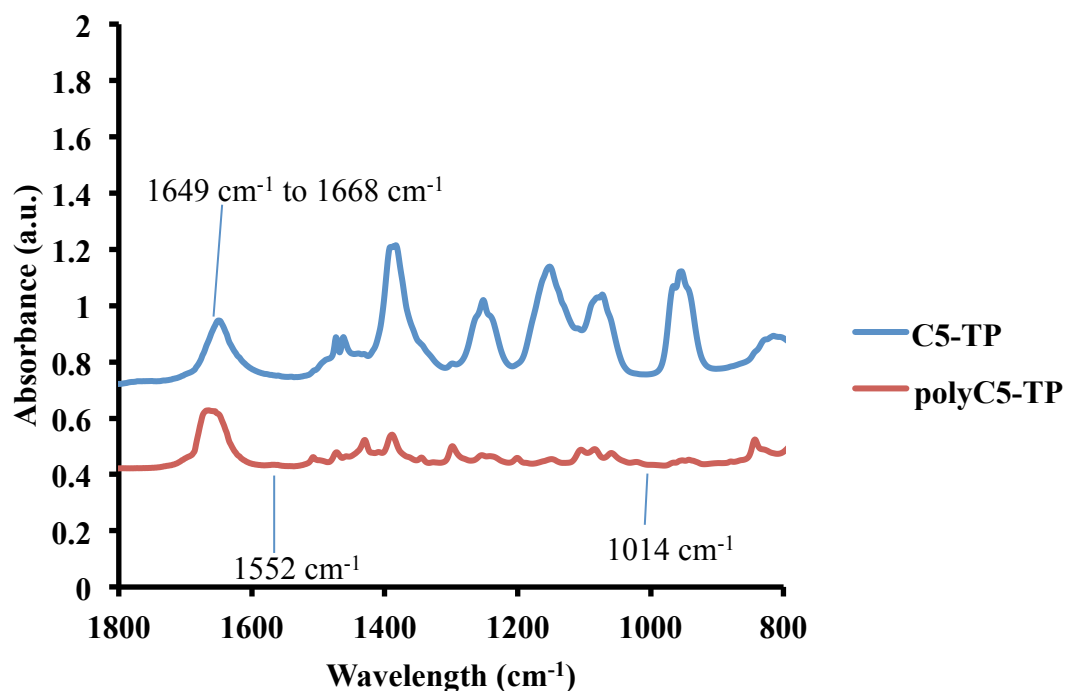


Figure 3.12. FTIR spectra (1800 – 800 cm^{-1} region) of C5-TP (blue) and polyC5-TP (red). Bands attributed to the monomer species are shown to diminish and shift in conjunction with the appearance of new bands. For clarity, 0.3 has been added to the absorbance values of C5-TP

The increase in intensity of the band at 1552 cm^{-1} indicates coupling of ring vibrations to the motion of charge carriers, providing further confirmation of polymerisation taking place.¹⁷ This data supports electrochemical/visual observations that conversion of each monomer unit to the corresponding polymer can be achieved either chemically and electrochemically.

For C5-TPT, the formation of precipitate upon addition of FeCl_3 to C5-TPT solution was immediate. However, a less obvious colour change than with the formation of polyC5-TP was observed. The isolated precipitate was found to be robust in nature and more metallic-like than polyC5-TP. As with C5-TP, precipitate formation from incubation with ferric chloride indicated polymer formation by oxidative polymerisation, in support of the observations made in Section 3.3.3 based on electrochemical data.

Polymerisation of C5-TPT was less evident by FTIR (Figure 3.13, 1800 – 600 cm^{-1} region) than C5-P and C5-TP. The ring breathing mode at 1105 cm^{-1} was shown to be reduced in intensity in conjunction with a sharpening of the ring breathing mode at 1089 cm^{-1} .^{17, 34, 35} This was thought to be due to the constriction of the ring system

from polymerisation, preventing ring breathing. A new band at 663 cm^{-1} was also found, likely as a result of the formation of polymer chains formed through the 3-position of the thiophene ring.³⁷

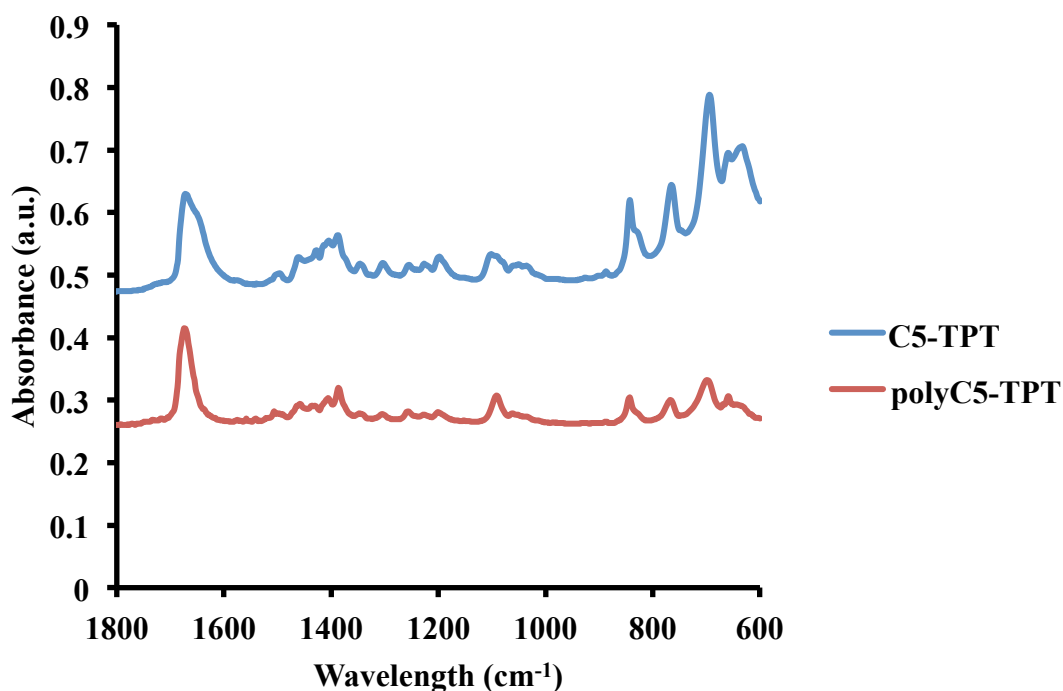


Figure 3.13. FTIR spectra ($1800 - 600\text{ cm}^{-1}$ region) of C5-TPT (blue) and polyC5-TPT (red). Bands attributed to the monomer species are shown to recede in conjunction with the appearance of new bands attributed to polymer formation. For clarity, 0.3 has been added to the absorbance values of C5-TPT

As with C5-P, and C5-TP, the most obvious indication of polymerisation is the overall reduction of absorbance with time due to the reflective nature of the conductive polymer.

The differences between the monomer units upon polymerisation may also be rationalised through other experimental observations. Upon treatment of C5-TP or C5-TPT with FeCl_3 , precipitate was formed immediately and fewer new bands were observed in the spectra than compared to C5-P, where precipitate formation took place over a longer period of time. It is considered that any steric influence exhibited by the pendant pentynyl chain is reduced by the addition of the thiophene moiety in both systems, which effectively acts as a ‘spacer’ unit facilitating enhanced access to the C2 carbons on the thiophene by reducing steric hindrance posed by the alkyne terminated carbon chain and promoting consistent formation of

longer oligomers, resulting in immediate precipitation. Polymerisation will also be influenced by the increase in energy of the HOMO and decrease in the LUMO as a result of the extended ring system, resulting a smaller band gap.³¹

3.4 Conclusions

The alkylated monomers of **C5-P**, **C5-TP** and **C5-TPT** were synthesized and characterized by ^1H NMR, ^{13}C NMR, FTIR and mass spectroscopy. A crystal structure of **TPT** was also obtained.

Characterisation of the polymer formed both chemically and electrochemically was also performed. No evidence of polymer degradation was observed by either method, indicating the stability of these materials as formed polymer. Importantly, polymerisation of all three monomers units using FeCl_3 was demonstrated; as it is the standard method for polymerisation in templating reactions.

3.5 Experimental

All chemicals were purchased from Aldrich and/or Alfa Aesar and used as received unless otherwise stated. All ^1H and ^{13}C NMR spectroscopy was performed on a 300 or 400 MHz Bruker Spectrospin. Infrared spectra were recorded on a Varian 800 FT-IR; high resolution mass spectra with electrospray ionization (HRMS-ESI) were measured on a Waters Micromass LCT Premier mass spectrometer.

3.5.1 Thiophene *N*-allylcarboxamide³¹

Thiophene carbonyl chloride (5.0 g, 34 mmol) was added to allylamine (2.5 mL, 34 mmol) in anhydrous pyridine (30 mL) under N_2 . The mixture was stirred vigorously for 24 hours. The pyridine was removed *in vacuo* with the aid of toluene affording a yellow/orange oil which was subsequently dissolved in CH_2Cl_2 and washed with water. The orange organic layer produced was dried with magnesium sulfate and the solvent removed *in vacuo* to give an orange crystalline solid (5.76 g, 34 mmol, 100%). ^1H NMR (300 MHz, CDCl_3): δ 4.08 (2H, CH_2), 5.29 (2H, m; CH_2), 5.96 (1H, quint; CH), 6.33 (1H, s; NH), 7.10 (1H, m; CH), 7.49 (1H, d; CH), 7.56 (1H, d; CH).

3.5.2 Imidoyl Chloride³¹

N-allylcarboxamide (6.93 g, 41 mmol), thionyl chloride (9 mL in 35 mL toluene) and DMF (1 mL) were combined giving a red/orange solution. The mixture was stirred vigorously for 18 hours in a closed round bottomed flask affording a red solution. The solvent was removed *in vacuo* producing an oil of yield 6.30 g, 34 mmol, 83%. ^1H NMR (300 MHz, CDCl_3): δ 4.11 (2H, t; CH_2), 5.31 (2H, m; CH_2), 5.96 (1H, m, CH_2), 7.10 (apparent t, 2H), 7.50 (d, 1H), 7.53 (d, 1H).

3.5.3 2-(2-Thienyl)-pyrrole from Imidoyl Chloride³¹

KOtBu (4.5 g, 40.2 mmol) was added to anhydrous DMF (25 mL) under nitrogen at 0 °C. A solution of imidoyl chloride (2.5 g, 13.5 mmol) in THF (15 mL) was added dropwise to the reaction mixture and left to stir for 18 hours in the dark. The brown/black solution produced was poured into iced water (500 mL) and extracted using ether. The organic solution was dried using magnesium sulphate and

concentrated to afford a dark brown solid with a black/brown oil. The crude product was purified using column chromatography (SiO₂, 80:20 hexane-EtOAc). Yielding an oil which was dried *in vacuo* (1.53 g, 10 mmol, 74%). ¹H NMR (CDCl₃): δ 6.29 (dd, 1H, CH_{py}), 6.44 (s, 1H, CH_{py}), 6.83 (s, 1H, CH_{py}), 7.03 (t, 2H, 2 CH_{th}), 7.18 (dd, CH_{th}), 8.33 (broad s, 1H, NH).

3.5.4 Preparation of 1, 4-Bis(2-thienyl)-1, 4-butanedione¹⁴

A solution of thiophene (96.1 mL, 1.20 mol) and succinyl chloride (40 mL, 0.3 mol) in dry CH₂Cl₂ (100 mL) was added to a suspension of powdered anhydrous AlCl₃ (160 g, 1.2 mol) in dry CH₂Cl₂ (150 mL) over a period of 2 hours under N₂. The temperature was maintained within 16-22 °C by cooling in ice-water and the mixture stirred vigorously for 3 hours. A green solution containing large solid pellets formed. The mixture was hydrolyzed with ice (2 kg) and conc. HCl (50 mL). The organic phase was extracted using DCM and washed with 2 M HCl, H₂O and NaHCO₃ and dried using MgSO₄. The solvent was removed *in vacuo* affording a solid which was then washed in cold EtOH (150 mL). (85.30 g, 0.34 mol, 94%). ¹H NMR (CDCl₃): δ 3.38 (s, 2H, CH), 7.13 (t, 1H, CH_{th}), 7.62 (d, 1H, CH_{th}), 7.80 (d, 1H, CH_{th}).

3.5.5 Preparation of 2,5-Di(thiophen-2-yl)-pyrrole¹⁴

1, 4-bis(2-thienyl)-1, 4-butanedione (5 g, 20 mmol) was dissolved in excess hot HOAc. NH₄OAc (38.54 g, 0.5 mol) and acetic anhydride (15.1 mL, 0.16 mol) were added and the reaction left to stir under reflux for 16 hours. After cooling to room temperature the solvent was evaporated to dryness. The green solution was neutralized using 2 M NaOH (200 mL) and the organic product extracted using CH₂Cl₂. The mixture was washed with sodium bicarbonate (excess 2x), brine (excess 1x) and dried with MgSO₄. The green solution was concentrated *in vacuo* affording a solid/oil, **TPT**, (2.46 g, 10 mmol, 53%) ¹H NMR (CDCl₃): δ 6.40 (s, 2H, CH_{py}), 7.02 (t, 2H, CH_{th}), 7.06 (apparent s, 2H, CH_{th}), 7.24 (d, 2H, CH_{th}), 8.40 (broad s, 1H, NH).

3.5.6 General procedure for Alkylation of Monomer Units using 5-Chloro-1-pentyne

A typical procedure for alkylation is given. **TP** (1.00 g, 6.80 mmol) was added to anhydrous DMF (100 mL) under nitrogen and left to stir for 20 minutes. Sodium hydride (0.55 g, 13.6 mmol) was added and the reaction mixture which was left to stir for a further 40 minutes. 5-chloro-1-pentyne (1.42 mL, 13.6 mmol) was added and the reaction mixture allowed to stir overnight. The dark brown/black solution was produced which was filtered using celite, dissolved in CH_2Cl_2 and washed with water then dried over magnesium sulphate. The product was concentrated *in vacuo* and purified by column chromatography (SiO_2 , 80:20 hexane-EtOAc), to yield an oil, **C5-TP** (0.78 g, 61%). ^1H NMR (CDCl_3): δ = 1.92 (m, 2H, CH_2), 2.03 (t, 1H, CH), 2.19 (m, 2H, CH_2), 4.19 (t, 2H, CH_2), 6.23 (m, 1H, CH_{py}), 6.36 (m, 1H, CH_{py}), 6.84 (s, 1H, CH_{py}), 7.08 (m, 2H, CH_{th}), 7.31 (m, 1H, CH_{th}). ^{13}C -NMR (CDCl_3): δ = 135.33, 127.51, 126.73, 125.93, 125.21, 123.37, 111.19, 108.49, 83.26, 69.62, 46.43, 30.36, 16.08. HRMS (ESI): m/z: calc. for $\text{C}_{13}\text{H}_{13}\text{NS}$ $[\text{M}+\text{H}]^+$: 216.0843; found: 216.0847.

C5-P: Yield: 89% as an oil. ^1H NMR (CDCl_3): δ = 1.96 (m, 2H, CH_2), 2.03 (t, 1H, CH), 2.16 (m, 2H, CH_2), 4.05 (t, 2H, CH_2), 6.16 (t, 2H, CH_{py}), 6.68 (t, 2H, CH_{py}). ^{13}C -NMR (CDCl_3): δ = 120.70, 108.45, 83.10, 69.68, 47.92, 30.38, 15.75. HRMS (ESI): m/z: calc. for $\text{C}_9\text{H}_{11}\text{N}$ $[\text{M}+\text{H}]^+$: 134.0958; found: 134.0970.

C5-TPT: Yield: 44% as a solid, mp 36-40 °C. ^1H NMR (CDCl_3): δ = 1.78 (m, 2H, CH_2), 1.86 (t, 1H, CH), 2.03 (m, 2H, CH_2), 4.28 (m, 2H, CH_2), 6.36 (s, 2H, CH_{py}), 7.11 (m, 4H, CH_{th}), 7.33 (m, 2H, CH_{th}). ^{13}C -NMR (CDCl_3): δ = 135.30, 128.84, 127.58, 126.51, 125.65, 111.53, 83.05, 69.22, 44.61, 30.12, 16.12. HRMS (ESI): m/z: calc. for $\text{C}_{17}\text{H}_{15}\text{NS}_2$ $[\text{M}+\text{H}]^+$: 298.0724; found: 298.0718.

3.5.7 General Procedure for Electrochemical Polymerisation

Cyclic voltammograms of dissolved monomers were collected on a CH Instrument Inc. electrochemical workstation 760B (using CHI Version 5.21 software). A platinum working electrode, gold counter electrode and silver quasi-reference electrode were used. All data were collected at room temperature using acetonitrile

as solvent, with 10 mM of the compound under investigation and 100 mM LiClO₄ as electrolyte.

3.5.8 General Procedure for Chemical Polymerisation

FeCl₃ (2 ml, 0.3 M) was added to a DMF/water solution (1:4) of the appropriate monomer (2 ml, 0.1 M) and left to stand until precipitate formation occurred. After which the reaction mixture was centrifuged for 10 minutes (10,000 rpm) and the remaining FeCl₃ removed. The precipitate produced was rinsed 3 times with excess nanopure water via the same method. The sample was subsequently dried in a vacuum oven (60°C) overnight.

3.5.9 Preparation of Si/SiO₂ Wafers for FTIR

N doped Si <111> wafers were sequentially cleaned using a cotton bud soaked in acetone, propanol and finally water. The wafers were then soaked in a solution of sodium dodecyl sulphate and water (0.01 g in 100 mL) and heated to 50 °C for 20 minutes after which, the wafers were sonicated in nanopure water for 10 minutes. Following a further rinse they were dried using a nitrogen stream and the wafer was placed in 'piranha solution' (4:1, H₂SO₄:H₂O₂) for 1 hour, rinsed again with nanopure water and then dried in an oven for 15 minutes.

3.5.10 Fourier Transform Infrared Spectroscopy (FTIR)

FTIR spectra (in the range 600–4000 cm⁻¹) were recorded in transmission mode with a Bio-Rad Excalibur FTS-40 spectrometer (Varian Inc., Palo Alto, CA, USA) equipped with a liquid nitrogen cooled deuterated triglycine sulfate (DTGS) detector, and were collected at 128 scans with 4cm⁻¹ resolution. All samples were prepared through drop casting of polymer solutions described in 3.4.8 onto chemically oxidized Si<n-100> substrates. Data acquisition and analysis were carried out using Digilab Merlin version 3.1 software (Varian Inc.).

3.6 References

1. M. Hamed, A. Elfving, R. Gabrielsson and O. Inganas, *Small*, 2012, **9**, 363-368.
2. X. Lu, W. Zhang and C. Wang, *Progress in Polymer Science*, 2011, **36**, 671.
3. U. Lange, N. V. Roznyatovskaya and V. M. Mirsky, *Analytica Chimica Acta*, 2008, **614**, 1-26.
4. C. M. Hangarter, M. Bangar, A. Mulchandani and N. V. Myung, *Journal of Materials Chemistry*, 2010, **20**, 3131-3140.
5. F. Garnier, H. Korri-Youssoufi, P. Srivastava, B. Mandrand and T. Delair, *Synthetic Metals*, 1999, **100**, 89-94.
6. T. Livache, B. Fouque, A. Roget, J. Marchand, G. Bidan, R. Téoule and G. Mathis, *Analytical Biochemistry*, 1998, **255**, 188-194.
7. K. K. Kanazawa, A. F. Diaz, M. T. Krounbi and G. B. Street, *Synthetic Metals*, 1981, **4**, 119-130.
8. J. Hegewald, L. Jakisch and J. Pionteck, *Synthetic Metals*, 2009, **159**, 103-112.
9. G. Zotti, S. Zecchin, G. Schiavon and L. B. Groenendaal, *Chemistry of Materials*, 2000, **12**, 2996-3005.
10. K. Zong and J. R. Reynolds, *The Journal of Organic Chemistry*, 2001, **66**, 6873-6882.
11. G. Sonmez, P. Schottland, K. Zong and J. R. Reynolds, *Journal of Materials Chemistry*, 2001, **11**, 289-294.
12. E. Rodlovskaya, N. Frolova, E. Savin and V. Nedel'kin, *Polymer Science Series C*, 2006, **48**, 58-84.
13. R. Kiebooms, R. Menon and K. Lee, in *Handbook of Advanced Electronic and Photonic Materials and Devices*, eds. N. Hari Singh, M.Sc and M. S. P. D. Ph.D.A2 - Hari Singh Nalwa, Academic Press, Burlington, 2001, pp. 1-102.
14. R. E. Niziurski-Mann and M. P. Cava, *Advanced Materials*, 1993, **5**, 547-551.
15. N. Engel and W. Steglich, *Angewante Chemie International Edition English*, 1978, **17**, 676-676.
16. P.-G. Cristina, J. A. Pomposo, J. A. Alduncin, M. Salsamendi, A. b. I. Mikhaleva, L. B. Krivdin and B. A. Trofimov, *Electrochimica Acta*, 2007, **52**, 4784-4791.
17. Z. Ping and G. E. Nauer, *Journal of Electroanalytical Chemistry*, 1996, **416**, 157-166.

18. C. Alemán, V. M. Domingo, L. Fajarí, L. Juliá and A. Karpfen, *The Journal of Organic Chemistry*, 1998, **63**, 1041-1048.
19. S. Srinivasan and G. B. Schuster, *Organic Letters*, 2008, **10**, 3657-3660.
20. M. Gerard, A. Chaubey and B. D. Malhotra, *Biosensors and Bioelectronics*, 2002, **17**, 345-359.
21. R. Huisgen, *Angewante Chemie International Edition English*, 1963, **2**, 633.
22. L. G. G. V. V. Rostovtsev, V. V. Fokin, K. B. Sharpless, *Angewante Chemie International Edition English*, 2002, **41**, 2596.
23. J.-F. Lutz, *Angewandte Chemie - International Edition*, 2007, **46**, 1018.
24. B. A. Merrill and E. LeGoff, *The Journal of Organic Chemistry*, 1990, **55**, 2904-2908.
25. A. Merz and F. Ellinger, *Synthesis*, 1991, 462-464.
26. J. P. Parakka, J. A. Jeevarajan, A. S. Jeevarajan, L. D. Kispert and M. P. Cava, *Advanced Materials*, 1996, **8**, 54-59.
27. M. L. Hallensleben, M. van Hooren and M. Peters, *Polymer Bulletin*, 1998, **40**, 167-172.
28. S. Naitoh, K. Sanui and N. Ogata, *Journal of the Chemical Society, Chemical Communications*, 1986, 1348-1350.
29. C. J. DuBois Jr and R. L. McCarley, *Journal of Electroanalytical Chemistry*, 1998, **454**, 99-105.
30. I. Rodríguez, B. R. Scharifker and J. Mostany, *Journal of Electroanalytical Chemistry*, 2000, **491**, 117-125.
31. M. Vautrin, P. Leriche, A. Gorgues and M. P. Cava, *Electrochemistry Communications*, 1999, **1**, 233-237.
32. M. A. Galindo, J. Hannant, R. W. Harrington, W. Clegg, B. R. Horrocks, A. R. Pike and A. Houlton, *Organic & Biomolecular Chemistry*, 2011, **9**, 1555-1564.
33. D. H. Williams, Fleming, Ian, *Spectroscopic Methods in Organic Chemistry*, 5th edn., McGraw-Hall, 1995.
34. D. Brezoi, *Journal of Science and Arts*, 2010, **12**, 53-58.
35. M. Omastová, M. Trchová, J. Kovářová and J. Stejskal, *Synthetic Metals*, 2003, **138**, 447-455.
36. N. V. Blinova, J. Stejskal, M. Trchová, J. Prokeš and M. Omastová, *European Polymer Journal*, 2007, **43**, 2331-2341.
37. D. Kelkar and A. Chourasia, *Macromolecular Symposia*, 2013, **327**, 45-53.

Chapter 4

DNA-Based Nanowires

4.1 Chapter Overview

Overall Goal

To use DNA-templating as a route to the formation of hybrid DNA/polymer nanowires.

Hypothesis

DNA-templating will serve as a route to the formation of 1-D hybrid DNA/polymer nanostructures based on C5-P, C5-TP and C5-TPT.

Manipulating the surface chemistries, deposition procedure and templating conditions will enable a degree of control over nanowire size and surface coverage.

Objectives

To assess the suitability of each system (C5-P, C5-TP and C5-TPT) for DNA-templating through comparison of FTIR spectra of bulk polymeric and DNA-templated materials.

To establish a fixed protocol for DNA/polymer nanowire immobilization via brief study of Si/SiO₂ surface chemistries.

Elucidate the appropriate conditions for consistent deposition of DNA-templated polymer nanowires of C5-P, C5-TP and C5-TPT onto Si/SiO₂ substrates.

4.2 Introduction

1-D nanostructures of conducting polymer nanowires have attracted significant interest due to the potential advantages of combining an organic semi-conductor with low dimensionality.¹⁻⁴ Efforts to exploit CPs include the development of new generations of solar cells,^{5, 6} rechargeable batteries,⁷ transistors,⁸ capacitors⁹ and bio/chemical sensors.^{10, 11}

With the current drive towards small-scale technologies, recent years have seen a growing emphasis placed upon the fabrication of materials with nanoscale dimensions. In particular, attention has focused on devising methods for producing highly anisotropic forms such as nanowires, nanoropes, and nanotubes.^{4, 12, 13} Nanowires are of interest as they represent the smallest structure for effective electrical charge transport and are promising for use in nanoscale electronics. However, the search for simple and efficient synthetic methods to prepare conducting polymers with deliberate control of morphologies and sizes on a large scale is still a major challenge.

Template-directed growth is the most frequently used approach for preparing such 1-D nanostructures and several different methods have been shown to be effective.¹⁴⁻¹⁶ Here, an external ‘membrane’ is used to direct the growth of the polymer into the desired architecture. As discussed in Chapter 1, a variety of alternative materials have been used to facilitate this process which can be broadly split into two categories; ‘hard’ or ‘soft’ templates. One approach is the use of naturally occurring biopolymers, such as duplex DNA, as a template.

DNA-templating has been shown to provide a practical and reproducible route to single CP nanowire formation for materials such as polyaniline,¹⁷ polypyrrole^{13, 18} and polyindole;¹⁹ with the resulting materials considered supramolecular polymers, comprising of anionic DNA and cationic conducting polymer strands.

The ability of DNA to act as a template for CPs principally arises from the complementary nature of the DNA duplex and the CP chains. DNA contains a high anionic charge, due to the phosphodiester backbone, a wealth of hydrogen bonding sites and numerous van der Waals surfaces in the grooves of the duplex. The general class of CPs derived from aromatic heterocyclic systems, such as pyrrole, are

formed in their conducting cationically charged form through oxidative polymerization and also tend to have a significant capacity for hydrogen bonding. Such molecules interact with the different proton donors and proton acceptors of the base-pairs that are exposed to solution at the major and minor grooves (Figure 4.1).

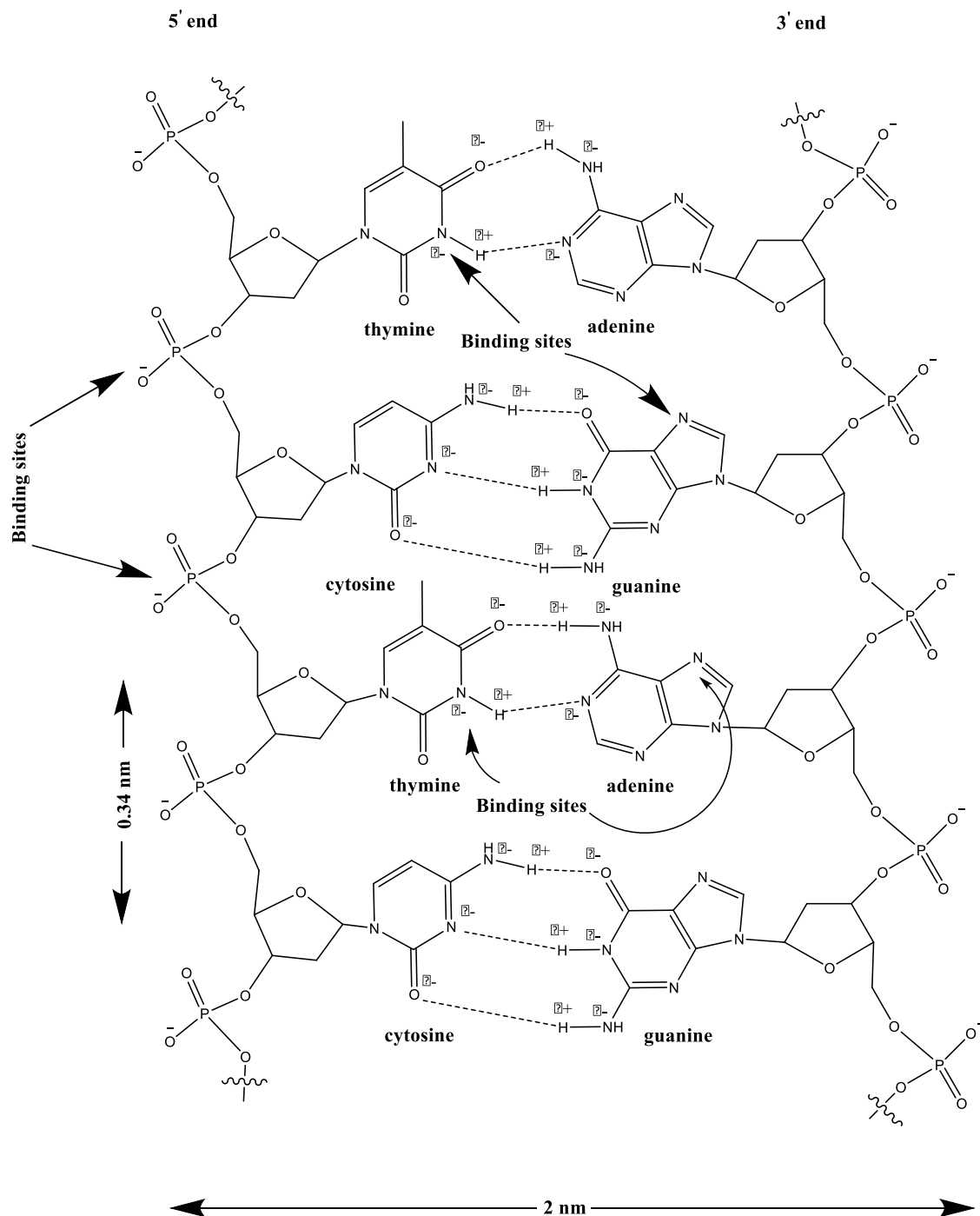


Figure 4.1. Recognition groups in the major and minor grooves of dsDNA. Redrawn from reference²⁰

Hence electrostatic attraction between the growing cationic CP and the anionic DNA template, allied with additional non-covalent interactions, provide an effective means by which the CP growth is affected.

The use of DNA to direct the growth of polyC5-**P**, polyC5-**TP** and polyC5-**TPT** into 1-D nanostructures presents an interesting challenge. While each of these CP systems can interact with the DNA-template electrostatically, the number and strength of hydrogen bonding interactions that can be envisaged between DNA and each of these systems is reduced compared to materials such as polypyrrole (Figure 4.2, a)).

Figure 4.2 shows the chemical structure of each system under investigation. In the case of polyC5-**TP** (Figure 4.2, c)) and polyC5-**TPT** (Figure 4.2, d)), strong hydrogen-bond donor sites (NH) are replaced by relatively weak acceptor sites (-S-), as a result of alkylation at the *N*-position. With polyC5-**P** (Figure 4.2, b)), no hydrogen bonding sites remain. This could be expected to have a detrimental effect on DNA-templating; as such these novel polymer systems may less well-suited materials for nanowire formation by this method.

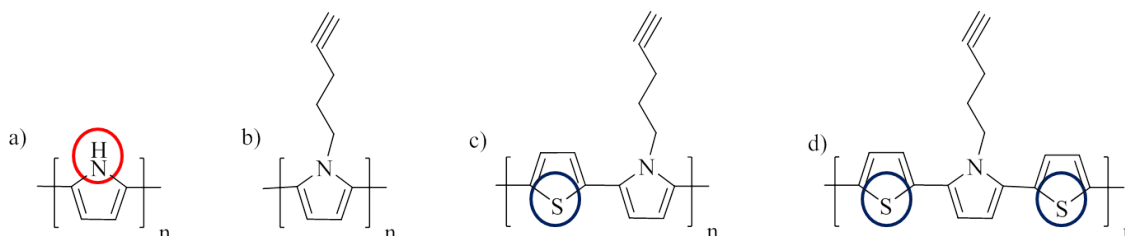


Figure 4.2. Hydrogen bonding sites available in a) polypyrrole; b) polyC5-**P**; c) polyC5-**TP** and d) polyC5-**TPT**. These have quite different hydrogen bonding capabilities, the red circle indicates strong (NH) hydrogen-bond donor sites while blue circle denotes relatively weak acceptor sites (-S-)

Silicon/Silicon Dioxide (Si/SiO₂) Substrates

In order to gather topographical and electrical data (Chapter 5) pertaining to DNA-templated polymer nanowires of polyC5-**P**, polyC5-**TP** and polyC5-**TPT** by scanning probe microscopy (SPM), it was necessary to first immobilize the samples onto a suitable substrate. As a high-quality electrical insulator, silicon dioxide is used extensively as a barrier for electrical isolation of semiconductor devices. Moreover, the silicon dioxide layer produced from thermal oxidation is relatively flat. These two characteristics, combined with the ability to tune the surface

properties have made Si/SiO₂ the preferred substrate on which to examine DNA/polymer nanowires.^{18, 21, 22}

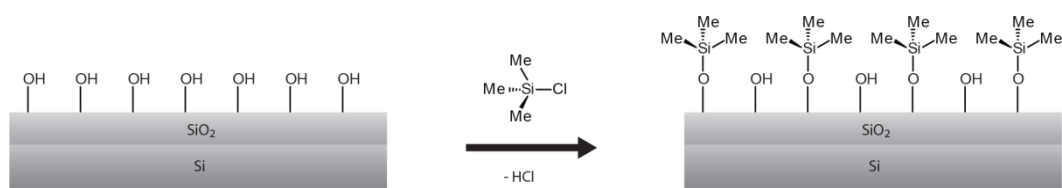
Si/SiO₂ wafers are typically produced through the thermal oxidation of silicon with a native oxide layer at ~1200 °C. At this temperature, oxygen combines with silicon at the surface to form a thicker oxide layer. Subsequent exposure to moisture in the air produces a partial hydroxyl terminated surface (Scheme 4.1).

Three different types of Si substrates were used during this project according to the purpose of the sample. Si<111> was employed for gathering topographical information while substrates with thicker oxide layers (*ca.* 200 nm), which screen electronic charge more effectively were used for electrical characterization (Chapter 5).

Substrate Surface Modification

The formation of siloxane bonds with appropriately functionalised chlorosilane (-SiCl₃) head groups enables the tuning of surface hydrophobicity and the coupling of a wide range of desired entities to Si/SiO₂ surfaces.²³ The quality of the monolayer produced is highly dependent upon the temperature and moisture content of the reagents used.²⁴⁻²⁶ However, the broad surface modification afforded provides the level of control required for this work. Furthermore, unlike Langmuir-Blodgett films,²⁷ the robust nature of the Si-O-Si-C bound layers make the monolayers significantly stable.

The effective deposition and alignment of DNA-based nanowires onto Si/SiO₂ surfaces is highly dependent upon the hydrophobicity of the substrate surface; hydrophilic surfaces such as freshly cleaved mica and silicon dioxide have been shown to cause nanowires to coil up or align in random directions.¹³ In the case of silicon dioxide, treatment with chlorotrimethylsilane (TMS, Scheme 4.1) modifies the surface with methyl groups, producing a hydrophobic surface which reduces surface interactions with the hydrophilic nanowires. A fine balance must be found in order to enable an appropriate surface density to allow inspection of individual nanowires.



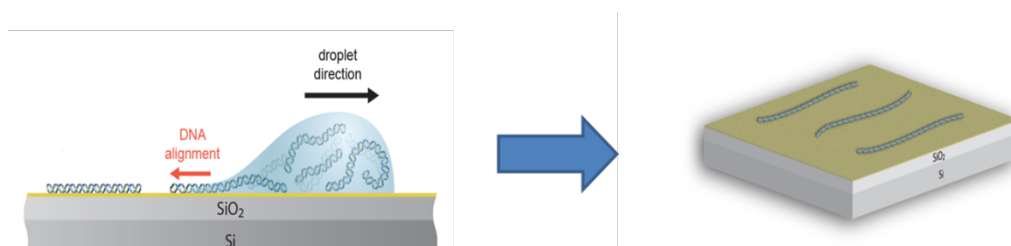
Scheme 4.1. Surface modification of Si/SiO₂ surfaces with TMS in order to facilitate molecular combing²⁸

As such, Si/SiO₂ surface modification with chlorotrimethylsilane served two purposes in this project; firstly, allowing for nanowire alignment and secondly to enable an appropriate surface density to allow inspection of individual nanowires.

DNA and Nanowire Alignment

A fundamental requirement for the characterization and eventual integration of nanowires into the circuitry of many applications is the development of cost effective and reproducible methods for nanowire deposition/alignment. One approach is to essentially make use of the fluid and surface tension forces of the solution to elongate nanowires or DNA onto a surface. This approach forms the basis of methods such as continuous flow or spin coating²⁹⁻³², molecular combing^{33, 34} and electronic field alignment³⁵, which have previously been shown to facilitate reproducible alignment of nanowires or DNA onto silicon oxide and mica.

Methods most applicable to this work are molecular combing and spin coating, largely due to the simplicity and cost effectiveness. First developed by Bensimon *et. al.*³⁴, molecular combing involves the direct manipulation of a drop of solution, with the alignment of the DNA/nanowires perpendicular to the receding meniscus of the solution through movement of the droplet (Scheme 4.2).



Scheme 4.2. An illustration of DNA alignment across Si/SiO₂ surfaces using molecular combing²⁸

Spin-coating of DNA was first demonstrated by Ye *et. al.*³⁰ onto mica. Treatment of the surface with a cationic dye molecule induced a strong adhesion force between DNA and the substrate. Subsequent spinning of the sample provided an elongation force in the form of fluid flow, stretching the DNA across the mica surface. This method was extended to silicon oxide surfaces pre-treated with cationic polyelectrolyte by Yokota *et. al.*³¹ when examining the surface morphology of cellulose films.

In this Chapter, as with previous related work,^{13, 18, 36} molecular combing was the primary method for immobilization of DNA and DNA/polymer nanowires onto Si/SiO₂ surfaces, with spin-coating employed only when molecular combing proved unsuccessful.

Chapter Outline: *In an effort to explore DNA-templating as a route to the formation of 1-D nanostructures using the novel polymeric materials described, this chapter presents studies assessing the suitability of each system, C5-P, C5-TP and C5-TPT, for DNA-templating through comparison of FTIR spectra of bulk polymeric and DNA-templated materials. Also presented in this chapter is characterization of DNA-templated polymer nanowires of polyC5-P, polyC5-TP and polyC5-TPT by atomic force microscopy (AFM).*

4.3 Results and Discussion

4.3.1 Large Scale DNA-Templating

Hypothesis: Interaction between DNA and polymeric materials (DNA-templating) will be evident by the appearance of new bands and shifts in the Fourier Transform Infra-Red spectra of DNA-templated materials when compared to spectra of bulk polymeric material and DNA respectively.

In order to establish the feasibility of polymer nanowire formation by DNA-templating of the monomer units described, large scale reactions were first attempted. This was useful as it enables the use of Fourier Transform Infra-Red spectroscopy (FTIR) to characterize the hybrid materials produced. Typically, a 0.1 M solution of monomer in DMF (1 mL) was added to an aqueous mixture of calf thymus DNA (CT-DNA), 40 $\mu\text{g mL}^{-1}$ (1 mL) and 0.5 M MgCl_2 (1 mL). 0.1 M aqueous FeCl_3 (1 mL) as an oxidant was added to begin polymerisation. A silicon chip, cut to *ca.* 1 cm^2 , was deposited in the reaction mixture and left for 8 hours. Subsequently, the chip was removed, dried in a vacuum oven (25 °C) rinsed with nanopure water and dried again.

Spectra of the isolated DNA/polyC5-**P** material provided evidence of the formation of a supramolecular polymer structure containing both DNA and polyC5-**P** (Figure 4.3, green). The presence of the polyC5-**P** in the material was evident from the bands attributed to the alkane C-H asymmetric and symmetric vibrations (2924 cm^{-1} , 2854 cm^{-1}) and the weak alkyne stretch at 2086 cm^{-1} .³⁷ The position of these bands were observed to be shifted to lower wavenumbers relative to the corresponding stretches in the spectrum of polyC5-**P** (2958 cm^{-1} , 2868 cm^{-1} and 2156 cm^{-1} respectively, Figure 4.3, red), suggesting that interaction with the CT-DNA was taking place.¹⁸ Unfortunately, bands pertaining to alkyne and aromatic C-H vibrations were masked by the broad O-H stretch of water trapped in the DNA.

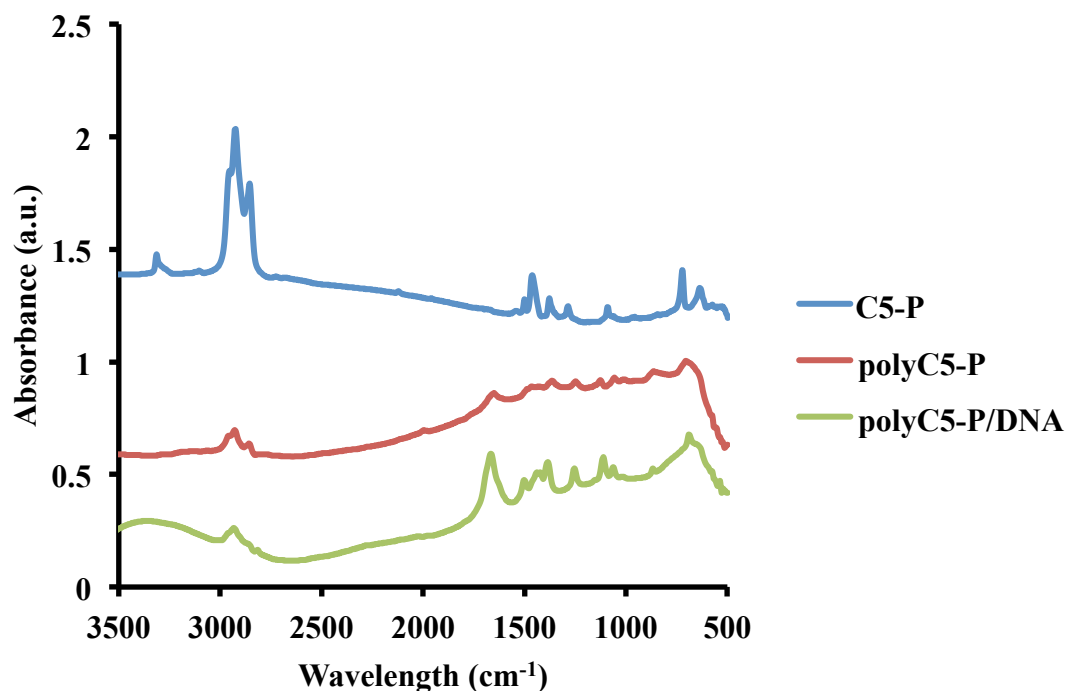


Figure 4.3. FTIR spectra of (blue) C5-P, (red) polyC5-P and (green) polyC5-P/DNA. For clarity, absorbance values have been altered to stack plot the spectra

Similar effects were observed throughout the spectrum, with the majority of the bands shifted to a lower wavenumbers (Appendix). Comparison with the spectra of free DNA (Figure 4.4) also provided evidence that the hybrid material was not a simple mixture of DNA and polyC5-P, but that an intimate interaction between the two polymer types existed. For example, bands at 1496 cm^{-1} and 995 cm^{-1} corresponding to ring vibration of cytosine/guanine and the C-O deoxyribose stretch in CT-DNA were observed and shifted to lower wavenumbers (normally 1487 cm^{-1} and 962 cm^{-1} respectively).^{38,39} Bands corresponding to phosphate groups (1077 cm^{-1} and 1253 cm^{-1}) were not visible; consequently any interaction could not be directly elucidated.

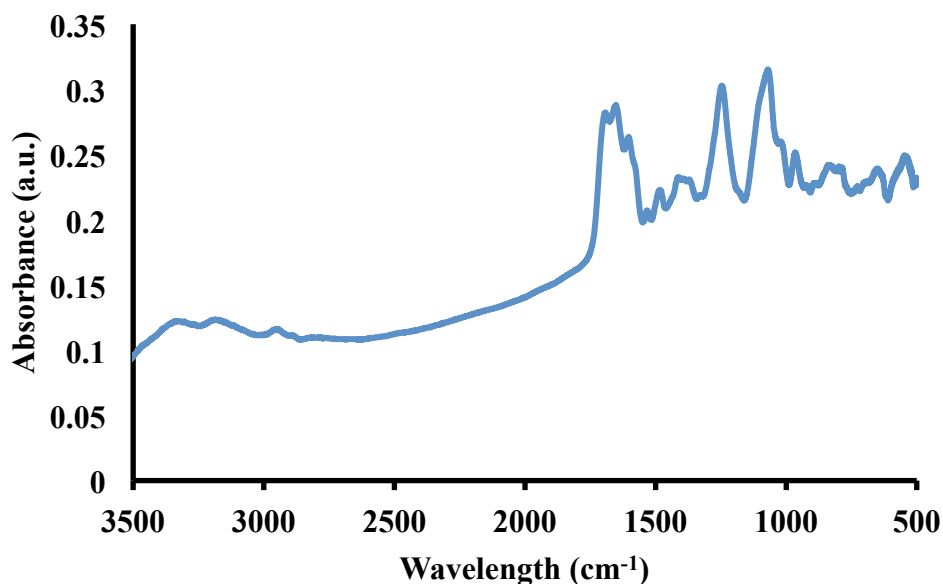


Figure 4.4. FTIR spectra of CT-DNA

Similar observations were made for the isolated DNA/polyC5-**TP** material (Figure 4.5, green). As with DNA/polyC5-**P**, templated material showed that the majority of bands were shifted to higher wavenumbers; with the presence of the polyC5-**TP** in the hybrid material evident from absorptions in the 3500 – 2800 cm⁻¹ region (Appendix). Bands attributed to the alkyne, aromatic C-H stretches/vibrations (3302 cm⁻¹, 3107 cm⁻¹ and 2955 cm⁻¹ respectively) of the C5-**TP** monomer units were observed to be shifted to higher wavenumber relative to the corresponding stretches in the spectrum of polyC5-**TP** (3283 cm⁻¹, 3097 cm⁻¹ and 2929 cm⁻¹ (Figure 4.5, blue and red respectively, Chapter 3).

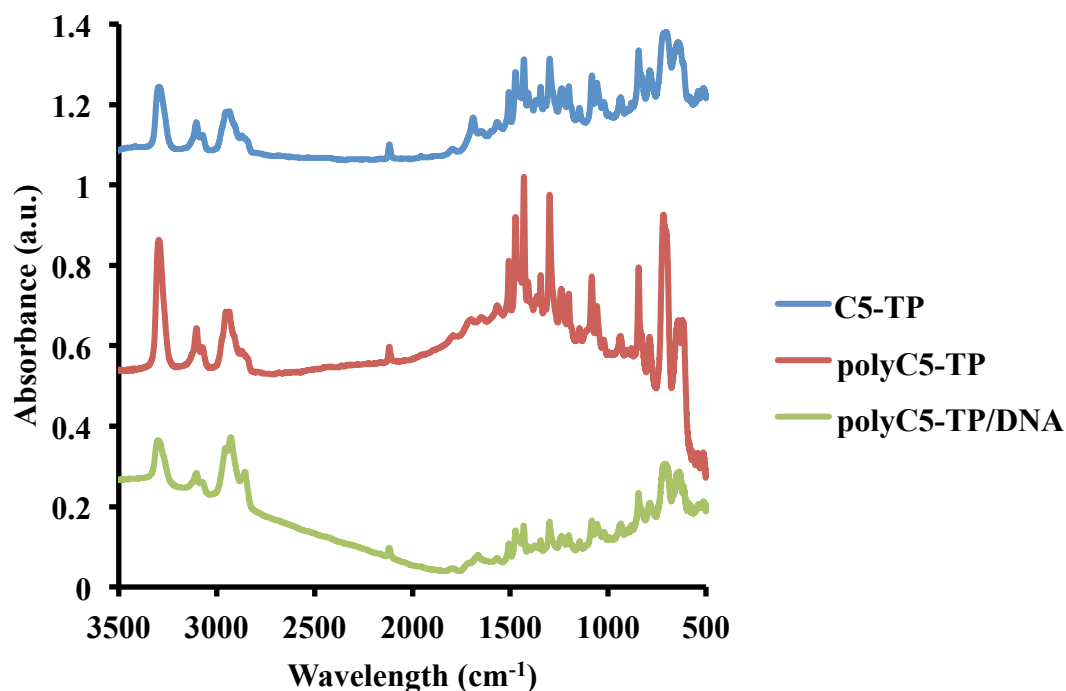


Figure 4.5. FTIR spectra of C5-TP (blue), polyC5-TP (red) and DNA/polyC5-TP (green). For clarity, absorbance values have been altered to stack plot the spectra

Unlike the DNA/polyC5-P hybrid material, the broad band centred at *ca.* 3300 cm^{-1} in DNA due to O-H stretching vibrations from bound to water molecules was markedly reduced in intensity in the DNA/polyC5-TP sample; likely as a result of displacement of the DNA bound water by the hydrophobic polymer chains. Whilst the bands corresponding to phosphate groups (1077 cm^{-1} and 1253 cm^{-1}) were not visible, the characteristic bands at 1723 cm^{-1} and 1674 cm^{-1} corresponding to C=O stretching of nucleobases in CT-DNA were observed and were shown to have shifted to a higher wavenumber (normally 1705 cm^{-1} and 1658 cm^{-1} respectively).^{39,}

40

In the case of DNA/polyC5-TPT, the most notable effect on the spectra upon templating was an increase in absorbance and sharpening of the alkyne stretch at 2117 cm^{-1} (Figure 4.6, green).³⁷ Both polyC5-TP and polyC5-TPT possess unsymmetrical alkynes, however only exhibit weak absorbance at *ca.* 2100 cm^{-1} . The significant increase in the dipole required to cause such a change in intensity, as seen with polyC5-TPT, suggests a stronger electrostatic interaction between polyC5-TPT and DNA taking place.

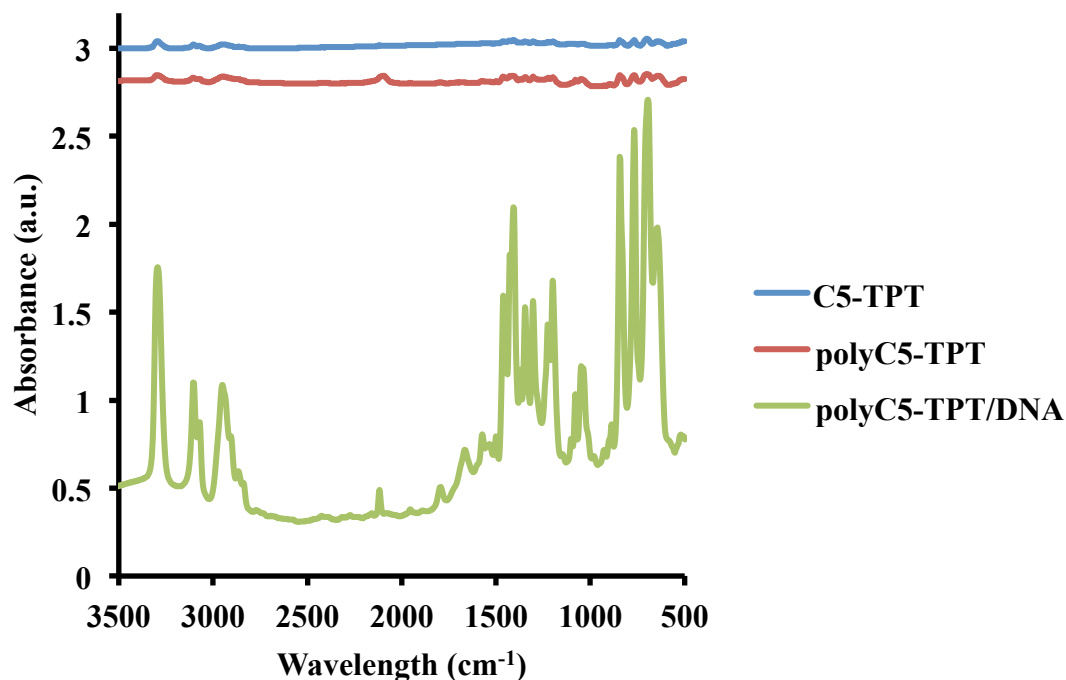


Figure 4.6. FTIR spectra of C5-TPT (blue), polyC5-TPT (red) and DNA/polyC5-TPT (green). For clarity, absorbance values have been altered to stack plot the spectra

As with DNA/polyC5-P and DNA/polyC5-TP, isolated DNA/polyC5-TPT material provided evidence of supramolecular polymer formation through the majority of bands being shifted to higher wavenumbers (Appendix). The presence of polyC5-TPT was again confirmed through bands attributed to the alkyne, aromatic and alkene C-H (3282 cm^{-1} , 3101 cm^{-1} , 3070 cm^{-1} and 2939 cm^{-1} respectively, Chapter 3). Notable shifting of bands attributed to C=O stretch of cytosine/thymine, PO_2^- asymmetric stretch and C-O deoxyribose stretch were also observed (1653 cm^{-1} to 1658 cm^{-1} , 1102 cm^{-1} to 1110 cm^{-1} and 962 cm^{-1} to 975 cm^{-1} respectively).³⁹

These studies confirm that despite the reduction in strong hydrogen-bond donor sites (NH), as a result of alkylation at the *N*-position, polymeric C5-P, C5-TP and C5-TPT are suited to nanowire formation via DNA-templating.

4.3.2 Si/SiO₂ Surface Modification

Hypothesis: By standardizing cleaning and surface modification protocols for Si/SiO₂ chips, a reproducible level of surface wettability will be attained.

As described earlier, effective deposition and alignment of DNA-based nanowires onto Si/SiO₂ surfaces is highly dependent upon the hydrophobicity of the substrate

surface.¹³ Treatment of silicon dioxide with chlorotrimethylsilane (TMS, Scheme 4.1) modifies the oxide surface to produce a surface layer presenting methyl groups to afford a hydrophobic surface. This reduces the surface interactions with the hydrophilic nanowires.

Previous work with DNA-templated polypyrrole nanowires¹³ has shown exposure to TMS for 20 minutes affords a contact angle of 60-70° which facilitates molecular combing and the desired level of surface adhesion of DNA/PPy nanowires. Contact angles greater than 70° were shown to prevent both DNA and nanowire adhesion, while values below 60° result in wholesale deposition of material.

In order to gain relative control over the density of nanowires on the surface, initial work focused upon determining the contact angle and therefore hydrophobicity of the silicon surface after exposure to chlorotrimethylsilane vapour. Figure 4.7 shows the change in contact angle for a droplet of nanopure water deposited onto Si<111> substrates with varied TMS exposure time (averaged over three data sets with four values in each).

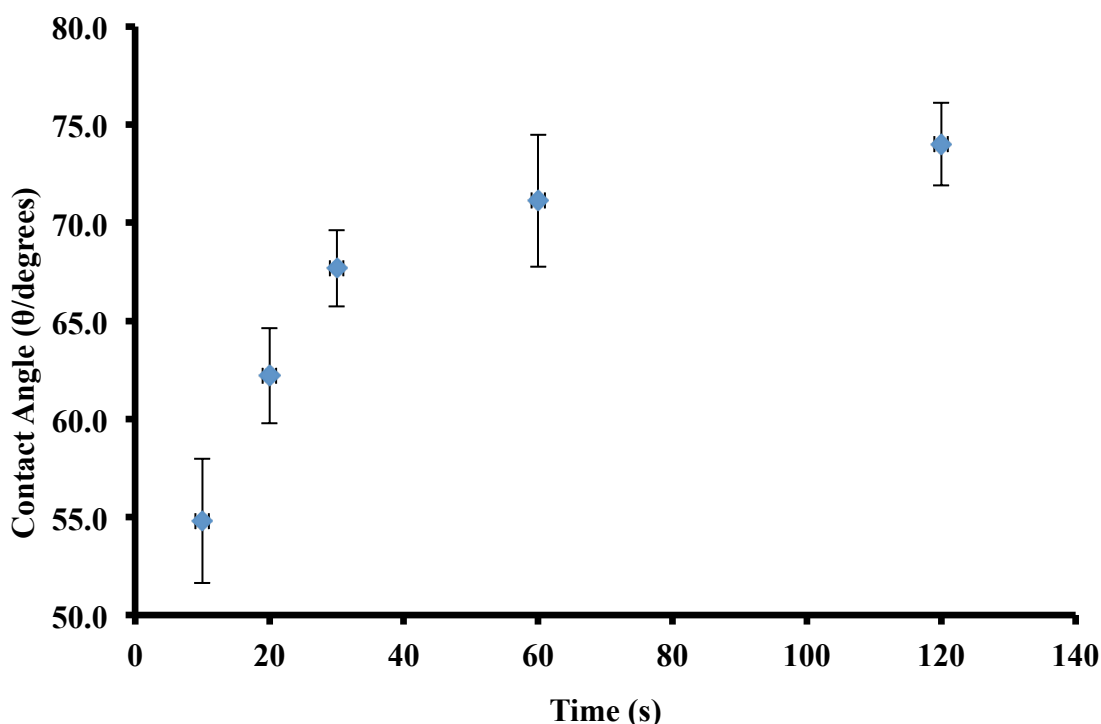


Figure 4.7. Contact angle variation with exposure of Si/SiO₂ surfaces to TMS vapour

Clearly, the contact angle significantly increases initially and then plateaus after ~20 seconds exposure. The data shows that at these shorter exposure times (20-60 seconds), it is considered that only a fraction of the surface is modified and the

optimum contact angle falls (60-70°) well within the error range.¹³ With longer exposure times (>60 seconds), it would seem the entire surface is modified, promoting discrimination against DNA/nanowire adhesion. The longer exposure times employed by comparison to results shown here are thought to be due to the alternative surface cleaning method employed.

4.3.3 Nanowire Formation and Deposition

Hypothesis: DNA-templating will serve as a route to the formation of 1-D hybrid DNA/polymer nanostructures based on C5-**P**, C5-**TP** and C5-**TPT**.

When implementing consistent deposition and surface modification procedures, a degree of reproducibility over the size and morphologies of nanowires immobilized from solution can be attained through tuning the incubation time and monomer/DNA concentrations of templating reactions.

Preparation of DNA/polymer nanowires of C5-**P**, C5-**TP** and C5-**TPT** was broadly similar to those previously reported for comparable systems.^{13, 18} However, as the monomers for C5-**TP** and C5-**TPT** are not water soluble, modification of the procedure was required whereby the reaction medium was a solvent mixture (H₂O:DMF) rather than pure water. In the case of each system, the monomer unit was introduced into the aqueous DNA solution containing MgCl₂ (0.5 mM), giving a 5:1 H₂O/DMF final ratio. Polymerisation was induced using an aqueous solution of FeCl₃ as previously described (Chapters 1 and 3).

Atomic force microscopy (AFM) was used to probe the size and morphology of the polymer/DNA structures immobilized on TMS-modified Si/SiO₂ <111> substrates using deposition techniques described earlier (Chapter 2). TMS incubation times elucidated in Section 4.3.2, were used throughout.

DNA/polyC5-**P** Nanowires

During studies to elucidate the appropriate conditions to obtain the single DNA/polyC5-**P** nanowires, the importance of tuning the incubation time with monomer unit and DNA concentrations to find an agreeable balance between non-specific deposition, rope formation and nanowire coverage was clearly evident. It would seem that when high concentrations of monomer (500 μM), DNA and/or

extended incubation times are employed, polymerisation is no longer directed along the duplex in a linear fashion but instead DNA/polymer simply aggregates in an uncontrolled manner, similar to condensation of DNA by multivalent cations and cationic polymers.⁴¹ Giving rise to a greater degree of height variation in addition to difficulties during nanowire deposition.

For example, when 500 μM of C5-P monomer unit was employed ($\sim 80 \mu\text{g mL}^{-1}$, 1.5 hour incubation, 0.5 mM MgCl_2 , 1 mM FeCl_3), significant deposition of non-templated material was observed (Figure 4.8). These large features were considered to be aggregates or bundles of polymer/DNA or non-templated polymer, the formation of both promoted by the high C5-P concentration.

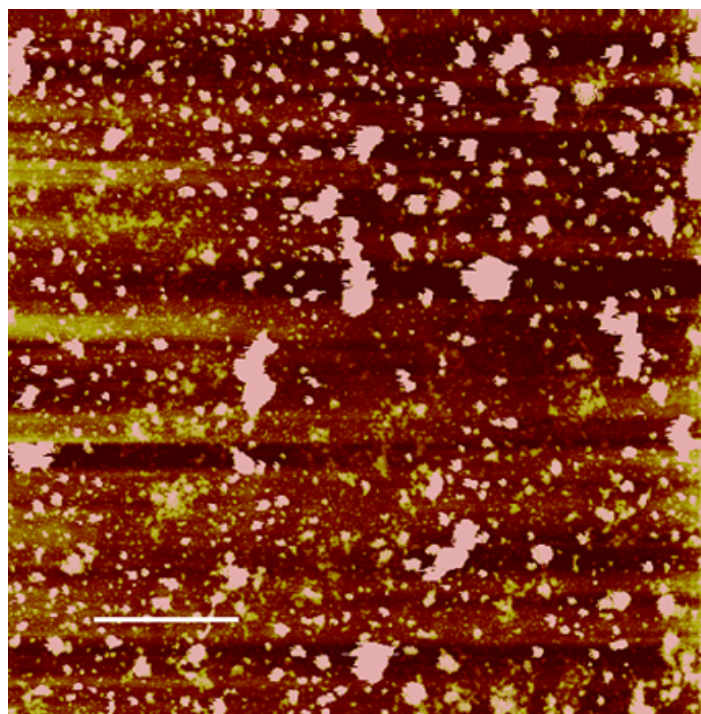


Figure 4.8. DNA/polyC5-P on silanised silicon $\langle 111 \rangle$ surface, scale bar = 4 μm , z-scale range 0- 20 nm dark to bright contrast, (0.5 mM C5-P, DNA $\sim 80 \mu\text{g mL}^{-1}$, 0.5 mM MgCl_2 , 1 mM FeCl_3 , incubated for 1.5 hours

At incubation times beyond 1.5 hour while implementing a lower concentrations of C5-P (300 μM), rope formation was clearly evident (Figure 4.9). In each case, typically thicker wires ($>10 \text{ nm}$) were produced with greater height variations along the length of individual structures (for example, up to 5.0–15.0 nm, Figure 4.11, black arrow 60.0 nm, green arrow 29 nm and white arrow 48.0 nm).

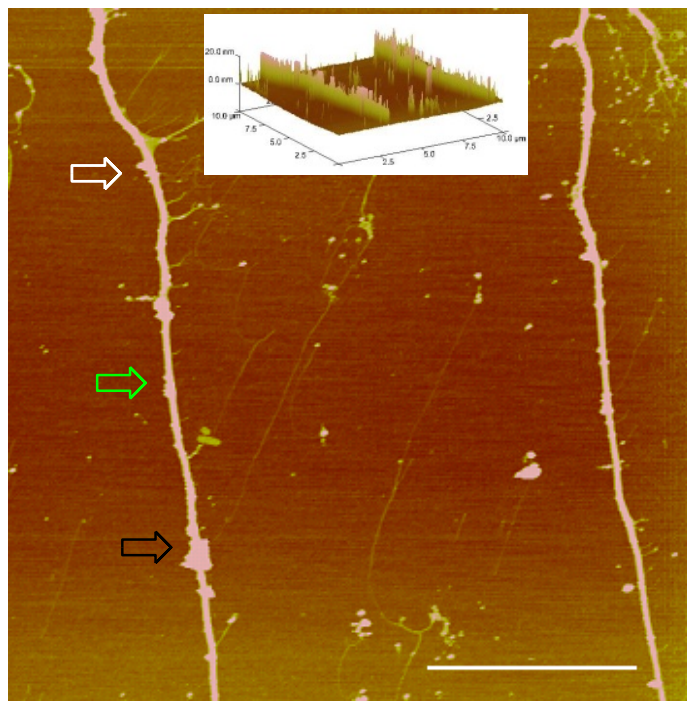


Figure 4.9. DNA/polyC5-P nanowires aligned on silanised silicon <111> surface, scale bar = 3 μm , z-scale range 0- 20 nm dark to bright contrast, DNA $\sim 80 \mu\text{g mL}^{-1}$, 0.5 mM MgCl_2 , 1 mM FeCl_3 , incubated for 2 hours

Significantly increasing DNA concentration above $\sim 80 \mu\text{g mL}^{-1}$ to $500 \mu\text{g mL}^{-1}$, had a similar effect, with larger wires/ropes being consistently observed (Figure 4.10). Successful deposition in this case was only achieved when the spin-coating method of nanowire immobilization was employed.

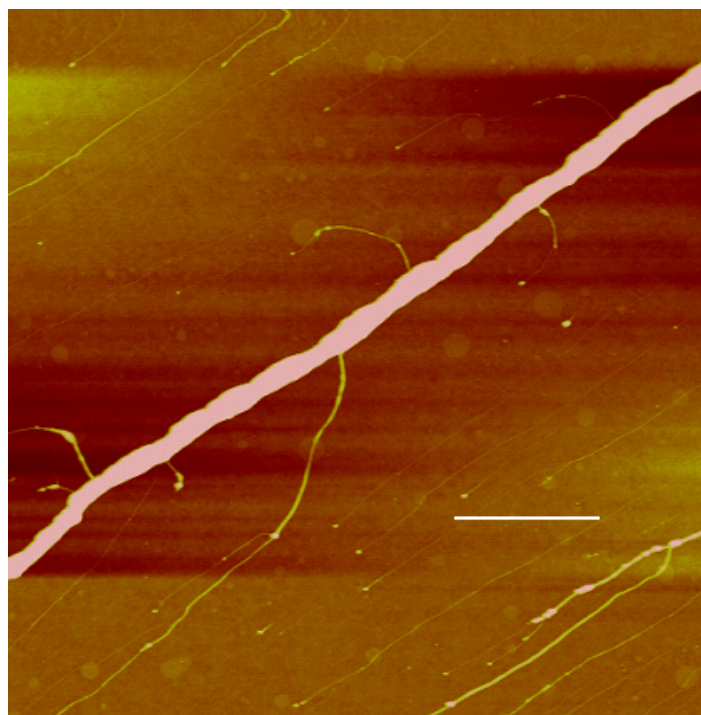


Figure 4.10. An AFM image of DNA/polyC5-P drop cast onto Si/SiO₂, height average 65.2 nm, the scale bar = 2 μm , z-scale range 0- 10 nm dark to bright contrast, 500 $\mu\text{g ml}^{-1}$, 1.5 hour incubation, 0.5 mM MgCl₂, 1 mM FeCl₃. Demonstrating the ability of this approach to deposit large wires/ropes and the effect of DNA concentration on rope formation

Samples isolated after 1.5 hour reaction time revealed successful templating of well-aligned, individual wires with regular coverage (Figure 4.11) extended across the substrate. The material isolated from the reactions was also shown to contain both a small number of bare CT-DNA strands (white arrow), indicating that not all of the CT-DNA in the reaction is involved in templating. The nanowire also appears continuous and quite smooth in comparison to DNA-templated metal-based materials (black arrow).⁴² The inset illustrates a surface plot, highlighting the height variation along the DNA/CP nanowire. This was quantified further by calculating the standard deviation of the mean nanowire diameters which was found to consistently fall within a range of 2.7–5.5 nm.

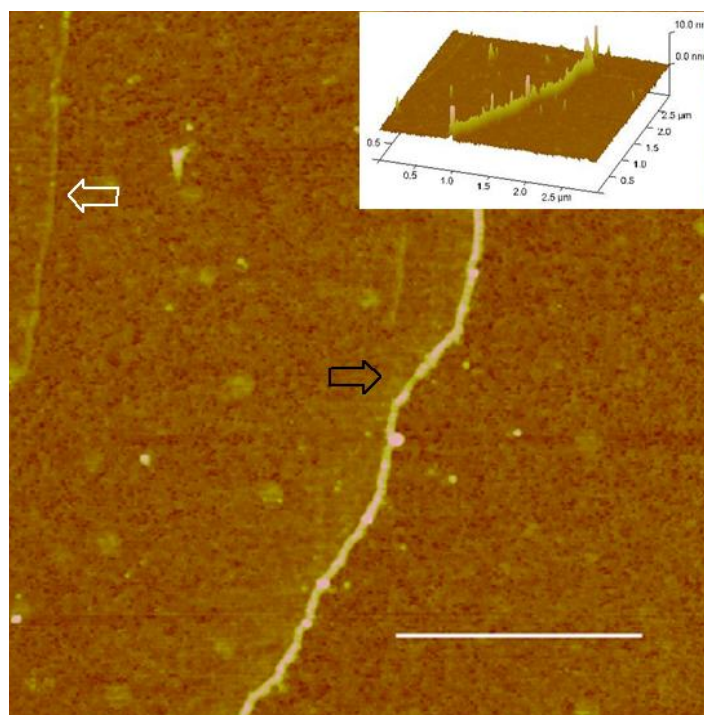


Figure 4.11. DNA/polyC5-P stretched on silanised silicon <111> surface, scale bar = 1 μm , z-scale range 0- 10 nm dark to bright contrast. 300 μM C5-P, DNA $\sim 80 \mu\text{g mL}^{-1}$, 1.5 hour incubation, 0.5 mM MgCl_2 , 1 mM FeCl_3

Further statistical treatment carried out on 100 DNA/polyC5-P nanowires over 5 samples reveals the distribution of the mean diameters, with a modal diameter of 4.0–5.0 nm when employing the specified conditions (Figure 4.12). A small number of larger structures were also observed with diameters >10 nm. These structures are attributed to the ‘bundling’ of DNA/polyC5-P structures into larger rope-like assemblies formed in the solution. Bare DNA was omitted from this study by ignoring structures which heights fell below 2.0 nm.

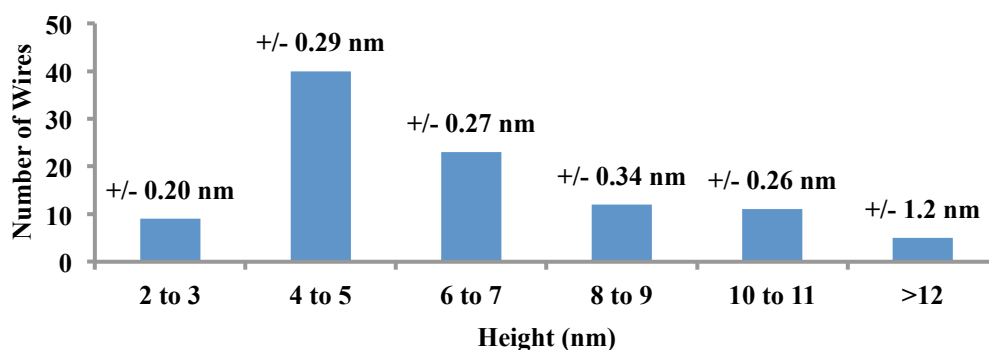


Figure 4.12. A histogram displaying the mean diameters of 100 DNA/polyC5-P nanowires. The standard deviation for each data set is displayed above the relevant column

In summary, these findings demonstrate that despite the removal of hydrogen bonding interactions between DNA and polyC5-**P**, thought to be a key requirement of DNA-templating (Section 4.2), this approach remains a viable route to nanowire formation.

Moreover, in order to successfully form and align single nanowires on the substrate an agreeable balance between concentrations and incubation time must be reached. Several parameters have been shown to significantly affect both nanowire dimensions and the ability to deposit such wires on the surface. As a consequence, the ability exhibit a degree of control over the size and number of nanowires immobilized on the surface through appropriate tuning of the conditions seems possible. However, it is noted, that such observations are also a function of the specific surface chemistries, deposition procedure and imaging in relatively the same area of the deposition pathway in each experiment (Chapter 2). It is unlikely that the remaining nanowires in the templating solution are all of the same dimensions. What has been observed is the preferential adhesion of nanowires of a particular size due to the hydrodynamic sheer forces at different locations within the droplet as it is being combed. Tuning the templating conditions merely provides the point at which the templating reaction is compatible with the surface chemistries/deposition procedure. As such, complete reproducibility and control over nanowire dimensions remains difficult.

DNA/polyC5-TP Nanowires

Successful synthesis and deposition of well-aligned, individual wires was also achieved with polyC5-**TP**. Figure 4.13 is a typical AFM image of polyC5-**TP** nanowires prepared using similar conditions to those employed for polyC5-**P** (~80 $\mu\text{g mL}^{-1}$ CT-DNA, 1.5 hour incubation, 0.5 mM MgCl_2 and 1 mM FeCl_3) however using a much lower monomer concentration (C5-**P** 300 μM and C5-**TP** 30 μM). The inset illustrates a surface plot, highlighting the height variation along the DNA/polyC5-**TP** nanowire. This was quantified further by calculating the standard deviation of the mean nanowire diameters which in this case was found to consistently lie within a range of 3.1 –7.6 nm. The material isolated from the templating reactions was also shown to contain both a small number of bare DNA strands (white arrow), again indicating that not all the DNA in the reaction is

involved in templating, while the beginnings of rope formation were also evident, indicated by the frayed strands protruding from the nanowires shown.

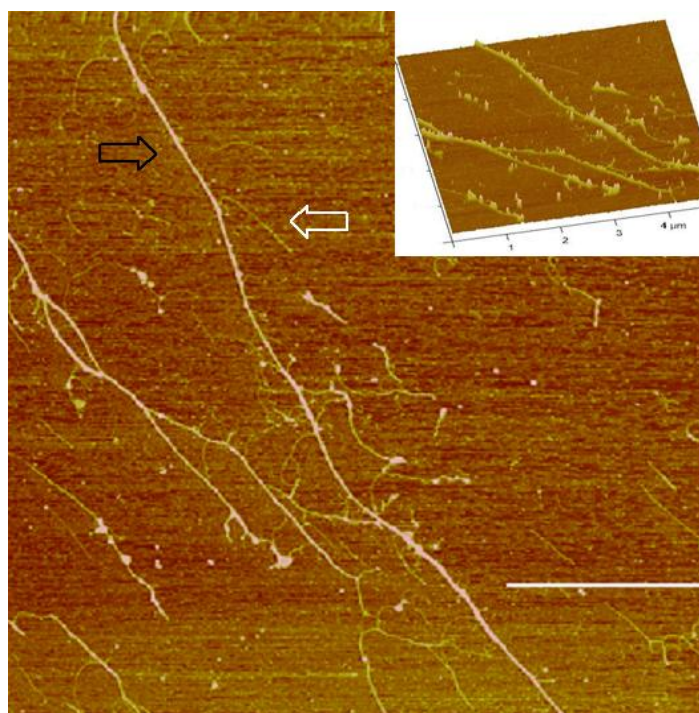


Figure 4.13. DNA/C5-**TP** stretched on silanised silicon <111> surface, scale bar = 3 μm , z-scale range 0- 10 nm dark to bright contrast. 30 μM C5-**TP**, $\sim 80 \mu\text{g mL}^{-1}$ CT-DNA, 2 hour incubation, 0.5 mM MgCl_2 and 1 mM FeCl_3

In the synthesis of DNA/polyC5-**TP** nanowire a lower concentration of monomer unit was employed than in the synthesis of DNA/polyC5-**P** nanowire (30 μM compared to 300 μM) with a longer incubation period implemented (2 hours compared to 1.5 hour). These alternative conditions were used in order to mitigate against aggregation of polyC5-**TP** impeding both nanowire synthesis and deposition.

This strategy was effective in that, over longer incubation times (Figure 4.14, right, 3 hours) nanowires could still be observed on the surface unlike with DNA/polyC5-**P**. However, aggregation in the templating solution was still evident and rope formation at these time-frames was also observed in addition to significant height variation along the wires (Figure 4.14., right, 2.1-15.4 nm of image shown).

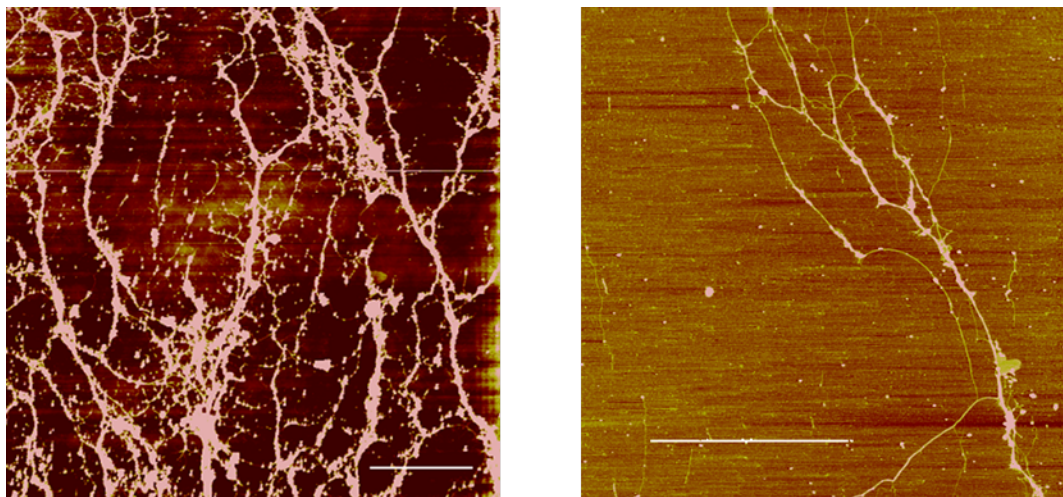


Figure 4.14. DNA/C5-TP stretched on silanised silicon <111> surface, scale bar = 4 μm , z-scale range 0- 20 nm dark to bright contrast, left, 0-10 nm, right. Left; demonstrates the effect of increasing monomer concentration (500 μM C5-TP, DNA $\sim 80 \mu\text{g mL}^{-1}$, 2 hour incubation). Right; indicates the formation of ropes at incubation times of 3 hours with reduced monomer concentrations (30 μM C5-TP, DNA $\sim 80 \mu\text{g mL}^{-1}$, 3 hour incubation)

This greater degree of height variation was reflected in the statistical treatment carried out on DNA/polyC5-TP nanowires. Nanowires prepared using the conditions described in Figure 4.14 revealed a modal diameter of 8.0–14.0 nm; far greater than that observed in DNA/polyC5-P. This was considered to be due to the greater degree of aggregation and non-specific deposition as described previously.

As described in Chapter 3, the addition of the thiophene moiety in the C5-TP monomer unit is considered to promote polymerisation by reducing the steric influence of the alkynyl chain, this is further supported by the successive reduction in oxidation potential of each monomer unit. These characteristics are thought to promote the aggregation of DNA/polymer in the templating solution in the respect that more polyC5-TP will be produced over a shorter space of time by comparison to polyC5-P and hence lower monomer concentrations were employed in order minimize these effects.

DNA/polyC5-TPT Nanowires

DNA-templated nanowires of C5-TPT were prepared in an optimized fashion similar to both DNA/polyC5-P and DNA/polyC5-TP. However, in order to achieve similar architectures, the concentration of the monomer unit was required to be

significantly reduced by comparison ($10\ \mu\text{M}$). Figure 4.15 is a typical AFM image of nanowires (black arrow) prepared over an incubation time of 1.5 hour.

As with DNA/polyC5-**P** and DNA/polyC5-**TP**, the material isolated from the templated reactions was also shown to contain bare DNA strands (white arrow), indicating that not all the DNA in the reaction is involved in templating. One of the significant features of the wires produced was the uniform coverage of the DNA with polymer with only a small height deviation typically found along each wire, illustrated by the 3-D plot (inset). This is useful when considering electrical characterization, as the absence of breaks in the conductance pathway removes the need to consider significant contact resistance between sections of wire. The inset illustrates a surface plot, highlighting the height variation along the DNA/polyC5-**TP** nanowire; the nanowire appears continuous and quite smooth. This was quantified further by calculating the standard deviation of the mean nanowire diameters which was found to consistently fall within a range of 2.7 – 4.4 nm.

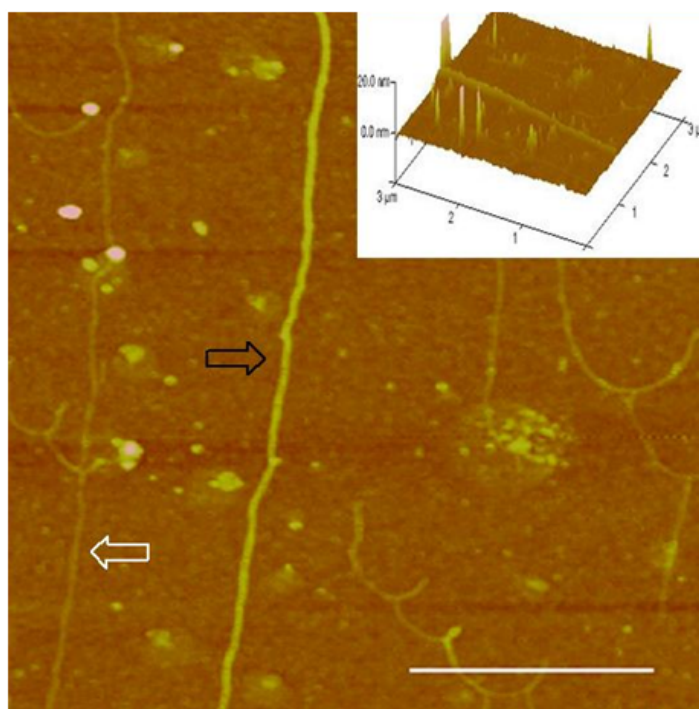


Figure 4.15. DNA/polyC5-**TPT** stretched on silanised silicon <111> surface, scale bar = $1\ \mu\text{m}$, z-scale range 0- 20 nm dark to bright contrast

As observed with C5-**TP**, significantly lower concentrations of monomer unit (compared to C5-**P**, $30\ \mu\text{M}$) and DNA concentrations were required in conjunction with tailored incubation times to avoid the effects of aggregation in solution. Of the three systems studied, C5-**TPT** seems to exhibit the greatest degree on aggregation,

which is in agreement with other experimental observations (Chapter 6). C5-TPT consists of two thiophene rings which act as spacer molecules to reduce the steric interaction of the alkynyl moiety while also increasing the hydrophobicity of the molecule. Unfortunately, as deposition was inconsistent, statistical treatment of DNA/polyC5-TPT nanowires could not be carried out. The spin-coating method of deposition was seemingly the only route to consistent deposition of DNA/polyC5-TPT nanowires (Figure 4.16), which was deemed an unsuitable approach for sensor device applications due to the lack of control over alignment and size of wires deposited.

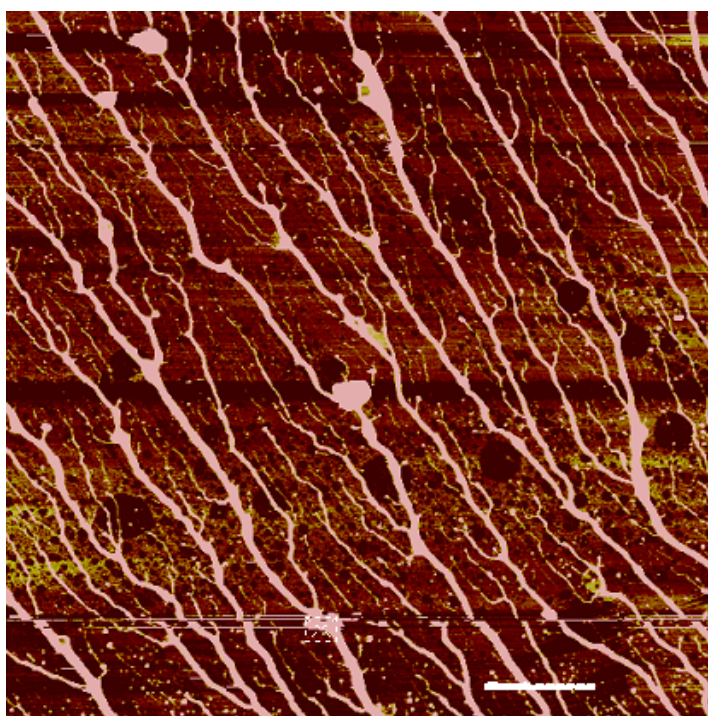


Figure 4.16. DNA/polyC5-TPT drop cast on silanised silicon (111) surface, scale bar = 3 μm z-scale range 0- 20 nm dark to bright contrast. 10 nm. 300 μM $\sim 80 \mu\text{g mL}^{-1}$, 1.5 hour incubation, 0.5 mM MgCl_2 and 1 mM FeCl_3 . Typical height $\sim 30\text{-}40$ nm

In summary, these findings demonstrate that despite the apparent reduction in the number and strength of hydrogen bonding interactions that can be envisaged between DNA and polyC5-P, polyC5-TP or polyC5-TPT, DNA-templating remains a viable route to nanowire formation using this material. Moreover, in order to successfully form and align single nanowires on the substrate an agreeable balance between surface chemistries, deposition procedure, concentrations and incubation time must be reached.

4.3.4 Iron-free DNA Catalysed Nanowire Formation

Goal: To assess iron-free DNA catalysed polymerisation as a route to conducting polymer nanowire formation.

An interesting observation that came from the optimized approach to DNA-templating of C5-**P**, C5-**TP** and C5-**TPT** described in Section 4.3.3, was the lack of evident nanowires from preparation at higher concentrations. Aggregation of polymer/DNA was thought to be a common occurrence when higher concentrations of DNA, monomer unit and/or longer incubation times were employed. In consideration of this obstacle, and the necessity to control a number of parameters (incubation time, DNA/monomer concentration), a milder manner of polymerization was explored in an attempt to consistently obtain samples containing single wires of a uniformed height.

Acidic conditions have previously been employed to polymerize monomer units such as pyrrole in the absence of a chemical oxidant.^{43, 44} Therefore iron-free templating reactions in acidic conditions potentially offered an alternative route to DNA based nanowires. Using short reaction times (1 hour), relatively mild acidic conditions (pH 5, Tris-HCl in order to preserve the DNA-template) and CT-DNA, DNA/polyC5-**P** nanowire formation was achieved, as demonstrated by AFM (Figure 4.17). To the top right of the image bare DNA is evident while running north-south down the center of the image is DNA/polyC5-**P** nanowire while to the left of this wire is a thinner partially polymer covered DNA strand.

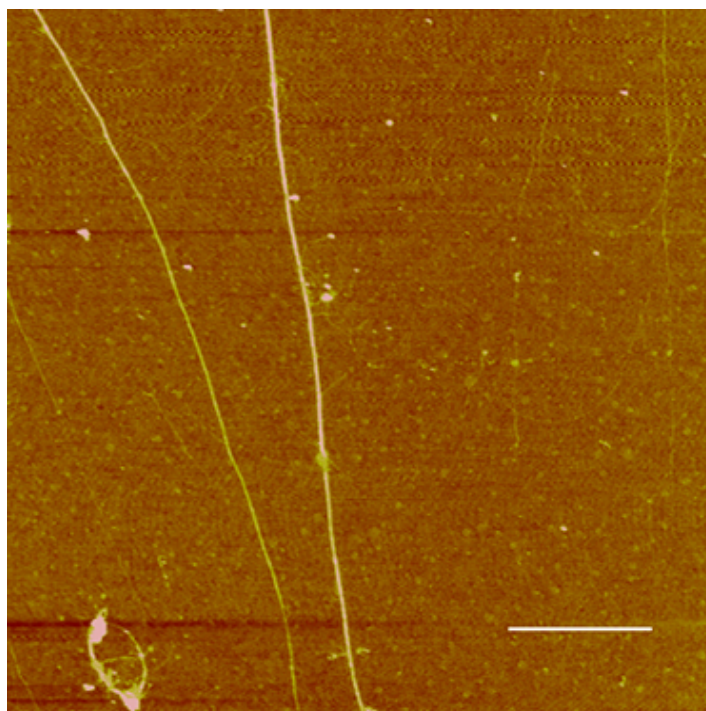


Figure 4.17. A typical AFM image of DNA/polyC5-P ~9.08 nm in height aligned on Si/SiO₂ using molecular combing, the scale bar = 2 μ m and the z-scale range 0- 10 nm dark to bright contrast. (200 μ g ml⁻¹ CT-DNA, 0.5 mM C5-P, pH 5, 1 h incubation)

The larger structures produced were uniform in height (4.55 nm, +/- = 1.05 nm, 343 data points). Additionally, there was little non-specific polymer deposition shown on the surfaces. Possibly indicating DNA-templating influences the oxidation process or that low concentrations of polymer formed binds to the DNA in a more elegant charge driven process with only a thin layer of polymer produced to encapsulate the DNA.

Given the indications that polymerization and templating occurs by simply lowering the pH of the monomer/DNA solution, it became apparent that the DNA itself could act as a localized region of low pH. Washizu *et. al.*⁴⁵ have reported that a relatively high H⁺ concentration resides along the duplex in the proximity of the phosphate backbone, with a calculated drop in pH of 3.5 relative to the bulk solution.

UV-Vis studies of the addition of C5-P to CT-DNA indicate that molecular oxygen dissolved in the solvent acts as an initiator for the polymerisation process, with DNA acting as a catalyst with the lower pH helping drive the reaction. Figure 4.18 illustrates the change in UV-Vis absorbance (400-500 nm) when polymerisation is initiated by FeCl₃. As expected, an increase in absorbance is observed over time which is as expected with the extension of the conjugated π -system.

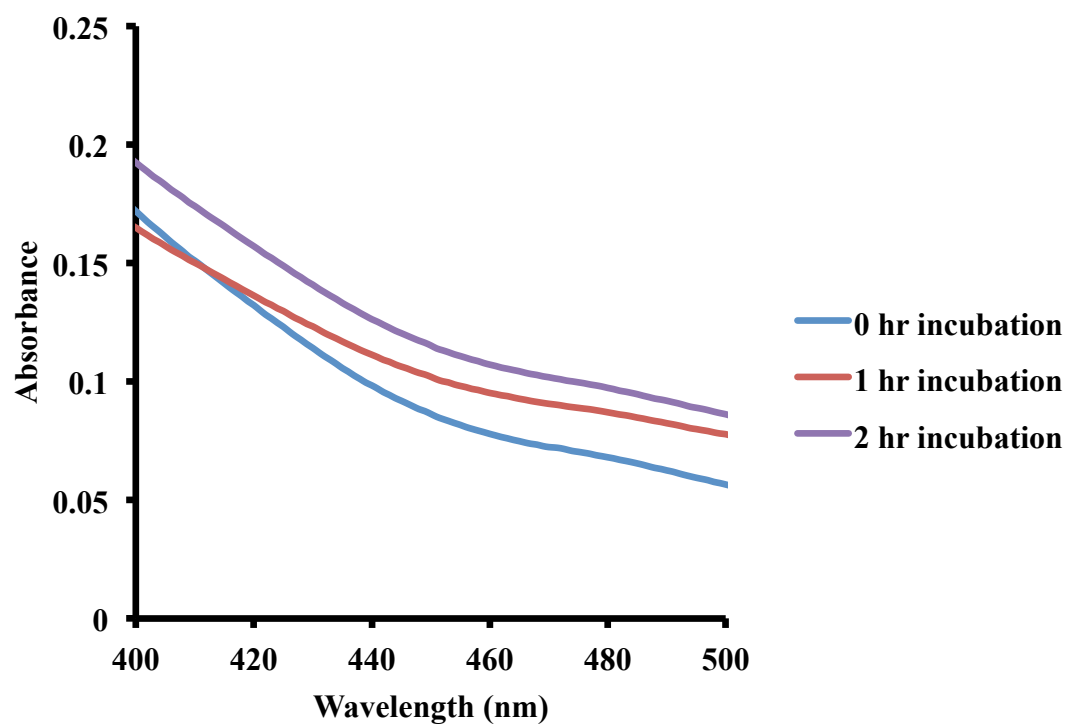


Figure 4.18. UV-Vis spectrum (400-500 nm) of C5-P incubated with FeCl₃ over 0-2 hours

Figure 4.19 shows the control experiment in which C5-P was dissolved in an aqueous solution (pH 5, Tris-HCl). A very small increase in absorbance was observed after incubation for 2 hours. This was considered to be due to very low levels of polymerisation initiated by the presence of molecular oxygen with the acidic nature of the solution increasing the rate of the reaction.

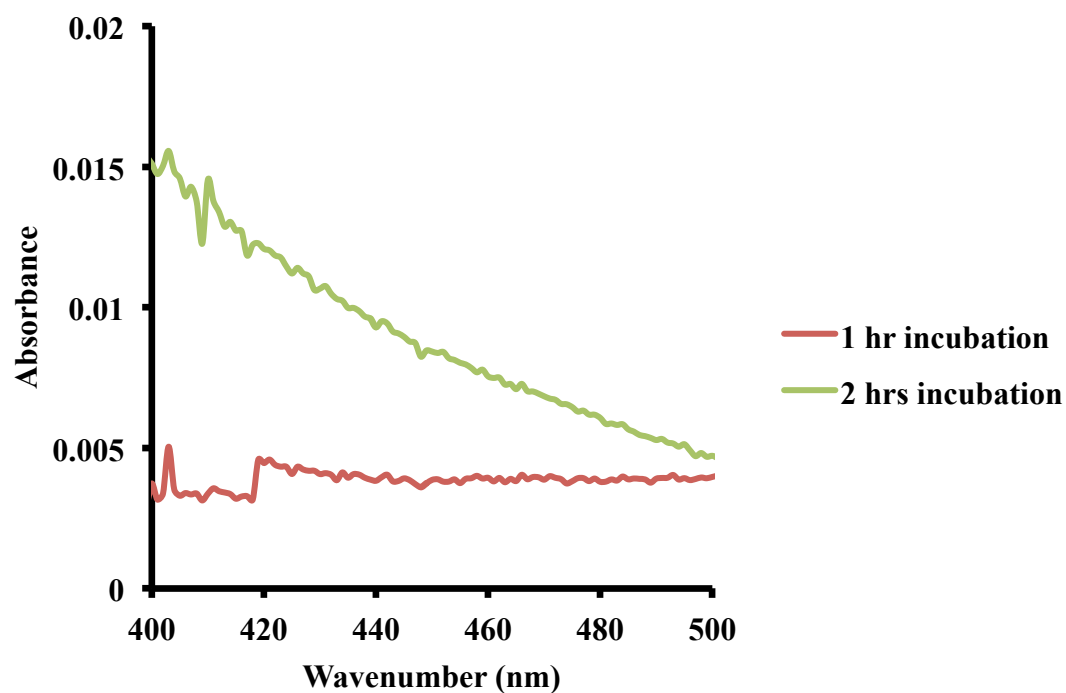


Figure 4.19. UV-Vis spectrum (400-500 nm) of C5-P in pH 5 media over 0-2 hours

Figure 4.20 illustrates the catalytic effect DNA has on this polymerisation process. When CT-DNA was added to a solution of C5-P dissolved in pH 5 media a significant increase in absorbance was observed in comparison to the control shown in Figure 4.21 where all solutions were degassed (flowed through with N₂ for 1 hour) prior to mixing.

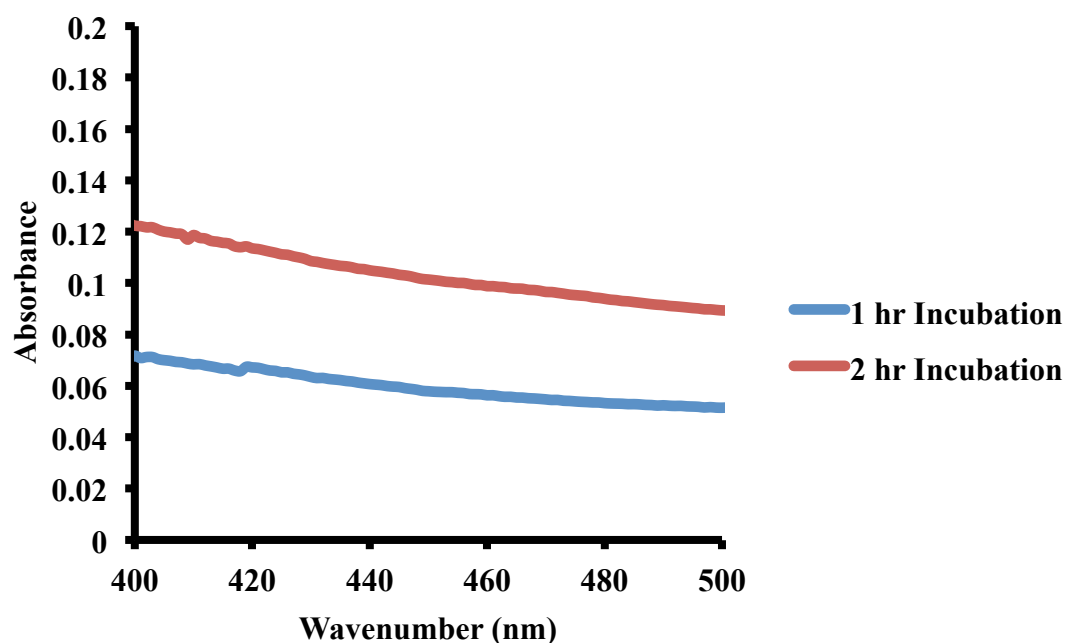


Figure 4.20. UV-Vis studies of the addition of C5-P to CT-DNA at pH 5, the increase in absorbance indicates polymer systems through an extended conjugated system

The final control experiment is shown in Figure 4.21. Here, DNA was added to solution of C5-P dissolved in pH 5 media as before, however all solvents were degassed prior to use. Clearly, very little change in absorbance was observed, with the small change likely due to the acidic nature of the solution or brief exposure to light when setting up the experiment. As a result of these findings it is proposed that molecular oxygen dissolved in the solvent acts as the primary initiator for the polymerisation process with the localized pH of the DNA driving the reaction.⁴⁵

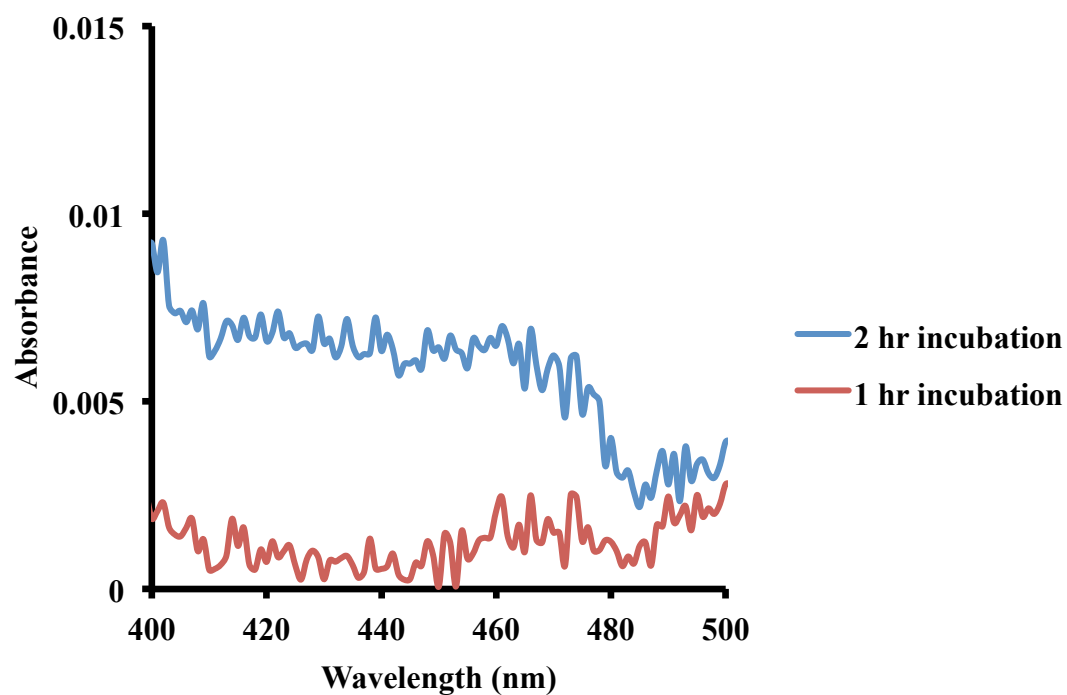


Figure 4.21. UV-Vis studies of the addition of C5-P to CT-DNA at pH 5 when all solutions were degassed prior to mixing

Furthermore, wires formed using this method have exhibited extremely interesting electrical properties; further discussion can be found in Chapter 5.

4.4 Conclusions

Bulk DNA/polymeric hybrid materials of **C5-P**, **C5-TP** and **C5-TPT** were successfully synthesized and characterized by FTIR spectroscopy. The use of FTIR demonstrated the materials to be supramolecular polymers rather than simple mixture, as evident by shifts in band positions compared to the parent compounds.

C5-P, **C5-TP** and **C5-TPT** monomer units have been successfully utilized in the preparation of DNA-templated polymer nanowires. The use of these monomer units in particular, provides a route to preparing co-polymer materials which offer improved structural regularity compared to alternative approaches whereby polymerization of mixtures of pyrrole and thiophene is carried out to form the polymer material.

Similar to previous examples of DNA/CP hybrid materials, DNA is demonstrated to be an effective template for directing polymer formation despite the reduced hydrogen bonding capacity of these compounds. Statistical analysis of DNA/poly**C5-P** and DNA/poly**C5-TP** nanowires revealed a modal diameter of 4.0–5.0 nm and 8.0–14.0 nm respectively. The resulting 1-D DNA/polymer structures formed appear to consist of a continuous polymer coating encapsulating the DNA template, based on height comparisons to bare DNA. However, in the absence of compositional data, it remains unknown if the structures are indeed polymer encapsulating the DNA or intertwined ropes of DNA and polymer.

Additionally, it has also been shown that DNA-templating of **C5-P** under very mild acidic conditions is possible. It is postulated that the low local pH of the DNA may promote a more elegant polymerization process. Polymerization has been shown to be initiated by molecular oxygen present in solution. This novel method may be applied to a variety of different monomer units, facilitating further modification in device construction whilst also allowing for the formation of smaller DNA templated structures than those achievable by chemical oxidation.

4.5 Experimental

4.5.1 Preparation of SiO₂ wafers for AFM/FTIR

N doped Si <111> wafers were sequentially cleaned using cotton buds soaked in acetone, propanol and finally water. The wafers were then soaked in a solution of sodium dodecyl sulphate and water (0.01 g in 100 mL) and heated to 50 °C for 20 minutes after which, the wafers were sonicated in nanopure water for 10 minutes. Following a further rinse they were dried using a nitrogen stream and the wafer was placed in 'piranha solution' (4:1, H₂SO₄:H₂O₂) for 1 hour, rinsed again with nanopure water and then dried in an oven for 15 minutes.

For AFM studies only; following these cleaning procedures, the surface of the cleaned Si substrates was subsequently modified through the formation of a trimethylsilane (TMS) self-assembled monolayer at the substrate surface. The Si substrate was positioned on top of specimen bottle containing 200 µL of chlorotrimethylsilane (Me₃SiCl) (polished side of the wafer facing upwards) and sealed inside a larger specimen bottle. The Si wafer was exposed to the vapour of the chlorotrimethylsilane in the specimen bottle for 30 seconds at room temperature.

4.5.2 Fourier Transform Infrared (FTIR)

FTIR spectra (in the range 600–4000cm⁻¹) were recorded in transmission mode with a Bio-Rad Excalibur FTS-40 spectrometer (Varian Inc., Palo Alto, CA, USA) equipped with a liquid nitrogen cooled deuterated triglycine sulfate (DTGS) detector, and were collected at 128 scans with 4 cm⁻¹ resolution. The DNA used was calf thymus DNA and all samples were prepared through drop casting of solutions of the DNA (0.5mg mL⁻¹) or DNA/polymer upon chemically oxidized Si<n-111> substrates. Data acquisition and analysis were carried out using Digilab Merlin version 3.1 software (Varian Inc.).

4.5.3 General Procedure for DNA-templated Synthesis for FTIR Studies

Typically, a 0.1 M solution of monomer in DMF (1 mL) was added to an aqueous mixture of CT-DNA, 40 $\mu\text{g mL}^{-1}$ (1 mL) and 0.5 M MgCl_2 (1 mL). 0.1 M aqueous FeCl_3 (1 mL) as an oxidant was added. The solution was stirred for 30 minutes at room temperature in darkness. A silicon chip, prepared as above, was deposited in the reaction mixture and left for 8 hours. The chip was removed, dried in a vacuum oven (25 °C) rinsed with nanopure water and dried again.

4.4.4 General Procedure for DNA-templated Synthesis for SPM Studies

5 μL of aqueous MgCl_2 solution (0.5 mM) was added to 10 μL of an aqueous solution of CT-DNA ($\sim 81.1 \mu\text{g mL}^{-1}$), followed by 5 μL of appropriate monomer in DMF (typically, C5-P = 500 μM , C5-TP = 30 μM and C5-TPT = 10 μM). 5 μL of a freshly prepared aqueous solution of FeCl_3 (1 mM) was then added to the DNA/monomer solution, and incubated for the specified period ((typically, C5-P = 1.5 h, C5-TP = 2 h and C5-TPT = 1.5 h) at room temperature to form the final DNA-templated polymer structures.

Following templating, the DNA/polymer nanowires were aligned upon the TMS-modified Si substrate using molecular combing techniques. 5 μL of the DNA/polymer/ FeCl_3 solution was applied to the substrate surface and combed back and forth 20 times using a micropipette. This typically left a small residual amount of solution on the substrate surface (ca. <1mm diameter), within which individually aligned DNA/polymer nanowires could be located.

4.5.5 Atomic Force Microscopy (AFM)

Surface topography images were obtained by TappingMode™ AFM performed in air on both Multimode Nanoscope IIIa and Dimension Nanoscope V systems (Veeco Instruments Inc., Metrology Group, Santa Barbara, CA, USA), using TESP7 probes (n-doped Si cantilevers, Veeco Instruments Inc., Metrology Group) with a resonant frequency of 234–287kHz, and a spring constant of 20–80 Nm^{-1} . Tap300Al-G (Budget Sensors, Monolithic silicon cantilevers) with a resonance

frequency of 100-400 kHz, and a spring constant of 20-75 Nm^{-1} (Windsor Scientific, Sloughm Berks., U.K.). Data acquisition was carried out using Nanoscope version 5.12b36 software on the Multimode Nanoscope IIIa and Nanoscope version 7.00b19 software (Veeco Instruments Inc., Digital Instruments) on the Nanoscope Dimension V. For both AFM systems, vibrational noise was reduced with an isolation table/acoustic enclosure (Veeco Inc., Metrology Group)

4.5.5 General Procedure for DNA-Catalyzed Nanowire Formation

5 μL of aqueous MgCl_2 solution (pH 5 (Tris-HCl)) (0.5 mM) was added to 10 μL of an aqueous solution (pH 5 (Tris-HCl)) of CT-DNA ($\sim 81.1 \mu\text{g mL}^{-1}$), followed by 5 μL of C5-**P** in DMF (500 μM). The DNA/C5-**P** solution was then incubated for 1 hour at room temperature.

4.5.6 General Procedure for UV-Vis Studies

UV-Vis absorption spectra were recorded on a Thermo-Spectronic GENESYS 6 spectrophotometer using a Quartz cuvette. 200 μL of C5-**P** in DMF (500 μM) was added to 400 μL of an aqueous solution (pH 5 (Tris-HCl)) of CT-DNA ($\sim 81.10 \mu\text{g mL}^{-1}$) and diluted accordingly. The DNA/C5-**P** solution was then incubated for 1 hour at room temperature while flowing through with N_2 prior to analysis by UV-vis. All manipulations were performed in darkness where possible.

4.6 References

1. T. A. Skotheim, R. L. Elsenbaumer and J. R. Reynolds, eds., *Handbook of Conducting Polymers*, New York, 1998.
2. H. Shirakawa, E. J. Louis, A. G. MacDiarmid, C. K. Chiang and A. J. Heeger, *Journal of the Chemical Society, Chemical Communications*, 1977, **0**, 578-580.
3. H. D. Tran, D. Li and R. B. Kaner, *Advanced Materials*, 2009, **21**, 1487-1499.
4. Y. Xia, P. Yang, Y. Sun, Y. Wu, B. Mayers, B. Gates, T. Yin, F. Kim and H. Yan, *Advanced Materials*, 2003, **15**, 353-387.
5. H. Xin, F. S. Kim and S. A. Jenekhe, *Journal of the American Chemical Society*, 2008, **130**, 5424-5425.
6. W. Liang, J. Lei and C. R. Martin, *Synthetic Metals*, 1992, **52**, 227-239.
7. F. Cheng, W. Tang, C. Li, J. Chen, H. Liu, P. Shen and S. Dou, *Chemistry – A European Journal*, 2006, **12**, 3082-3088.
8. T. K. Tam, M. Pita, M. Motornov, I. Tokarev, S. Minko and E. Katz, *Advanced Materials*, 2010, **22**, 1863-1866.
9. K. Wang, J. Huang and Z. Wei, *The Journal of Physical Chemistry C*, 2010, **114**, 8062-8067.
10. F. Wang, H. Gu and T. M. Swager, *Journal of the American Chemical Society*, 2008, **130**, 5392-5393.
11. C. M. Hangarter, M. Bangar, A. Mulchandani and N. V. Myung, *Journal of Materials Chemistry*, 2010, **20**, 3131-3140.
12. M. Hasegawa and M. Iyoda, *Chemical Society Reviews*, 2010, **39**, 2420-2427.
13. S. Pruneanu, S. A. F. Al-Said, L. Dong, T. A. Hollis, M. A. Galindo, N. G. Wright, A. Houlton and B. R. Horrocks, *Advanced Functional Materials*, 2008, **18**, 2444-2454.

14. C. R. Martin, R. Parthasarathy and V. Menon, *Synthetic Metals*, 1993, **55**, 1165-1170.
15. E. Braun, Y. Eichen, U. Sivan and G. Ben-Yoseph, *Nature*, 1998, **391**, 775-778.
16. Y. Eichen, E. Braun, U. Sivan and G. Ben-Yoseph, *Acta Polymerica*, 1998, **49**, 663-670.
17. Y. Ma, J. Zhang, G. Zhang and H. He, *Journal of the American Chemical Society*, 2004, **126**, 7097-7101.
18. L. Dong, T. Hollis, S. Fishwick, B. A. Connolly, N. G. Wright, B. R. Horrocks and A. Houlton, *Chemistry – A European Journal*, 2007, **13**, 822-828.
19. R. Hassanien, M. Al-Hinai, S. A. Farha Al-Said, R. Little, L. Šiller, N. G. Wright, A. Houlton and B. R. Horrocks, *ACS Nano*, 2010, **4**, 2149-2159.
20. G. Qun, C. Chuanding, G. Ravikanth, S. Shivashankar, A. Sathish, D. Kun and T. H. Donald, *Nanotechnology*, 2006, **17**, R14.
21. W. U. D. Patrick Nickels, Stefan Beyer, Jörg P Kotthaus and Friedrich C Simmel, *Nanotechnology*, 2004, **15**, 1524-1529.
22. A. Eftekhari, *Nanostructured Conducting Polymers*, 2010, John Wiley & Sons, LTD.
23. L. D. S. Ernst Sudholter, Marleen Mescher and Daniela Uliien ed., Organic Surface Modification of Silicon Nanowire-Based Sensor Devices, *Nanowires - Implementations and Applications*, *InTech*, 2011.
24. Y. Wang and M. Lieberman, *Langmuir*, 2003, **19**, 1159-1167.
25. P. Silberzan, L. Leger, D. Ausserre and J. J. Benattar, *Langmuir*, 1991, **7**, 1647-1651.
26. J. A. Howarter and J. P. Youngblood, *Langmuir*, 2006, **22**, 11142-11147.
27. F. Embs, D. Funhoff, A. Laschewsky, U. Licht, H. Ohst, W. Prass, H. Ringsdorf, G. Wegner and R. Wehrmann, *Advanced Materials*, 1991, **3**, 25-31.

28. Image drawn by Dr. J. D. Watson, 2010.
29. W. Wang, J. Lin and D. C. Schwartz, *Biophysical Journal*, 1998, **75**, 513-520.
30. J. Y. Ye, K. Umemura, M. Ishikawa and R. Kuroda, *Analytical Biochemistry*, 2000, **281**, 21-25.
31. H. Yokota, D. A. Nickerson, B. J. Trask, G. van den Engh, M. Hirst, I. Sadowski and R. Aebersold, *Analytical Biochemistry*, 1998, **264**, 158-164.
32. T. Thundat, D. P. Allison and R. J. Warmack, *Nucleic acids research*, 1994, **22**, 4224-4228.
33. D. Bensimon, A. J. Simon, V. Croquette and A. Bensimon, *Physical Review Letters*, 1995, **74**, 4754-4757.
34. A. Bensimon, A. Simon, A. Chiffaudel, V. Croquette, F. Heslot and D. Bensimon, *Science*, 1994, **265**, 2096-2098.
35. J. Li, C. Bai, C. Wang, C. Zhu, Z. Lin, Q. Li and E. Cao, *Nucleic acids research*, 1998, **26**, 4785-4786.
36. A. Houlton, A. R. Pike, M. Angel Galindo and B. R. Horrocks, *Chemical Communications*, 2009, 1797-1806.
37. D. H. Williams, Fleming, Ian, *Spectroscopic Methods in Organic Chemistry*, 5th edn., McGraw-Hall, 1995.
38. J. A. Taboury, J. Liquier and E. Taillandier, *Canadian Journal of Chemistry*, 1985, **63**, 1904-1909.
39. H. Fritzsche and C. Zimmer, *European Journal of Biochemistry*, 1968, **5**, 42-44.
40. T. Theophanides, *Applied Spectroscopy*, 1981, **35**, 461-465.
41. V. A. Bloomfield, *Biopolymers*, 1991, **31**, 1471-1481.
42. S. Pruneanu, L. Dong, T. A. Hollis, N. G. Wright, M. A. Galindo, A. R. Pike, B. A. Connolly, B. R. Horrocks and A. Houlton, *AIP Conference Proceedings*, 2008, **1062**, 33-42.

43. S. J. Hawkins and N. M. Ratcliffe, *Journal of Materials Chemistry*, 2000, **10**, 2057-2062.
44. B. S. Lamb and P. Kovacic, *Journal of Polymer Science: Polymer Chemistry Edition*, 1980, **18**, 1759-1770.
45. S. Suzuki, T. Yamanashi, S. Tazawa, O. Kurosawa and M. Washizu, Industry Applications, *IEEE Transactions on*, 1998, **34**, 75-83.

Chapter 5

Electrical Characterisation of DNA- Templated Polymer Nanowires

5.1 Chapter Overview

Overall Goal

To investigate the electrical properties of hybrid DNA/polymer nanowires based on C5-P, C5-TP and C5-TPT formed by DNA-templating.

Hypothesis

Hybrid DNA/polymer nanowires based on C5-P, C5-TP and C5-TPT will exhibit low levels of conductivity with DNA/poly C5-TPT proving to be the most conductive system.

Electron hopping will be the dominant mechanism for electron transport in all systems investigated.

Objectives

To study the electrical properties of DNA/polymer nanowires of C5-P, C5-TP and C5-TPT using scanned conductance microscopy (SCM).

Apply surface chemistries and templating conditions described in Chapter 4 to align DNA/polymer nanowires of C5-P, C5-TP and C5-TPT between two bespoke micro-fabricated Au electrodes embedded in SiO₂.

To explore the basic conduction mechanism of these hybrid materials and to investigate the thermal stability of the polymer nanowires using two-terminal current-voltage (I-V) measurements.

5.2 Introduction

The field of electrically conducting polymers has grown rapidly since the discovery of a sharp increase in conductivity when intrinsically insulating organic conjugated polymers are doped with oxidizing or reducing agents.¹ Combining the attractive properties of conducting polymers with the advantages of down-scaling devices to the nano-scale, presents challenges not only in the controlled synthesis of desired architectures but also in the characterization of these new materials.

Characterization of the electronic properties of 1-D nano-materials such as DNA-templated conducting polymer nanowires is difficult for two primary reasons. Firstly, the diameter and length of these nano-sized structures prohibits the application of well-established testing techniques. Secondly, the small size of the nanostructure makes their manipulation rather difficult with specialized techniques needed for installing individual nanostructures.

The pursuit of new methods of characterization for detailed examination and prediction of the properties of nanomaterials constitutes a significant field within nanotechnology. Techniques such as Transmission Electron microscopy (TEM), Surface Plasmon Resonance (SPR), X-ray photoemission spectroscopy (XPS), Scanning Tunneling Microscopy (STM), Scanning Electron Microscopy (SEM), four-probe Field Emission Scanning Electron Microscopy (FE-SEM) Atomic Force Microscopy (AFM, Chapter 2), Conductive Atomic Force Microscopy (c-AFM, Chapter 2) and Scanned Conductance Microscopy (SCM, Chapter 2) have all been developed to meet these needs.

Many of the applications envisage for CPs are based around their electronic properties. As such, the necessity to appropriately characterize these materials is paramount to their development and a number of techniques have been used to achieve such goals. For example, Scanning Tunneling Spectroscopy (STS), a form of STM, has been used provide a useful insight onto conduction and charge transport mechanisms in semiconducting poly(phenylenevinylene) (PPV).²⁻⁴ However, STM is only able to probe semi-conductive surfaces, since a current between the tip and sample is used to keep a constant tip-sample distance and to

probe the topography. This means that in STM measurements topography and electrical information are linked and especially for electrically heterogeneous samples like bulk hetero-junctions separation of electrical data from topography is difficult.

The most conventional technique for analyzing electrical properties in semiconductor materials is current-voltage measurements. The electrical properties of a number of conducting polymers such as polythiophene,^{5, 6} polyaniline^{7, 8} and poly(3,4-ethylenedioxythiophene) (PEDOT)⁹ have been characterized using this technique which may be performed using a four or two terminal sensing set-up.

Four-terminal sensing is an electrical impedance measuring technique that uses separate pairs of current-carrying and voltage-sensing electrodes to make more accurate measurements than traditional two-terminal (two-terminal) sensing. The key advantage of four-terminal sensing is that the separation of current and voltage electrodes eliminates the impedance contribution of the wiring and contact resistances as there is no current flow in the voltage sensing circuit. However, the diameter and length of the nano-sized structures such as nanowires, prohibits conventional application of this technique due to the size of the materials under investigation and difficulties in orientating the probes required for the measurement.

In an effort to circumvent the difficulties, a method utilizing a combination of SEM in-conjunction with four probe current-voltage measurements has been developed; this has led to the inception of the UHV NANOPROBE system also referred to as four-probe Field Emission Scanning Electron Microscope (FE-SEM). Specifically designed for local and non-destructive 4-point contact measurements and function testing of nano devices, the UHV NANOPROBE is equipped with four SEM's capable of <4 nm resolution (Figure 5.1). The SEMs remove the barrier posed by the size of nano-scale samples and facilitates application of a conventional 4-probe technique by accurate probe positioning and safe approach of the probe tips with diameters in the range of a few tens of nanometers.

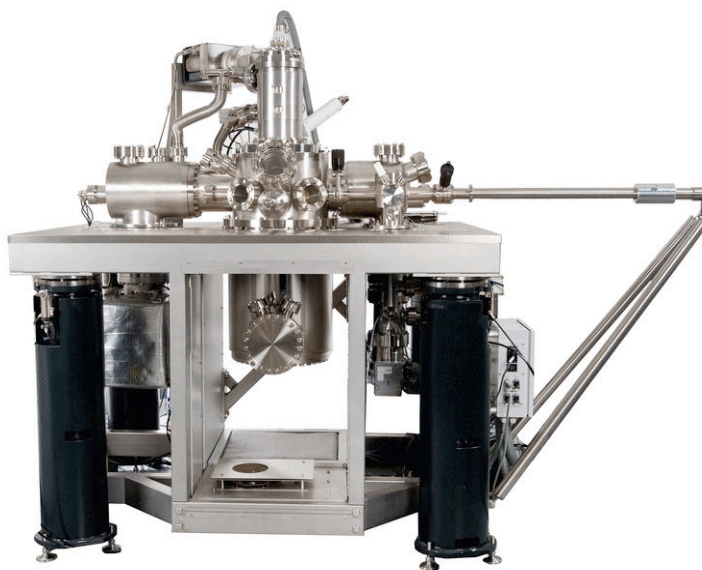


Figure 5.1. A UHV NANOPROBE equipped with four SEM's capable of <4 nm resolution

A common draw-back of this technique for materials such as conducting polymers is that organic materials disintegrate as a result of low pressures employed and electron bombardment of the four SEMs, making such materials unsuitable for examination in conventional SEMs. Low vacuum and environmental SEMs exist meaning many of these types of samples can be successfully examined in these specialized instruments.

An alternative approach, and the most common, for examining 1-D conducting polymer nanowires is to employ a two-probe I - V technique (Chapter 2). Here, the material is either grown/immobilized between the two probes or between two-terminal electrodes to provide an interface between the nanowire and the probe station.⁹⁻¹⁴

In this project, quantitative data on the electrical properties of individual DNA-based nanowire structures was gathered through two-probe I - V measurements; this required the fabrication of bespoke two-terminal devices (Figure 5.2). These devices were used as an interface between the nanowire and the probe station and were constructed using Au electrode pairs, micro-fabricated using photolithography, embedded in a thermally grown insulating SiO_2 layer, on a silicon substrate. The Au

electrodes were typically separated by a gap of 2–8 μm , across which a DNA-based nanowire was be aligned using molecular combing as described in Chapter 4.

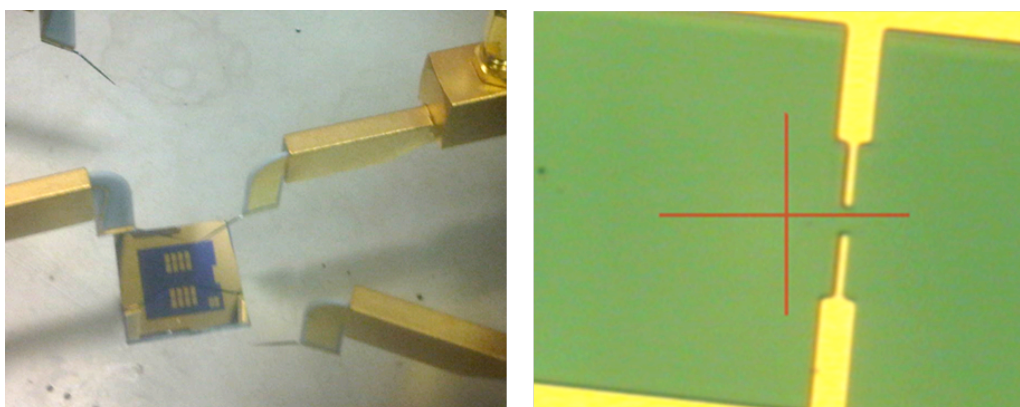


Figure 5.2. Optical images of Au electrode pairs, micro-fabricated using photolithography, embedded in a thermally grown insulating SiO_2 layer, on a silicon substrate. The Au electrodes were typically separated by a gap of 2–8 μm

Scanned Conductance Microscopy (SCM) was first developed by Bockrath *et al.*¹⁵ in 2001 and is a technique based on EFM which enables imaging of a sample's conductivity on a microscopic scale. The group demonstrated the usefulness of this approach by probing the electrical properties of single-walled carbon nano-tubes (SWNTs) on length scales as small as 0.4 μm (Figure 5.3).

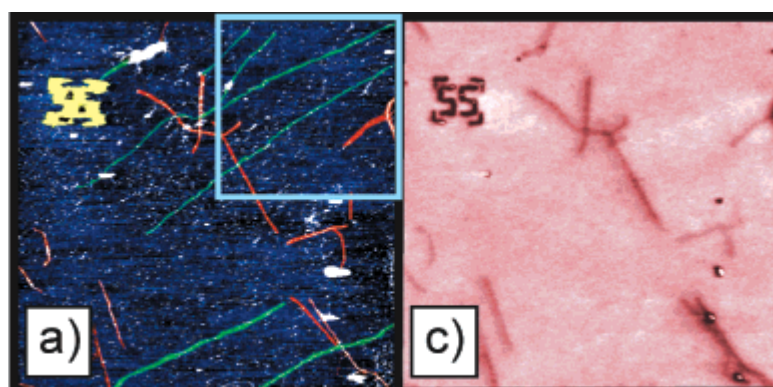


Figure 5.3. (a) Colorized topographic image of SWNT bundles and single tubes, colored red, and λ -DNA molecules, colored green. (c) Scanned conductance image of the region shown in part (a).

Reproduced from reference¹⁵

As described in Chapter 2, SCM provides a non-contact method for probing the electronic properties of one-dimensional nanomaterials in qualitative manner. The

technique involves a ‘two-pass’ method in which the first pass of a metal-coated AFM probe over the sample surface is used to record the topography while in the second pass over the same scan line a bias is applied above the sample.

The sign of the phase shift ($\Delta\phi$) of the cantilever associated with the nanowire under investigation, relative to the substrate background, indicates whether the wire is electrically conducting or insulating through the generation of a phase image. Negative phase shifts (black features, negative phase) are only observed for conductive materials, whilst insulating materials exhibit positive phase shifts (white or positive phase).¹⁵⁻¹⁷

SCM provides a simple method to rapidly screen materials to find potential conductors which may otherwise be difficult through the necessity to attach electrical leads/contacts. As such, the electrical properties of a number of materials have been investigated using this technique.^{12, 15-21}

In the case of conducting polymers, Staii *et. al.*¹⁶ investigated the electrical properties of doped polyaniline/PEO nanofibers to develop a quantitative model for phase shifts. By using simple approximate geometries, the group determined the dielectric constant of the PEO nanofibres to be between 2.28-2.32, which was in agreement with tabulated values.

Recently, McGrath *et. al.*²² used SCM to confirm the conductance of colloidal dispersions of emeraldine salt state polyaniline (ES-PAni) nanofibres (Figure 5.4). The fibres were prepared through the template-directed synthesis of PAni using monodisperse, solution-self-assembled, cylindrical, block copolymer micelles as nanoscale templates, affording controlled lengths of 200 nm–1.1 μm .

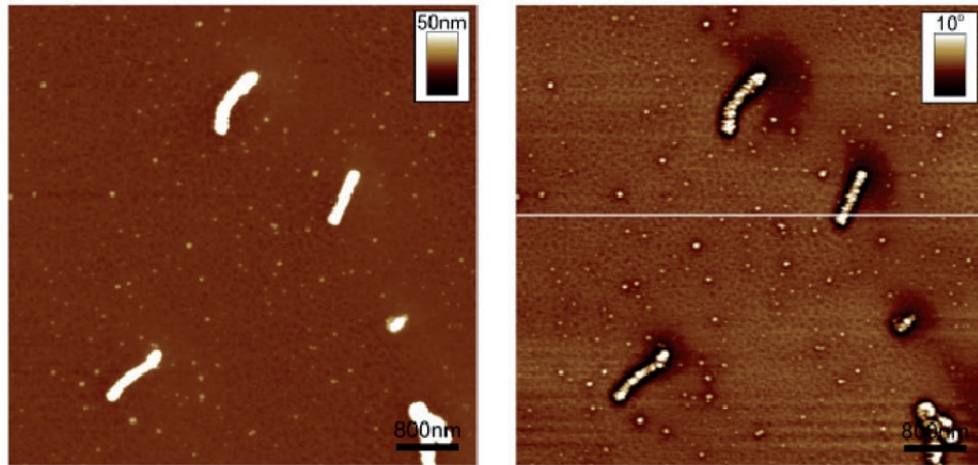


Figure 5.4. ES-state PANi nanofibres. Left; tapping mode AFM height image of the structures, right; the corresponding SCM phase image. The negative-positive-negative phase shifts in the scanned conductance image is characteristic of semi-conducting materials; this corresponds to a negative phase shift as the tip crosses the nanowire and demonstrates the existence of charge conduction in the wire. Reproduced from reference²²

Houlton *et. al.*^{11, 12, 20, 23} have also used SCM to aid the characterization of a number of DNA-templated conducting polymer nanowires such as polyindole (PIn)²⁰ and polypyrrole (PPy).¹¹ Figure 5.5 shows an AFM image and a scanned conductance images of PIn/DNA nanowire. The nanowire appears as a dark line in the scanned conductance image; this corresponds to a negative phase shift as the tip crosses the nanowire and demonstrates the existence of charge conduction in the wire.

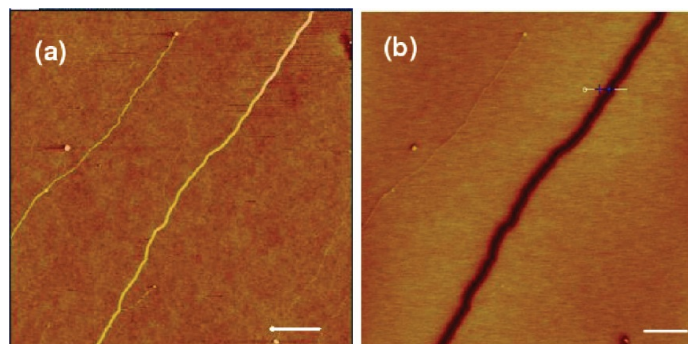


Figure 5.5. AFM and scanned conductance (SCM phase) images of PIn/DNA nanowires on SiO₂/Si surface with a SiO₂ thickness of 220 nm. (a) AFM image of a nanowire with a diameter of 5 nm (grayscale 10 nm). (b) Phase image of the same nanowire. Reproduced from reference²⁰

Chapter Outline: *In this chapter, studies into the electrical properties of DNA/polymer nanowires of C5-P, C5-TP and C5-TPT are presented. Initial studies made use of scanned conductance microscopy (SCM) as a qualitative approach. Subsequent studies using two-terminal current-voltage (I-V) measurements as a function of temperature were used to explore the basic conduction mechanism of these hybrid materials and to investigate the thermal stability of the polymer nanowires. Temperature-dependent measurements were performed on a single DNA/polymer nanowires aligned between two bespoke micro-fabricated Au electrodes embedded in SiO₂ (Appendix).*

5.3 Results and Discussion

5.3.1 SCM Studies of Conductive Polymer Nanowires

Goal: To investigate the electrical properties of nanowires formed in Chapter 4 by SCM.

Nanowires for SCM studies were prepared and deposited using protocols developed in Chapter 4. In each case, a 1 cm^2 Si/SiO₂ chip with an oxide thickness of *ca.* 200 nm was used in as a substrate. Figure 5.6 is a typical cross-sectional plot of a nanowire imaged by SCM. The negative-positive-negative phase shifts is characteristic of semi-conducting materials.^{11, 20, 23}

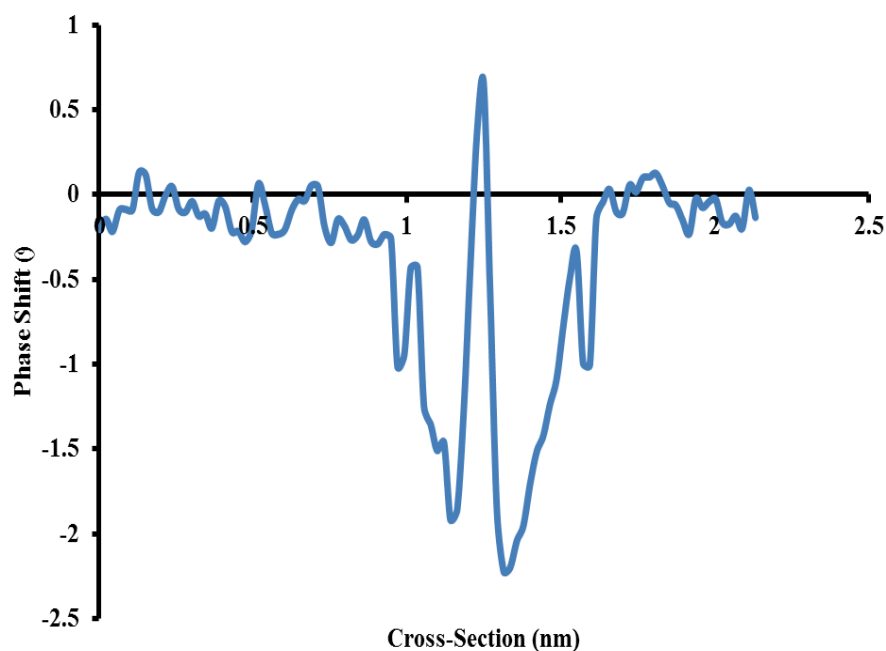


Figure 5.6. A typical cross-section of a conducting DNA/C5-P nanowire, illustrating the negative-positive-negative phase shifts is characteristic of semi-conducting materials

SCM phase images of DNA hybrid C5-P, C5-TP and C5-TPT nanowires prove consistent with the predicted observations for conductive objects (Figure 5.7). The features running left-right (Figure 5.7, a) and top-bottom (Figure 5.7, b and c) are SCM phase images of DNA hybrid C5-P, C5-TP and C5-TPT nanowires. The

material isolated from the templated reactions was also shown to contain both a small number of bare DNA strands located non-specifically around the main features of each image; exhibiting a positive phase shift due to their insulating nature.

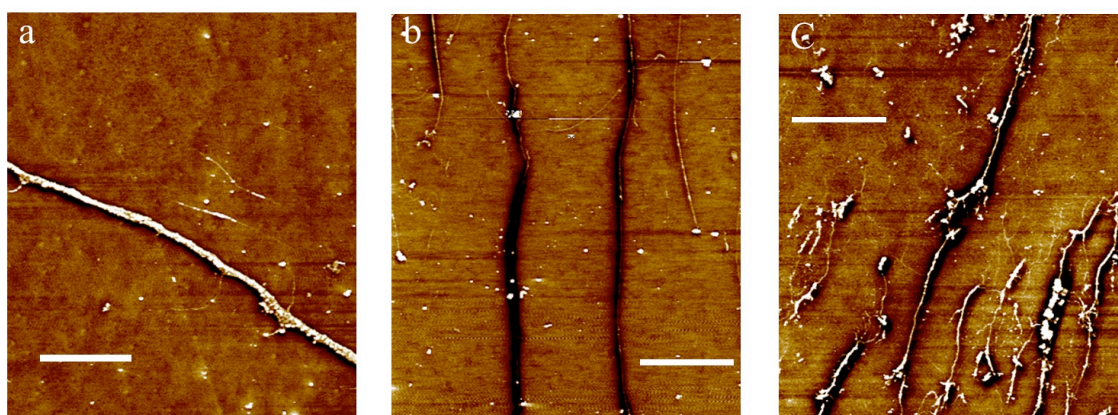


Figure 5.7. SCM phase images of a) DNA/polyC5-P; b) DNA/polyC5-TP; c) DNA/polyC5-TPT nanowires stretched on silanised silicon <111> surface, scale bar = 3 μm , z-scale range 0- 10 nm dark to bright contrast when a -7 V bias was applied. The negative-positive-negative phase shifts characteristic of semi-conducting materials was observed in each case (Figure 5.2 and Appendix)

Typically at lower bias (± 1 V) no phase image was observed. However, upon gradually increasing the bias to ± 7 V a negative phase shift was observed, indicating a very weak electric field gradient in the sample.

Figure 5.8 shows the effect of different tip/sample biases on the same DNA/polyC5-TPT nanowires displayed in Figure 5.7, c. SCM studies of extended conducting objects can be influenced by electrostatic forces generated from trapped charges, Van der Waal's forces or capacitive effects.¹⁶ The proportional relationship of the phase shift to the square of the applied bias shows the interaction of the conducting AFM probe with the electric field gradient above the samples is dominated by capacitance effects; meaning changes in the cantilever resonance frequency are a result of the attractive or repulsive forces of the electrically conducting wire not as a result of electrostatic forces on the substrate surface.

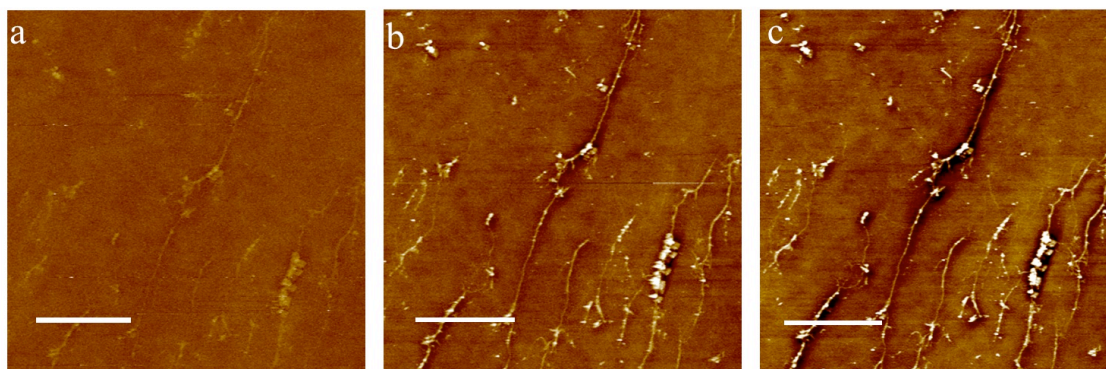


Figure 5.8. DNA/polyC5-TPT nanowires stretched on silanised silicon <111> surface, scale bar = 3 μm , z-scale range 0- 10 nm dark to bright contrast when different tip/sample biases. a) 0 bias; b) -2 V; c) -3 V

This behaviour is more clearly illustrated by the parabolic relationship shown when plotting the (tangent) phase shift against the DC bias applied to the substrate. Figure 5.9 shows a typical plot for DNA/polyC5-P.

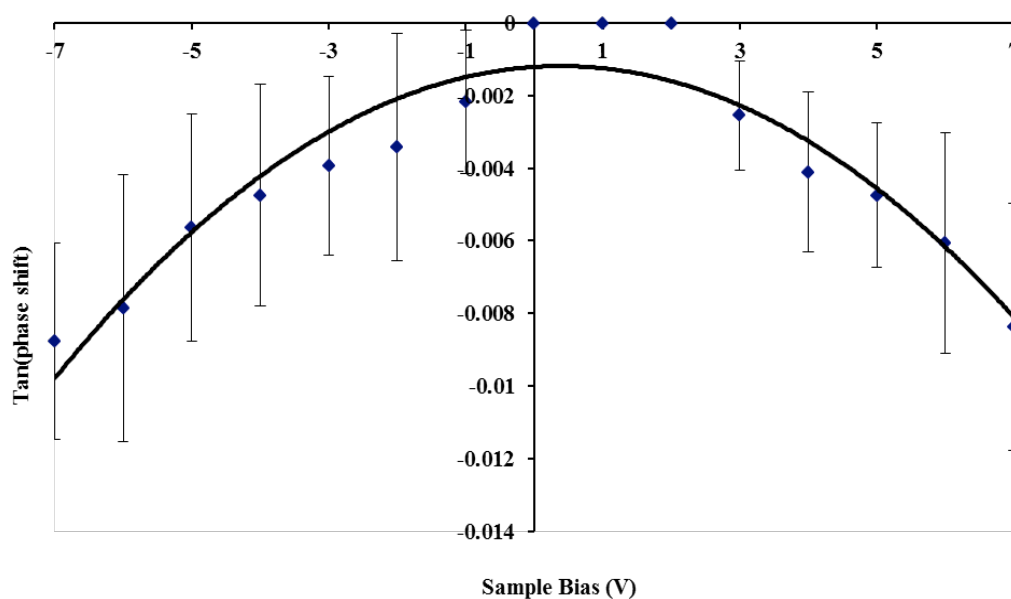


Figure 5.9. A plot of the (tangent) phase shift against the dc bias applied to the substrate for DNA/polyC5-P (10.80 nm in diameter). Error bars produced by taking the standard deviation of ten points along the wire at each bias

The significance of plotting the (tangent) phase shift against the DC bias applied was demonstrated by Bockrath *et. al.*¹⁵ when investigating force gradients of carbon nanotubes and λ -DNA using Electronic Force Microscopy (EFM). This can be

rationalised by considering the capacitive coupling to an insulating substrate i.e. Si/SiO₂ and conductive materials i.e. NWs, respectively.

At resonance, the bare substrate exhibits zero phase shift. This is because $\pi/2$ is subtracted from all measured phase shifts:

$$\Phi = \emptyset - \left(-\frac{\pi}{2}\right) = \emptyset + \pi/2$$

Since the total energy stored in the tip is,

$$E_{tot} = 1/2 k h^2 + 1/2 C(h)V^2$$

Where, $C(h)$ is the tip-substrate capacitance, k , is the spring constant of the cantilever and V is the bias voltage applied between the tip and the substrate. Therefore,

$$1/2 C(h)V^2$$

is equivalent to a change in spring constant of the tip, k . The frequency shift, $\Delta\omega$, and the phase shift, $\Delta\Phi$ are proportional to the force gradient $F'(h)$ or degree of capacitive coupling between the tip and the substrate. The presence of the nanowire changes the tip/substrate capacitance because the electrons in the nanowire move in the electric field in the tip/substrate gap and affect the charge stored. Since the bare substrate exhibits zero phase shift, plotting the change in phase against the applied voltage shows the effect of capacitive coupling from the NW on the tip independent of the applied voltage, which alters the resonance frequency of the tip.

Should a linear plot be obtained then the phase shift is a result of electrostatic forces generated from trapped charges, Van der Waal's forces or capacitive effects (i.e. changes in tip oscillation are proportional to the applied bias). Further data pertaining to DNA/polyC5-**TP** and DNA/polyC5-**TPT** can be found in the Appendix.

In summary, SCM phase images of DNA hybrid C5-P, C5-TP and C5-TPT nanowires prove consistent with the predicted observations for conductive objects with the proportional relationship of the phase shift to the applied bias showing the interaction of the conducting AFM probe with the electric field gradient above the samples is dominated by capacitance effects.

5.3.2 Nanowire Two-Probe I - V Measurements

Goal: *To explore the electrical properties of DNA hybrid C5-P, C5-TP and C5-TPT nanowires quantitatively and elucidate the basic conduction mechanism of charge transport using two-terminal current-voltage (I - V) measurements.*

In order to obtain further insight into the electrical properties of DNA hybrid C5-P, C5-TP and C5-TPT nanowires, direct two-terminal I - V characterization of DNA/CP nanowires was performed using the micro-fabricated Au electrodes (Figure 5.10). These devices were used as an interface between the nanowire and the probe station and were constructed using Au electrode pairs, micro-fabricated using photolithography, embedded in a thermally grown insulating SiO₂ layer, on a silicon substrate. The Au electrodes were typically separated by a gap of 2–8 μm . Whilst extremely useful, this technique relies heavily on the ability to align a nanowire across the electrode gap using molecular combing and is therefore less straightforward to implement than SCM.

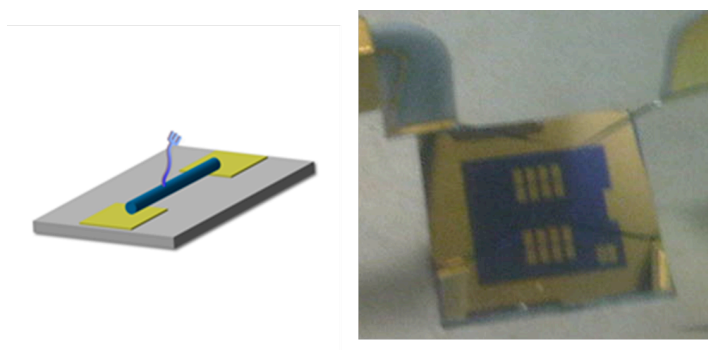


Figure 5.10. Left, a representation of a polymer nanowire with a terminal alkyne group aligned between two gold micro-electrodes using molecular combing; right, bespoke micro-fabricated Au electrodes for I - V measurements. The Au electrodes were typically separated by a gap of 2–8 μm while the chip was $\sim 1\text{ cm}^{2,24}$

Unfortunately, due to this experimental difficulty (aligning single nanowires across the Au microelectrode gap), no I - V data for DNA/C5-**P** or DNA/C5-**TPT** nanowires was obtained, despite extensive efforts to do so. It was possible to obtain data for DNA/polyC5-**TP** and DNA/polyC5-**TPT** prepared by chemical oxidation and DNA/polyC5-**P** prepared in acidic conditions.

In each case, the surface of the devices was treated with chlorotrimethylsilane (TMS) to afford a hydrophobic surface. As discussed in Chapter 4, treatment with TMS reduces the density of nanowires adhering to the surface and therefore increases the chance of immobilising single nanowires. In order to align a single nanowire across the microelectrode gap a droplet of template solution was combed across the chip 10 times. Consistently, no deposition of any kind was observed, likely due to the hydrophobic nature of the surface. When treatment of TMS was not performed, significant levels of aggregates or bundles of polymer/DNA or non-templated polymer were observed due to the increasing hydrophilic nature of the surface. While tuning of the templating conditions in conjunction with the surface chemistry allowed alignment of single nanowires in Chapter 4, application of the same approach here proved unsuccessful.

Unfortunately, treatment of the Au micro electrodes with the same cleaning method employed with Si/SiO₂ chips used for AFM and SCM resulted in degradation of the adhesion layer connecting the Au microelectrode pads to the silicon. Surface cleaning was therefore conducted by wiping the surface sequentially with acetone, propanol and water using a cotton bud. As result of this less aggressive cleaning, the surface was considered to be less reactive towards TMS than surfaces prepared by ‘piranha’ solution, resulting in the need for longer incubation times to enable molecular combing. Furthermore, due to the limited number of Au micro electrodes, chips were re-used despite regeneration of the Si/SiO₂ not being possible (removal of TMS layer). Consequently, a reproducible surface was difficult to obtain; as such true control over the surface properties for nanowire adhesion/alignment was impossible. The hydrophobicity of the surface was likely to be significant higher than in previous work due to the longer exposure times and continued surface modification.

Furthermore, it was also considered that the difficulties encountered in Chapter 4 with respect to polymer aggregation, were also a significant factor to being unable to immobilise single DNA/polymer nanowires onto the surface; difficulties found with DNA/polyC5-**TPT** in nanowire alignment for AFM studies were mirrored here. This complication in addition to the inherent technical difficulties of obtaining single nanowires aligned across the micro electrode gap made obtaining electrical data from two-probe I - V measurements extremely difficult. Despite these obstacles, successful alignment of single DNA/polyC5-**TP**, DNA/poly**TPT** and DNA/polyC5-**P** (prepared in the absence of FeCl_3) was achieved.

*Two-Probe I - V studies of DNA/polyC5-**TP** Nanowires*

Unlike DNA/polyC5-**P** and DNA/polyC5-**TPT**, a single DNA/polyC5-**TP** wire was successfully aligned across an electrode gap, possibly due in part to the greater degree of sulphur content and its high affinity for gold. Figure 5.11 shows an AFM image of a DNA/polyC5-**TP** nanowire (8 nm in diameter) located across a 6 μm electrode gap.

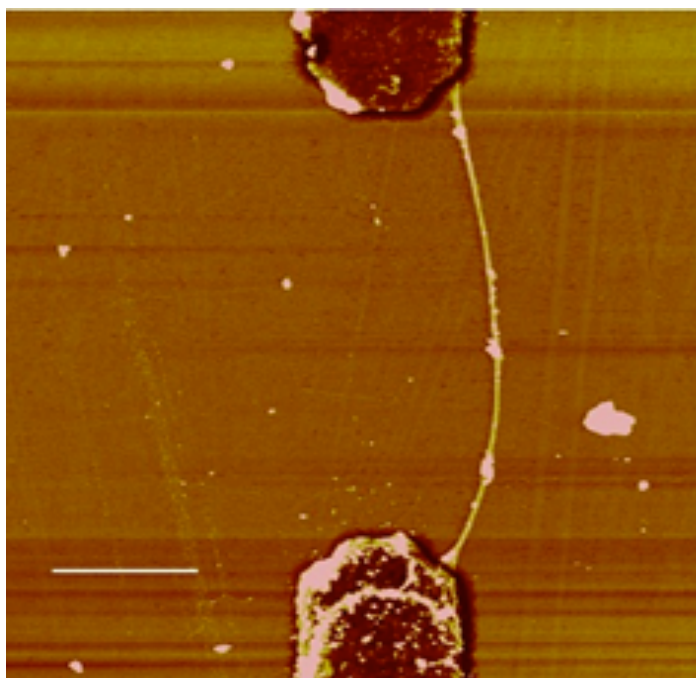


Figure 5.11. An AFM image of DNA/polyC5-**TP** 8 nm in height stretched between two Au micro-electrodes, the scale bar = 2 μm and the z-scale range 0- 20 nm dark to bright contrast. The Au electrodes are embedded in a thermally grown, 200 nm thick insulating SiO_2 layer on a Si substrate

Figure 5.12 shows a 3-D image of the same device, DNA/polyC5-**TP** illustrating the connection between the electrodes to the nanowire in addition to the relatively regular morphology of the wire.

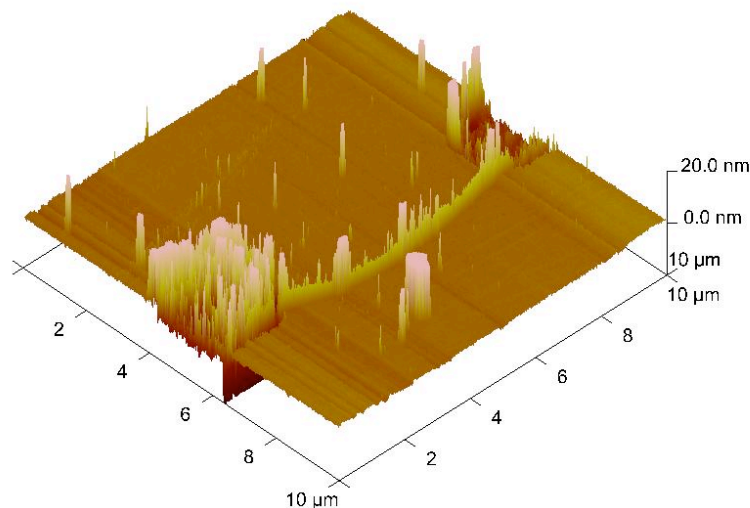


Figure 5.12. A 3-D image of the same wire illustrating the connection between the Au electrodes and the DNA/polyC5-**TP** nanowire

Using two probe current-voltage sweeps, typically over a range of -5 to $+5$ V, quantitative electrical data was obtained for this wire. A typical I - V plot obtained for the DNA/polyC5-**TP** nanowire (Figure 5.11) is shown in Figure 5.13. The I - V curves are nonlinear, as previously reported for similar measurements on polypyrrole/DNA and polyindole/DNA nanowires.^{10, 11, 20} The reason for this behaviour is most likely to be a small tunneling barrier at the Au/polymer contacts.

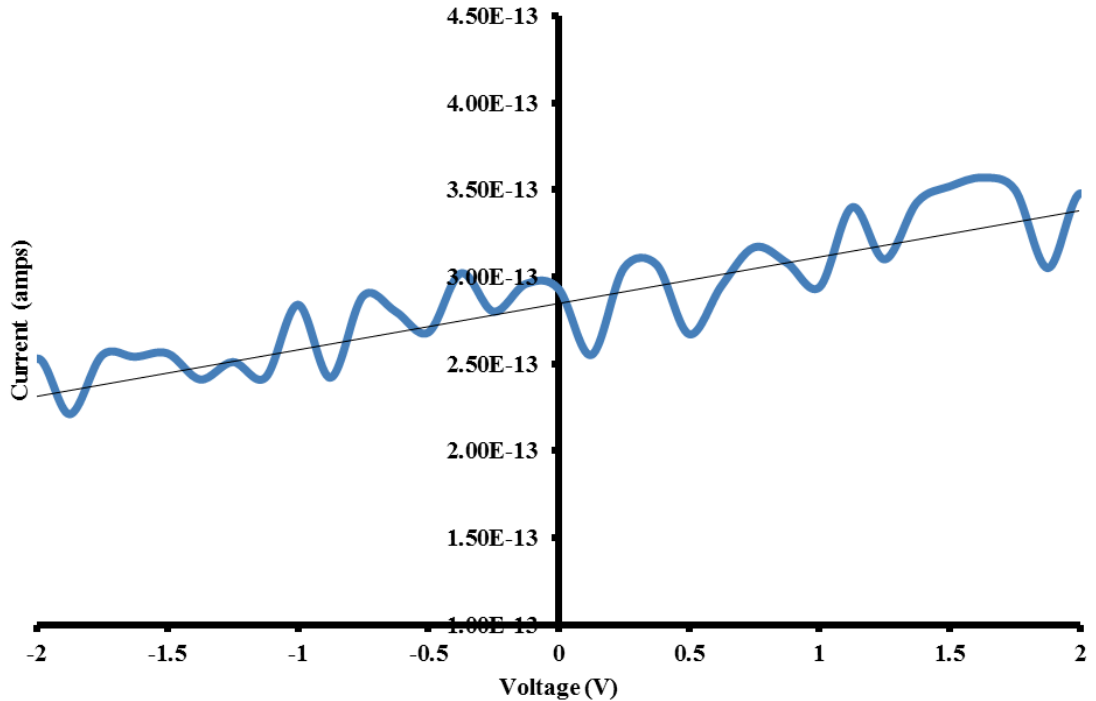


Figure 5.13. A typical current-voltage plot for a DNA/polyC5-TP nanowire obtained from the Agilent B1500 probe station

In order to calculate a conductivity value from the current-voltage (I - V) data, conductance values must be first extrapolated from the gradient of the I - V plots around zero bias; giving conductance (G) which is the reciprocal of resistance (R).

$$G = \frac{I}{V} \quad R = \frac{V}{I}$$

Conductivity (σ , S cm^{-1}) can then be calculated from the resistance, R , of a material of given cross sectional area, A , and length, l , using equation:

$$\sigma = l/RA$$

The cross-sectional area of the nanowire under investigation can be calculated by evaluating the dimensions of the nanowire aligned across the Au electrodes using AFM. Assuming the nanowire is a cylinder, with an average diameter, then the cross sectional area of the nanowire is equal to:

$$A = \pi \cdot R^2$$

A significant contribution to resistance from electrical contact made between the CP nanowire and the Au electrodes is possible, known as contact resistance. The term

contact resistance refers to the contribution to the total resistance of a material which comes from the electrical leads and connections as opposed to the intrinsic resistance of the wire, which is an inherent property, independent of the measurement method.²⁵ The term ‘contact resistance’ is traditionally applied for the consideration of the metal to semi-conductor interface as a main contribution to this phenomenon.

However, if the contact resistance is ignored, an estimate (lower bound) of the wire conductivity can be made. Based on the dimensions of the single DNA/polyC5-**TP** nanowire shown in Figure 5.11, a conductivity value was calculated to be $2.9 \times 10^{-5} \text{ S cm}^{-1}$ at 303K. Unfortunately, reports detailing conductivity values for bulk poly**TP** are absent from the literature (this data is presented in Chapter 6). However, some comparison may be made to pyrrole nanowires prepared in a similar fashion; in this instance this value is significantly lower than expected. For example, Bocharova *et al.* measured the conductivity of a single polypyrrole nanowire (50-60 nm in diameter) grown onto a device comprising Au microelectrodes (1 μm apart) and found it to be in the range 1-3 S cm^{-1} .²⁶ Houlton *et al.*¹⁰ reported similar levels of conductivity for DNA-templated nanowires of polypyrrole. Using FeCl_3 as an oxidant, conductivity was determined to be in the range of 4 S cm^{-1} , the same order as the conductivity of bulk polypyrrole powder (1.7 S cm^{-1}) prepared chemically by FeCl_3 .

As discussed in Chapter 1, the conduction pathway and therefore level of conductance in this class of polymers (CPs) is dependent upon, (i) planarity and anisotropy ratio (i.e. the interchain conductivity is much larger than inter-chain conductivity), (ii) the doping percentage, (iii) the alignment of the polymer chains, (iv) the conjugation length, and (v) the purity of the sample. Given the uniformed structure and morphology of the nanowire under investigation, it is unlikely conductance is significantly affected by breaks in the current pathway. Instead, this low level of conductance may be a consequence of modification at the *N*-position of the pyrrole moiety or an influence of the three possible configurations of polyC5-**TP**, “head-to-tail”, “tail-to-tail”, or “head-to-head” (Chapter 3) resulting in a loss of planarity/conjugation length; these consideration are investigated further in Chapter 6.

Most conducting polymers show an increase in conductivity with temperature typical of hopping conductors; the charge carriers are considered to be substantially localized and make thermally-assisted tunneling transitions or hops, between sites. As such the precise nature of the temperature dependence might be affected by many factors such as the polymer structure, degree of crystallinity and dimensionality. In general, several hops may be possible from a given site, which differ with respect to the energy barrier or hopping distance. This situation is called variable range hopping because the thermal average over the different hops leads to a hopping range that is temperature-dependent.

Characterisation of this temperature dependence therefore provides valuable insight into the conduction mechanism of the DNA/CP nanowires. Variable-temperature I - V studies of the two-terminal device were performed over a temperature range of 293 to 373 K in order to elucidate details of the conduction mechanism. The temperature dependence of the nanowire conductivity is shown in Figure 5.14, with the conductivity values calculated from the gradient of the I - V plots around zero bias. The data confirms semi-conducting behaviour with the nanowire whilst also demonstrating the thermal stability of the DNA/polyC5-**TP** nanowire. The expected increase in conductivity is a result of the low levels of doping and disorder order within the material. This behaviour is typical of disordered semiconductors, where conduction occurs by hopping between localized states.²⁷ A small degree of hysteresis was evident between the heating and cooling phases of the cycle, possibly due to the loss of residual water bound to the polymer during the heating of the sample. The resistance of the nanowire, determined from variable temperature I - V measurements, was found to be in the order of $10^{13}\Omega$.

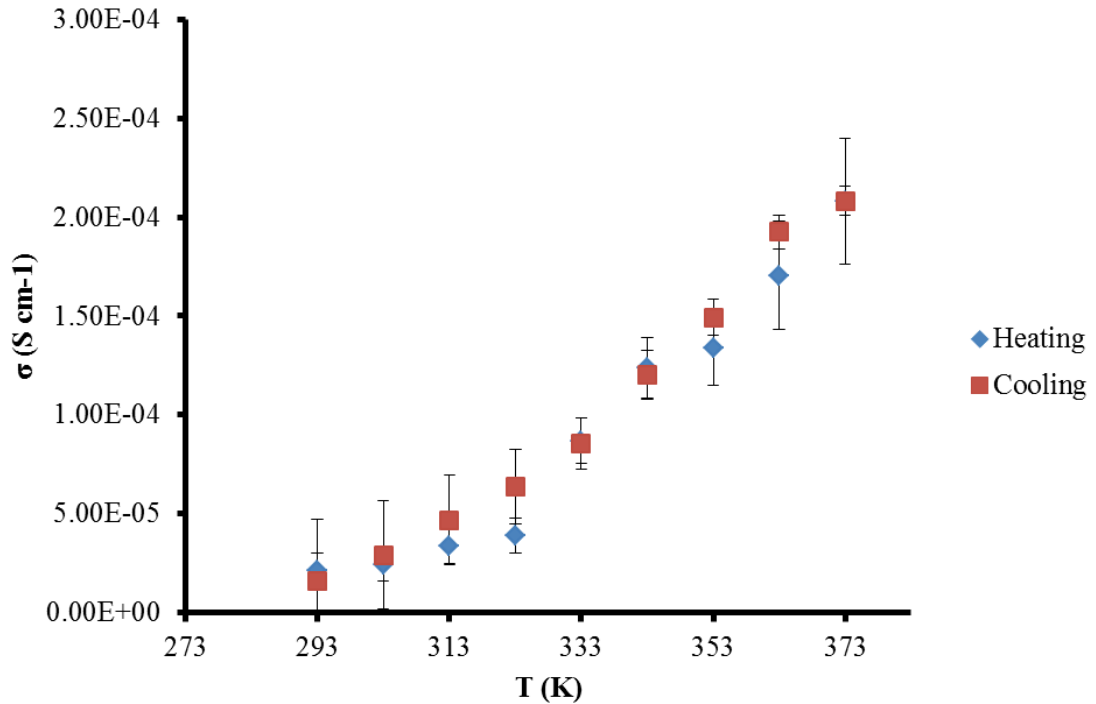


Figure 5.14. Variable temperature I - V measurements carried out upon a DNA/polyC5-TP nanowire aligned across two Au electrodes. Error bars were plotted using the standard deviation of each conductivity value

Analysis of the temperature dependence of conductance in conjugated polymers gives a more in-depth of the conduction mechanism and is typically carried out through fitting conductance (G) values to the following equation:

$$\ln G = \ln G_0 - (T_0/T)^\beta$$

This expression is used when describing the conductance behaviour of a conjugated polymer system through a variable range hopping (VRH) model (Chapter 1). This in turn describes the low temperature conductance behaviour in strongly disordered systems where electronic states are localized. In this approach, the outcome is dependent upon the dimensionality of the system which is described by the parameter $\beta=1/(1+D)$, where ' D ' is the dimensionality of the system. Following the VRH approach for a 1-D system such as our DNA/CP nanowires, predicts that $\beta=1/2$. However, this model breaks down for one-dimensional systems as the conduction is dictated by large barriers to charge carrier transport which cannot be avoided. As a consequence, such one-dimensional systems tend to follow Arrhenius behaviour,

where $\beta=1$, as previously reported for CP nanowires.²⁰ Figure 5.15 shows the corresponding Arrhenius plot of the conductance of the DNA/polyC5-TP nanowire, confirming the nanowire to follow this behaviour. The plot illustrates the temperature dependence of the rate constant and suggests electron hopping is the dominant mechanism for electron transport, shown through the exponential behaviour of the conductance upon increasing the temperature.

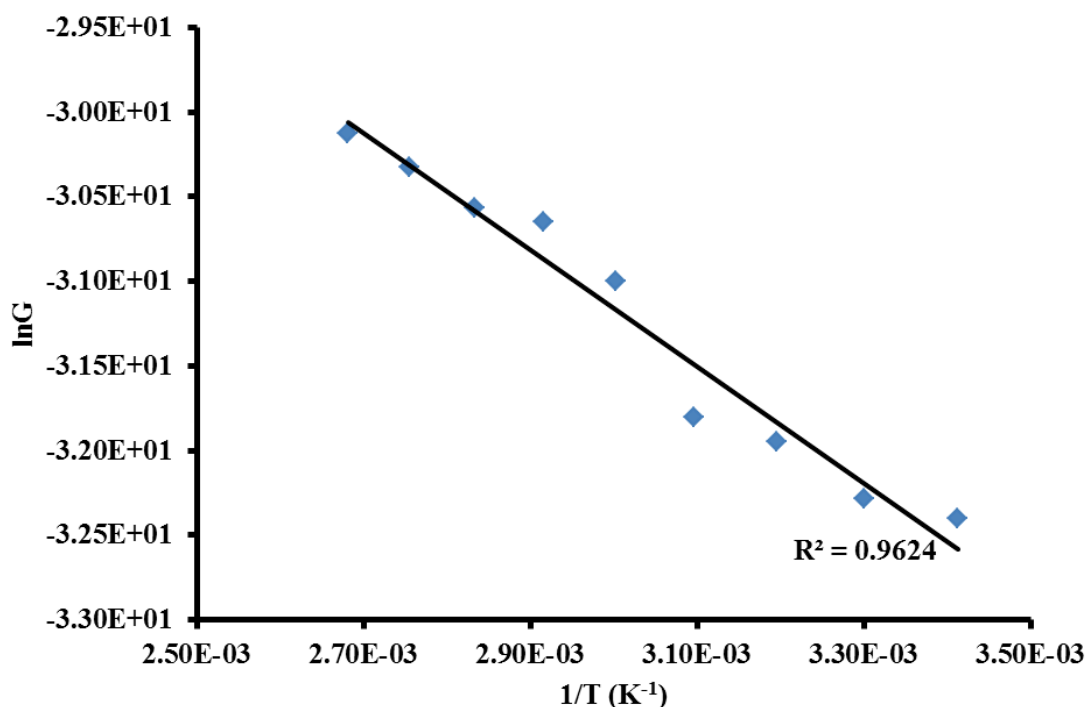


Figure 5.15. Arrhenius plot for the conductance of a DNA/polyC5-TP nanowire

Two-Probe I-V studies of DNA/polyC5-TPT aligned across Au micro-Electrodes

While quantitative information about the electrical behaviour of individual DNA/polyC5-TPT nanowires was not obtained, data pertaining to DNA/polyTPT was. Figure 5.16 shows an AFM height image of a DNA/polyTPT nanowire aligned across a 2.5 μm electrode gap. The resistance of the nanowire, determined from variable temperature I - V measurements, was found to be in the order of $10^{14} \Omega$. By evaluating the dimensions of the nanowire a conductivity value was extracted and calculated to be $1.9 \times 10^{-7} \text{ S cm}^{-1}$ at 303K.

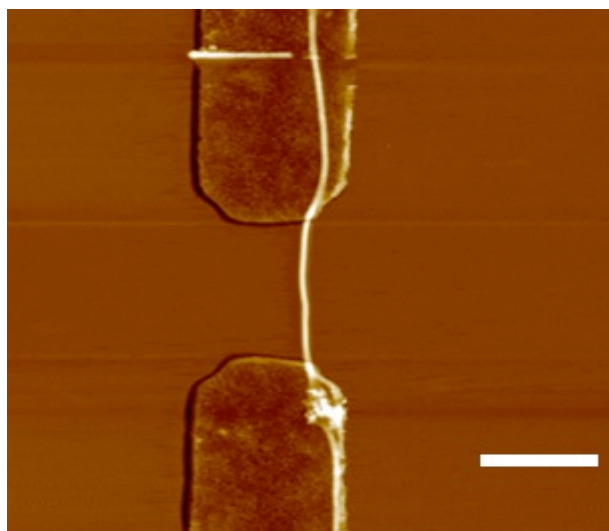


Figure 5.16. An AFM image of DNA/polyTPT nanowire (25 nm diameter) aligned across a 2.5 μm gap between two Au micro-electrodes, the scale bar = 2 μm and the z-scale range 0- 20 nm dark to bright contrast¹²

The temperature dependence of the nanowire conductivity is shown in Figure 5.17 with the conductivity values again calculated from the gradient of the I - V plots around zero bias while Figure 5.18 shows the corresponding Arrhenius plot. As with DNA/polyC5-TP, the plot illustrates the temperature dependence of the rate constant and suggests electron hopping is the dominant mechanism for electron transport, shown through the exponential behaviour of the conductance upon increasing the temperature. This data also confirms semi-conducting behaviour and thermal stability of the DNA/polyC5-TPT nanowire. Over the temperature range specified, as with DNA/C5-TP, a small degree of hysteresis was also evident between the heating and cooling phases of the cycle, which is again likely due to the loss of residual water bound to the nanowire during the heating of the sample.

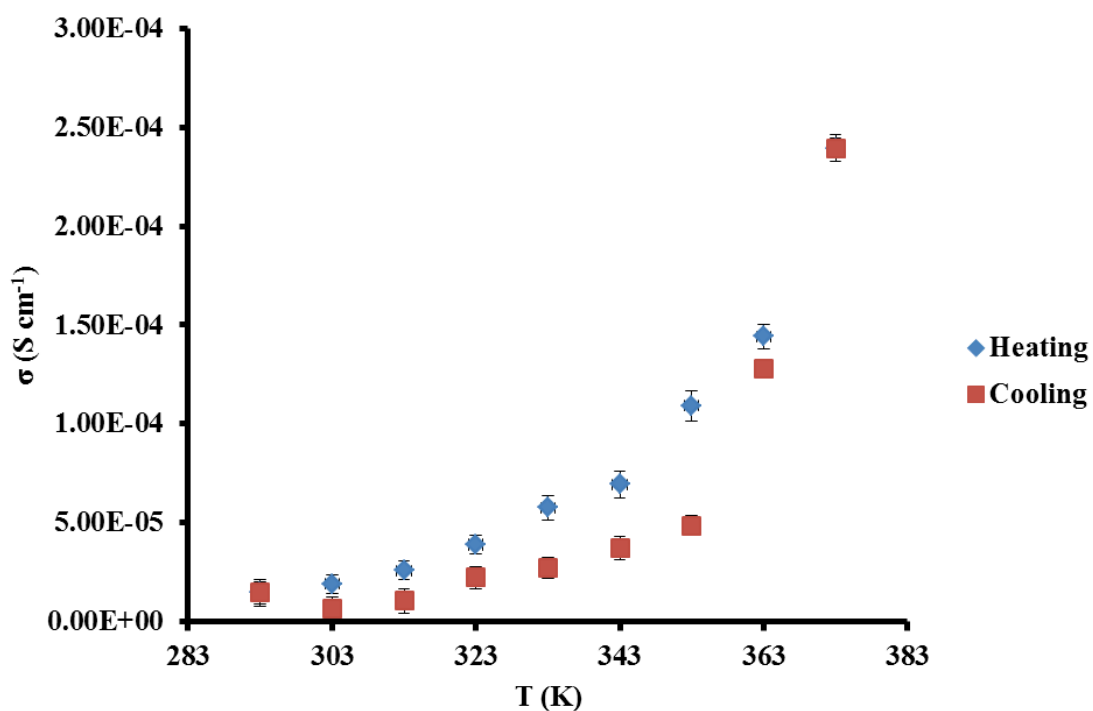


Figure 5.17. Variable temperature I - V measurements carried out upon a DNA/polyTPT nanowire aligned across two Au electrodes. Error bars were plotted using the standard deviation of each conductivity value

As with polyC5-TP, this value is significantly lower than anticipated. As this system remains unmodified at the N -position of pyrrole and that the DNA/CP material produced is structurally well-defined, these results would suggest the low conductivity values observed are an inherent characteristic of the pyrrole-thiophene monomer units. Unfortunately, reports detailing conductivity values for bulk polyTPT are absent from the literature.

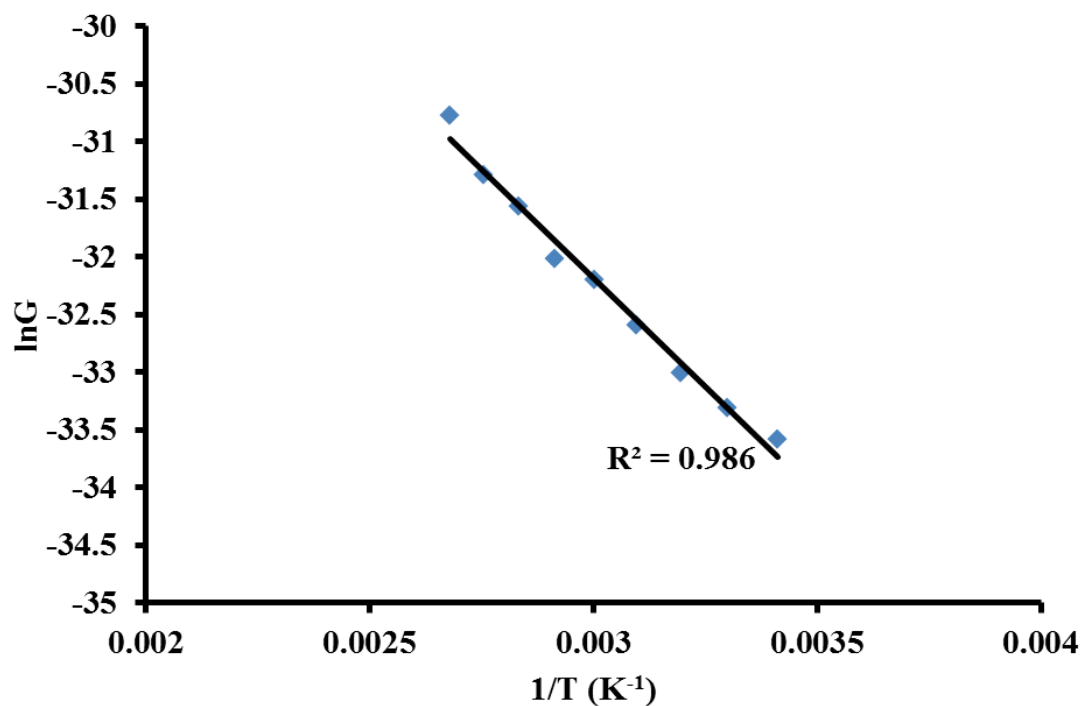


Figure 5.18. Arrhenius plot for the conductance of a DNA/polyTPT nanowire

Two-point probe I-V studies of DNA/C5-P aligned across Au micro-Electrodes

Figure 5.19 shows an AFM image of a single DNA/polyC5-P nanowire ~ 9.1 nm in diameter prepared in the absence of a chemical oxidant, stretched between two micro-electrodes ($2.5 \mu\text{m}$ gap).

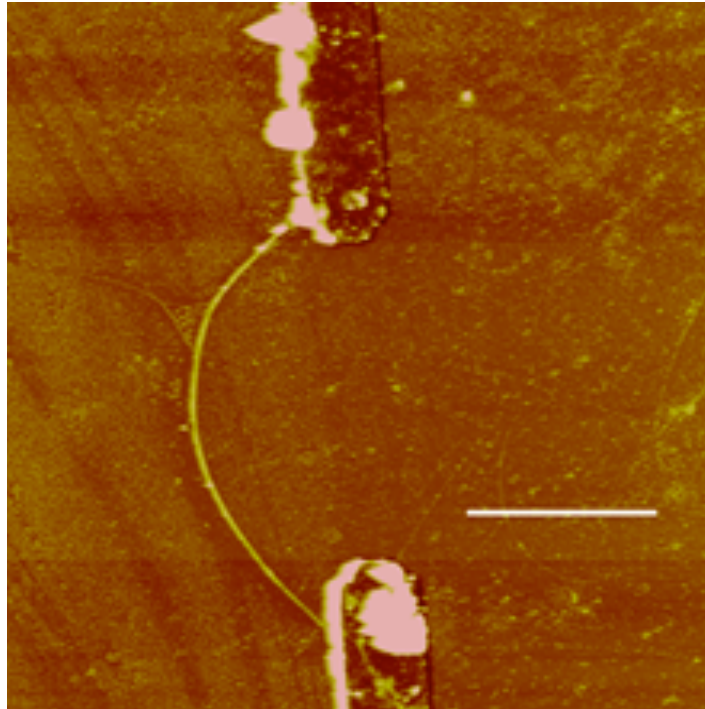


Figure 5.19. An AFM image of DNA/polyC5-P ~9 nm in diameter stretched between two Au microelectrodes, the scale bar = 5 μm and the z-scale range 0- 40 nm dark to bright contrast. The Au electrodes are embedded in a thermally grown, 200nm thick insulating SiO₂ layer on a Si substrate

Figure 5.20 is a 3-D image shows the connection between the nanowire and the gold electrodes and the good uniformity of the wire morphology.

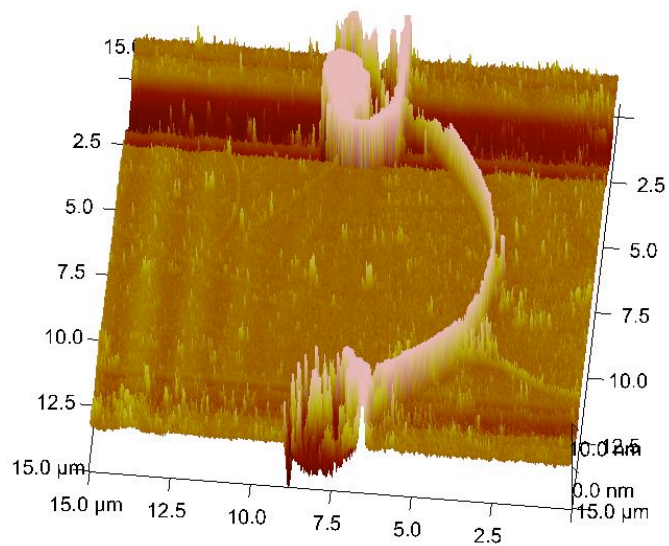


Figure 5.20. A 3-D image of DNA/polyC5-P ~9 nm in diameter stretched between two gold microelectrodes indicating the connection between the gold electrodes and the nanowire

The resistance of the nanowire determined from variable temperature I - V measurements found to be in the order of $10^{12} \Omega$. Again, by evaluating the dimensions of the nanowire (~ 9 nm) a conductivity value was calculated to be $3.8 \times 10^{-4} \text{ S cm}^{-1}$ at 303K. Unfortunately, comparison to pyrrole nanowires prepared in a similar fashion this value is significantly lower. As discussed earlier, Houlton *et. al.*¹⁰ reported levels of conductivity for DNA-templated nanowires of polypyrrole to be in the range of 4 S cm^{-1} using FeCl_3 as an oxidant. Given the uniform structure and morphology of the nanowire under investigation, it is unlikely conductance is significantly affected by breaks in the current pathway. Instead, this low level of conductance may be a consequence of modification at the N -position of the pyrrole moiety or as a result of low levels of doping within the material through the absence of FeCl_3 during the templating reaction.

Variable-temperature I - V studies over a temperature range of 293 to 373 K yielded some interesting behaviour. Figure 5.21 shows the conductivity calculated from the gradient of the I - V plots around zero bias plotted against temperature.

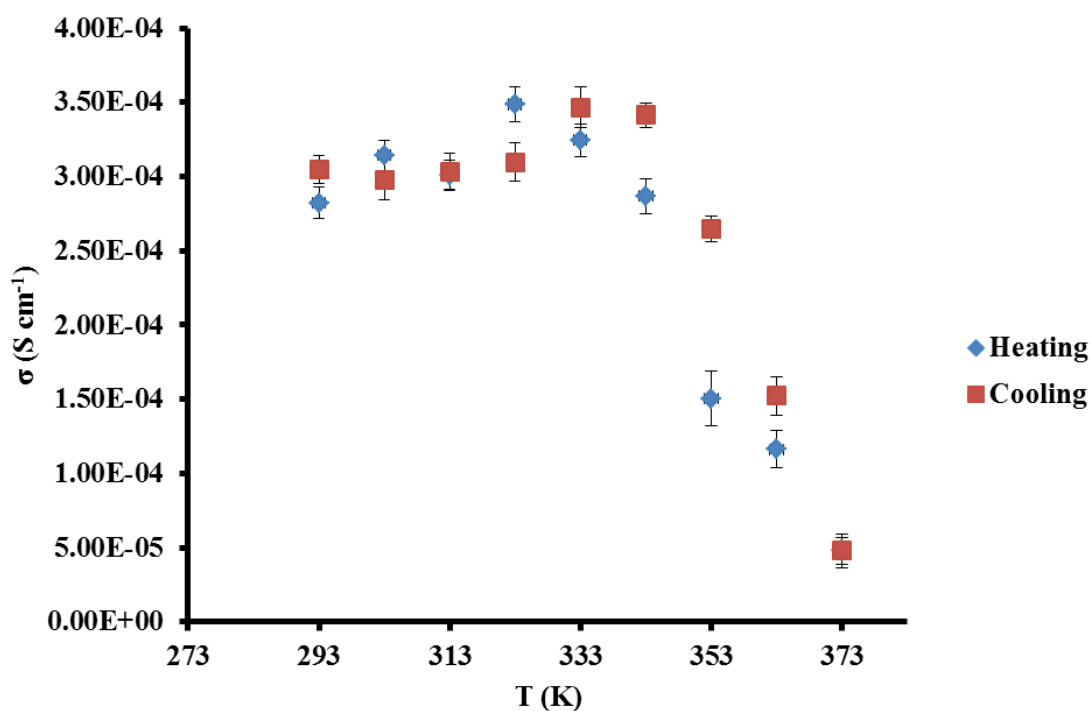


Figure 5.21. Variable temperature I - V measurements carried out upon a DNA/polyC5-P nanowire prepared in the absence of a chemical oxidant, aligned across two Au micro-electrodes. Error bars were plotted using the standard deviation of each conductivity value

Figure 5.21 shows that by elevating the temperature above 333 K a net reduction in conductivity was observed; with a final value of $3.83 \times 10^{-5} \text{ S cm}^{-1}$ recorded at 373 K compared to $2.27 \times 10^{-4} \text{ S cm}^{-1}$ at 293 K. Upon cooling from 373 K, this process was reversed over the same temperature range ($\sim 333 \text{ K}$), with a return to similar levels conductivity to those observed during the heating process ($2.45 \times 10^{-4} \text{ S cm}^{-1}$ at 293 K). This is unlike the behaviour of the other materials studied here or elsewhere.^{10, 12, 20}

This data confirms the DNA/C5-P nanowires prepared without a chemical oxidant are indeed conductive, whilst also suggesting heating may induce a molecular switch type process. The return of the conductivity upon cooling to similar levels observed prior to heating indicates that these observations were not a result of trapped water in the sample but may in fact a property of the wire.

As discussed in Chapter 4, it is considered that nanowires prepared in this manner (pH 5, in the absence of a chemical oxidant) may have a thinner polymer coating encapsulating the DNA and/or a more homogenous structure rather than aggregated polymer. Upon heating the sample above 333 K this is thought to provide more freedom to the template and thus allowing for denaturing of the DNA. Denaturing disrupts the polymer chains in such a way as to make charge transport less efficient between the electron holes and donors of the polymeric material is increased, resulting in a reduction in the degree of electron hopping and lower observed conductivity values. It is postulated, the polymer coating remains in the proximity of the denatured DNA strands and hence upon cooling hybridization occurs, restoring the nanowire to the original state. Efforts to examine DNA denaturing on Si surfaces by AFM were un-successful due to the AFM heating stage not having the necessary temperature range.

It was also considered that this switch type process may have alternatively been the result of short, poorly crystalline polymer chains or the significant presence of monomer units in the sample, due to the absence of a chemical oxidant. This explanation was examined by depositing FeCl_3 (1 mM, 5 μL) over the wire in question for a period of 1 minute in an effort to oxidize any remaining monomer units and provide a more tightly packed structure. No change to conductivity was

observed and consequently this anomaly is clearly based in the interior formation of the wire, not due to monomeric material.

5.4 Conclusions

The electrical properties of DNA-templated polymer nanowires of C5-**P**, C5-**TP** and C5-**TPT** were investigated using scanned conductance microscopy (SCM) and in some cases two-terminal I - V measurements using bespoke Au micro electrodes. SCM phase images of DNA hybrid C5-**P**, C5-**TP** and C5-**TPT** nanowires prove consistent with the predicted observations for conductive objects, with the negative-positive-negative phase shifts characteristic of semi-conducting materials observed.

The resistance of the DNA/polyC5-**TP** nanowire, determined from variable temperature I - V measurements, was found to be in the order of $10^{13}\Omega$. By evaluating the dimensions of the nanowire a conductivity value was calculated to be $2.9 \times 10^{-5} \text{ S cm}^{-1}$ at 303K

The resistance of the DNA/poly**TPT** nanowire, determined from variable temperature I - V measurements, was found to be in the order of $10^{14} \Omega$. A conductivity value was calculated to be $1.9 \times 10^{-7} \text{ S cm}^{-1}$ at 303K. In both cases, electron hopping was determined to be the dominant mechanism for electron transport shown through the exponential behaviour of the conductance upon increasing the temperature.

A DNA/polyC5-**P** prepared in the absence of a strong oxidant was shown to exhibit a resistance in the order of $10^{12}\Omega$. Again, by evaluating the dimensions of the nanowire, a conductivity value was calculated to be $3.75 \times 10^{-4} \text{ S cm}^{-1}$ at 303K. DNA/C5-**P** nanowires prepared without a chemical oxidant are shown to be conductive, while the temperature dependence of this was unusual.

Whilst the DNA/CP nanowires produced are structurally well-defined, electrical measurements show the polymer material to exhibit significantly lower conductivities in comparison to polypyrrole and polythiophene nanowires. This low level of conductance may be a consequence of modification at the N -position of the pyrrole moiety in some cases, or an inherent characteristic of the materials being

investigated as opposed to any significant effects from breaks in the current pathway.

In order for progress to be made towards application of these materials in sensory devices, methods for improving the intrinsic electrical conductivity of each material would, realistically, be required. Routes to achieving this include alternative approaches within the chemical polymerization strategies currently used, such as changing the oxidant/dopant used which may have a notable impact upon the CPs intrinsic properties.

5.5 Experimental

5.5.1 Scanned Conductance Microscopy (SCM)

SCM studies were carried out upon DNA/polymer nanowires immobilised upon Si(111) substrates with a 200 nm thick, SiO₂ layer, modified with a TMS self-assembled monolayer, as in Chapter 3. All experiments were performed in air with a Dimension Nanoscope V system (Veeco Instruments Inc., Metrology Group), using MESP probes (n-doped Si cantilevers, with a Co/Cr coating, Veeco Instruments Inc., Metrology Group) with a resonant frequency of *ca.* 70kHz, a quality factor of 200–260, and a spring constant of 1–5Nm⁻¹. Acquisition and processing of SCM data was carried out using Nanoscope version 7.00b19 software (Veeco Instruments Inc., Digital Instruments). During SCM experiments, an independently controlled bias, typically set between -7 V and +7 V, was applied to the sample whilst the tip was kept grounded, and lift heights of 50–70nm were typically employed.

5.5.2 Two-Point probe Current-Voltage Measurements

I-V measurements were carried out upon individual DNA/polymer nanowires through the fabrication of tailor-made two-terminal nanowire devices, comprised of Au microelectrodes embedded in a thermally grown SiO₂ layer, supported on a Si substrate. Electrical measurements were made using a Probe Station (Cascade Microtech, Inc., Oregon, USA) and B1500A Semiconductor analyzer (Agilent Technologies UK Ltd., Edinburgh, United Kingdom), equipped with Agilent EasyEXPERT software. Prior to electrical testing, the two-terminal devices underwent a heating/cooling cycle between 293-373K, using a heating/cooling chuck (Model ETC-200L, ESPEC Corp., Osaka, Japan), under a N₂ atmosphere, to drive off any water bound to the nanowire. Subsequent *I-V* measurements were conducted under a N₂ atmosphere, without light illumination, and using a voltage range of -3 to +3 V in steps of 0.05 V. Variable temperature *I-V* measurements were carried out between a temperature range of 293–373K, at increments of 10 K.

5.6 References

1. H. Shirakawa, E. J. Louis, A. G. MacDiarmid, C. K. Chiang and A. J. Heeger, *Journal of the Chemical Society, Chemical Communications*, 1977, **0**, 578-580.
2. S. F. Alvarado, W. Rieß, P. F. Seidler and P. Strohriegl, *Physical Review B*, 1997, **56**, 1269-1278.
3. R. Rinaldi, R. Cingolani, K. M. Jones, A. A. Baski, H. Morkoc, A. Di Carlo, J. Widany, F. Della Sala and P. Lugli, *Physical Review B*, 2001, **63**, 075311.
4. M. Kemerink, S. F. Alvarado, P. Müller, P. M. Koenraad, H. W. M. Salemink, J. H. Wolter and R. A. J. Janssen, *Physical Review B*, 2004, **70**, 045202.
5. D. Kelkar, A. Chourasia and V. Balasubramanian, *Macromolecular Symposia*, 2012, **315**, 66-72.
6. D. Kelkar and A. Chourasia, *Macromolecular Symposia*, 2013, **327**, 45-53.
7. P. K. Upadhyay and A. Ahmad, *Chinese Journal of Polymer Science (CJPS)*, 2010, **28**, 191-197.
8. P. D. Gaikwad, D. J. Shirale, V. K. Gade, P. A. Savale, H. J. Kharat, K. P. Kakde, S. S. Hussaini, N. R. Dhumane and M. D. Shirsat, *Bulletin of Materials Science*, 2005.
9. C. Musumeci, J. A. Hutchison and P. Samori, *Nanoscale*, 2013, **5**, 7756-7761.
10. L. Dong, T. Hollis, S. Fishwick, B. A. Connolly, N. G. Wright, B. R. Horrocks and A. Houlton, *Chemistry – A European Journal*, 2007, **13**, 822-828.
11. S. Pruneanu, S. A. F. Al-Said, L. Dong, T. A. Hollis, M. A. Galindo, N. G. Wright, A. Houlton and B. R. Horrocks, *Advanced Functional Materials*, 2008, **18**, 2444-2454.

12. S. M. D. Watson, J. H. Hedley, M. A. Galindo, S. A. F. Al-Said, N. G. Wright, B. A. Connolly, B. R. Horrocks and A. Houlton, *Chemistry – A European Journal*, 2012.
13. Y.-Z. Long, Z. Chen, C. Gu, M. Wan, J.-L. Duvail, Z. Liu and S. P. Ringer, *A Review on Electronic Transport Properties of Individual Conducting Polymer Nanotubes and Nanowires*, 2010.
14. A. L. Briseno, S. C. B. Mannsfeld, S. A. Jenekhe, Z. Bao and Y. Xia, *Materials Today*, 2008, **11**, 38-47.
15. M. Bockrath, N. Markovic, A. Shepard, M. Tinkham, L. Gurevich, L. P. Kouwenhoven, M. W. Wu and L. L. Sohn, *Nano Letters*, 2002, **2**, 187-190.
16. C. Staii, A. T. Johnson and N. J. Pinto, *Nano Letters*, 2004, **4**, 859-862.
17. J. Heo and M. Bockrath, *Nano Letters*, 2005, **5**, 853-857.
18. S. M. D. Watson, A. R. Pike, J. Pate, A. Houlton and B. R. Horrocks, *Nanoscale*, 2014.
19. H. Reda, A. F. A.-S. Said, Š. Lidija, L. Ross, G. W. Nicholas, H. Andrew and R. H. Benjamin, *Nanotechnology*, 2012, **23**, 075601.
20. R. Hassanien, M. Al-Hinai, S. A. Farha Al-Said, R. Little, L. Šiller, N. G. Wright, A. Houlton and B. R. Horrocks, *ACS Nano*, 2010, **4**, 2149-2159.
21. S. A. Farha Al-Said, R. Hassanien, J. Hannant, M. A. Galindo, S. Pruneanu, A. R. Pike, A. Houlton and B. R. Horrocks, *Electrochemistry Communications*, 2009, **11**, 550-553.
22. N. McGrath, A. J. Patil, S. M. D. Watson, B. R. Horrocks, C. F. J. Faul, A. Houlton, M. A. Winnik, S. Mann and I. Manners, *Chemistry – A European Journal*, 2013, **19**, 13030-13039.
23. J. Hannant, J. H. Hedley, J. Pate, A. Walli, S. A. Farha Al-Said, M. A. Galindo, B. A. Connolly, B. R. Horrocks, A. Houlton and A. R. Pike, *Chemical Communications*, 2010, **46**, 5870-5872.

24. Image drawn by Dr. J. D. Watson, 2010.
25. M. Weis, J. Lin, D. Taguchi, T. Manaka and M. Iwamoto, *Applied Physics Letters*, 2010, **97**.
26. V. Bocharova, A. Kiriya, H. Vinzelberg, I. Mönch and M. Stamm, *Angewandte Chemie International Edition*, 2005, **44**, 6391-6394.
27. A. B. Kaiser, *Advanced Materials*, 2001, **13**, 927-941.

Chapter 6

Conductivity Studies of Pyrrole-Thiophene Co-Polymer Films

6.1 Chapter Overview

Overall Goal

To improve the intrinsic electrical conductivity of each polymer system (polyC5-P, polyC5-TP and polyC5-TPT) by first elucidating sources of poor conductivity and optimizing polymer preparation accordingly.

Hypothesis

Low level of conductance observed in each system is a consequence of modification at the N-position of the pyrrole moiety. Introduction of pyrrole as a co-monomer unit will increase the conductivity of each system.

Objectives

Perform and compare bulk conductivity measurements of polyC5-P, polyC5-TP and polyC5-TPT and the relevant non-alkylated monomer units, polyP, polyTP and polyTPT.

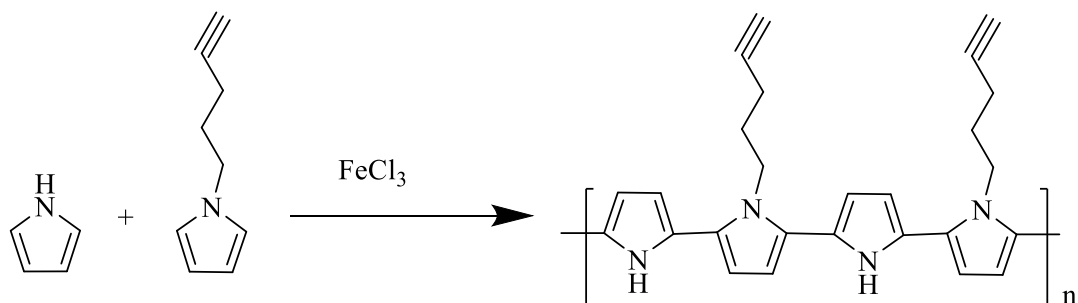
Establish reaction conditions which afford the highest level of conductivity in polypyrrole.

Prepare and electrically characterize bulk polymer systems of polyC5-P, polyC5-TP and polyC5-TPT co-polymerized with polypyrrole from the corresponding monomer mixtures.

6.2 Introduction

The use of semiconductor materials in sensor devices involves the measuring of small currents, with the limit to sensitivity in any measurement determined by the noise generated from the resistance in the circuit, current leakage, dielectric quality and the conducting compounds electrical properties. A fundamental requirement for future diagnostic (biosensor) technologies is the removal for the necessity of cumbersome and expensive instrumentation to facilitate such measurements, with ideally, a move toward portable device manufacture.

Unfortunately, electrical characterization (Chapter 5) of DNA/polyC5-**P** and DNA/polyC5-**TP** nanowires showed levels of conductivity that make these materials currently unsuitable for such application. The low level of conductance observed was considered to be a consequence of modification at the *N*-position of the pyrrole moiety or an influence of the three possible configurations of polyC5-**TP**, “head-to-tail”, “tail-to-tail”, or “head-to-head” (Chapter 3) resulting in a loss of planarity/conjugation length. Therefore efforts for improving the intrinsic electrical conductivity were made by introducing pyrrole, to produce a co-polymer (Scheme 6.1). Co-polymers can have tailor-made properties depending upon the choice of the two semi-conducting components, their relative amounts and their arrangement in the polymer chain. By increasing the proportion of highly conductive components (i.e. pyrrole) improves the overall conductivity of the co-polymer chain yet retaining functionality afforded by modified, less conductive components.



Scheme 6.1. Chemical co-polymerization of pyrrole and C5-**P**. The resulting product retains the alkyne functionality with the improved conductivity afforded by the additional un-modified pyrrole moieties

Here, C5-P, C5-TP and C5-TPT are used to retain the functionality afforded by the alkyne moiety but with increased level of conductivity provided by the addition of the large band-gap component, pyrrole. This approach is similar to that implemented by Livarche *et. al.*^{1, 2} amongst others,^{3, 4} using pyrrole bearing oligonucleotides (ODN) and unmodified pyrrole to construct DNA sensor arrays.

The conductivity of polypyrrole has been reported to vary according the final form and the preparation technique employed (10^{-12} - 10^5 S cm⁻¹).⁵⁻¹⁰ Therefore, in order to effectively improve the intrinsic electrical conductivity of the DNA-templated nanowires by implementation a co-polymer system, it was useful to investigate the effect how the preparation technique employed thus far may be optimised to produce the highest level of conductivity feasible from the polypyrrole component.

Defects and degradation during the formation of polypyrrole can take several forms, with the method of preparation shown to significantly affect the electronic properties of polymer produced.¹¹⁻¹⁴ In addition to the adverse effect polymerisation through the β -position has on conductivity, over-oxidation of pyrrole has been observed to cause a reduction in conductivity during both electrochemical¹⁵ and chemical preparation.¹¹ The presence of water and in particular $-OH$ ions is instrumental in this process through hydroxylation of the polymer and subsequent carbonyl formation (Figure 6.1).

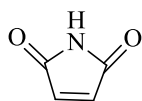


Figure 6.1. The chemical structure of maleimide, formed through over oxidation of pyrrole

Of particular importance to retaining the conductive nature of the polypyrrole produced is the role of acidic conditions upon pyrrolidine formation (Figure 6.2). There have been reports where acidic conditions have been employed to polymerize monomer units such as pyrrole.^{14, 16} In this approach low conductivity (in the order of 10^{-6} S cm⁻¹ in some cases), attributed to structural defects, such as the formation of pyrrolidine units (Figure 6.2), are known to occur during extended

polymerisation of pyrrole at low pH (7.5 M HCl).¹⁴ An alternative study has shown that when milder acidic conditions and lower concentrations are used an increased conductivity was observed.¹⁷

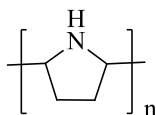


Figure 6.2. The structure of pyrrolidine units implicated in the acid initiated polymerisation of pyrrole

Given the pH of the DNA-templating solution drops during polymerisation (~pH 3, after 1 hour) as a result HCl formation (Figure 6.3). It was envisaged to be useful to investigate the effect of varying oxidant to monomer ratio, incubation times and pH of bulk polymerisation reactions upon the conductivity of polypyrrole prior to implementation a co-polymer system.

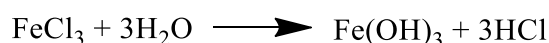


Figure 6.3. The chemical hydrolysis of ferric chloride yielding HCl

Chapter Outline: *In this chapter, initial studies focused upon bulk conductivity measurements of polyC5-P, polyC5-TP and polyC5-TPT and the relevant non-alkylated monomer units, polyP, polyTP and polyTPT, in order to compare values to those gathered in Chapter 5 and elucidate sources of poor conductivity. Subsequent studies investigating the effect of varying oxidant to monomer ratio, incubation times and pH of bulk polymerisation reactions upon the conductivity of polypyrrole are also presented. Finally, in an effort to prepare CP systems with functionality and high conductivity, bulk of polyC5-P, polyC5-TP and polyC5-TPT co-polymerized with polypyrrole samples were prepared from the corresponding monomer mixtures and the conductive properties of these materials investigated.*

6.3 Results and Discussion

6.3.1 Bulk Conductivity Measurements

Hypothesis: Low level of conductance observed in each system is a consequence of modification at the N-position of the pyrrole moiety evident by comparative bulk conductivity studies.

Bulk polymer samples of polyC5-**P**, polyC5-**TP** and polyC5-**TPT** were prepared by chemical polymerisation of the corresponding monomer units, with the precipitate formed isolated from solution as described in Chapter 3. The appearance and morphology of the precipitate formed was similar to that observed in Chapter 3, with isolated precipitate of polyC5-**P** again found to be both brittle and foam like. PolyC5-**TP** and polyC5-**TP** were both found to be robust and metallic-like.

As in Chapter 5, two probe current-voltage sweeps typically over a range of -5 to +5 V were used to gain quantitative electrical data for all samples. A typical I - V plot obtained is shown in Figure 6.4 and has the classic shape expected for hopping polymers in the case of fixed counter anions.¹⁸

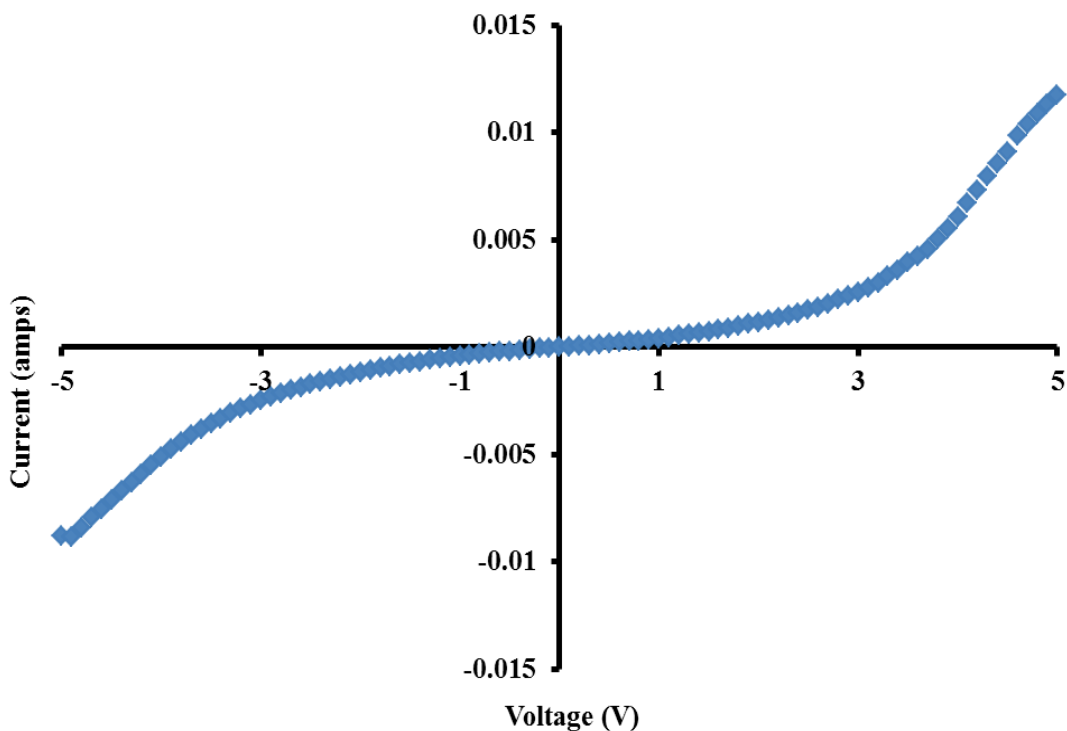


Figure 6.4. A typical current-voltage plot for bulk polypyrrole samples obtained from the Agilent B1500 Agilent probe station

The dimensions used for calculating the conductivity of each material were based on electrons taking shortest route between two points, i.e. the distance between the two probes. In this study, the diameter (D) of the probes used was $3.8 \mu\text{m}$. The cross-sectional area can be calculated using the equation:

$$A = 0.784 \times D^2$$

Assuming the electron path is direct, the length (l) is estimated distance between the two probes. This can then be used to calculate conductivity as described in Chapter 5. A significant contribution to resistance from electrical contact made between the CP and the electrical probes is possible. However, if the contact resistance is ignored, an estimate (lower bound) of the sample conductivity can be made.

Despite the likely dispersion of the electron path around the entire sample it was hoped conductivity values accurate within an order of magnitude could be obtained using this approach. Table 6.1 shows conductivity values calculated from the gradient of the I - V plots around zero bias (303 K and averaged over 5 values taken from different 5 samples) for the three alkynyl derivatized polymers.

Polymer	σ (S cm ⁻¹)
polyp	$2.22 \times 10^2 \pm 40.10$
polyTP	$1.05 \times 10^{-2} \pm 2.75 \times 10^{-5}$
polyTPT	$1.9 \times 10^{-2} \pm 6.10 \times 10^{-3}$
polyC5-P	$1.13 \pm 0.016 \times 10^{-6}$
polyC5-TP	$6.04 \pm 3.28 \times 10^{-10}$
polyC5-TPT	$1.98 \pm 0.17 \times 10^{-6}$

Table 6.1. Bulk conductivity values of polyP, polyTP, polyTPT and polyC5-P, polyC5-TP and polyC5-TPT

Overall, the conductivity values observed for each system are significantly low. PolyC5-P and polyC5-TPT exhibit comparable levels of conductivity (1.13×10^{-6} S cm⁻¹ and 1.98×10^{-6} S cm⁻¹ respectively), whereas polyC5-TP showing conductive properties several orders of magnitude lower (6.04×10^{-10} S cm⁻¹).

By comparison to measurements taken for non-alkylated polymers (polyP, and polyTPT, Table 6.1) it appears that alkylation of the central pyrrole ring at the *N*-position has a major impact on the poor conductivity, as higher conductivity levels were observed across all three non-alkylated systems analysed (polyP = 2.22×10^2 S cm⁻¹, polyTP = 1.05×10^{-2} S cm⁻¹ and polyTPT = 1.90×10^{-2} S cm⁻¹).

As described in Chapter 1, alkylation at the *N*-position of pyrrole has been shown to adversely affect the electrical properties of the polymer and this has been rationalised as being due to disruption of the conjugated system. *N*-methyl-polypyrrole for instance, is reported to exhibit conductivities of $\sim 10^{-3}$ S cm⁻¹.¹⁹ It is likely the increased size of the moiety attached at the *N*-position may cause similar disruption to the co-planar arrangement of the ring system, accounting for such a significant reduction in conductivity.

Furthermore, the fact that the TP based materials (polyTP, polyTPT, polyC5-TP and polyC5-TPT) show the lowest conductivity values of the systems studied may be due to additional irregularities in the polymer chain structure arising from the different possible configurations for lining the TP units. These are ‘head-to-tail’, ‘tail-to-tail’, or ‘head-to-head’ of polyC5-TP (Chapter 3) which may reduce the planarity and hence the significant reduction in conductive properties observed in polyC5-TP by comparison to polyC5-TP and polyC5-TP.

It is also noted that the conductivity of the bulk poly**TP** and poly**TPT** materials exhibit conductivity values which are 4 – 5 orders of magnitude lower in conductivity than that of polypyrrole and polythiophene ($10^2 - 10^3 \text{ S cm}^{-1}$) materials. Indicating that tailoring of the monomer units to incorporate thiophene ring system to *N*-alkylated polymer systems with high intrinsic conductivity actually has the opposite effect.

Interestingly, DNA/polyC5-**P** nanowires prepared in the absence of a chemical oxidant exhibit conductivity values higher than that of the corresponding bulk material prepared using FeCl_3 . Similar observations have been made elsewhere²⁰ and may be a result of structural regularity afforded by the templated directed growth. However, this is not the case with polyC5-**TPT** where the conductivity the bulk sample was shown to lie in the range 1.0×10^{-2} to $2.3 \times 10^{-2} \text{ S cm}^{-1}$; an increase by several orders of magnitude compared to the nanowire.

Interestingly, the dependence of the conductivity on the polymer form and size was clear when comparing these values to those gained from two-probe *I-V* measurements i.e. bulk *vs.* nanowire, of DNA templated nanowires of polyC5-**P**, polyC5-**TP** and poly-**TPT** (Chapter 5). While it is difficult to make precise comparisons given the absence of the DNA-template and the uncertainties in the geometry of current path in the bulk material, comparison of the quantitative two-probe *I-V* studies for DNA/polyC5-**P**, DNA/polyC5-**TP** show the conductivity of the nanowire structure ($3.75 \times 10^{-4} \text{ S cm}^{-1}$ and $2.9 \times 10^{-5} \text{ S cm}^{-1}$ at 303K respectively) to be several orders of magnitude higher than that of the bulk material ($1.13 \times 10^{-6} \text{ S cm}^{-1}$ and $6.04 \times 10^{-10} \text{ S cm}^{-1}$ respectively). The difference between these values was so large that this cannot be attributed on the uncertainties in the measurements.

6.3.2 Optimised Preparation of Polypyrrole

Goal: Elucidate the appropriate conditions to provide the highest level of conductivity from polypyrrole.

Prior to attempts to prepare co-polymer based systems of polyPy/polyC5-**P**/polyC5-**TP**/polyC5-**TPT**, studies were conducted to establish suitable reaction conditions

for obtaining polypyrrole with good conductivity levels. Specifically the ratio of oxidant to monomer and reaction time were considered.

Figure 6.5 is a plot of conductivity measurements against varied oxidant ratio (1:1 to 3:1) after 1 hour incubation ($\text{H}_2\text{O}:\text{DMF}$, 4:1). As expected, as the ratio of oxidant employed is increased (0.25-2, increasing the level of doping enhances conductivity) the conductivity of the bulk material also generally increases (15.5–222 S cm^{-1}); this is thought to be due substantial polymerisation and the subsequent formation of a more homogeneous structure. Interestingly, as the oxidant to monomer ratio is extended to 3:1, a reduction in conductivity is observed (2:1=222 S cm^{-1} , 3:1=109 S cm^{-1}). Initially this was considered to be due to over oxidation of the pyrrole ring however inspection of the FTIR spectra (Chapter 3) reveals little evidence of such degradation taking place (typically observed through C=O band at *ca.* 1720 cm^{-1}).

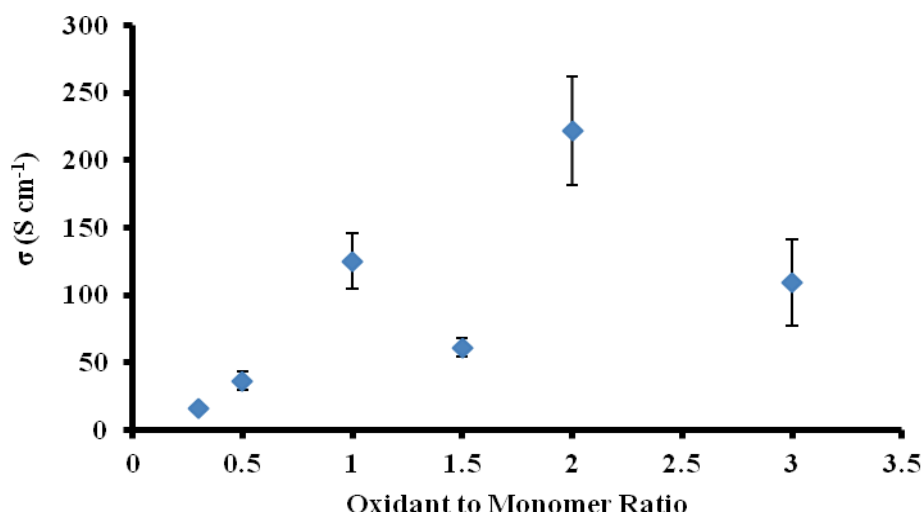


Figure 6.5. Conductivity measurements of polypyrrole against varied oxidant ratio (1:1 to 3:1) after 1 hour incubation

A possible explanation of the observed trend in conductivity can be found by considering the role of HCl and iron chloride concentration. With increased FeCl_3 , a greater degree of HCl is produced which is likely to cause minor defects in the polymer through pyrrolidine formation, as described in Section 6.2. While these defects remained untraceable by FTIR this may be due to the reflective nature of the conductive polymer produced and the density of defects in the samples.

Furthermore, work elsewhere^{21, 22} has shown maleimide formation from over-oxidation of pyrrole is strongly enhanced at the early stages of the polymerisation reaction, as degradation occurs more readily in shorter polymer chains with larger, more conductive material produced later in the reaction.

It was considered from data presented here, that over an extended time period continued degradation may also take place, resulting in the observed peak in conductivity and subsequent reduction in observed conductivity at later longer time periods.

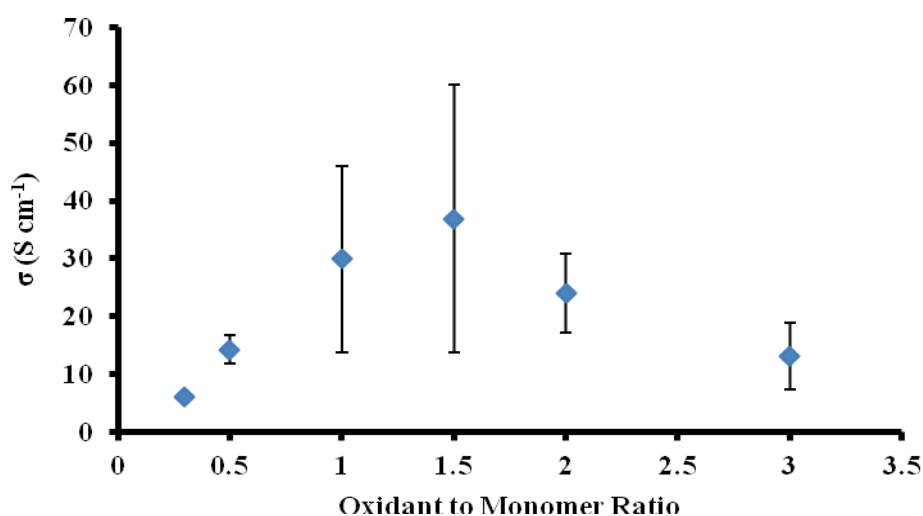


Figure 6.6 Conductivity measurements of polypyrrole against varied oxidant ratio (1:1 to 3:1) after 3 hour incubation

In order to examine the role longer reaction times in the degradation of polypyrrole, the effect of extended incubation times upon conductivity were also investigated (3 and 24 hours (Figure 6.6 and 6.7)). It is clear that by extending the reaction time the overall conductivity was significantly reduced in each case (for 2:1 1 hour, 222 S cm^{-1} compared to 24 S cm^{-1} after 3 hours and 13.6 S cm^{-1} after 24 hours). It is likely, extended incubation times give rise to more degeneration in the polymer and hence the observed reduction in conductivity.

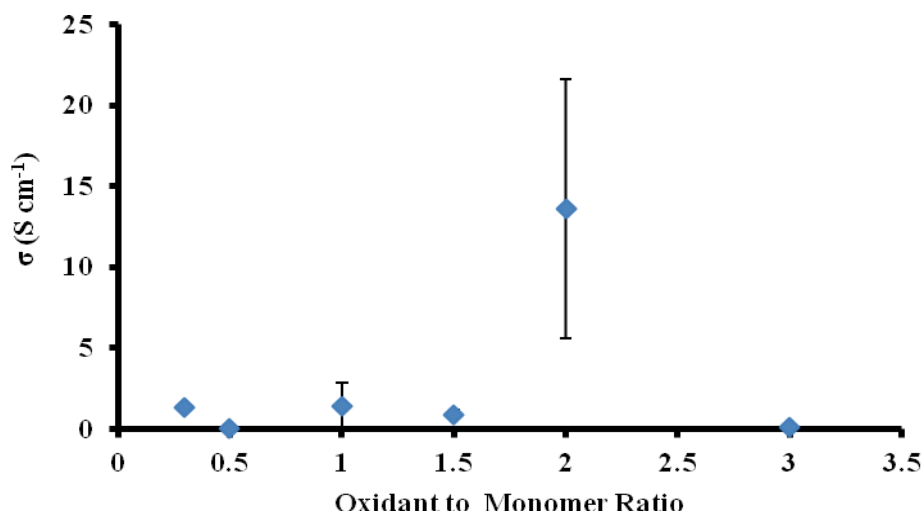


Figure 6.7. Conductivity measurements of polypyrrole against varied oxidant ratio (1:1 to 3:1) after 24 hour incubation

It is considered that beyond 1 hour reaction time the majority of the monomer unit has been used to form polymer. After which, HCl formation (rapidly) becomes the dominant process and polymer degradation begins, reducing the overall conductivity. When excess $FeCl_3$ was employed (2:1 or 3:1), a peak in conductivity was observed followed by a reduction, likely due to the increasing level of HCl in the reaction mixture over-time, with a 2:1 ratio of oxidant to monomer seeming to provide the highest level of conductivity in each set of experiments.

To investigate the effect of pH further, bulk polymerisation experiments in which the pH was deliberately lowered were carried out. Table 6.2 shows conductivity data for oxidant-to-Py ratios of 1:1, 2:1, 3:1, 1 hour incubation, at pH=5 (Tris-HCl). Despite the initial pH 5, levels of conductivity similar to those observed in a where the pH was not initially lowered were observed. However, the drop in conductivity at a 3:1 oxidant to monomer ratio was much more pronounced.

Ratio	σ ($S\ cm^{-1}$)
1:1	29.70 (± 19.69)
2:1	217.79 (± 79.34)
3:1	6.97 (± 7.20)

Table 6.2. Oxidant to Py ratio 1:1, 2:1, 3:1, 1 hour incubation, pH 5 (Tris-HCl)

Table 6.3 shows conductivity values with the pH=7 maintained (Tris-HCl buffer). A continued increase in conductivity is observed regardless of the oxidant to monomer ratio. Furthermore, polymerisation conducted at pH 7 produces materials with highest conductivity. Therefore it is considered that the acidic conditions of the system reduce the conductivity of the polymer produced. However, by maintaining an oxidant ratio below 3:1 or maintaining pH 7, pH is controlled, therefore reducing the overall degradation of the polymer.

Ratio	σ (S cm ⁻¹)
1:1	38.8 (\pm 18.68)
2:1	105.9 (\pm 56.08)
3:1	254.2 (\pm 89.42)

Table 6.3. Oxidant to Py ratio 1:1, 2:1, 3:1, 1 hour incubation, pH 7 (Tris-HCl buffer)

6.3.3 Co-Polymer Systems

Goal: To prepare and electrically characterize bulk polymer systems of polyC5-P, polyC5-TP and polyC5-TPT co-polymerized with polypyrrole from the corresponding monomer mixtures.

In an effort to prepare CP systems with functionality and high conductivity, bulk of polyC5-P, polyC5-TP and polyC5-TPT co-polymerized with polypyrrole, samples were prepared from the corresponding monomer mixtures using the optimised conditions described in Section 6.3.2. Here, each sample was prepared in a 2:1 oxidant to monomer ratio with 1 hour incubation time at pH=7. Unfortunately, efforts to elucidate the proportion of each unit present in the final co-polymeric mixture by FTIR were unsuccessful. In each instance isolation of the precipitate formed showed no absorbance bands at all. This was believed to be due to the reflective nature inherent of highly conductive materials. The intention of this study was to observe a gradual reduction in the alkyne stretch (*ca.* 2100 cm⁻¹) associated with each modified polymer unit (Chapter 3) and a gradual appearance of an N-H stretch (*ca.* 2600-3500 cm⁻¹) associated with polypyrrole.

Table 6.4 shows bulk conductivity values calculated from the gradient of the *I-V* plots around zero bias of bulk polypyrrole/polyC5-P, polypyrrole/polyC5-TP and

polypyrrole/polyC5-**TPT** (303 K and averaged over 5 values taken from different 5 samples). The dimensions were based on electrons taking shortest route between two points, the distance between the two probes.

Polymer/Ratio	1:1 (S cm⁻¹)	2:1 (S cm⁻¹)	3:1 (S cm⁻¹)
Py/C5- P	5.71 x 10 ⁻⁵ (±7.24 x 10 ⁻⁸)	0.30 (±0.21)	1.84 (±1.01)
Py/C5- TP	2.10 x 10 ⁻⁵ (±1.90 x 10 ⁻⁶)	7.65 x 10 ⁻⁶ (±2.14 x 10 ⁻⁶)	1.18 x 10 ⁻⁵ (±9.53 x 10 ⁻⁷)
Py/C5- TPT	2.13 x 10 ⁻⁶ (±3.06 x 10 ⁻⁷)	0.11 (±0.015)	7.94 (±5.85)

Table 6.4. Bulk conductivity data for co-polymer systems of Py/polyC5-**P**, polyC5-**TP** and polyC5-**TPT** prepared

As expected as the degree of pyrrole monomer introduced into the system was increased, the conductivity was shown to increase significantly in each case. A 3:1 ratio of pyrrole with an alkylated monomer unit of either polyC5-**P** or polyC5-**TPT**, incubated over 1 hour in a 2:1 ratio of oxidant to monomer was shown to provide the co-polymer with the highest level of conductivity. While efforts to elucidate the proportion of each unit present in the final co-polymeric mixture by FTIR were unsuccessful, the *I-V* data indicates that the alkynyl-monomer is incorporated by the expected reduction in conductivity observed compared to polypyrrole alone prepared under similar conditions;¹⁰ this is useful evidence that co-polymer formation was achieved.

6.4 Conclusions

Samples of polyC5-**P**, polyC5-**TP** and polyC5-**TPT** were prepared by chemical polymerisation and the electrical properties probed by two-point I - V measurements. Conductivity values for each material were calculated; polyC5-**P** and C5-**TPT** exhibit comparable levels of conductivity ($1.13 \times 10^{-6} \text{ S cm}^{-1}$ and $1.98 \times 10^{-6} \text{ S cm}^{-1}$ respectively), while polyC5-**TP** showed disappointing conductive properties ($6.04 \times 10^{-10} \text{ S cm}^{-1}$). Studies to optimise the preparation of polypyrrole prior to incorporation into a co-polymer system were also carried out. It seems the increasing presence of HCl in the polymerisation reaction through extended incubation times or high oxidant ration showed a detrimental effect of conductivity. Incubation for 1 hour at a 2:1 ratio of oxidant to monomer was shown to produce polypyrrole with highly conductive properties. Subsequent co-polymerisation with polyC5-**P**, polyC5-**TP** and polyC5-**TPT** under these conditions yield co-polymeric materials with higher levels of conductivity than the homopolymer systems.

In summary, as expected increased ‘doping’ enhances conductivity. However, clearly a balance is required between ensuring sufficient oxidation in order to achieve a sufficient ‘doping level’ while not promoting polymer degradation.

6.5 Experimental

6.5.1 General Procedure for Bulk Polymerisation and Conductivity Measurements

FeCl₃ (2 ml, 0.3 M) was added to a DMF/water solution (1:4) of pyrrole (2 mL, 0.1 M) and left to stand for 1 hour. After which the solution/precipitate was placed in a centrifuge for 10 minutes (10,000 rpm, rotor size 10 cm) and the remaining FeCl₃ removed. The black solid produced was rinsed 3 times with excess nanopure water via the same method. The sample was subsequently dried in a vacuum oven (60°C) overnight. This procedure was followed for all bulk polymer preparation and subsequent conductivity measurements unless otherwise stated. Variations of the procedure include incubation time (typically 3 hours and 24 hours), oxidant ratio (0.3, 0.5, 1, 1.5, 2, and 3) and co-polymer systems as stated.

6.5.2 General Procedure for Bulk Two-Probe I-V Measurements

Electrical measurements of the bulk polymer were recorded with the sample, supported on a Si<n-111>/200nm SiO₂ substrate, placed in the probe station chamber and purged with N₂ for 3 hours, prior to measurements being made. Measurements were repeated 4 times with the probes positioned at different locations on the bulk polymer material each time (though the distance between the probes was kept constant), from which an average conductivity was calculated. All measurements were taken at 303K, with an applied voltage range of -1 to +1V in steps of 0.05V.

6.6 References

1. T. Livache, A. Roget, E. Dejean, C. Barthet, G. Bidan and R. Teoule, *Nucleic acids research*, 1994, **22**, 2915-2921.
2. T. Livache, B. Fouque, A. Roget, J. Marchand, G. Bidan, R. Téoule and G. Mathis, *Analytical Biochemistry*, 1998, **255**, 188-194.
3. F. Garnier, H. Korri-Youssoufi, P. Srivastava, B. Mandrand and T. Delair, *Synthetic Metals*, 1999, **100**, 89-94.
4. A. Ramanavičius, A. Ramanavičienė and A. Malinauskas, *Electrochimica Acta*, 2006, **51**, 6025-6037.
5. S. Pouzet, N. Le Bolay, A. Ricard and F. Jousse, *Synthetic Metals*, 1993, **55**, 1079-1084.
6. J. Mansouri and R. P. Burford, *Journal of Materials Science*, 1994, **29**, 2500-2506.
7. M. Omastová, J. Pionteck and S. Košina, *European Polymer Journal*, 1996, **32**, 681-689.
8. J. Kim, D. Sohn, Y. Sung and E.-R. Kim, *Synthetic Metals*, 2003, **132**, 309-313.
9. V. Bocharova, A. Kiriya, H. Vinzelberg, I. Mönch and M. Stamm, *Angewandte Chemie International Edition*, 2005, **44**, 6391-6394.
10. L. Dong, T. Hollis, S. Fishwick, B. A. Connolly, N. G. Wright, B. R. Horrocks and A. Houlton, *Chemistry – A European Journal*, 2007, **13**, 822-828.
11. J. C. Thiéblemont, J. L. Gabelle and M. F. Planche, *Synthetic Metals*, 1994, **66**, 243-247.
12. R. Myers, *Journal of Electronic Materials*, 1986, **15**, 61-69.

13. W. Liang, J. Lei and C. R. Martin, *Synthetic Metals*, 1992, 52, 227-239.
14. S. J. Hawkins and N. M. Ratcliffe, *Journal of Materials Chemistry*, 2000, 10, 2057-2062.
15. S. Sadki, P. Schottland, N. Brodie and G. Sabouraud, *Chemical Society Reviews*, 2000, 29, 283-293.
16. B. S. Lamb and P. Kovacic, *Journal of Polymer Science: Polymer Chemistry Edition*, 1980, 18, 1759-1770.
17. M. M. Ayad, *Journal of Polymer Science Part A: Polymer Chemistry*, 1994, 32, 9-14.
18. H. Nishihara, K. Pressprich, R. W. Murray and J. P. Collman, *Inorganic Chemistry*, 1990, 29, 1000-1006.
19. J. Hegewald, L. Jakisch and J. Pionteck, *Synthetic Metals*, 2009, 159, 103-112.
20. R. Hassaniien, M. Al-Hinai, S. A. Farha Al-Said, R. Little, L. Šiller, N. G. Wright, A. Houlton and B. R. Horrocks, *ACS Nano*, 2010, 4, 2149-2159.
21. T. A. Skotheim, R. L. Elsenbaumer and J. R. Reynolds, eds., *Handbook of Conducting Polymers*, New York, 1998.
22. D. S. Park, Y. B. Shim and S. M. Park, *Journal of The Electrochemical Society*, 1993, 140, 2749-2752.

Chapter 7

DNA-Based Nanowire Modification

7.1 Chapter Overview

Overall Goal

To covalently immobilize probe DNA onto a hybrid DNA/polymer nanowire using 'click' chemistry.

Hypothesis

The terminal alkyne group present in each polymer will facilitate coupling of both chemical and biological azide terminated molecules.

Successful coupling of azido terminated DNA to an alkyne terminated DNA/polymer nanowire will result in a reduced level in conductance of the wire when compared to the unmodified state.

Objectives

Establish the appropriate reaction conditions for 'click' chemistry by the coupling 3-azido propan-1-ol to C5-P, C5-TP and C5-TPT monomer units and the respective DNA/polymer hybrid materials.

Synthesis azido-modified probe DNA and its complement via solid-phase phosphoramidite oligonucleotide synthesis and perform hybridization studies to assess the stability of the formed duplex.

Covalently immobilize azido-modified probe DNA onto a hybrid DNA/polymer nanowire and confirm attachment by C-AFM.

Hybridize complement DNA to the modified nanowire and stain with YOYO-1 to optically validate probe immobilization and hybridization to nanowire bound DNA.

7.2 Introduction

Nanowires based on conducting polymers or silicon lack the specificity/selectivity necessary to function as electrochemical biosensors. Biological recognition molecules (or capture probes), such as antibodies, enzymes or oligonucleotides, impart the desired selectivity and specificity in order for these materials to be used in this manner. The most conventional approach to achieving such function beyond their conductive nature is through the formation of covalent bonds between the biological recognition molecules and the nanowire. It is therefore necessary to introduce complementary functionalisation to both the nanowire and the desired recognition molecule.

The functionalisation of silicon nanowires is typically achieved via the formation of siloxane bonds to the native Si/SiO₂ surfaces. The appropriately functionalized silane head groups enables the coupling of a wide range of desired entities to the surface (Figure 7.1).^{1, 2} A stable, densely packed organic monolayer covalently bound directly to surface is produced and allows the detection of charge transfer across the Si/SiO₂/organic-electrolyte interface.

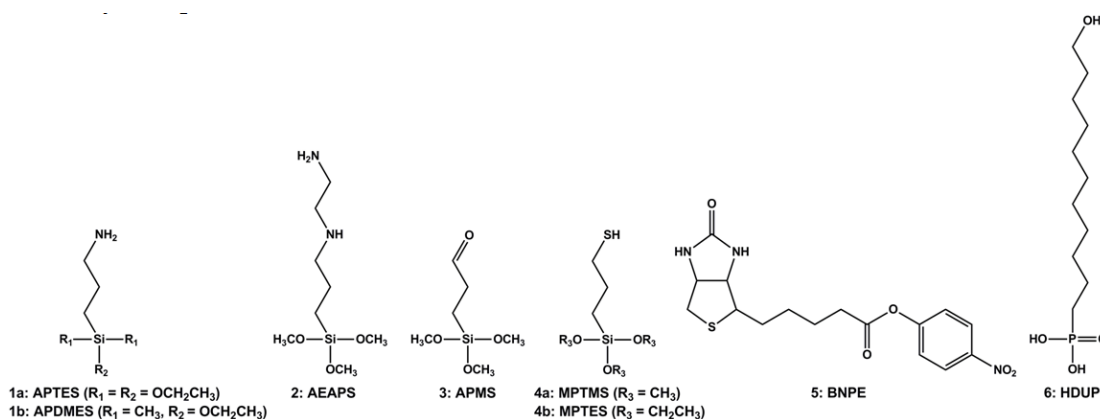
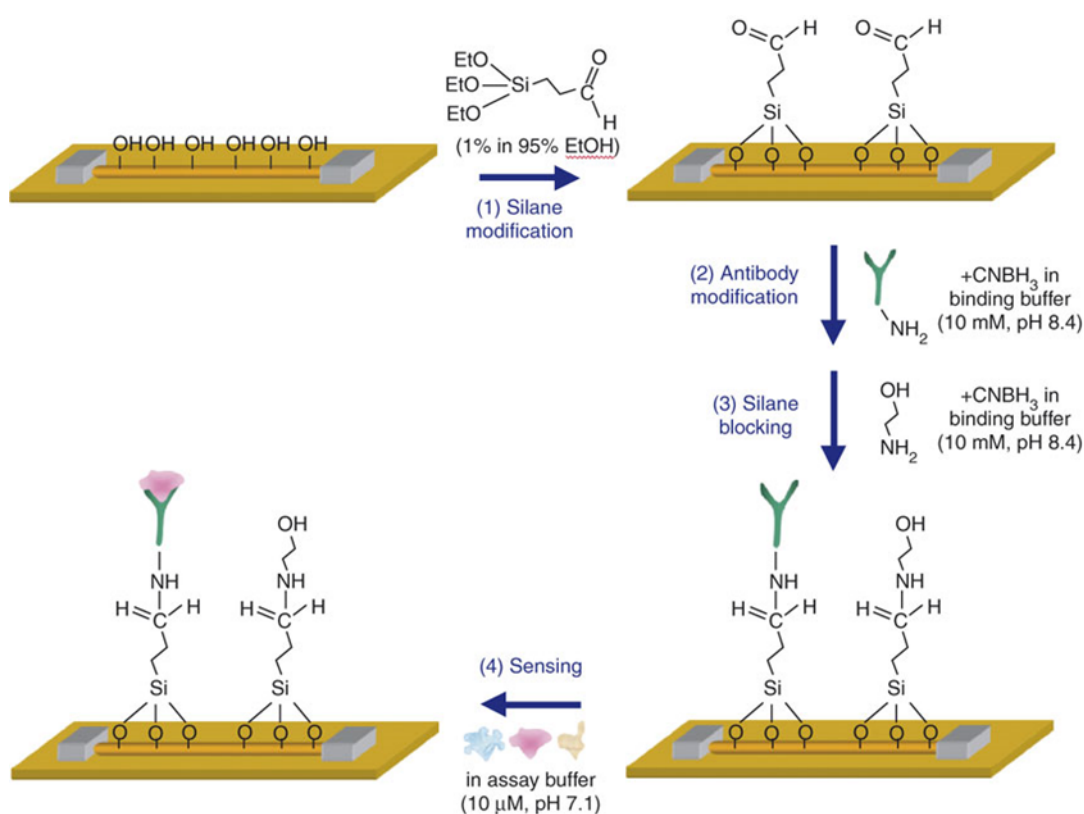


Figure 7.1. A range of silane compounds have been used in the modification on SiO₂-coated NWs: 3-aminopropyltriethoxysilane (APTES, 1a), (3-aminopropyl)-dimethyl-ethoxysilane (APDMES, 1b), *N*-(2-aminoethyl)-3-aminopropyltrimethoxysilane (AEAPS, 2), 3-aldehydepropyltrimethoxysilane (APMS, 3), mercaptopropyltrimethoxysilane (MPTMS, 4a), mercaptopropyltriethoxysilane (MPTES, 4b), biotin 4-nitrophenyl ester (BNPE, 5) and 11-hydroxyundecyl-phosphonate (HUP, 6)²

Silicon NW's constructed and modified in this way have been shown to be highly sensitive and selective sensors for direct and label-free detection of metal-ions,³

nucleic acids,⁴ proteins,⁵⁻⁷ virus⁸ and cells.⁹ Lieber *et. al.*^{5, 10-12} amongst others,¹³⁻¹⁶ has extensively demonstrated the use of silicon nanowire based field effect transistors (FETs) for label-free, electrical detection of a variety of species, such as antibodies, DNA and cancer markers.^{5, 11, 12, 17, 18} Notably the group demonstrated the capability for multiplexed real-time monitoring of analytes present in femtomolar concentrations.⁵ This was achieved by firstly developing an integrated nanowire array of distinct nanowires so surface bound capture probes could be incorporated as individual device elements. The nanowire array was subsequently modified with aldehyde propyltrimethoxysilane (APTMS, Figure 7.1) to afford terminal aldehyde groups at the nanowire surface (Scheme 7.1, (1)). Coupling of monoclonal antibodies (mAbs) via reductive amination provided individual device elements for the detection of prostate specific antigen (PSA), PSA-a1-antichymotrypsin, carcinoembryonic antigen and mucin-1 (Scheme 7.1., (2) and (4)).



Scheme 7.1. The Lieber group demonstrated the capability for multiplexed real-time monitoring of analytes present in femtomolar concentrations by firstly developing an integrated nanowire array of distinct nanowires so surface bound capture probes. The nanowire array was subsequently modified with aldehyde propyltrimethoxysilane⁵

As discussed in Chapter 1, the immobilization of bioactive macromolecules in or on electrically conductive polymers can be achieved through a number of techniques, one of which is covalent attachment. The most common approach for covalent biomolecule attachment is for modifications to be made post-polymerization. Here, functionalized monomer units are first polymerized followed by covalent attachment of the desired capture probe onto the surface of the functional conducting polymer. A significant advantage to this method is that the conducting polymer can be prepared under conditions that are potentially incompatible with the capture probe, such as organic solvents or high electropolymerization potentials; while probe attachment can be performed under mild conditions to ensure probe integrity.

Generally, capture probes functionalised with an amine, alkyne, or thiol are covalently attached to the functionalised surfaces.^{3, 11, 13, 15, 19} The synthesis of modified oligonucleotides for such applications is now common practice with a number of commercial companies in existence offering a wide range of modifications. Figure 7.2 illustrates some commercially available oligonucleotide modifications.

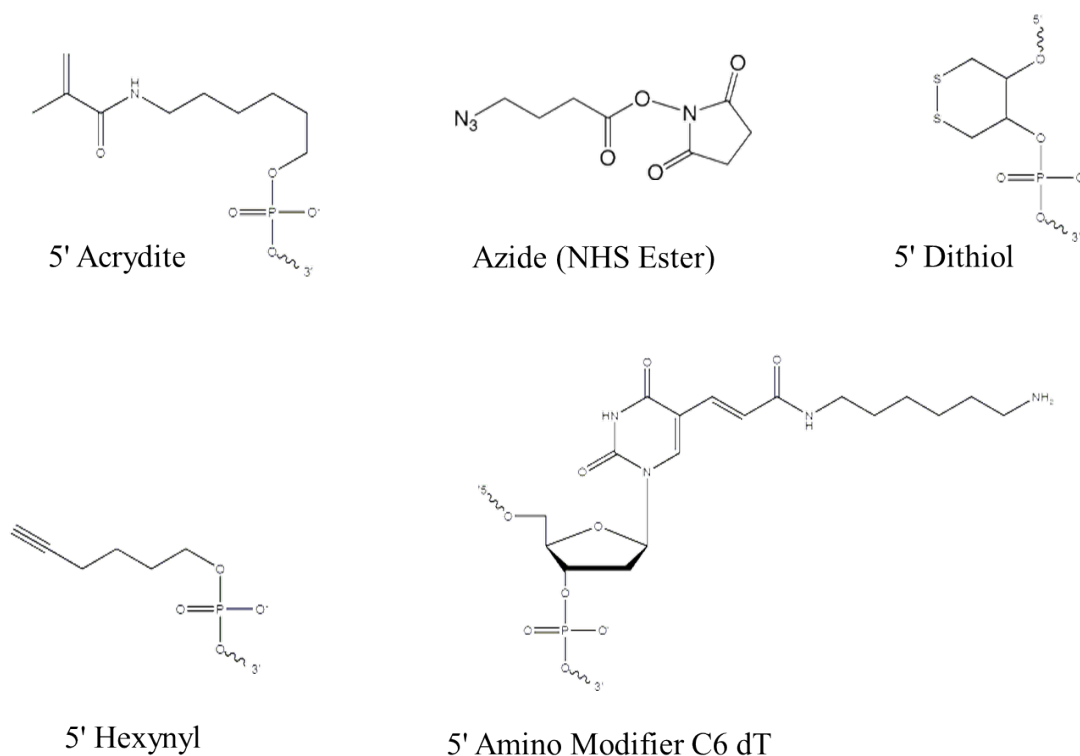


Figure 7.2. Some commercially available oligonucleotide modifications

The required functionality may be introduced either through the terminal phosphate group or through modified nucleotides. In the latter approach, modified nucleosides containing the desired functional group are first synthesized and subsequently introduced into a standard solid-phase oligonucleotide synthesis cycle at the desired position (Section 7.2.3). The development of such nucleotides constitutes a significant research area of synthetic chemistry. Briefly, nucleoside modification has been demonstrated at various sites,²⁰⁻²³ the most advantageous site is to modify the C5 position of pyrimidines as it does not disturb the supramolecular bonding between the nucleobases or interfere with the phosphodiester backbone (Figure 7.3). Numerous laboratory groups have reported the C5 modification of thymidine with the subsequent incorporation into DNA.^{24, 25}

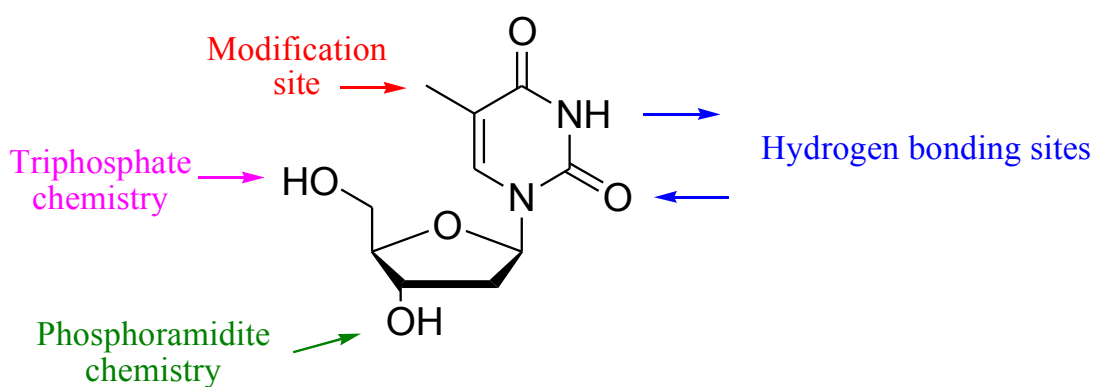


Figure 7.3 Possible modification sites at C-5, 3'-OH and 5'-OH prevents disruption of possible hydrogen bonding

Solid-phase Oligonucleotide Synthesis

Solid-phase chemical synthesis of peptides was invented in the 1960s by Bruce Merrifield for which he was awarded the Nobel Prize for Chemistry in 1984.²⁶ The methodology of which has since been extended to oligonucleotide synthesis.

Here, solid supports (also called resins) are insoluble particles, typically 50-200 μm in diameter, to which the oligonucleotide is bound during synthesis. Many types of solid support have been used on solid-phase oligonucleotide synthesis, but controlled pore glass (CPG) and polystyrene have proved to be the most useful.

The standard method for oligonucleotide synthesis is solid-phase phosphoramidite oligonucleotide synthesis, which proceeds in the 3'- to 5'-direction (opposite to the

5'- to 3'-direction of DNA biosynthesis in DNA replication). The phosphoramidite DNA synthesis cycle consists of a series of steps outlined in Figure 7.4.

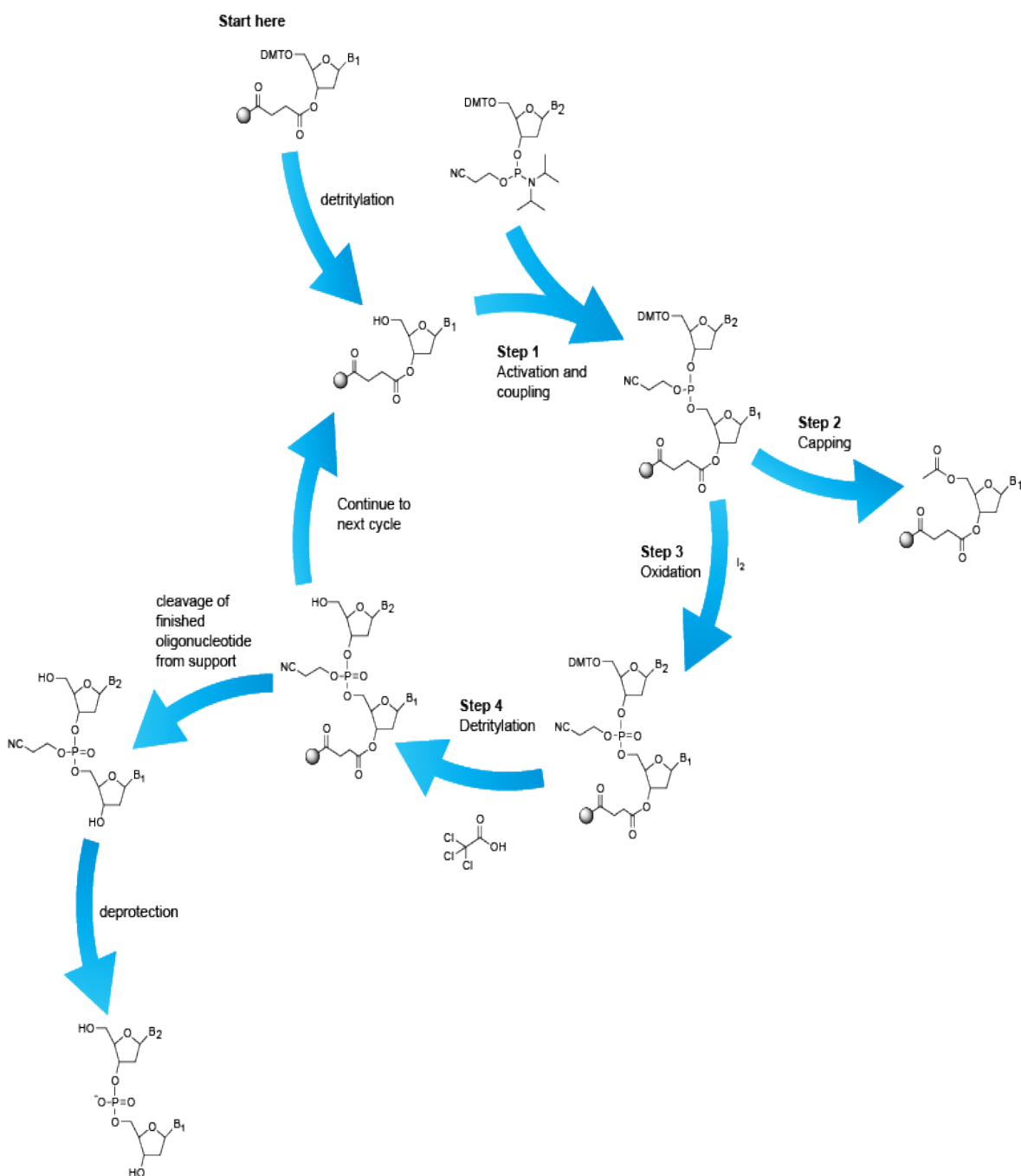


Figure 7.4. The phosphoramidite oligonucleotide synthesis cycle. Reproduced from reference²⁷

At the beginning of oligonucleotide synthesis the first protected nucleoside is pre-attached to the resin and the operator selects an A, G, C or T synthesis column depending on the nucleoside at the 3'-end of the desired oligonucleotide. The support-bound nucleoside has a 5' protecting group, 4,4'-dimethoxytrityl (DMT), the role of which is to prevent polymerization during resin functionalization. This

protecting group must be removed (detritylation) from the support-bound nucleoside before oligonucleotide synthesis can proceed.

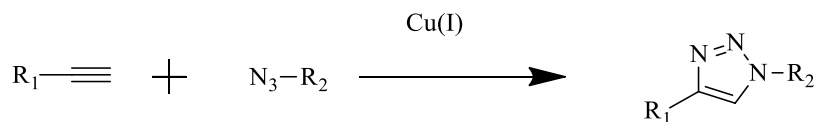
Following detritylation, the support-bound nucleoside is ready to react with the next base, which is added in the form of a nucleoside phosphoramidite monomer. It is not unreasonable to expect a yield of 99.5% during each coupling step. This still means that there will be some unreacted 5'-hydroxyl groups on the resin-bound nucleotide; if left unchecked, these 5'-hydroxyl groups would be available to react with the incoming phosphoramidite. The resulting oligonucleotide would lack one base, and would correspond to a deletion mutation of the desired oligonucleotide. Deletion mutations are avoided by introducing a 'capping' step after the coupling reaction, to block the unreacted 5'-hydroxyl groups. (Figure 7.4, Step 2).

The phosphite-triester (P(III)) formed in the coupling step is unstable to acid and must be converted to a stable (P(v)) species prior to the next detritylation step. This is achieved by iodine oxidation in the presence of water and pyridine (Figure 7.4, Step 3). The resultant phosphotriester is effectively a DNA backbone protected with a 2-cyanoethyl group. The cyanoethyl group prevents undesirable reactions at phosphorus during subsequent synthesis cycles.

After phosphoramidite coupling, capping and oxidation, the DMT protecting group at the 5'-end of the resin-bound DNA chain must be removed so that the primary hydroxyl group can react with the next nucleotide phosphoramidite (Figure 7.4, Step 4). The cycle is repeated, once for each base, to produce the required oligonucleotide.

As discussed earlier, a fundamental requirement in the covalent immobilisation of specific capture probes is the biological compatibility of the reaction and conditions. Mild, aqueous, conditions and highly specific orthogonal bond formation to the groups present in the biomolecule are required in order to retain the functionality and specificity of the probe itself, post immobilisation.

As described in Chapter 3, copper catalyzed 1,3-dipolar cycloaddition ('click' chemistry, Scheme 7.2) is a highly specific reaction compatible with biological, aqueous conditions.²⁸



Scheme 7.2. A general scheme for the formation of 1,4-triazoles via ‘click’ chemistry

The synthesis of alkyne terminated monomers of **C5-P**, **C5-TP** and **C5-TPT** was also described in this chapter (Figure 7.5). Attachment of an alkyne group to each monomer unit allows the use of ‘click’ chemistry to form a triazole linkage between azide-terminated DNA and the DNA-based conducting polymer nanowires described in Chapters 4 and 5.

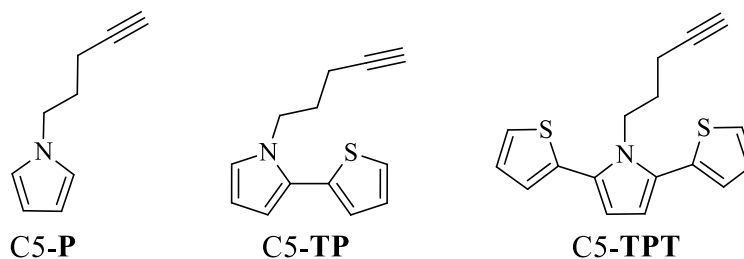


Figure 7.5. Structures of *N*-alkylated alkynyl units

Chapter Outline: This final results chapter describes functionalisation of **C5-P**, **C5-TP** and **C5-TPT**. Initial studies focused upon the use of bulk hybrid materials to demonstrate the feasibility of ‘click’ chemistry as a route to probe attachment. Synthesis and characterisation of an azido-modified oligonucleotide is also presented in addition to efforts made to achieve probe attachment to DNA/poly**C5-P** nanowires.

7.3 Results and Discussion

7.3.1 Functionalization of Bulk DNA/Polymer Hybrid Materials

Goal: To establish the appropriate reaction conditions for ‘click’ chemistry by the coupling 3-azido propan-1-ol to C5-P, C5-TP and C5-TPT monomer units and the respective bulk DNA/polymer hybrid materials.

In order to establish the appropriate reaction conditions for ‘click’ chemistry, the coupling 3-azido propan-1-ol (Figure 7.6) to C5-P, C5-TP and C5-TPT monomer units and the respective DNA/polymer hybrid materials was performed. This work was also useful in investigating alternative strategies in the synthesis DNA modified conducting polymer nanowires. As discussed earlier, modification of nanowires with ssDNA probes is typically achieved via covalent attachment of appropriately functionalised oligonucleotides, in this project azido-modified oligonucleotides. An alternative route is to synthesize the desired oligonucleotides directly at the CP surface, akin to conventional solid phase synthesis however using a nanowire as a solid support. Successful coupling 3-azido propan-1-ol to the C5-P, C5-TP and C5-TPT monomer units and the respective DNA/polymer hybrid materials provides an alternative route to ssDNA probe immobilization through the terminal OH moiety afforded post modification. While it is not the intention to do so in this project, direct DNA synthesis using phosphoramidite chemistry could potentially be performed at the CP surface as a means to synthesizing DNA modified conducting polymer nanowires in future work.

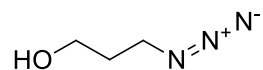
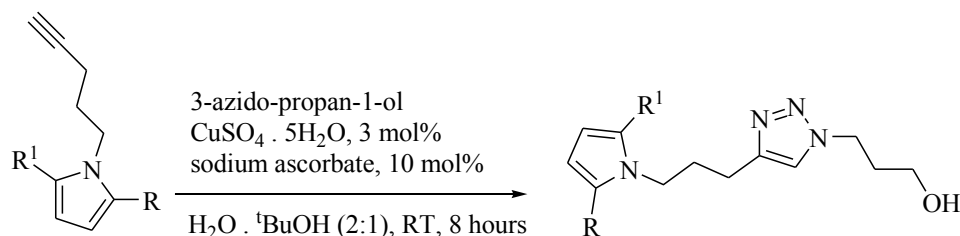


Figure 7.6. The chemical structure of 3-azido propan-1-ol

In order to establish the appropriate reaction conditions for ‘click’ chemistry, initial experiments involved coupling 3-azido propan-1-ol to each monomer unit. Characterization was performed using LC-MS, ¹H and ¹³C NMR spectroscopy to ascertain the reactions had yielded the desired products.

The coupling of the azido group to the alkylnyl monomers C5-**P**, C5-**TP** and C5-**TPT** was achieved in solution (Scheme 7.3) without need to significantly vary the conditions between systems. Yields in the region of 80% after 8 hours incubation were typical.



Scheme 7.3. Reaction scheme for coupling 3-azido propanol, C5-**P**, when R1 and R are H, C5-**TP**, when R1 is H and R is thiophene, and C5-**TPT** when R1 and R are thiophene

Having identified suitable reaction conditions for the coupling reaction, it was important to establish that when in nanowire form the same reaction was still accessible and that the alkyne group was still available for reaction. To ensure the terminal alkyne group was still available/active for further chemistry upon templating and polymerization, this method was extended to the DNA-templated materials. Experiments here involved the suspension of bulk DNA-templated material, dried onto a silicon wafer in a similar manner to that in Chapter 4 in a ‘click’ solution with gentle agitation. Typically, the silicon wafer was suspended in a solution of water:*tert*-butyl alcohol (2:1, 20 mL) containing sodium ascorbate (0.03g, 0.15 mmol), copper^(II) sulphate (4.72 mg, 0.03 mmol) and 3-azido propanol (0.3 g, 2.95 mmol). The mixture was stirred gently in darkness for 8 hours prior to being washed with excess of nanopure water and dried in a vacuum oven (60 °C).

Analysis by FTIR allowed comparison between DNA-templated materials and ‘clicked’ products. 3-azido propan-1-ol was extremely useful in this aspect, as there were no additional functional groups to which were already present in the hybrid material i.e. O-H stretches, alkane C-H stretches, preventing further complication of the spectra from its presence or upon attachment. Significantly, the region attributed to alkyne moiety also remained clear, allowing for relatively straightforward monitoring of the coupling reaction.

As discussed in Chapter 4, spectra of the isolated DNA/polyC5-**P** material provided evidence of the formation of a supramolecular polymer structure containing both

DNA and polyC5-P (Figure 7.7., blue). The presence of the polyC5-P in the material was evident from the three bands attributed to the characteristic aromatic, alkene and alkane C-H stretches (2924 cm^{-1} , 2854 cm^{-1} and 2812 cm^{-1} respectively, alkyne C-H masked by O-H stretch of water) and importantly the weak alkyne stretch at 2071 cm^{-1} (Chapter 3).²⁹

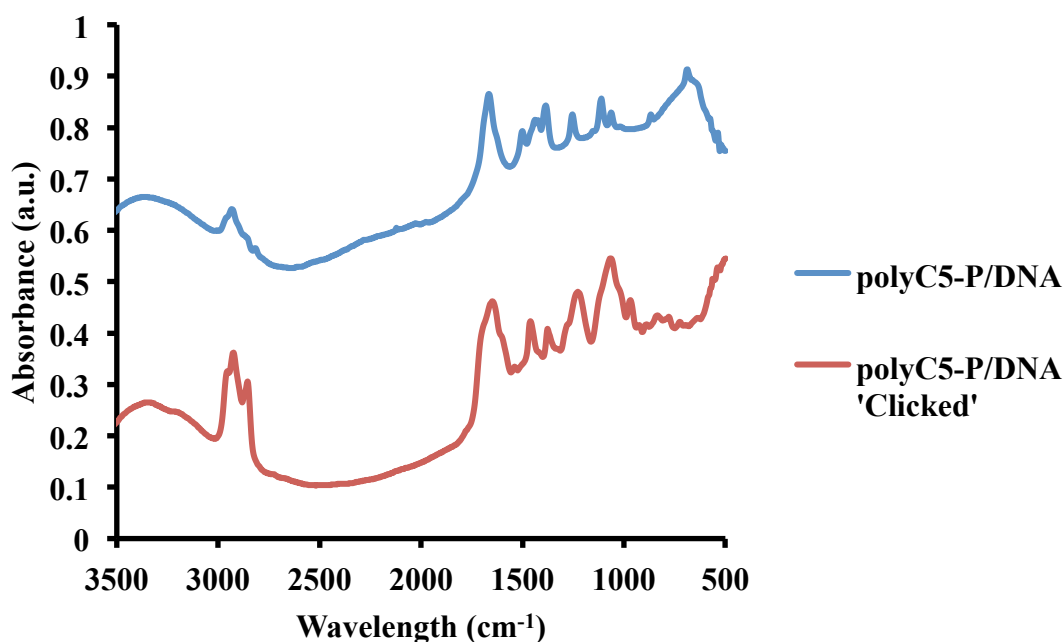


Figure 7.7. FTIR spectra ($3500\text{-}500\text{ cm}^{-1}$) of DNA/polyC5-P (blue) and DNA/ polyC5-P 'clicked' (red). For clarity, absorbance values have been altered to stack plot the spectra

Subsequent clicking of 3-azido propan-1ol to the DNA/polyC5-P hybrid material was evident primarily through the disappearance of the alkyne carbon-carbon bond (Figure 7.7, *ca.* 2100 cm^{-1}). Closer inspection of the spectra (Figure 7.8, red) revealed characteristic absorptions bands at 1597 cm^{-1} (triazole ring vibration), 1215 cm^{-1} (triazole breathing) and 829 cm^{-1} (triazole nucleus) showing the formation of the 1,2,3-triazole ring.^{29, 30}

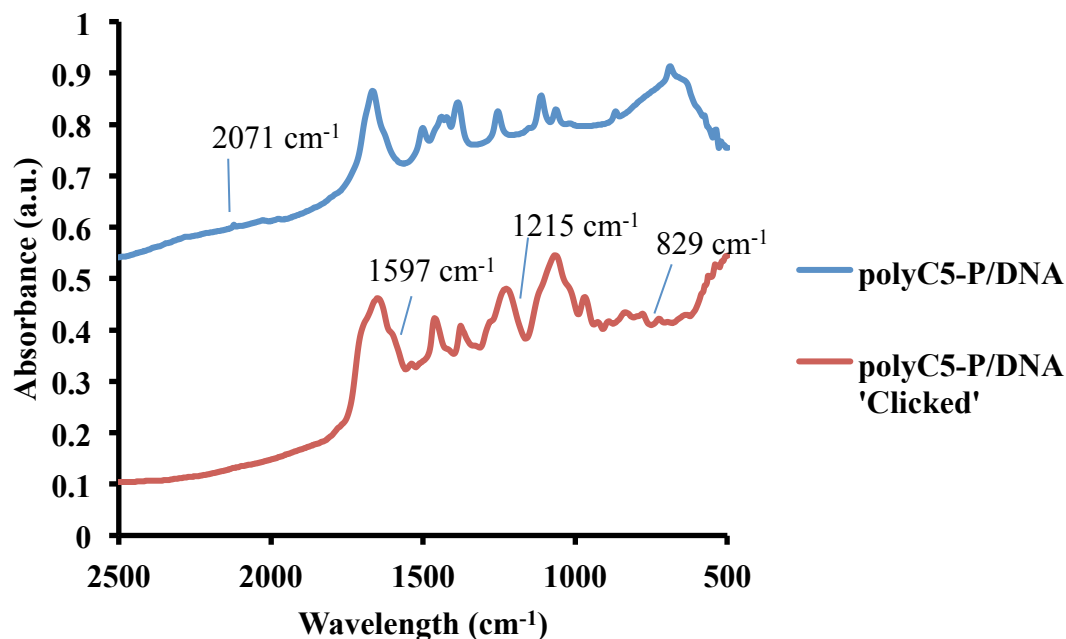


Figure 7.8. FTIR spectra (1800–500 cm^{-1}) of DNA/polyC5-P (blue) and DNA/ polyC5-P ‘clicked’ (red). For clarity, absorbance values have been altered to stack plot the spectra

Similar observations were made for the DNA/polyC5-TP material (Figure 7.9). Again, as described in Chapter 4, templating resulted in the majority of the bands being shifted to higher wavenumbers upon templating with the presence of the polyC5-TP in the hybrid material, evident from absorptions in the 3500–2800 cm^{-1} region. Bands attributed to the alkyne, aromatic and alkene C-H’s (3302 cm^{-1} , 3107 cm^{-1} and 2955 cm^{-1} respectively) of the C5-TP monomer units were observed to be shifted to lower wavenumbers relative to the corresponding stretches in the spectrum of polyC5-TP itself (3283 cm^{-1} , 3097 cm^{-1} and 2929 cm^{-1} , Chapter 3), again, thought to be as a result of interaction with the DNA.

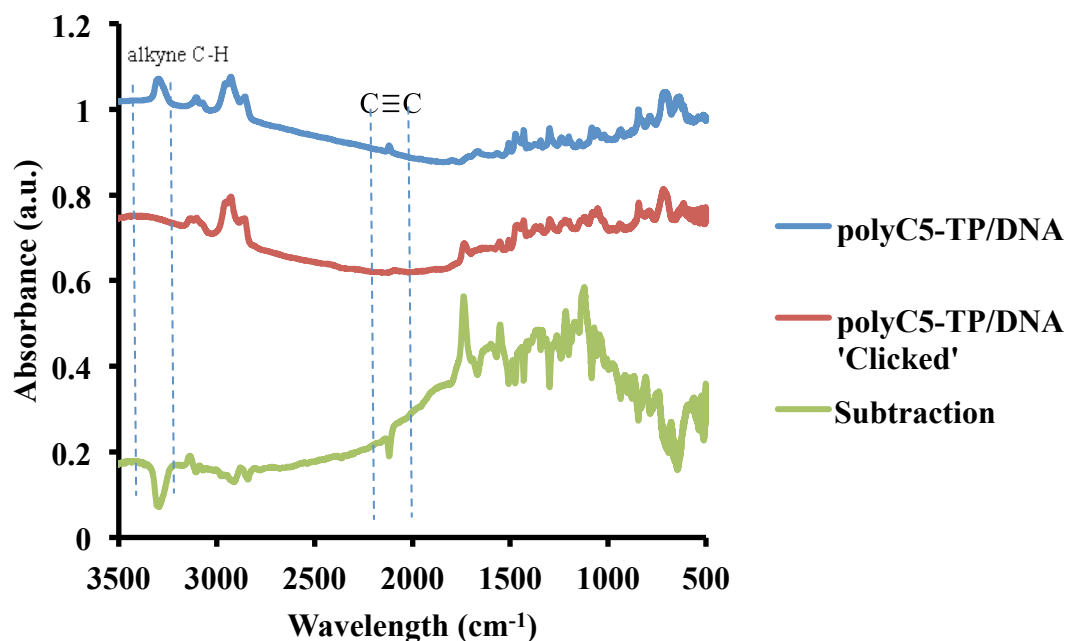


Figure 7.9. FTIR spectra of polyC5-TP, blue; DNA/polyC5-TP 'clicked', red and the subtraction of polyC5-TP 'clicked' from DNA/polyC5-TP, green. For clarity, absorbance values have been altered to stack plot the spectra

As with DNA/polyC5-P, subsequent clicking of 3-azido propan-1-ol to the polyC5-TP hybrid was evident through the disappearance of the alkyne carbon-carbon bond (*ca.* 2100 cm^{-1}) and the appearance of characteristic triazole absorptions at 1100-1150 cm^{-1} (triazole breathing mode) and 965-945 cm^{-1} (C-N).²⁹ In addition to the disappearance of the alkyne C-H band (*ca.* 3300 cm^{-1}) visible due to the displacement of DNA bound water molecules. This is shown more clearly in the subtraction spectra (green).³¹

Isolated DNA/polyC5-TPT material provided evidence of supramolecular polymer formation through a number of bands being shifted to higher wavenumbers (Figure 7.10, blue). The presence of polyC5-TPT was again confirmed through bands attributed to the alkyne, aromatic and alkene C-H's (3282 cm^{-1} , 3101 cm^{-1} , 3070 cm^{-1} and 2939 cm^{-1} respectively, Chapter 3). Notable shifting of bands attributed to C=O stretch of cytosine/thymine, PO_2^- asymmetric stretch and C-O deoxyribose stretch were also observed (1653 cm^{-1} to 1658 cm^{-1} , 1102 cm^{-1} to 1110 cm^{-1} and 962 cm^{-1} to 975 cm^{-1} respectively).³²

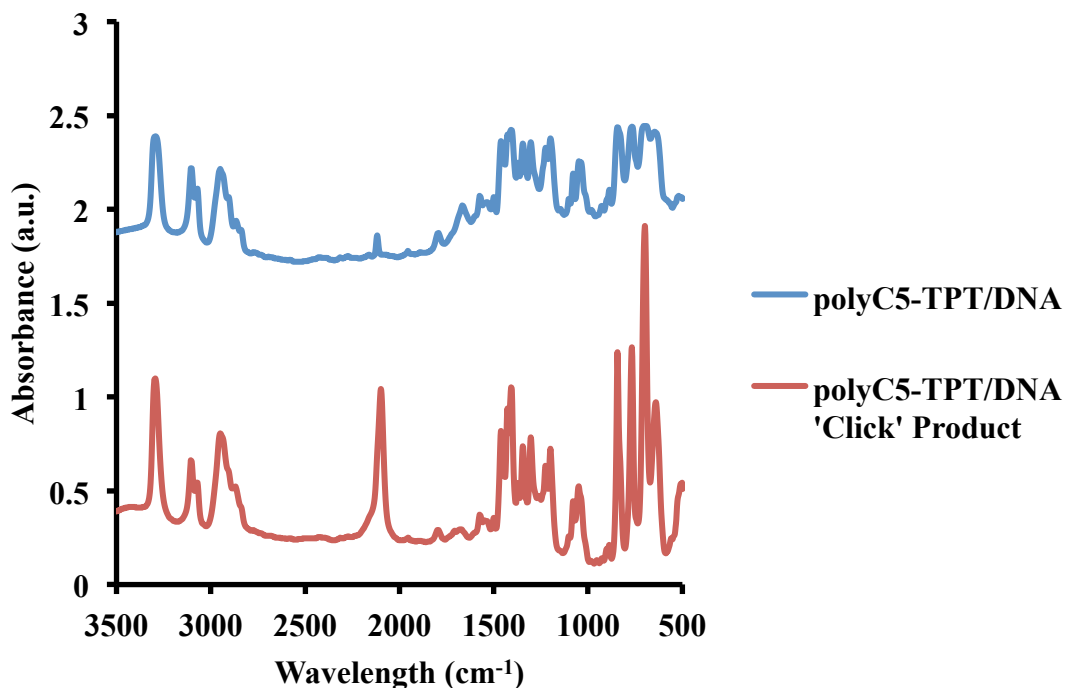


Figure 7.10. FTIR spectra of DNA/polyC5-TPT (blue) and ‘clicked’ result (red). For clarity, absorbance values have been altered to stack plot the spectra

Evidence of ‘clicking’ of 3-azido propan-1-ol to the polyC5-TPT hybrid could not be elucidated by FTIR, despite several attempts. Figure 7.10, red, shows polyC5-TPT hybrid following the attempted ‘click’ reaction.

The continued presence of the alkyne stretch at 2117 cm^{-1} is clear evidence that the ‘click’ reaction was not successful. However, the increase in intensity and broadening of the band indicates the formation of a nitrile group (usually *ca.* 2200 cm^{-1}). It was not clear why this should be possible but may relate to the accessibility of the alkyne group or degeneration of the material, perhaps during the drying step ($60\text{ }^{\circ}\text{C}$). While the stability of triazole linkages is well known,²⁸ the polyC5-TPT hybrid may cause destabilization of the triazole linker, making it susceptible to degradation. Importantly, this degradation would only be possible if a triazole was formed in the first instance, as a nitrile group could only be derived from the linker. Thermal degradation of pyrrole results in imine formation indicated by a new absorbance band *ca.* 1670 cm^{-1} , this band is absent from the spectra.²⁹

In summary, the synthesis and coupling of 3-azido propanol to monomer units of C5-P, C5-TP and C5-TPT was achieved in solution with high yield. ‘clicking’ of 3-azido propanol to bulk DNA/polymeric hybrid materials of C5-P, C5-TP was

shown through FTIR spectroscopy. Sample degradation during preparation of 'clicked' DNA/polyC5-TPT was also observed.

7.3.2 Modified Oligonucleotide Synthesis

Goal: Synthesis azido-modified probe DNA and its complement via solid-phase phosphoramidite oligonucleotide synthesis.

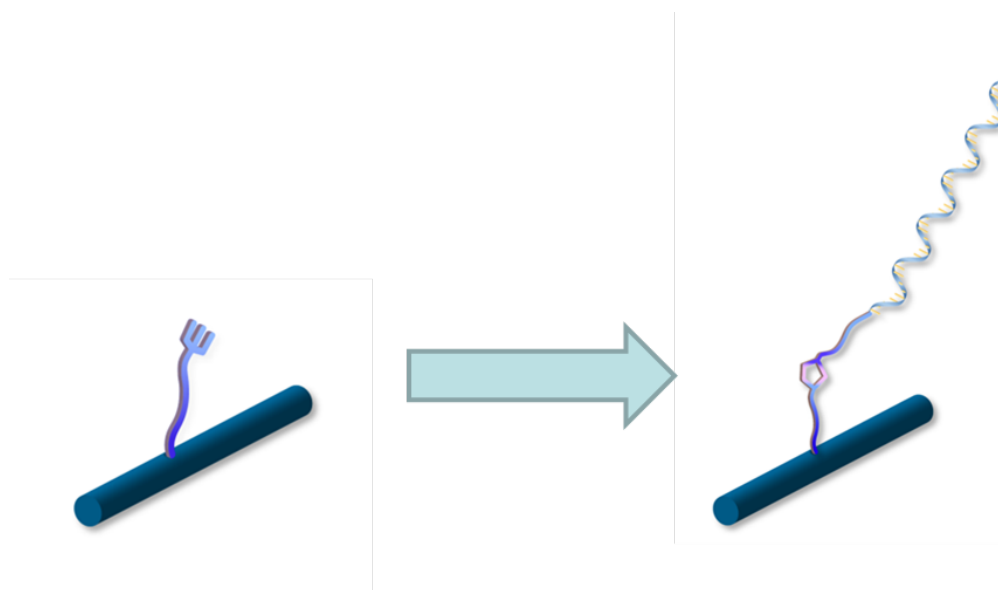
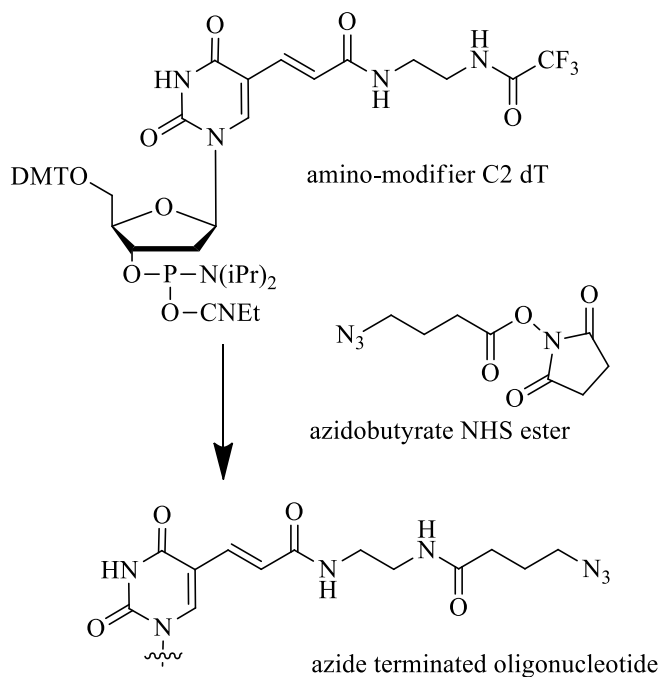


Figure 7.11. An illustration of ssDNA probe attachment to an alkyne terminated DNA-templated CP. The azide terminated DNA reacts with the alkyne group to form a highly stable triazole linkage³³

In order to synthesize azido-terminated oligonucleotides suitable for nanowire modification via 'click' chemistry (Figure 7.11 and Chapter 3), an amino-modifier C2 dT was introduced at the 5' end of the DNA synthesis cycle to facilitate modification to an azide, post-synthesis (Scheme 7.5).³⁴ Here, an additional T is added to the complementary sequence in the form of an amino-modifier C2 dT. This modified nucleotide can be readily converted to possess an azide terminated side chain through treatment with azidobutyrate NHS ester, after removal from the solid support.



Scheme 7.4. The synthetic pathway to 5'azido-modified oligonucleotides. Reproduced from reference³⁴

Using solid phase DNA synthesis and the methods outlined above, the following azido modified 25mer and the appropriate complement were prepared:

azido-hexyl-25mer (T* = the additional azido-modified T to the complementary sequence)



Complement



Purification and initial indication of the successful conversion to the modified oligonucleotide was performed by HPLC (Appendix). Subsequent analysis by MALDI-TOF MS confirmed successful synthesis of the azido-modified oligonucleotide (negative mode for azido modified 25mer 4109.42, Appendix). The sequence of the modified oligonucleotide was chosen specifically to contain a G-C content between 40-60% in order to ensure stable binding. G-C interactions contribute more to stability than A-T due to the greater number of hydrogen bonds. In this study, the 25mer duplex has a GC content of 53.8%.

Unfortunately, the synthesis of the azido-modified oligonucleotide was low yielding, with the concentrations of the final solutions of the 25mer found to be $3.94 \times 10^{-7} \text{ mol L}^{-1}$ (260 nm, extinction coefficient = $231677.6 \text{ L mol}^{-1} \text{ cm}^{-1}$, using Cavaluzzi-Borer correction)

The importance of a high average stepwise yield is significantly important in order to avoid the ‘arithmetic demon’ associated with linear synthesis. In practice, yields in the region of 98.5% are readily attainable with carefully dried anhydrous solvents. The cumulative effect of a series of poor couplings is two-fold, resulting in a poor overall yield of the desired oligonucleotide, a product that is extremely difficult to purify. The bulky amino-modifier C2 dT is also likely to have contributed to the number of poor couplings.

The synthesis of the desired complement was performed using standard DNA synthesis protocol described earlier. As expected this reaction was significantly higher yielding by comparison to the modified oligonucleotide. The 25mer complement final solution concentration was found to be $2.58 \times 10^{-6} \text{ mol L}^{-1}$ (260 nm, extinction coefficient = $237901.0 \text{ L mol}^{-1} \text{ cm}^{-1}$, using Cavaluzzi-Borer correction).

7.3.3 Hybridization Studies

Goal: *To perform hybridization studies assessing the stability of the formed duplex from the modified oligonucleotides synthesized in 7.3.2.*

Hybridization studies using the azido-modified oligonucleotide and its complement were performed in order to assess the stability of the formed duplex. The hexyl azide modified 25 mer and its complement were diluted ($\sim 0.72 \mu\text{M}$) using buffer (25 mM HEPES, pH 7, 1 M NaCl) and combined. The mixture was heated to suspended $80 \text{ }^\circ\text{C}$ for 20 minutes then allowed to cool to room temperature. Using UV-Vis spectrometry, absorption spectra (200-500 nm, $20\text{-}85 \text{ }^\circ\text{C}$) was recorded over a temperature range of $20\text{-}40 \text{ }^\circ\text{C}$.

Figure 7.12 shows the UV-Vis spectra for the melting of the modified 25mer duplex. As expected, denaturing was indicated by an increase in absorbance. The ability of DNA to absorb light (260 nm) increases as denaturation progresses, this is

because absorbance is primarily a property of the nitrogenous bases. An increase in absorbance is observed upon denaturation since the bases contained within the DNA duplex are in too close proximity to absorb as much light as when they are exposed (known as Hyperchromicity).

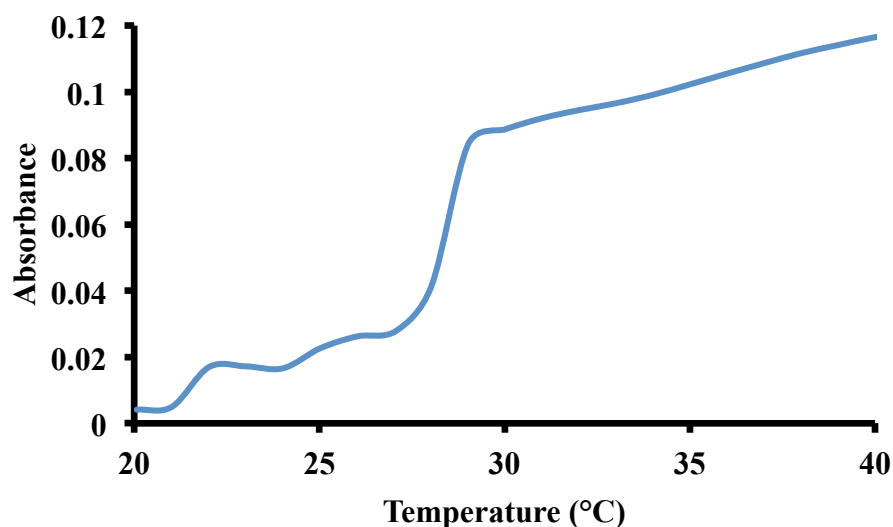


Figure 7.12. Denaturation of 5'azido-hexyl-25mer duplex with increased temperature shown by an increase in absorbance in the UV-Vis spectra (260 nm)

The T_m of a DNA duplex is defined as the temperature in degrees Celsius, at which 50% of all molecules of a given DNA sequence are hybridized into a double strand and 50% are present as single strands. The theoretical T_m for the unmodified 25mer duplex was calculated to be 61°C, while the actual T_m for the modified duplex was found to be significantly low by comparison, ~29°C.

While discrepancies between predicted and actual T_m 's are common, the low actual T_m value is interesting. This was considered to be largely due to instability caused by the 5' azido-modification weakening the binding between the two strands of DNA. Additionally, HEPES buffer is similar water in that its dissociation decreases as the temperature decreases. Good *et. al.*³⁵ reported the PKa of HEPES to be 7.55 at 20 °C with a change in PKa of approximately -0.14 per 10 °C upon increasing temperature. It is possible that the heating procedures before and during the UV-Vis studies may have resulted in a reduction in pH to more acidic conditions. Acidic solutions are well known to denature DNA. While it is likely that this change in pH is not large and therefore not wholly the source of the low T_m value observed, it may

have contributed to the overall instability of the duplex. Furthermore, Lepe-Zuniga *et. al.*³⁶ reported a phototoxicity of HEPES when exposed to ambient light by the production of hydrogen peroxide. Reactive oxygen species such as hydrogen peroxide have been shown to produce oxidized bases.³⁷ Again, this may be a contributing factor to the low T_m , as no effort was made to perform this study in the dark.

7.3.4 Nanowire Modification

Goal: Covalently immobilize azido-modified probe DNA onto a hybrid DNA/polymer nanowire and confirm attachment by C-AFM.

Using protocols developed in Section 7.3.1, ssDNA probe attachment to DNA/polyC5-**P** wires formed in an ‘iron-free’ templating solution was attempted and intended to be confirmed by cAFM *I-V* measurements (Chapter 2) due to the difficulties associated with the two-probe technique outlined in Chapter 5.

cAFM involves applying a droplet of templating solution onto the Si/SiO₂ substrate with subsequent solvent evaporation leaving a dense network of nanowires on the surface, at the periphery of which individual nanowires can be found to extend out. The dense nanowire network can effectively be used as a macroscopic electrical contact to the nanowire under study. Electrical contact of the network to the metallic sample chuck can be made using a drop of Ga/In eutectic. The second electrical contact to the nanowire is made using the conductive metal-coated AFM probe itself

It was anticipated that the introduction of ssDNA probes to the nanowire surface would modulate the conductivity of the wire through a charge accumulation of polarons or bipolarons in conducting polymer backbone. Upon the introduction of a second ssDNA, it was hoped the detection of label-free DNA hybridization using a conducting polymer nanowire could be demonstrated.

As discussed in Chapter 5, DNA/polyC5-**P** nanowires displayed the highest level of conductivity ($3.75 \times 10^{-4} \text{ S cm}^{-1}$ at 303K) when formed as a homopolymer. In this instance, ropes were deliberately formed by implementing high DNA concentrations ($\sim 500 \mu\text{g ml}^{-1}$) in the templating solutions as described previously (Chapter 4). This approach provided several advantages; by increasing the size of the wire the level of

current passed will be greater, offsetting the low sensitivity of the instrument (nAmps) and the relatively poor conductive properties of DNA/polyC5-P. It was also envisaged that many of the practical problems associated with cAFM could be avoided by making wires in the >100 nm range. cAFM operates in contact mode, as a result a common drawback of this technique is that the high vertical forces exerted by the tip on the sample can destroy smaller, less robust wires when scanning.

Figure 7.13 shows an example of a contact mode AFM height image of a DNA/polyC5-P nanowire (left) approximately 170 nm in height and a zoomed cAFM current image (right) of the same wire recorded with a dc bias of +10 V applied between the cantilever and the metallic chuck. Essentially, zero current was observed when the tip was above Si/SiO₂ but currents on the order of magnitude of 100's of nA were observed when the tip was in contact with the nanowire, thus confirming the electrical conductivity.

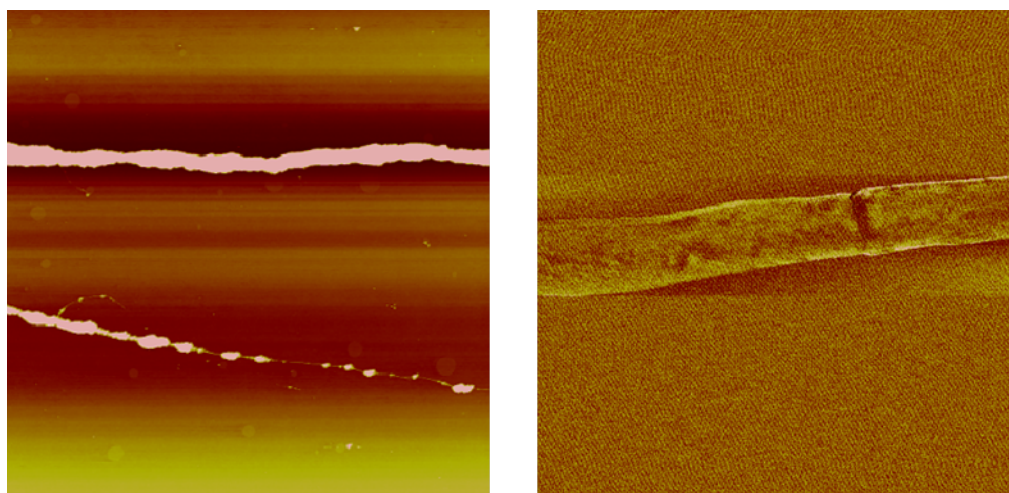


Figure 7.13. Left; contact mode AFM height image of a DNA/polyC5-P nanowire, 25 μm scan size, z-scale 0-100 nm dark to bright contrast. Right; a zoomed cAFM current image of the same wire acquired at a dc bias of +10 mV, 5 μm scan size

Unfortunately, efforts to retain a level of measurable current response by cAFM in order to elucidate any change in the conductance of the nanowire upon ssDNA immobilisation proved unsuccessful. This was largely due to time constraints and the difficulty in making and maintaining a good eutectic connection between the nanowire and the metallic sample chuck.

Despite this drawback, efforts to ‘click’ a 25mer duplex to DNA/polyC5-**P** nanowires were made. The azide modified 25mer and its complement were hybridized in solution (30 μM) using protocols described in Section 7.3.3 and introduced, in a ‘click’ solution, to nanowires spin coated onto a Si/SiO₂ surface. After washing with buffer, YOYO-1 dye was introduced (0.1 mM in DMSO) and incubated for 2 hours.

YOYO-dyes consist of two chromophores connected with a bis-cationic linker which is capable of bis intercalating into dsDNA. YOYO-1 exhibits a high fluorescence quantum yield when bound to dsDNA and zero fluorescence when unbound in solution. The ability of these dyes to interact with DNA has been well investigated and hence YOYO-1 staining provided a simple and fast way of confirming if attachment of the azido-modified duplex was successful.^{38,39}

Unfortunately in these experiments, no fluorescence could be observed, indicating one of three possible outcomes had taken place: duplex coupling was unsuccessful, YOYO-1 binding was unsuccessful or the nanowire had some-how quenched the YOYO-1. Given the extensive application of YOYO-1 in similar experiments, it was considered likely that coupling or quenching were the main sources of failure, with the former the favoured explanation. This experiment was repeated with a higher duplex concentration (67 μM compared to 30 μM), a higher copper catalyst loading (6.25 mM compared to 2.6 mM) and a longer incubation time (24 hours compared to 2 hours) in addition to agitation, however the same result was obtained. It was considered that the very low diffusion mobility of DNA fragments and relatively low DNA concentrations were impacting significantly on successful surface duplex coupling. Unfortunately, due to time constraints and limited availability of the modified oligonucleotides further efforts to overcome these problems were not possible.

However, other studies using C5-**TP** have demonstrated DNA/polyC5-**TP** nanowires may be functionalised via click reaction with 3-azido-1-*N*-dansylpropylamine for example.³¹ The DNA/polyC5-**TP** nanowires were immobilized on a silicon chip and then incubated for 16 hours with a ‘click’ solution containing dansyl azide.

Figure 7.14, B, shows a typical AFM image of a DNA/polyC5-TP nanowire after treatment of DNA/polyC5-TP with the azido-dansyl fluorophore under ‘click’ conditions similar to those employed in Section 7.3.1, indicating that the 1-D wire-like structure remains intact. Fluorescence microscopy indicated the successful labeling of the wires with the dansyl derivative by excitation at 365 nm (Figure 7.14, D). The fluorescence from the nanowire is clearly evident, thus confirming the modification was successful. Furthermore, Figure 7.14, C, indicates that the conductive nature of the nanowire remains intact, despite the modification.

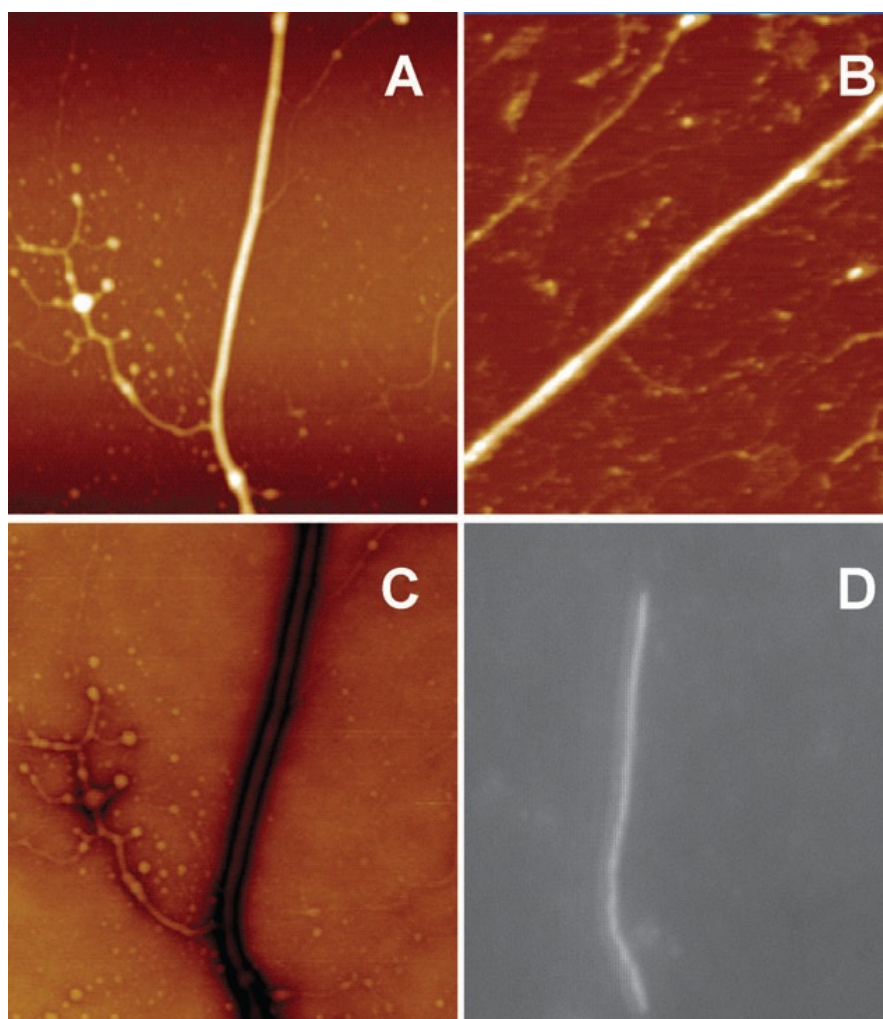


Figure 7.14. AFM images of DNA/polyC5-TP nanowires before (A, 4 μm scan size, 15 nm height scale) and after modification with dansyl azide (B, 7 μm scan size, 50 nm height scale). EFM image of the DNA/polyC5-TP nanowire (C, 4 μm scan size, grey scale corresponds to negative-positive-negative phase shift). Fluorescence image of a DNA/polyC5-TP nanowire after click reaction with dansyl azide. Reproduced from reference³¹

7.4 Conclusions

Synthesis and coupling of 3-azido propanol to monomer units of C5-**P**, C5-**TP** and C5-**TPT** was achieved in high yield. ‘Clicking’ of 3-azido propanol to bulk DNA/polymeric hybrid materials of C5-**P** and C5-**TP** was also shown through FTIR spectroscopy. Unfortunately, similar coupling using DNA/polyC5-**TPT** was deemed unsuccessful.

A 25mer azido modified ssDNA probe oligonucleotide and the relative complement, was synthesized for nanowire modification using solid phase phosphoramadite chemistry. The T_m for the modified duplex was found to be relatively lower than that of the theoretical value. This was considered to be largely due to instability caused by the 5’ azido-modification weakening the binding between the two strands of DNA.

Using protocols developed on bulk and solution based ‘click’ reactions, azido modified duplex attachment to DNA/polyC5-**P** wires formed in ‘iron-free’ templating solutions was attempted. Unfortunately, duplex coupling was deemed unsuccessful.

7.5 Experimental

7.5.1 Preparation of 3-Azido Propanol from 3-Bromo Propanol

Sodium azide (1.30g, 20 mmol) was added to an aqueous solution of 3-bromopropanol (1.36g, 9.78 mmol in 30 mL). The reaction was fitted with a reflux condenser and heated to 80 °C for 18 hours. The product was extracted from the aqueous solution using ethyl acetate (5 x 40 mL). The organic layer was washed with brine (30 mL) and dried using MgSO₄. The product was concentrated *in vacuo* affording a colourless oil (0.82g, 8 mmol, 83%). ¹H NMR spectrum (300 MHz, CDCl₃): δ 1.73 (m, 2H, CH₂), 2.59 (broad s, 1H, OH), 3.43 (t,t, 2H, CH₂), 4.02 (m, 2H, CH₂) ¹³C NMR spectrum (400 MHz, CDCl₃): δ 31 (CH₂), 48 ppm (CH₂), 60 (CH₂).

7.5.2 General Procedure for ‘Click’ Chemistry of 3-Azido Propanol with Monomer Units

Typically, 3-azido-propanol (48.5mg, 480 μmol) and C5-TP (63.8mg, 480 μmol) were suspended in 1:1 mixture of *tert*-butyl alcohol and water (2 mL). Freshly prepared aqueous 1M sodium ascorbate solution (50 μL, 50 μmol) was added, followed by copper^(II) sulphate pent-hydrate (1.70mg, 7.00 μmol). The mixture was stirred vigorously in a small capped vile overnight in darkness. The organic phase was dissolved in CH₂Cl₂ and washed with nanopure water (3 x 2 mL). The solvent was removed *in vacuo* affording a pale yellow oil (0.09 g, 0.38 mmol, 80%) ¹H NMR spectrum (400 MHz, CDCl₃): δ 2.0 (m, 4H), 2.63 (t, 2H), 4.0 (t, 2H), 4.41 (t, 2H), 6.15 (d, 1H), 6.26 (d, 1H), 6.75 (d, 1H), 6.94 (d, 1H), 7.0 (t, 1H), 7.10 (d, 1H), 7.24 (d, 1H). ¹³C NMR spectrum (400 MHz, CDCl₃): δ 22.58, 30.85, 32.54, 46.51, 46.73, 58.8, 108.0, 110.5, 121.2, 122.8, 124.8, 125.5, 126.3, 127.3. LCMS (ESI): m/z: calc. for C₁₆H₂₁N₄OS [M+H]⁺: 317.1445; found: 317.1436.

‘Clicked N-(pent-4-ynyl)pyrrole: Yield: 78% as an oil. (400 MHz, CDCl₃): δ 2.0 (m, 4H), 2.65 (t, 2H), 3.62 (t, 2H), 3.98 (t, 2H), 4.46 (d, 1H) 5.29 (d, 1H), 6.13 (t, 2H), 6.65 (d, 2H), 7.29 (d, 1H). ¹³C NMR spectrum (400 MHz, CDCl₃): δ 22.50,

30.83, 32.86, 46.79, 46.59, 58.4, 107.92, 120.4, 121.36, LCMS (ESI): m/z: calc. for $C_{12}H_{18}N_4ONa$ $[M+H]^+$:257.14 found: 257.13.

'Clicked' *N*-(pent-4-ynyl)-2,5-bis(2-thienyl)pyrrole: Yield: 83% as an oil(400 MHz, $CDCl_3$): δ 1.83 (m, 4H), 2.0 (t, 2H), 3.4 (t, 2H), 3.7 (t, 2H), 4.26 (t, 1H), 6.3 (d, 1H), 7.08 (d, 1H), 7.22 (d, 1H) ^{13}C NMR spectrum (400 MHz, $CDCl_3$): δ 15.7 29.61, 31.40, 32.54, 44.09, 48.46, 59.9, 68.9, 82.65, 110.84, 110.98, 125.32, 126.06, 127.29, 128.33.

7.5.3 General Procedure for 'Click' Chemistry of DNA Hybrid Polymers on Si/SiO₂

Typically, the sample prepared in 2.2.1 was suspended in a solution of water:*tert*-butyl alcohol (2:1, 20 mL) containing sodium ascorbate (0.03g, 0.15 mmol), copper^(II) sulphate (4.72 mg, 0.03 mmol) and 3-azido propanol (0.3 g, 2.95 mmol). The mixture was stirred gently in darkness for 8 hours. The chip was washed with excess of nanopure water, dried in a vacuum oven (60 °C) and analysed by FTIR

7.5.4 Oligonucleotide Synthesis

All oligonucleotides were synthesized using a standard elongation cycle. An amino modifier C2 dT was introduced at the 5' end to facilitate modification to an azide post-synthesis. After cleavage, purification by HPLC, deprotection and desalting the amino terminated oligo was re-dissolved in sodium bicarbonate (200 μ L, 0.2 M, pH 8.5). An azido group was subsequently introduced through the addition of azidobutyrate ester (60 μ L, 0.17 M) in acetonitrile and incubated at room temperature for 3 hours. Monitoring of the reaction and purification was performed by HPLC. Desalting of the product afforded the desired product. MALDI-TOF MS negative mode for azido modified 24mer 4109.42.

7.5.5 UV-Vis Oligonucleotide Hybridisation Studies

The hexyl azide modified 25 mer and its complement was diluted (~0.72 μ M) using buffer (25 mM Hepes, pH 7, 1 M NaCl) and combined. The mixture was suspended in a beaker of nanopure water (80 °C) for 20 minutes then allowed to cool to room

temperature. UV-vis absorption spectra (200-500 nm, 20-85 °C) was recorded on a Thermo-Spectronic GENESYS 6 spectrophotometer using a Quartz cuvette.

7.5.6 Electrical Characterisation by c-AFM General Procedure

For c-AFM measurements, MESP probes (n-doped Si cantilevers, with Co/Cr coating, Veeco Inc.). These probes are 200-250 μm long, with a resonant frequency of about 79 KHz, a quality factor (Q) between 200 and 260 and a spring constant between 1 and 5 N m^{-1} . A constant bias was also applied between the tip and the sample (the tip was grounded). Electrical contact was made by applying a drop of In/Ga eutectic to one corner of the chip and to the metallic chuck. c-AFM imaging was performed in contact mode, with an applied bias of 10 V. The imaged area was approximately 1 mm away from the In/Ga contact unless otherwise stated. The closed loop system of the Dimension V instrument makes it possible to reproducibly position the tip at a point of interest identified in the image of the nanowire and to record I - V measurements at that point. The resistance was measured was estimated from the reciprocal of the slope of the I - V curve at zero bias. Samples were prepared as in Chapter 4. 2-3 μL of template solution was deposited onto 1 cm^{-3} SiO_2/Si substrates at room temperature and allowed to dry for 1 h.

7.5.7 Azide Modified Duplex Coupling Method 1

A stock solution of copper^(II) sulfate pentahydrate (2.6 mM), sodium ascorbate (2.6 mM) and TBTA (2.6 mM) was made up in DMSO (1.5 mL). Azido 25mer duplex (30 μM , 8.5 μL) in HEPES buffer (0.6mM), was added to 1.5 μL of stock solution. 5 μL of the ‘click-azide solution’ was deposited on the wire and incubated for 2 h. After which, the droplet was removed and the area washed 3 times with nanopure water.

7.5.8 Azide Modified Oligonucleotide Coupling Method 2

A Si/SiO₂ substrate with DNA/C5-polyP wires deposited on the surface was cut into $\sim 2\text{ mm}^2$ and placed in a mass spec vile. Azido 25mer duplex (67 μM , 50 μL) in HEPES buffer (0.6mM), sodium ascorbate (6.25 mM in buffer, 4 μL) and a solution of Cu-TBTA (6.25 mM in 1:1, buffer: DMSO, 4 μL) were added, submerging the

substrate. The reaction mixture was mixed using a vortex. Upon completion the substrate was rinsed with buffer (3x).

7.5.9 Fluorescence Microscopy

Fluorescence images were collected on an Axioplan 2 microscope (Zeiss) using Axiovision Viewer software (Zeiss). The fluorescence was excited using the light from a Hg lamp passed through a 500-800 nm band-pass filter with a maximum transmission of 65% at $\lambda = 365$ nm. The emitted light was separated from scattered light using a long pass filter with a cutoff at 420 nm.

7.6 References

1. L. D. S. Ernst Sudholter, Marleen Mescher and Daniela Ullien ed., Organic Surface Modification of Silicon Nanowire-Based Sensor Devices, Nanowires - Implementations and Applications, *InTech*, 2011.
2. L. C. P. M. d. Smet, D. Ullien, M. Mescher and E. J. R. Sudhölter, Organic Surface Modification of Silicon Nanowire-Based Sensor Devices, 2011.
3. X. Bi, A. Agarwal and K.-L. Yang, *Biosensors and Bioelectronics*, 2009, **24**, 3248-3251.
4. G.-J. Zhang, G. Zhang, J. H. Chua, R.-E. Chee, E. H. Wong, A. Agarwal, K. D. Buddharaju, N. Singh, Z. Gao and N. Balasubramanian, *Nano Letters*, 2008, **8**, 1066-1070.
5. G. Zheng, F. Patolsky, Y. Cui, W. U. Wang and C. M. Lieber, *Nature Biotechnology*, 2005, **23**, 1294-1301.
6. B. Dorvel, B. Reddy and R. Bashir, *Analytical chemistry*, 2013.
7. X. Duan, Y. Li, N. K. Rajan, D. A. Routenberg, Y. Modis and M. A. Reed, *Nature Nanotechnology*, 2012, **7**, 401-407.
8. F. Patolsky, G. Zheng, O. Hayden, M. Lakadamyali, X. Zhuang and C. M. Lieber, *Proceedings of the National Academy of Sciences of the United States of America*, 2004, **101**, 14017-14022.
9. T.-S. Pui, A. Agarwal, F. Ye, N. Balasubramanian and P. Chen, *Small*, 2009, **5**, 208-212.
10. Y. Huang, X. Duan, Q. Wei and C. M. Lieber, *Science*, 2001, **291**, 630-633.
11. Y. Cui, Q. Wei, H. Park and C. M. Lieber, *Science*, 2001, **293**, 1289-1292.
12. J.-i. Hahm and C. M. Lieber, *Nano Letters*, 2003, **4**, 51-54.

13. A. K. Wanekaya, W. Chen, N. V. Myung and A. Mulchandani, *Electroanalysis*, 2006, **18**, 533-550.
14. A. Gao, N. Lu, Y. Wang, P. Dai, T. Li, X. Gao, Y. Wang and C. Fan, *Nano Letters*, 2012, **12**, 5262-5268.
15. G.-J. Zhang and Y. Ning, *Analytica Chimica Acta*, 2012, **749**, 1-15.
16. F. Patolsky, *Analytical chemistry*, 2006, **78**, 4260-4269.
17. C. M. Zheng, *Methods in molecular biology*, 2011, **790**, 223-237.
18. S. Su, Y. He, S. Song, D. Li, L. Wang, C. Fan and S.-T. Lee, *Nanoscale*, 2010, **2**, 1704-1707.
19. Z. Gao, A. Agarwal, A. D. Trigg, N. Singh, C. Fang, C.-H. Tung, Y. Fan, K. D. Buddharaju and J. Kong, *Analytical chemistry*, 2007, **79**, 3291-3297.
20. C. Wanninger-Weiß and H. A. Wagenknecht, *European Journal of Organic Chemistry*, 2008, 64-71.
21. K. L. Seley, L. Zhang, A. Hagos and S. Quirk, *The Journal of Organic Chemistry*, 2002, **67**, 3365-3373.
22. P. Liu, A. Sharon and C. K. Chu, *Journal of Fluorine Chemistry*, 2008, **129**, 743-766.
23. C. Mathé and C. Périgaud, *European Journal of Organic Chemistry*, 2008, 1489-1505.
24. J. A. Brazier, T. Shibata, J. Townsley, B. F. Taylor, E. Frary, N. H. Williams and D. M. Williams, *Nucleic Acids Research*, 2005, **33**, 1362-1371.
25. H. Ozaki, M. Mine, K. Shinozuka and H. Sawai, *Nucleosides Nucleotides Nucleic Acids*, 2004, **23**, 339-346.
26. R. B. Merrifield, *Journal of the American Chemical Society*, 1963, **85**, 2149-2154.
27. S. L. Beaucage and R. P. Iyer, *Tetrahedron*, 1992, **48**, 2223-2311.

28. J.-F. Lutz, *Angewandte Chemie - International Edition*, 2007, **46**, 1018.
29. D. H. Williams, Fleming, Ian, *Spectroscopic Methods in Organic Chemistry*, 5th edn., McGraw-Hall, 1995.
30. E. Borello and A. Zecchina, *Spectrochimica Acta*, 1963, **19**, 1703-1715.
31. J. Hannant, J. H. Hedley, J. Pate, A. Walli, S. A. Farha Al-Said, M. A. Galindo, B. A. Connolly, B. R. Horrocks, A. Houlton and A. R. Pike, *Chemical Communications*, 2010, **46**, 5870-5872.
32. T. Theophanides, *Applied Spectroscopy*, 1981, **35**, 461-465.
33. Image drawn by Dr. J. D. Watson, 2010.
34. J. Lietard, A. Meyer, J.-J. Vasseur and F. Morvan, *Tetrahedron Letters*, 2007, **48**, 8795-8798.
35. N. E. Good, G. D. Winget, W. Winter, T. N. Connolly, S. Izawa and R. M. M. Singh, *Biochemistry*, 1966, **5**, 467-477.
36. J. L. Lepe-Zuniga, J. S. Zigler Jr and I. Gery, *Journal of Immunological Methods*, 1987, **103**, 145.
37. J. Nakamura, E. R. Purvis and J. A. Swenberg, *Nucleic acids research*, 2003, **31**, 1790-1795.
38. K. Gnther, M. Mertig and R. Seidel, *Nucleic acids research*, 2010, **38**, 6526-6532.
39. S. G. Datta, C. Reynolds, Y. K. Goud and B. Datta, *Journal of Biomolecular Structure and Dynamics*, 2013, 1-9.

Chapter 8

Summary and Further Work

8.1 Achievements

Novel DNA-based conductive polymer nanowires formed from pyrrole and thiophene co-monomer units have been synthesized. Relative control over nanowire dimensions and deposition through tailoring of silicon surfaces and DNA-templating conditions has been demonstrated. The electronic properties of these materials have also been investigated. While undesirable levels of conductivity were observed the potential to tailor these systems further through co-polymerisation has been shown.

In Chapter 3, the alkylated monomers of **C5-P**, **C5-TP** and **C5-TPT** were synthesized with polymer formation demonstrated both chemically and electrochemically. Chapter 4 demonstrated how DNA-templating can be used to direct the growth of these materials into 1-D nanostructures despite the lack of available strong hydrogen bonding sites. Tuning of templating and surface conditions to facilitate relative control over nanowire dimensions was also shown. Interestingly, the low local pH of the DNA seems to promote a more elegant polymerisation process than when initiated by chemical oxidant, with polymerisation been shown to be initiated by molecular oxygen present in solution and catalyzed by DNA in solution.

In Chapter 5, the electrical properties of DNA polymer nanowires of **C5-P**, **C5-TP** and **C5-TPT** were investigated. The resistance of the DNA/polymer nanowires, determined from variable temperature I - V measurements, was found to be in the range of 10^{12} - $10^{14}\Omega$. Nanowire conductivity values were calculated to be in the range of 1.9×10^{-7} - $3.75 \times 10^{-4} \text{ S cm}^{-1}$ at 303K. In both cases, electron hopping was determined to be the dominant mechanism for electron transport shown through the exponential behaviour of the conductance upon increasing the temperature. While DNA/**C5-P** nanowires prepared without a chemical oxidant were shown to be conductive and when heated exhibit a molecular switch type process.

Studies to optimise the preparation of polypyrrole prior to incorporation into a co-polymer system were presented in Chapter 6. Optimisation of polymerisation conditions for polypyrrole formation was shown to produce polymer with highly conductive properties. Subsequent co-polymerisation with polyC5-**P**, polyC5-**TP** and polyC5-**TPT** under these conditions yield co-polymeric materials with higher levels of conductivity than homopolymer systems.

In the final chapter, Chapter 7, synthesis and coupling of 3-azido propanol to monomer units of C5-**P**, C5-**TP** and C5-**TPT** was achieved in high yield, in addition to ‘clicking’ of 3-azido propanol to bulk DNA/polymeric hybrid materials of C5-**P**, C5-**TP**. Synthesis and characterisation of an azido-modified oligonucleotide was also presented in addition to efforts made to achieve probe attachment to DNA/polyC5-**P** nanowires.

8.2 Further Work

Several areas for further investigation on the systems studied have been identified; the most important of which relates to the controlled deposition of nanowires across micro-electrode gaps. By mechanising this procedure with current technologies such as an a NanoInk DPN 2000; consistent nanowire deposition and device construction could be achieved. These printing platforms operate in a lateral position, travelling continuously across a chosen substrate, essentially combing. Small droplets of liquid (sample) are ejected from the print head nozzles and land on the substrate. The DPN 2000 can fabricate multiplexed, customized patterns with feature sizes as small as 50 nm or as big as 10 μm on a variety of substrates. This technology allow device construction to become routine which in-turn would allow for effective monitoring of nanowire modification by two-terminal I - V measurements allowing for optimisation of the chemistries involved. An alternative approach facilitated by such devices would be to print the polymer directly onto the substrate of choice; contact pads for the electrodes could also be formed by this method, removing any contact resistance between the pads and the nanowire. Interestingly, more straightforward routes to device construction would allow for the development and introduction of a micro-fluidic

flow system. This would improve the efficiency of the nanowire modification and potentially hybridization process by increasing mixing efficiency.

Furthermore, work in Chapter 5 demonstrated the potential to tune the electronic properties of these materials the co-polymer formation of pyrrole. An interesting study would be to further investigate the level of functionality afforded in such materials and produce wires accordingly. This could be achieved by FTIR studies by integrating under the alkyne C-H band and the N-H band produced from the alkyne moiety and non-alkylated pyrrole moiety respectively. Such data could be further validated by fluorescence microscopy through coupling of fluorescently labeled probes of a known quantum yield. This would allow estimation of the number of probes present on the surface based on the fluorescence intensity. An extension of this work would be then to examine different probes and linker lengths and the effect on coupling.

As discussed in Chapter 7, modification of nanowires with ssDNA probes is typically achieved via covalent attachment of appropriately functionalised oligonucleotides, in this project azido-modified oligonucleotides. An alternative route is to synthesize the desired oligonucleotides directly at the CP surface, akin to conventional solid phase synthesis however using a nanowire as a solid support. Successful coupling 3-azido propan-1-ol to the C5-**P**, C5-**TP** and C5-**TPT** monomer units and the respective DNA/polymer hybrid materials has been demonstrated. Direct DNA synthesis using phosphoramidite chemistry could potentially be performed at the CP surface as a means to synthesizing DNA modified conducting polymer nanowires in future work

9 Appendix

9.1 Molecular structure of 2-(2-thienyl)-pyrrole, TP

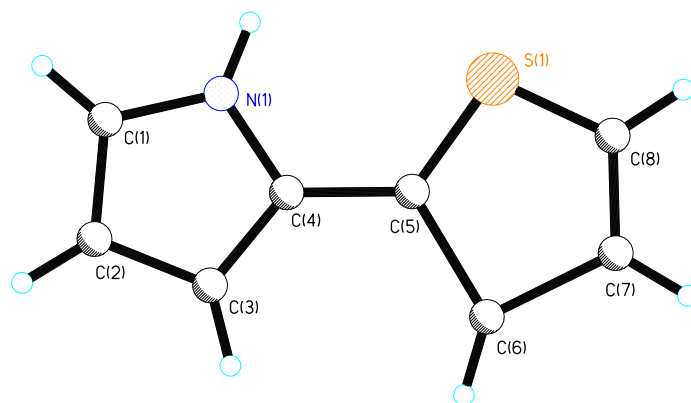


Figure 9.1.1 Molecular structure of 2-(2-thienyl)-pyrrole, **TP**, recrystallized from dichloromethane and obtained by a single crystal X-ray study

Table 9.1. Crystal data and structure refinement for ah156.

Identification code	ah156	
Chemical formula (moiety)	C ₈ H ₇ NS	
Chemical formula (total)	C ₈ H ₇ NS	
Formula weight	149.21	
Temperature	150(2) K	
Radiation, wavelength	MoK α , 0.71073 Å	
Crystal system, space group	monoclinic, P12 ₁ 1	
Unit cell parameters	a = 5.3335(2) Å b = 7.0736(3) Å c = 9.7363(5) Å	$\alpha = 90^\circ$ $\beta = 103.896(4)^\circ$ $\gamma = 90^\circ$
Cell volume	356.57(3) Å ³	
Z	2	
Calculated density	1.390 g/cm ³	
Absorption coefficient μ	0.363 mm ⁻¹	
F(000)	156	
Crystal colour and size	colourless, 0.20 × 0.18 × 0.18 mm ³	
Reflections for cell refinement	3141 (θ range 2.9 to 29.4°)	
Data collection method	Oxford Diffraction Gemini A Ultra diffractometer thin-slice ω scans	
θ range for data collection	3.6 to 29.5°	
Index ranges	h -7 to 6, k -7 to 9, l -12 to 13	
Completeness to $\theta = 26.0^\circ$	99.9 %	
Reflections collected	4009	
Independent reflections	1558 ($R_{\text{int}} = 0.0191$)	
Reflections with $F^2 > 2\sigma$	1453	
Absorption correction	semi-empirical from equivalents	
Min. and max. transmission	0.9309 and 0.9375	
Structure solution	direct methods	
Refinement method	Full-matrix least-squares on F^2	
Weighting parameters a, b	0.0584, 0.0202	
Data / restraints / parameters	1558 / 1 / 96	
Final R indices [$F^2 > 2\sigma$]	R1 = 0.0317, wR2 = 0.0862	
R indices (all data)	R1 = 0.0339, wR2 = 0.0872	
Goodness-of-fit on F^2	1.099	
Absolute structure parameter	-0.01(9)	
Largest and mean shift/su	0.000 and 0.000	
Largest diff. peak and hole	0.36 and -0.31 e Å ⁻³	

Table 9.2. Atomic coordinates and equivalent isotropic displacement parameters (\AA^2) for ah156. U_{eq} is defined as one third of the trace of the orthogonalized U^{ij} tensor.

	x	y	z	U_{eq}
S(1)	0.54692(19)	0.35899(16)	0.15648(10)	0.0350(4)
S(1A)	0.95525(11)	0.11561(8)	0.18558(6)	0.0284(2)
N(1)	0.5589(3)	0.2600(2)	0.47184(15)	0.0204(3)
C(1)	0.6255(3)	0.2199(2)	0.61272(18)	0.0236(4)
C(2)	0.8481(3)	0.1137(3)	0.63960(17)	0.0228(3)
C(3)	0.9183(3)	0.0889(2)	0.50909(17)	0.0206(3)
C(4)	0.7361(3)	0.1824(2)	0.40610(18)	0.0183(3)
C(5)	0.7314(3)	0.2156(2)	0.25861(17)	0.0185(3)
C(6)	0.95525(11)	0.11561(8)	0.18558(6)	0.0284(2)
C(6A)	0.54692(19)	0.35899(16)	0.15648(10)	0.0350(4)
C(7)	0.8542(4)	0.2256(3)	0.0337(2)	0.0327(4)
C(8)	0.6515(4)	0.3412(3)	0.0260(2)	0.0328(4)

Table 9.3. Bond lengths [\AA] and angles [$^\circ$] for ah156.

S(1)–C(5)	1.5863(19)	S(1)–C(8)	1.510(2)
S(1A)–C(5)	1.6849(16)	S(1A)–C(7)	1.643(2)
N(1)–H(1)	0.90(3)	N(1)–C(1)	1.362(2)
N(1)–C(4)	1.377(2)	C(1)–H(1A)	0.950
C(1)–C(2)	1.376(2)	C(2)–H(2A)	0.950
C(2)–C(3)	1.419(2)	C(3)–H(3A)	0.950
C(3)–C(4)	1.385(2)	C(4)–C(5)	1.449(2)
C(7)–H(7)	0.950	C(7)–C(8)	1.343(3)
C(8)–H(8)	0.950		
C(5)–S(1)–C(8)	100.09(11)	C(5)–S(1A)–C(7)	93.93(9)
H(1)–N(1)–C(1)	125(2)	H(1)–N(1)–C(4)	125(2)
C(1)–N(1)–C(4)	110.08(14)	N(1)–C(1)–H(1A)	126.0
N(1)–C(1)–C(2)	108.03(14)	H(1A)–C(1)–C(2)	126.0
C(1)–C(2)–H(2A)	126.3	C(1)–C(2)–C(3)	107.37(14)
H(2A)–C(2)–C(3)	126.3	C(2)–C(3)–H(3A)	126.3
C(2)–C(3)–C(4)	107.39(15)	H(3A)–C(3)–C(4)	126.3
N(1)–C(4)–C(3)	107.13(14)	N(1)–C(4)–C(5)	123.07(14)
C(3)–C(4)–C(5)	129.54(15)	S(1)–C(5)–S(1A)	113.55(10)
S(1)–C(5)–C(4)	125.82(13)	S(1A)–C(5)–C(4)	120.32(12)
S(1A)–C(7)–H(7)	122.4	S(1A)–C(7)–C(8)	115.11(15)
H(7)–C(7)–C(8)	122.4	S(1)–C(8)–C(7)	117.30(16)
S(1)–C(8)–H(8)	121.4	C(7)–C(8)–H(8)	121.4

Table 9.4. Anisotropic displacement parameters (\AA^2) for ah156. The anisotropic displacement factor exponent takes the form: $-2\pi^2[h^2a^{*2}U^{11} + \dots + 2hka^*b^*U^{12}]$

	U^{11}	U^{22}	U^{33}	U^{23}	U^{13}	U^{12}
S(1)	0.0328(6)	0.0488(7)	0.0243(6)	-0.0025(4)	0.0085(4)	-0.0085(5)
S(1A)	0.0292(3)	0.0325(3)	0.0252(3)	-0.0003(3)	0.0104(2)	0.0039(3)
N(1)	0.0182(7)	0.0198(7)	0.0228(7)	0.0002(6)	0.0040(5)	0.0016(6)
C(1)	0.0263(9)	0.0219(9)	0.0247(9)	-0.0016(7)	0.0105(7)	-0.0027(7)
C(2)	0.0238(7)	0.0202(7)	0.0223(8)	0.0036(7)	0.0017(6)	-0.0024(7)
C(3)	0.0190(8)	0.0169(8)	0.0254(8)	0.0021(6)	0.0044(6)	-0.0010(6)
C(4)	0.0179(7)	0.0140(7)	0.0235(9)	-0.0020(6)	0.0057(6)	-0.0034(5)
C(5)	0.0169(7)	0.0173(8)	0.0214(8)	-0.0032(6)	0.0048(6)	-0.0027(6)
C(6)	0.0292(3)	0.0325(3)	0.0252(3)	-0.0003(3)	0.0104(2)	0.0039(3)
C(6A)	0.0328(6)	0.0488(7)	0.0243(6)	-0.0025(4)	0.0085(4)	-0.0085(5)
C(7)	0.0360(10)	0.0385(11)	0.0275(10)	-0.0066(9)	0.0151(8)	-0.0053(9)
C(8)	0.0383(10)	0.0284(10)	0.0269(10)	0.0019(8)	-0.0014(8)	-0.0010(8)

Table 9.5. Hydrogen coordinates and isotropic displacement parameters (\AA^2) for ah156.

	x	y	z	U
H(1)	0.418(6)	0.326(5)	0.428(3)	0.080(12)
H(1A)	0.5342	0.2585	0.6806	0.028
H(2A)	0.9382	0.0659	0.7290	0.027
H(3A)	1.0636	0.0208	0.4950	0.025
H(6)	1.0905	0.0277	0.2197	0.034
H(6A)	0.4097	0.4346	0.1728	0.042
H(7)	0.9334	0.2088	-0.0430	0.039
H(8)	0.5770	0.4090	-0.0581	0.039

Table 9.6. Torsion angles [$^\circ$] for ah156.

C(4)-N(1)-C(1)-C(2)	-0.36(18)	N(1)-C(1)-C(2)-C(3)	-0.01(19)
C(1)-C(2)-C(3)-C(4)	0.37(19)	C(1)-N(1)-C(4)-C(3)	0.59(18)
C(1)-N(1)-C(4)-C(5)	-174.01(15)	C(2)-C(3)-C(4)-N(1)	-0.58(18)
C(2)-C(3)-C(4)-C(5)	173.55(16)	N(1)-C(4)-C(5)-S(1)	6.8(2)
N(1)-C(4)-C(5)-S(1A)	179.94(12)	C(3)-C(4)-C(5)-S(1)	-166.52(14)
C(3)-C(4)-C(5)-S(1A)	6.6(2)	C(8)-S(1)-C(5)-S(1A)	1.49(14)
C(8)-S(1)-C(5)-C(4)	175.05(15)	C(7)-S(1A)-C(5)-S(1)	-0.85(12)
C(7)-S(1A)-C(5)-C(4)	-174.80(14)	C(5)-S(1A)-C(7)-C(8)	-0.23(16)
S(1A)-C(7)-C(8)-S(1)	1.3(2)	C(5)-S(1)-C(8)-C(7)	-1.72(19)

9.2 Fourier Transform Infrared Spectroscopy (FTIR)

<i>DNA</i>	
Wavenumber (cm ⁻¹)	Assignment
ca 3300	OH stretch or NH stretch of nucleobases
1690	C=O stretch of Guanine/thymine; N-H thymine
1653	C=O stretch of cytosine/thymine
1487	ring vibration of cytosine/guanine
1420	CH, NH deformation; CN stretch of Guanine and cytosine
1365	CN stretch of cytosine and guanine
1241	PO ₂ - asymmetric stretch
1102	PO ₂ - asymmetric stretch
1060	C-O deoxyribose stretch
ca 1022 (as a shoulder)	C-O deoxyribose stretch
962	C-C deoxyribose stretch

Table 9.2.1 Assignment of FTIR spectra (500-4000 cm⁻¹) of CT-DNA

N-(pent-4-ynyl)pyrrole (*C5-P*)

<i>Monomer</i>	
Wavenumber (cm ⁻¹)	Assignment
3309 (w)	Alkyne CH
2951 (s, br)	Aromatic CH
2920 (s, br)	Alkene CH
2854 (s, br)	Alkane CH
2117 (vw)	Alkyne C=C
1531 (w)	C=C str. (ar)
1500 (m)	C=C, C-N str.
1458 (s)	C=C, C-N asym.
1377 (m)	C=C, C-N sym.
1342 (vw)	C-C str. in plane
1284 (m)	C-N & ring str.
1087 (m)	C-CH, sym NCH
1053 (vw)	Ring breathing
991 (vw)	Ring deformation
960 (w)	Ring deformation
945 (w)	Ring deformation
833 (w)	CH in plane
806 (w)	Ring deformation
775 (w)	CH out of plane
721 (s)	Alkene CH bending

Table 9.2.2. Assignment of FTIR spectra (500-4000 cm⁻¹) of *N*-(pent-4-ynyl)pyrrole (C5-P)

PolyC5-P	
Wavenumber	Assignment
3263 (w)	alkyne CH
3113 (br)	Aromatic CH
2924 (s)	Asym CH ₂
2854 (m)	Sym CH ₂
1978 (w)	alkyne
1643 (m)	inter-ring C-C bond of longer oligomers
1446 (w)	C=C str. (ar)
1408 (w)	C=C, C-N str.
1357 (m)	C=C, C-N asym.
1238 (m)	C=C, C-N sym.
1122 (m)	C-C str. in plane
1049 (m)	C-N & ring str.
983 (w)	CH oop ring def.
837 (m)	C=C
682 (m)	CH oop ring def.

Table 9.2.3. Assignment of FTIR spectra (500-4000 cm⁻¹) of polyC5-P

DNA/polyC5-P	
Wavenumber (cm⁻¹)	Assignment
ca 3300	O-H of water
2924	Aromatic CH
2854 appears as shoulder	Alkene CH
2812	Alkane CH
2086	Alkyne
1658	C-C inter ring, sym. with alkene C=C, str.
1496	ring vibration of cytosine/guanine
1419	C=C str. (ar)
1396	C=C, C-N str.
1381	C=C, C-N asym.
1249	C=C, C-N sym.
1134	C-C str. in plane
1107	C-N & ring str.
1060	CH oop ring def.
995	C-O deoxyribose stretch

864	C=C
678	CH oop ring def.

Table 9.2.4. Assignment of FTIR spectra (500-4000 cm^{-1}) of DNA/polyC5-P

Bulk 'Clicked' DNA/polyC5-P

<i>Wavenumber (cm⁻¹)</i>	<i>Assignment</i>
ca 3300	O-H of water/terminal OH
2939 (m, shoulder)	Aromatic CH
2920 (s)	Alkene CH
2854 (m)	Alkane CH
1639 (s)	C-C inter ring, sym. with alkene C=C, str.
1600 (w, shoulder)	triazole ring vibration
1516 (w)	C-H, C-N & C=C (Ar)
1458 (m)	C=C, C-N asym.
1388 (w)	C-H, C-N & C=C (Ar)
1373 (m)	C=C, C-N sym.
1269 (w, shoulder)	C-C str. in plane
1215 (s)	triazole breathing
1056 (s)	C-O deoxyribose stretch
1014 (w, shoulder)	C-N & ring str.
960 (m)	CH oop ring def./C-O deoxyribose stretch
902 (w)	C-O deoxyribose stretch
860 (w)	triazole nucleus
810 (w)	out of plane def. of H CH ₂
771 (w)	planar def. of triazole ring
698 (w)	CH oop ring def.
613 (w)	Ring, sugar, phosphate deformations

Table 9.2.5. Assignment of FTIR spectra (500-4000 cm^{-1}) of 'Clicked' DNA/polyC5-P

N-(pent-4-ynyl)-2-(2-thienyl)pyrrole (C5-TP)

<i>Wavenumber (cm⁻¹)</i>	<i>Assignment</i>
3302	Alkyne C-H
2107	Aromatic C-H
2955	Alkene C-H
2889	Alkane C-H
2120	Alkyne C=C
1801	Oxidised Py

1694	Alkene str.
1654	C=C, str. (Ar)
1571	Alkene C-H
1509	C=C, C-N str.
1475	C=C, C-N asym.
1410	C=C, C-N sym. (Py)
1373	C=C, C-N sym. (Py, T)
1346	C=C sym. (T)
1330	C-N-C str.
1300	C-C stretch in plane
1243	C-N and ring str.
1202	CCH, CNH bending
1149	Ring breathing (Py)
1084	Ring breathing (Py)
1059	C-CH, sym, NCH
1024	Ring deformation
942	Ring deformation
881	C-H in plane bending
845	Ring def., sym, C-S str.
790	C-H out of plane (2, 5 dist.)
715	Alkene C-H bending
647	Substitution of the ring
543	Substitution of the ring
518	Substitution of the ring

Table 9.2.6. Assignment of FTIR spectra (500-4000 cm^{-1}) of C5-TP

polyC5-TP

Wavenumber (cm ⁻¹)	Assignment
518	Substitution of the ring
543	Substitution of the ring
647	Substitution of the ring
715	Alkene CH bending?
790	C-H out of plane (2, 5 dist?)
845	Ring def., sym, C-S str.
881	C-H in plane bending
942	Ring deformation
1024	Ring deformation
1059	C-CH, sym, NCH
1084	Ring breathing (Py)
1149	Ring breathing (Py)
1202	CCH,CNH bending
1243	C-N and ring str.
1300	C-C stretch in plane
1330	C-N-C str.
1346	C=C sym. (T)
1373	C=C, C-N sym. (Py, T)
1410	C=C, C-N sym. (Py)
1475	C=C, C-N asym.
1509	C=C, C-N str.
1571	Alkene CH
1654	C=C str. (Ar)
1694	Alkene Str.
1801	Oxidised Py
2120	Alkyne
2889	Alkane C-H
2955	Alkene C-H
3107	Aromatic CH
3302	Alkyne CH

Table 9.2.7. Assignment of FTIR spectra (500-4000 cm⁻¹) of polyC5-TP

DNA/polyC5-TP

Wavenumber (cm ⁻¹)	Assignment
500-900	Ring, sugar, phosphate deformations
975	O-P-O Antisymmetric
1020	C-O deoxyribose
1077	PO ₂ - sym
1253	PO ₂ - asym
1380-1538	C-H, C-N & C=C (Ar)
1610	C=C, C=N stretching
1658	C=O stretching
1705	C=O stretching

Table 9.2.8. Assignment of FTIR spectra (500-4000 cm⁻¹) DNA/polyC5-TP

Bulk DNA/polyC5-TP ‘clicked’ to 3-azido propan-1-ol

Wavenumber (cm⁻¹)	Assignment
500-900	Ring, sugar, phosphate deformations
975	O-P-O Antisymmetric
1020	C-O deoxyribose
1077	PO2- sym
1253	PO2- asym
1380-1538	C-H, C-N & C=C (Ar)
1610	C=C, C=N stretching
1658	C=O stretching
1705	C=O stretching

Table 9.2.9. Assignment of FTIR spectra (500-4000 cm⁻¹) bulk DNA/polyC5-TP ‘clicked’ to 3-azido propan-1-ol

N-(pent-4-ynyl)-2,5-(di-2-thienyl)-pyrrole (C5-TPT)

Wavenumber (cm⁻¹)	Assignment
3290	Alkyne CH
3101	Aromatic CH
3070	Alkene C-H
2947	Alkane CH
2117	Alkyne
1778	Oxidised Py
1651	C=C str. (ar)
1566	Alken CH
1462	C=C, C-N asym. (Py, T)
1400	C-N and C=C stretches of pyrrolyl ring of poly TPT
1404	C-H, N-H deformation
1354	C=C, C-N sym. (Py, T)
1342	C=C sym. (T)
1303	C-C stretch in plane
1207	CCH, CNH bending
1195	Ring breathing (Py)
1080	Ring breathing (Py)
1049	Ring Deformation
1037	Ring deformation
864	C-H in plane bending
844	C-H out of plane bending of thiophene
767	C-H out of plane bending of pyrrolyl ring

Table 9.2.10. Assignment of FTIR spectra (500-4000 cm⁻¹) C5-TPT

polyC5-TPT

Wavenumber (cm-1)	Assignment
3381	NH
3290	alkyne CH
3099	aromatic CH
2926	alkene C-H
2852	alkane CH
2115 (w)	alkyne
1672	C=C str. (ar) of DMF C=O
1570	alkene CH
1494	C=C, C-N str.
1456	C=C, C-N asym. (Py, T)
1402	C-N and C=C stretches of pyrrolyl ring
1417	C-H, N-H deformation
1384	C=C, C-N sym. (Py, T)
1342	C=C sym. (T)
1301	C-C stretch in plane
1251	CCH, CNH bending
1219	C-N and ring str.
1195	Ring breathing (Py)
1089	Ring breathing (Py)
1049	Ring Deformation
1034	Ring deformation
887	C-H in plane bending
842	C-H out of plane bending of thiophene
765	C-H out of plane bending of pyrrolyl ring
692	2,5 Ring Substitution
657	2,5 Ring Substitution

Table 9.2.11. Assignment of FTIR spectra (500-4000 cm⁻¹)
bulk polyC5-TPT

DNA/polyC5-TPT

Wavenumber (cm-1)	Assignment
ca3300 (br)	OH of water
3282 (s)	alkyne CH

3101 (s)	aromatic CH
3070 (m)	alkene C-H
2939 (s)	alkane CH
2117 (m)	alkyne
1789 (m)	over oxidation?
1658 (m)	C=C str. (ar) of DMF C=O/C=O stretch of cytosine/thymine
1570 (w)	alkene CH
1504 (w)	C=C, C-N str.
1477 (w)	C=C, C-N asym. (Py, T)
1458 (m)	C-N and C=C stretches of pyrrolyl ring
1400 (m)	C-H, N-H deformation
1354 (w)	C=C sym. (T)
1342 (m)	C-C stretch in plane
1303 (m)	CCH, CNH bending
1203 (m)	C-N and ring str.
1195 (m)	ring breathing (Py)
1110 (w)	PO ₂ - asymmetric stretch
1056 (w)	ring Deformation
1033(m)	ring deformation
975 (w)	C-C deoxyribose stretch
829 (m)	C-H out of plane bending of thiophene
759 (m)	C-H out of plane bending of pyrrolyl ring
675 (m)	2,5 Ring Substitution
628 (m)	2,5 Ring Substitution

Table 9.2.12. Assignment of FTIR spectra (500-4000 cm⁻¹)
bulk DNA/polyC5-TPT ‘clicked’ to 3-azido propan-1-ol

9.3 Scanned Conductance Microscopy (SCM)

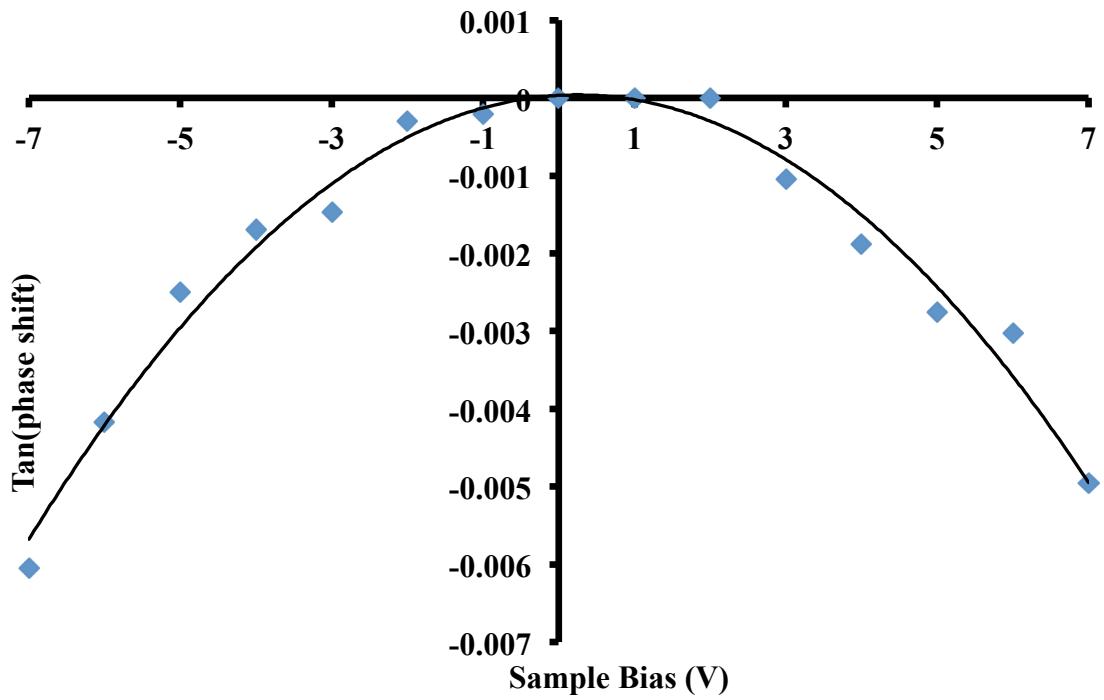


Figure 9.3.1. A plot of the (tangent) phase shift against the dc bias applied to the substrate for DNA/polyC5-P (10.80 nm in diameter)

Voltage vs. Phase Shift for a-TP-DNA polymer hybrid

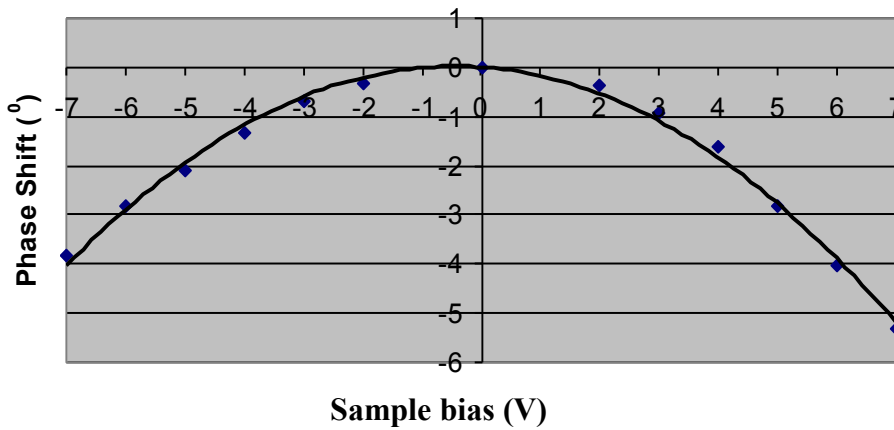


Figure 9.3.2. Parabolic dependence of phase shift on bias for voltages between -7 and +7 V for DNA/polyC5-TP nanowires

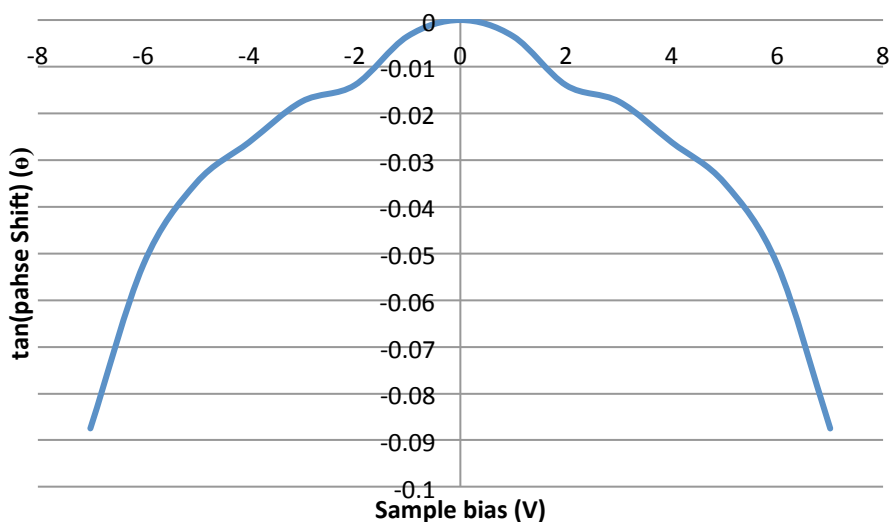


Figure 7.3.3. Parabolic dependence of phase shift on bias for voltages between -7 and +7 V for DNA/polyC5-TPT nanowires

9.4 Two-Probe *I-V* Measurements

The microelectrodes were prepared using an appropriate mask and reverse photolithography process to initially pattern the Si/SiO₂ substrate. A reactive ion etch was used to generate *ca.* 100 nm deep trenches in the patterned regions of the 100nm SiO₂ layer. Electron beam evaporation was used to fill the trenches with a *ca.* 10nm Cr adhesion layer, followed by a *ca.* 100nm Au layer to give the microelectrodes embedded in the SiO₂ layer. A lift-off process was finally applied to remove an unwanted Cr/Au from the substrate. The photolithography masks employed in this process directed the patterning of a series of microelectrode pairs upon the Si/SiO₂ substrate, where the gaps between the electrodes in each pair typically ranges from 2-8 μ m. The electrodes themselves each consist of a macroscale gold ‘pad’ (0.5mm wide and 1.0mm in length) which acts as an electrical contact, from which a smaller Au finger is connected (2.5 μ m wide and 16 μ m in length) (Figure 9.3.1). These fingers provide the contacts to the DNA-templated polymer nanowires, when they are aligned across the inter-electrode gap of the electrode pairs.

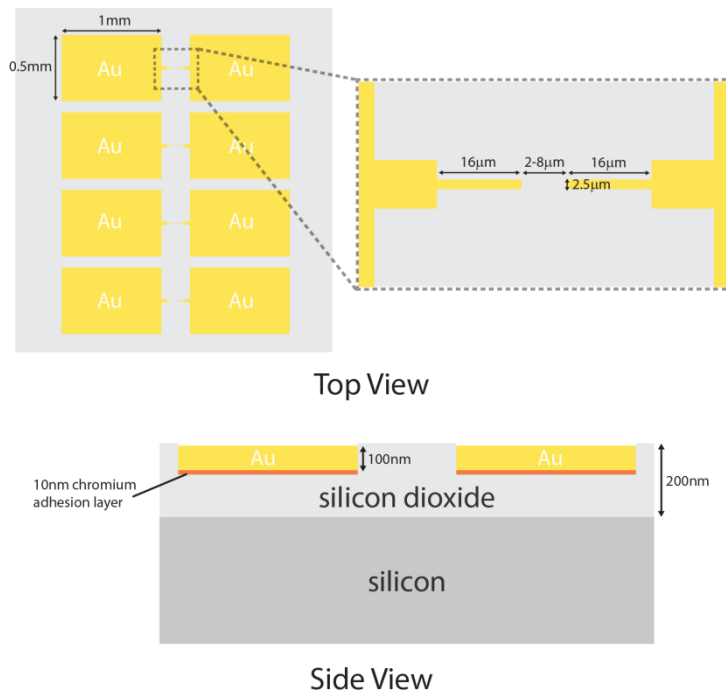
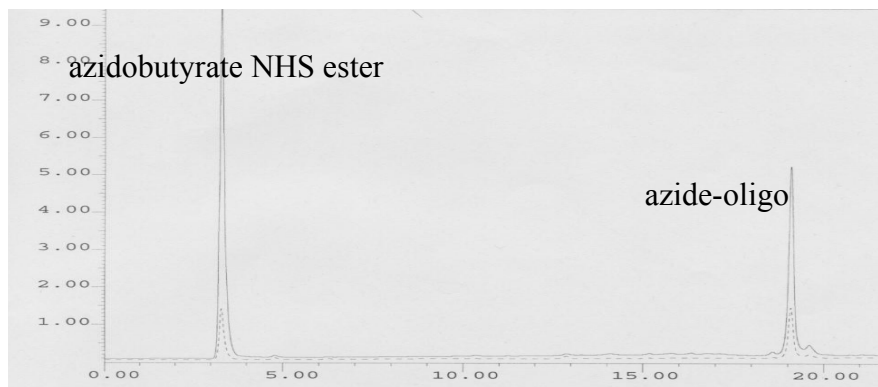


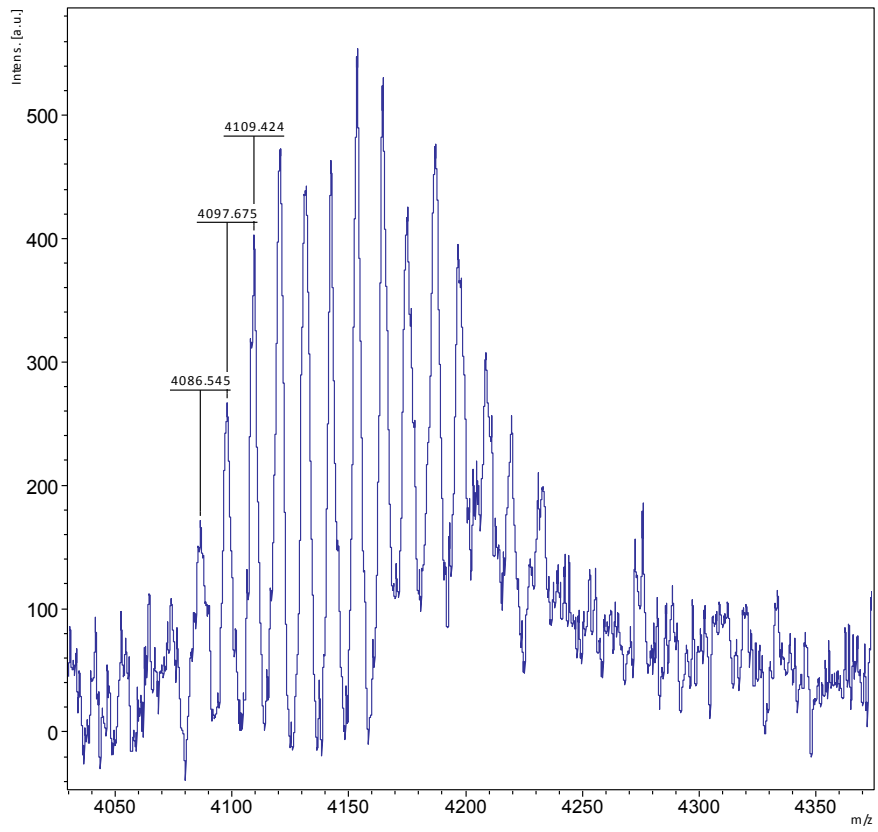
Figure 9.4.1. Design and dimensions of Au electrodes prepared upon Si/SiO₂ substrate, for use in two-terminal I - V measurements

9.5 DNA Synthesis

a) HPLC profile of 5' modified 25mer



MALDI-TOF MS – modified 25mer



Modification of DNA-templated conductive polymer nanowires *via* click chemistry†

Jennifer Hannant,^a Joseph H. Hedley,^a Jonathan Pate,^a Adam Walli,^b Said A. Farha Al-Said,^a Miguel A. Galindo,^a Bernard A. Connolly,^c Benjamin R. Horrocks,^a Andrew Houlton^a and Andrew R. Pike^{*a}

Received 31st March 2010, Accepted 25th June 2010

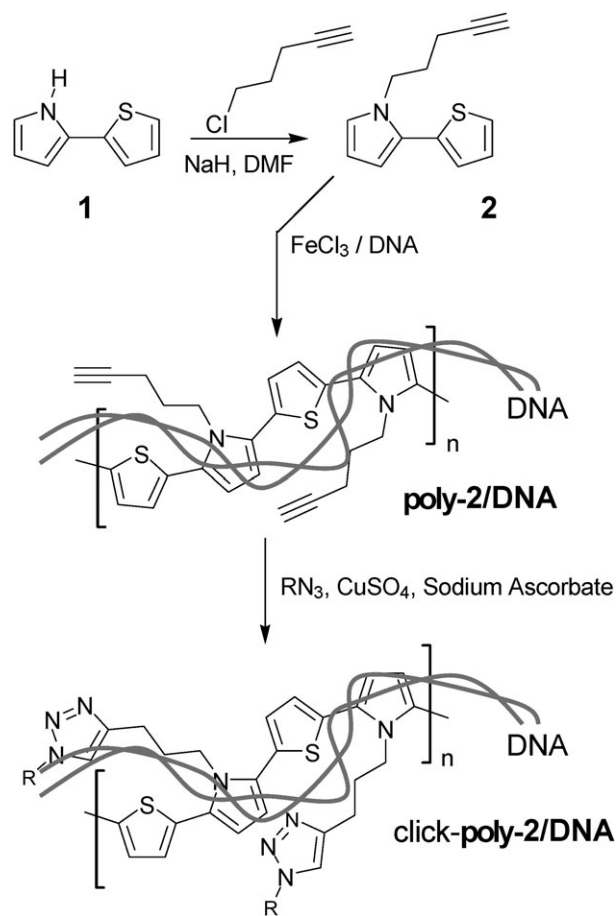
DOI: 10.1039/c0cc00693a

DNA templated nanowires of a pentynyl-modified poly-2-(2-thienyl)-pyrrole undergo functionalisation *via* “click chemistry” and retain their 1D-nanostructure and conductive properties.

There is considerable interest in the control of material growth so as to produce specifically sized, and topologically defined, nanostructures.^{1,2} Conductive 1D structures, so-called nanowires, are particularly important due to their potential use in photo-detectors,^{3,4} waveguides^{5,6} and chemical sensors.⁷ In the last of these devices advantage is taken of the highly sensitive nature of the electrical conduction to external perturbations, making them ideal as transducing elements. A variety of methods for preparing such structures have been developed, including the use of double helical DNA as a template.^{8,9} This approach has proved quite general and has enabled the preparation of conducting 1D nanostructures of metals, binary inorganics as well as molecular-based materials.^{9–11} This is possible because as individual molecules, the strands exhibit extensive non-covalent interactions with a wide variety of precursors, *e.g.* metal ions, small molecules, oligomers *etc.*^{9–12} This ability to “dope” the biopolymer with these precursors controls the resulting material formation. However, for use as sensing elements it is not sufficient to produce conducting structures; these must also be capable of functionalisation with appropriate receptors so as to prime them for capture of a target. Here we report the preparation of a conducting DNA-based nanowire system that can be readily functionalised.^{13,14} The approach uses individual strands of DNA¹⁵ to template the growth of a conducting polymer, **poly-2**, from monomers of *N*-pentynyl-2-(2-thienyl)-pyrrole, **2**. The resulting supramolecular **poly-2**/DNA material is formed as nanowires which can undergo functionalisation using “click” chemistry, demonstrated here with a variety of molecular groups. We also confirm that the **poly-2**/DNA nanowires are electrically conducting and importantly that they remain conductive after functionalisation

via the “click” reaction and therefore offer potential as versatile sensing elements.

Scheme 1 illustrates the approach for the preparation of **poly-2**/DNA hybrid nanostructures and the functionalisation of the terminal alkyne *via* “click chemistry”.¹⁶ 2-(2-Thienyl)-pyrrole, **1**, was synthesised in three steps according to the route developed by Cava *et al.*¹⁷ *N*-alkylation of **1** with 5-chloro-1-pentyne gave the target co-monomer, **2**. Hybrid polymer/DNA nanowires based on **poly-2** were formed *in situ* by reacting monomer **2** (30 mM), DNA (~80 μg μL⁻¹) as a template and FeCl₃ (1 mM) as oxidant in water/DMF. After incubation for 2 hours nanowire formation was confirmed using atomic force microscopy (AFM) by deposition and molecular combing of



Scheme 1 Synthetic route to the formation of alkyne bearing DNA-polymer hybrids and their subsequent “click” modification with an azide (R = 3-azido propan-1-ol or azido-dansyl sulfonamide).

^a Chemical Nanoscience Laboratory, School of Chemistry, Bedson Building, Newcastle University, Newcastle upon Tyne, UK. E-mail: a.r.pike@ncl.ac.uk; Fax: +44 (0)191 2226929; Tel: +44 (0)191 2227061

^b Institut für Anorganische Chemie, Georg-August-Universität Göttingen, Germany. Tel: +49 551 39 305

^c Institute for Cell and Molecular Biosciences, Newcastle University, Newcastle upon Tyne, UK

† Electronic supplementary information (ESI) available: Synthesis of the propanol and dansyl azido moieties, FTIR characterisation of **poly-2**/DNA nanowires, and further AFM, EFM, and fluorescence images of **poly-2**/DNA nanowires before and after modification are available. See DOI: 10.1039/c0cc00693a

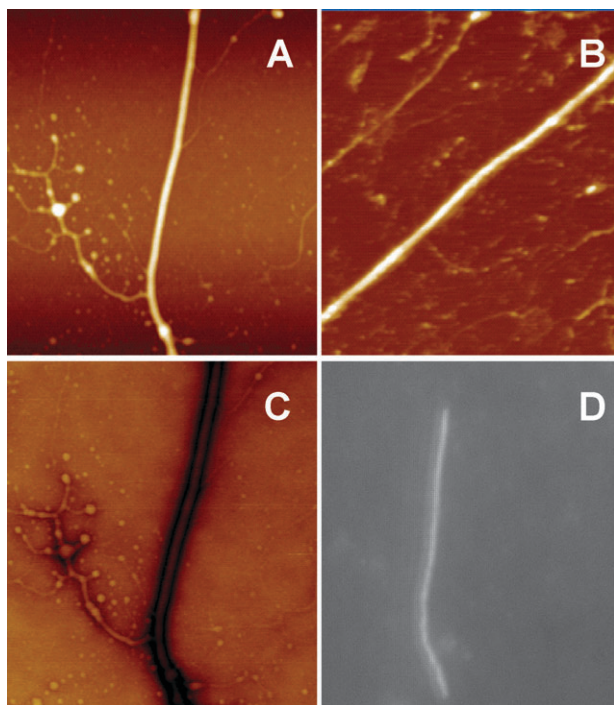


Fig. 1 AFM images of **poly-2**/DNA nanowires before (A, 4 μm scan size, 15 nm height scale) and after modification with dansyl azide (B, 7 μm scan size, 50 nm height scale). EFM image of the **poly-2**/DNA nanowire (C, 4 μm scan size, grey scale corresponds to 10° phase shift). Fluorescence image of a **poly-2**/DNA nanowire after click reaction with dansyl azide (D, $20 \times 20 \mu\text{m}$ image size).

droplets of these solutions across an n(111)-Si wafer.¹⁸ Tapping mode™ AFM of the **poly-2**/DNA hybrid material indicated the formation of wire-like structures aligned on the surface. Fig. 1A shows a typical single **poly-2**/DNA nanowire, height 9 nm, aligned across the surface with several smaller bare DNA strands in the background. The resulting nanowires exhibit diameters in the range 5–40 nm, which is comparable to our previous reports on polypyrrole/DNA hybrid nanowires.¹⁹

FTIR studies of **poly-2**, DNA and **poly-2**/DNA hybrids were used to illustrate the interaction of **poly-2** and DNA. **Poly-2** was prepared by the oxidative polymerisation of **2** as for **poly-2**/DNA (minus the DNA template) and samples of both polymeric materials were dried onto silicon wafers with native oxide. Fig. 2 shows transmission FTIR spectra of these samples. In **poly-2**/DNA hybrids the characteristic bands corresponding to the C=O stretching in the pyrimidine bases of DNA (1723 cm^{-1} and 1674 cm^{-1}) are shifted to a higher wavenumber than in natural DNA, 1705 cm^{-1} and 1658 cm^{-1} .²⁰ The reason for this shift is the electrostatic interaction of the cationic **poly-2** with the anionic DNA phosphate backbone.²¹

Analysis of the FTIR spectra was also used to establish that the terminal alkyne group of **2** does not react during the polymerisation step in the formation of **poly-2** and **poly-2**/DNA. The expected bands due to the C \equiv C bond (2124 cm^{-1}), alkyne C–H (3308 cm^{-1}) and alkane C–H (2879 cm^{-1}) stretches are observed in the spectra of the monomer **2** (Fig. 2A) and **poly-2**/DNA hybrids (Fig. 2C), and correlate well with that of **poly-2** (see ESI†, Fig. S4). Therefore upon polymerisation, the alkynyl group of **2** remains intact within

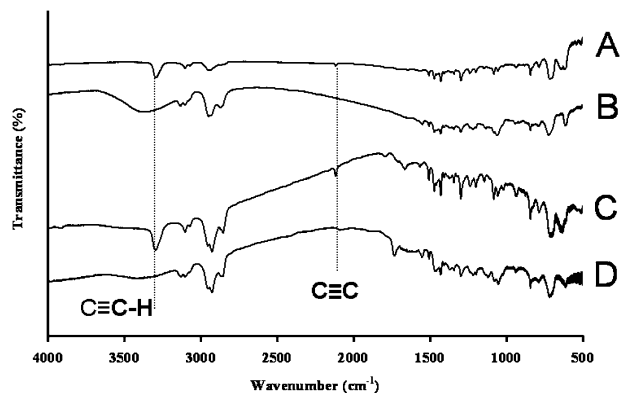


Fig. 2 FTIR spectra of (A) **2**, (B) **2** after click reaction with 3-azido propanol (C) **poly-2**/DNA and (D) **poly-2**/DNA after click reaction with 3-azido propanol.

the **poly-2**/DNA nanowires observed by AFM in Fig. 1A and is present for further reaction. To demonstrate that this alkynyl group is not buried in the polymeric material but can undergo functionalisation the copper catalysed azide–alkyne Huisgen cycloaddition reaction (“click”), was performed using 3-azido propan-1-ol.¹⁶

FTIR characterisation of the product of the click reaction of **2** with 3-azido propan-1-ol (Fig. 2B) was used as a basis for assessing the feasibility of performing the same reaction using **poly-2**/DNA hybrid nanowires. The standard click procedure involved the treatment of **2** or **poly-2**/DNA with a “click” solution of water/*tert*-butyl alcohol (2 : 1) containing sodium ascorbate, copper(II) sulfate and 3-azido propanol (details in ESI†). FTIR spectra of **poly-2**/DNA hybrid wires, before and after treatment showed that the alkynyl-hybrid material undergoes molecular modification (Fig. 2C and 2D). This is evident primarily through the disappearance of the C \equiv C (2124 cm^{-1}) and the alkyne C–H (3308 cm^{-1}) bands. In addition the terminal hydroxyl group of the propanol moiety appears in the spectra as a typically broad O–H stretching band at $3100\text{--}3600 \text{ cm}^{-1}$. The C=O stretching in the pyrimidine bases of DNA (1723 cm^{-1} and 1674 cm^{-1}) remain unaffected after the click reaction. These FTIR studies demonstrate that the “click” reaction can be successfully performed at alkynyl groups exposed along the **poly-2**/DNA nanowires.

Further demonstration that the nanowires could be functionalised was obtained by using the click reaction with 3-azido-1-*N*-dansylpropylamine (see ESI† for synthesis). Figure 1B shows a typical AFM image of a click-**poly-2**/DNA nanowire after treatment of **poly-2**/DNA with the azido-dansyl fluorophore under standard “click” conditions, indicating that the 1D wire-like structure remains intact. Fluorescence microscopy indicated the successful labelling of the wires with the dansyl derivative. Fluorescence micrographs of the silicon chip before modification were essentially dark (image is available in ESI†, Fig. S7) but after “click” modification with the dansyl azide the click-**poly-2**/DNA nanowires (Fig. 1D) were clearly visible under excitation at 365 nm. The functionalised nanowire shown (Fig. 1D) is approximately 17 μm in length, comparing well with the known length of λ -DNA.

Having confirmed that **poly-2**/DNA hybrids undergo modification *via* “click chemistry”, the electronic conductance

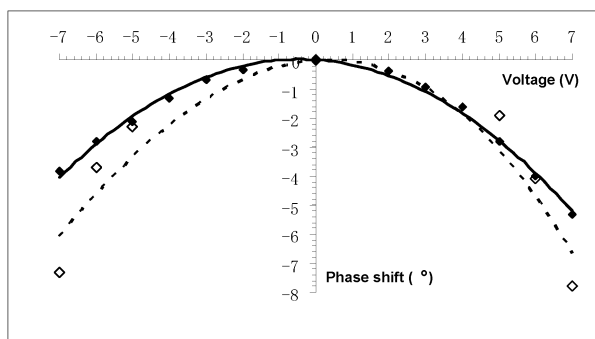


Fig. 3 Parabolic dependence of phase shift on bias for voltages between -7 and $+7$ V for **poly-2**/DNA hybrid nanowires before (solid points and line) and after click modification with dansyl azide (hollow points and dashed line).

of the nanowires was characterised by EFM phase imaging (“scanned conductance microscopy”). **Poly-2**/DNA nanowires were combed onto a silanised silicon oxide chip and then imaged *via* the same procedure as previously described.^{14,22} In EFM an extended conductive object shows a negative phase shift in relation to the background and appears as a darker region in the image (Fig. 1C). The EFM image of the **poly-2**/DNA nanowire shows the negative–positive–negative phase variation as the tip crosses the wire; this is typical of conducting polymers.²³ We observed a parabolic dependence of phase shift on bias for voltages between -7 and $+7$ V expected for a conductive nanowire, see Fig. 3. This observation, seen previously with polypyrrole/DNA hybrids confirms that the negative phase shift is due to the “scanned conductance effect” rather than trapped charge which produces phase shifts that depend linearly on bias voltage.²² The **poly-2**/ λ -DNA nanowires were immobilised on a silicon chip and then incubated for 16 hours with a “click” solution containing dansyl azide. AFM images of the click-**poly-2**/DNA nanowires, *i.e.* after reaction with the dansyl azide, again showed individual wires similar in height (5–40 nm) to polypyrrole/DNA hybrid materials previously reported.¹⁸

We conclude that the coupling reaction has no discernible detrimental effect on the 1D structure of the polymer/DNA hybrid material and so here have demonstrated the potential to incorporate new functionalities or sensing groups into a conductive nanowire *via* this method. In addition the click-**poly-2**/DNA hybrid nanowires were examined by EFM and the parabolic dependence of the negative phase was retained (see Fig. 3), confirming that the nanowires remain not only structurally intact but are also conductive after modification with the triazole-coupled fluorophore.

This work illustrates that **poly-2**/DNA nanowires are conductive and can be readily modified *via* “click chemistry”.

This methodology has potential for the development of conductive nanowires as sensing elements over a wide range of applications; the azido derivative of a receptor group is simply “clicked” onto the nanowire sensor/transducer. Conducting polymer nanowires bring the advantage of significantly enhanced sensitivity over an electrode/polymer-film system due to the massively increased surface/volume ratio. Therefore changes in the conductivity of the polymer/DNA nanowire hybrid system described here may hold potential for use in molecular electronics or even single molecule detection.

One, EPSRC, BBSRC, Marie Curie EU-FP7 and Newcastle University are thanked for funding.

Notes and references

- 1 *Self-Assembled Nanostructures*, ed. J. Zhang, Z. L. Wang, J. Liu, S. Chen and G. Y. Liu, Kluwer Academic Publishers, 2002.
- 2 J. Kim, Y. Piao and T. Heon, *Chem. Soc. Rev.*, 2009, **38**, 372–390.
- 3 M. S. Hu, H. L. Chen, C. H. Shen, L. S. Hong, B. R. Huang, K. H. Chen and L. C. Chen, *Nat. Mater.*, 2006, **5**, 102–106.
- 4 C. H. Hsieh, L. J. Chou, G. R. Lin, Y. Bando and D. Golberg, *Nano Lett.*, 2008, **8**, 3081–3085.
- 5 Y. S. Zhao, A. Peng, H. Fu, Y. Ma and J. Yao, *Adv. Mater.*, 2008, **20**, 1661–1665.
- 6 D. O’Carroll, I. Lieberwirth and G. Redmond, *Nat. Nanotechnol.*, 2007, **2**, 180–184.
- 7 Z. L. Wang, *Adv. Mater.*, 2003, **15**, 432–436.
- 8 Q. Gu, C. Cheng, R. Gonela, S. Suryanarayanan, S. Anagathula, K. Dai and D. T. Haynie, *Nanotechnology*, 2006, **17**, R14–R25.
- 9 A. Houlton, A. R. Pike, M. Galindo and B. R. Horrocks, *Chem. Commun.*, 2009, 1797–1806.
- 10 J. Richter, *Physica E (Amsterdam)*, 2003, **16**, 157–173.
- 11 K. Keren, R. S. Berman, E. Buchstab, U. Silvan and E. Braun, *Science*, 2003, **302**, 1380–1382.
- 12 E. Braun, Y. Eichen, U. Sivan and B. Ben-Yoseph, *Nature*, 1998, **391**, 775–778.
- 13 A. R. Pike, A. Houlton and B. R. Horrocks, *UK Pat.* 0918396.3, 2009.
- 14 S. A. Farha Al-Said, R. Hassanien, J. Hannant, M. A. Galindo, S. Pruneanu, A. R. Pike, A. Houlton and B. R. Horrocks, *Electrochem. Commun.*, 2009, **11**, 550–553.
- 15 Single duplexes of λ -DNA were used in probe microscopy investigations of the hybrid nanowires. FTIR studies were performed using calf thymus DNA as the template material.
- 16 V. V. Rostovtsev, L. G. Green, V. V. Fokin and K. B. Sharpless, *Angew. Chem., Int. Ed.*, 2002, **41**, 2596–2599.
- 17 M. Vautrin, P. Leriche, A. Gorgues and M. P. Cava, *Electrochem. Commun.*, 1999, **1**, 233–237.
- 18 L. Dong, T. Hollis, B. A. Connolly, N. G. Wright, B. R. Horrocks and A. Houlton, *Adv. Mater.*, 2007, **19**, 1748–1751.
- 19 L. Dong, T. Hollis, S. Fishwick, B. A. Connolly, N. G. Wright, B. R. Horrocks and A. Houlton, *Chem.–Eur. J.*, 2007, **13**, 822–828.
- 20 T. Theophanides, *Appl. Spectrosc.*, 1981, **35**, 461–465.
- 21 H. Fritzsche and C. Zimmer, *Eur. J. Biochem.*, 1968, **5**, 42–44.
- 22 S. Pruneanu, S. A. Farha Al-Said, L. Dong, T. Hollis, M. A. Galindo, N. G. Wright, A. Houlton and B. R. Horrocks, *Adv. Funct. Mater.*, 2008, **18**, 2444–2454.
- 23 Y. Zhou, M. Freitag, J. Hone, C. Staii, A. T. Johnson, N. J. Pinto and A. G. MacDiarmid, *Appl. Phys. Lett.*, 2003, **83**, 3800–3802.

Synthesis, characterization and electrical properties of supramolecular DNA-templated polymer nanowires of 2,5-(di-2-thienyl)-pyrrole

S. M. D. Watson,^[a] J. H. Hedley,^[a] M. A. Galindo,^[a] S. A. F. Al-Said,^[a] N. G. Wright,^[b] B. A. Connolly,^[c] B. R. Horrocks,^[a] A. Houlton*^[a]

Abstract: Supramolecular polymer nanowires have been prepared using DNA-templating of 2,5-(di-2-thienyl)-pyrrole (TPT) by oxidation with FeCl₃ in a mixed aqueous/organic solvent system. Despite the reduced capacity for strong hydrogen bonding in poly(TPT) compared to other systems, such as polypyrrole, the templating proceeds well. FTIR spectroscopic studies confirm that the resulting material is not a simple mixture and that the two types of polymer interact. This is indicated by shifts in bands associated with both the phosphodiester

backbone and the nucleobases. XPS studies further confirm the presence of DNA and TPT, as well as dopant Cl⁻ ions. Molecular dynamics simulations on a $[\{dA_{24}:dT_{24}\}/\{TPT\}_4]$ model support these findings and indicate a non co-planar conformation for oligo-TPT over much of the trajectory. AFM studies show the resulting nanowires typically lie in the 6-8 nm diameter range and exhibit a smooth, continuous, morphology. Studies on the electrical properties of the prepared nanowires, using a combination of scanned conductance microscopy, conductive

AFM and variable temperature two-terminal I-V measurements show, that in contrast to similar DNA/polymer systems, the conductivity is markedly reduced compared to bulk material. The temperature dependence of the conductivity shows a simple Arrhenius behaviour consistent with the hopping models developed for redox polymers.

Keywords: DNA · supramolecular polymer · nanowire · conducting polymer · templating

Introduction

Organic conducting polymers (CPs) have attracted much interest over the past 40 years due to their unique behaviour; exhibiting electronic and optical properties akin to metals and semiconductors, whilst maintaining the mechanical qualities, and ease of functionalisation, associated with organic materials.^{[1] [2] [3] [4] [5]} Efforts to exploit CPs include the development of new generations

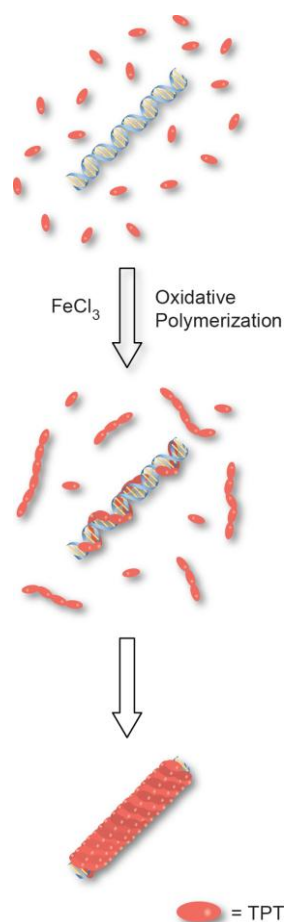
of solar cells,^{[6] [7] [8]} rechargeable batteries,^[9] electrochromic devices,^[10] transistors,^{[11] [12]} capacitors^[13] and bio/chemical sensors.^{[14] [15]} With the current drive towards small-scale technologies, recent years has seen a growing emphasis placed upon the fabrication of such materials with nanoscale dimensions. In particular, attention has focussed on devising methods for producing highly anisotropic forms such as nanowires, nanoropes, and nanotubes.^{[16] [17] [18] [19] [20]} Nanowires are of interest as they represent the smallest structure for effective electrical charge transport, and are promising for use in nanoscale electronics.

Template-directed growth is the most frequently used approach for preparing such 1D nanostructures, and several different methods have been shown to be effective. These include the use of an external, porous, templates like anodically etched aluminium oxide (AAO)^{[21] [22] [23]} or mesoporous silica,^{[24] [25] [26]} as well as “soft” templates such as surfactants which self-assembled in solution to provide the appropriately structured reaction space.^{[27] [28] [29] [30]}

[a] Dr. S.M.D. Watson, J. H. Hedley, Dr. M. A. Galindo, Dr. S. A. F. Al-Said, Dr. B. R. Horrocks, Prof. A. Houlton*
Chemical Nanoscience Labs, School of Chemistry
Newcastle University
Newcastle, U.K. NE1 7RU
Fax: (+) 44 191 222 6929
E-mail: andrew.houlton@ncl.ac.uk

[b] Prof. N. G. Wright
School of Electrical, Electronic and Computer Engineering
Newcastle University
Newcastle, U.K. NE1 7RU

[c] Prof. B. A. Connolly
Institute of Cell and Molecular Bioscience
Newcastle University
Newcastle, U.K. NE1 7RU



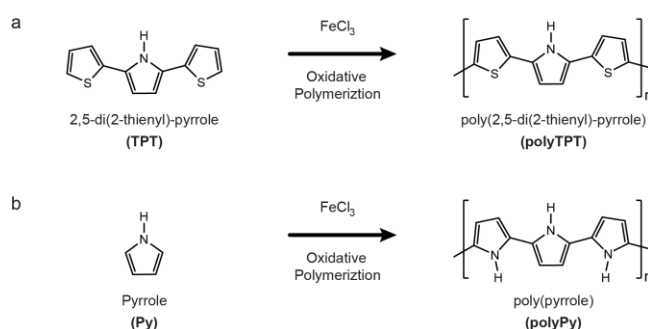
Scheme 1. Scheme highlighting the templating by the DNA molecules in directing the growth of polyTPT towards 1D structures. Oxidatively induced polymerisation of TPT forms cationic oligo(TPT) which bind to DNA molecules through supramolecular interactions. Further growth produces the final hybrid DNA/polymer nanowire.

An alternative approach is the use of naturally occurring biopolymers, such as duplex DNA, as a template (Scheme 1).^{[31] [32] [33] [17] [34] [35] [36]} For DNA, the duplex structure is just 2nm wide but is available over microns lengths and has a large persistence length, making it highly suited for 1D material growth.^[20] The ability of DNA to act as a template for CPs principally arises from the complementarity of the DNA duplex and the growing CP chains. DNA contains a high anionic charge, due to the phosphodiester backbone, a wealth of hydrogen bonding sites and numerous van der Waals surfaces in the grooves of the duplex. The general class of CPs derived from aromatic heterocyclic systems, such as pyrrole, indole *etc.* are formed in their conducting cationically charged form through oxidative polymerization and also tend to have a significant capacity for hydrogen bonding. Hence electrostatic attraction between the growing cationic CP and the anionic DNA template, allied with additional non-covalent interactions, provide an effective means by which the CP growth is affected. In contrast to templating in porous media *etc.* this approach yields *supramolecular polymers*, comprising both the template and the conducting strands, which are a relatively new class of materials.^{[37] [38] [39] [40]}

Previous reports demonstrate the formation of such supramolecular DNA/polymer nanowires for aniline,^{[31] [32]} pyrrole,^{[33] [17]} and indole,^[36] for example. In an effort to further explore the scope of this method we have investigated the DNA-templating of 2,5-(di-2-thienyl)-pyrrole (TPT). This compound has a quite different hydrogen bonding capacity compared to previously prepared materials and is also not water soluble therefore requiring changes to the solvent system. Here we report our findings.

Results and Discussion

DNA-templating reaction. As can be seen from Scheme 2, despite the similarity in structure, both the number and strength of potential hydrogen bonding interactions formed between DNA and poly(TPT) is reduced compared to poly(Py); two-thirds of the strong hydrogen-bond donor sites (NH) are replaced by relatively weak acceptor sites (-S-). This could be expected to have a detrimental effect on DNA-templating and that poly(TPT) is a less well-suited material for nanowire formation by this method.



Scheme 2. Oxidative polymerisation of (a) 2,5-(bis(di-2-thienyl)-pyrrole (TPT) and (b) pyrrole with FeCl_3 forms the corresponding conducting polymer. These have quite different hydrogen bonding capabilities with poly(TPT) having 1/3 of the strong H-bond donor sites as polyPy and a capacity for self-association through NH...S interactions.

The attempted preparation of DNA/polyTPT nanowires was broadly similar to those previously reported for similar systems (Scheme 1).^{[33] [17] [36]} However, as the monomer for polyTPT, 2,5-(di-2-thienyl)-pyrrole, is not water soluble modification of the procedure is required whereby the reaction medium is a solvent mixture ($\text{H}_2\text{O}:\text{MeCN}$) rather than pure water. The source of the DNA was either calf thymus (CT), used for experiments requiring larger quantities of material, *e.g.* FTIR spectroscopy or λ -DNA which, at *ca.* 16 μm long, is of sufficient length to facilitate single molecule measurements and fabrication of electrical devices. The TPT unit was introduced into the aqueous DNA-containing solution as a solution in acetonitrile giving a 6:1 $\text{H}_2\text{O}:\text{MeCN}$ final ratio. The polymerisation was induced by oxidation using an aqueous solution of FeCl_3 . The reaction was allowed to proceed for 24 hours.

Fourier Transform Infrared Spectroscopy.

FTIR spectra of the isolated DNA/polyTPT material reveals evidence of the formation of a supramolecular hybrid polymer containing both DNA and polyTPT (Fig. 1). The presence of the polyTPT in the material is evident from the N-H stretch at 3432cm^{-1} , attributed to the pyrrolyl ring of the TPT units.^[41] The position of this band is observed to be shifted relative to the corresponding N-H stretch in the spectrum of TPT (3429cm^{-1}), suggesting that hydrogen bonding with the acceptor groups on the DNA, e.g. phosphate groups or nitrogen or oxygen atoms of the nucleobases, is taking place. The broad band centred at *ca.* 3300cm^{-1} in DNA due to O-H stretching vibrations from groove-bound water molecules, as well as a contribution from N-H stretches in the DNA nucleobases, is also noted to be reduced in intensity in the DNA/polyTPT spectrum. This loss of intensity is proposed to be the result of displacement of water molecules which were bound to the DNA. Bands observed in the $900\text{--}1800\text{cm}^{-1}$ region of the spectrum further confirm the presence of DNA in the hybrid material. These features can be assigned to nucleobase vibrations, as well as stretches associated with the phosphate backbone.^{[42] [43] [44]} Several small shifts in the peak positions can be identified in this region of the DNA/polyTPT spectrum when compared to the corresponding bands in the spectrum of free DNA (see Supporting Information). The vibrational modes associated with the PO_2^- symmetric stretching (*ca.* 1102cm^{-1}) and C-O deoxyribose stretching (1060cm^{-1}) for example, show a change in intensity relative to one another when comparing the DNA and DNA/polyTPT spectra, whilst the PO_2^- asymmetric stretching vibration (1241cm^{-1}) is found to be shifted to lower frequency in the hybrid material (1233cm^{-1}). In addition, C-N stretches of the cytosine and guanine bases (1365cm^{-1}), along with the a cytosine or guanine ring vibration (1487cm^{-1}), are also shifted to lower frequency (1357cm^{-1} and 1474cm^{-1} , respectively). Similarly, changes in other spectral bands assigned to stretches and vibrations in the TPT units are also observed, with the peak at 1411cm^{-1} in the DNA/polyTPT spectrum, attributed to the C-N and C=C stretches of the pyrrolyl unit,^[41] showing a slight shift to higher frequency when compared to the corresponding band in the spectrum of polyTPT. In summary, these data provide strong evidence that the hybrid material is not a simple mixture of DNA and polyTPT, but instead *the materials is a supramolecular polymer are intimate interactions between the two strand types.*

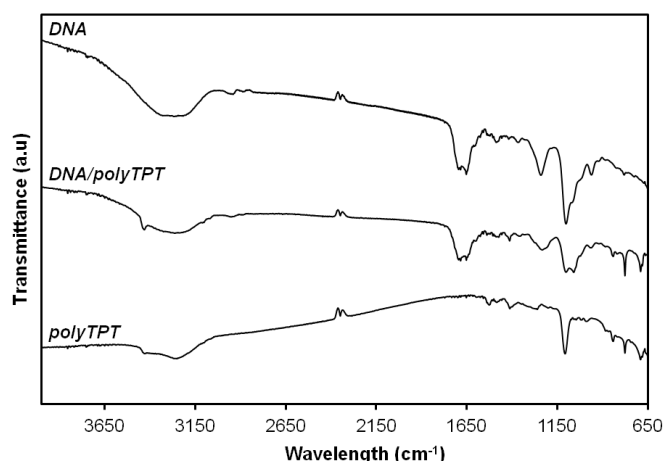


Figure 1. FTIR spectrum of DNA/polyTPT hybrid polymer along with spectra of control samples of DNA, and polyTPT.

X-Ray Photoelectron Spectroscopy.

Further chemical characterization of DNA/polyTPT was provided by XPS which confirmed the presence of C (C1s), O (O1s), N (N1s), S(2p), P(2p), and Cl (Cl2p) in the sample, Fig 2a. Observation of the N1s peak provided evidence of the presence of DNA and polyTPT in the sample material. Curve fitting of high resolution XPS spectra of the N1s region revealed two distinct peaks in the N1s envelope with binding energies at 399.5eV and 401.4eV , respectively (Fig. 2b). Contributions to both of these peaks can be assigned to the presence of the DNA and polyTPT. Previous XPS studies of both free DNA^{[45] [46] [47]} and polyPy^{[48] [49] [50]} have reported that spectra of the N1s core level of these materials can be fitted to at least two separate components. The N1s core level of DNA for example has been reported to comprise of a lower binding energy peak ($398.6\text{--}399.0\text{eV}$) arising from the contributions of sp^2 -bonded N atoms in the nucleobase base rings, and a higher binding energy peak ($400.1\text{--}401.4\text{eV}$) attributed to the sp^3 -bonded N atoms in the nucleobase rings and $-\text{NH}_2$ groups.^{[45] [46] [47]} Similarly, polyPy is also known to give at least two distinguishable peaks of the N1s core level.^{[48] [49] [50]} Here, a lower binding energy peak ($399.5\text{--}399.9\text{eV}$) tends to dominate, arising from the N-H groups present in the constituent pyrrolyl rings of the polymer. The higher binding energy species ($400.6\text{--}402.3\text{eV}$) arise from the presence of inequivalent nitrogen atoms in the polyPy structure which occur as a result of their electrostatic interaction with the dopant anions present in the polymer structure.

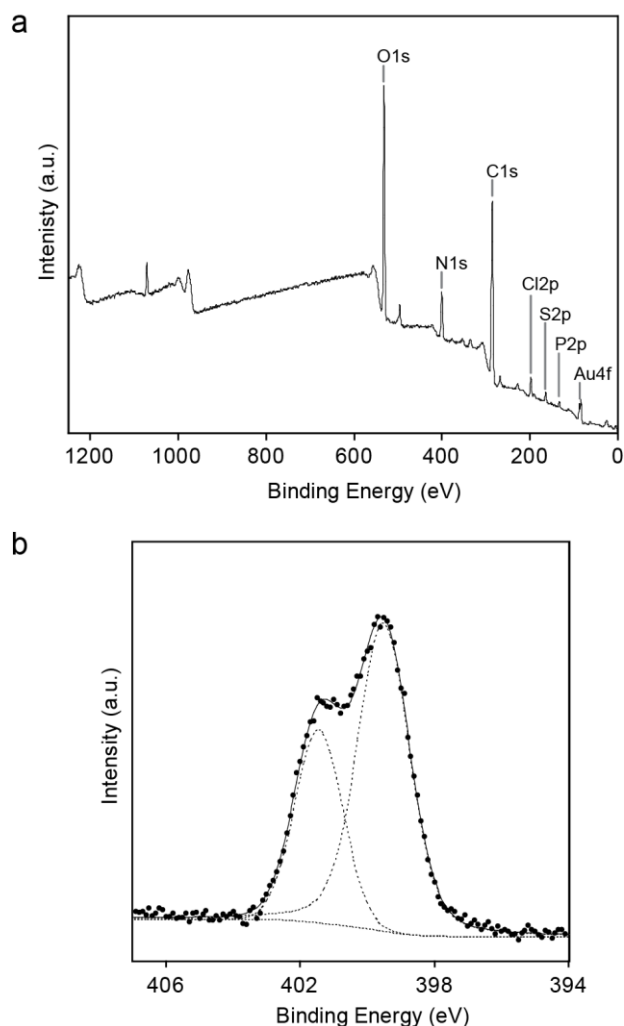


Figure 2 XPS spectra recorded from a sample of DNA/polyTPT nanowire structures deposited upon a gold substrate: (a) XPS survey scan spectrum, (b) High resolution XPS spectrum of N1s region, with curve fitting of the N1s envelope.

Clear evidence for the presence of DNA in the sample material is obtained from the P2p signal at 133.2eV, arising from the phosphorus in the phosphodiester backbone in the DNA. The presence of polyTPT is also confirmed by the observed S2p band, with the S2p_{3/2} peak centred at 163.8eV, consistent with the thiophene sulphur.^[51] The Cl2p peak in the survey spectrum reveals the presence of the Cl in the sample, suggesting that the anionic charge of the DNA is not sufficient to compensate the cationic charge of the bound polyTPT, and that Cl⁻ anions are also present as dopants in the material.

Scanning probe microscopy studies

Atomic force microscopy (AFM) was used to probe the size and morphology of the DNA/polyTPT structures. These were immobilised on trimethylsilane-modified (TMS) Si/SiO₂ substrates using molecular combing techniques.^{[52] [53] [33]} Samples isolated after 24 hours reaction revealed individual DNA/polyTPT

nanowires which have a regular appearance with complete coverage of the DNA template molecules by the polymer (Fig 3a). The uniformity of the polymeric coatings on single nanowires was quantified by calculating the standard deviation of the mean nanowire diameters. This was found to consistently fall within a range of *ca.* 0.5–1.3nm. As noted previously for other conducting polymers templated at DNA,^{[33] [17] [36]} the resulting structures have remarkably smooth, regular morphologies. This is in contrast to typical metal-based structures.^{[54] [55] [34]}

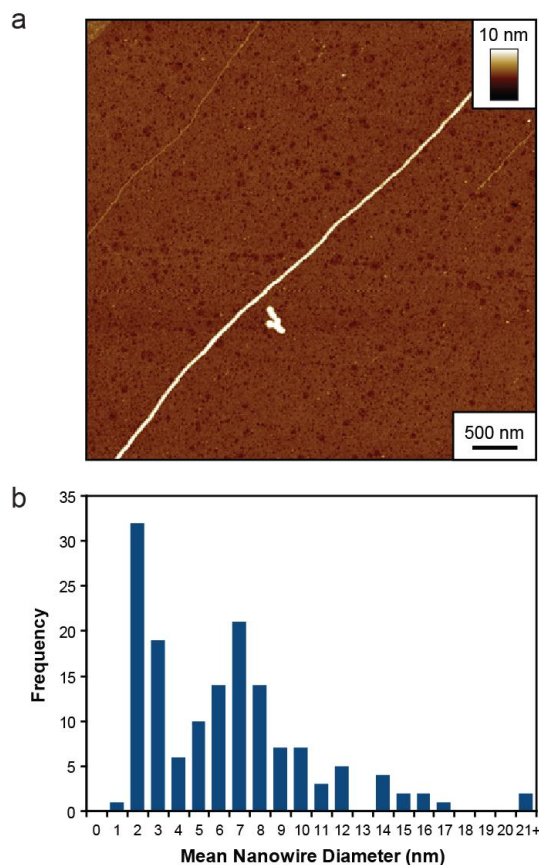


Figure 3. (a) Tapping mode AFM image of a DNA/polyTPT nanowire immobilised upon a Si/SiO₂ substrate modified with a TMS SAM. (b) Histogram showing the distribution of the mean DNA/polyTPT nanowire diameters for 150 nanowire structures. Mean diameter of structures were determined from AFM data.

Statistical treatment carried out on 150 DNA/polyTPT nanowires reveals the distribution of the mean diameters, with a modal diameter of 7.0–8.0nm, (Fig 3b). A small number of larger structures were also observed, with diameters *ca.* 17nm and even larger in a few instances. These structures are attributed to the “bundling” of DNA/polyTPT structures into larger ropelike assemblies formed in the solution, as previously described for DNA/polyPy (see Supporting Information).^[17] It is also apparent from inspection of the histogram (Fig. 3b) that not all the DNA in the reaction is involved in templating. This is evident from the large

peak value observed at 2.0–3.0nm, which represents some bare DNA present for the entire reaction.

MD simulations

In an effort to gain further insight into the details of the supramolecular interactions between the two polymer types a molecular dynamics (MD) calculation was performed. We simulated the interaction of a tetramer of TPT with a typical doping level of one charge per three aromatic rings, $[\{TPT\}_4]^{4+}$, with a $(dA)_{24}$ - $(dT)_{24}$ oligonucleotide duplex in aqueous solution for 100 picoseconds. Sodium cations were included to exactly balance the charge of the complex. Analysis of the results reveals the close association of the duplex and $\{TPT\}$ oligomer over the whole trajectory. The $\{TPT\}_4$ remains located in the major groove of the duplex and many molecular contacts (2.5-3.5Å) are evident between the two. At points in the trajectory the $\{TPT\}_4$ can be seen to interact with both the upper and lower edges of the groove simultaneously, as shown in Fig. 4a. Despite the four pyrrolyl NH sites with the capacity for strong hydrogen bonding with acceptor sites on the DNA, few are observed. The strongest of these is formed by a pyrrolyl unit in a more terminal position (second 5-membered ring in the $[\{TPT\}_4]$ oligomer) as either $NH_{Pyr} \dots N6H_{2adenine}$ or $NH_{Pyr} \dots O4_{thymine}$ interactions. Rather weaker interactions are also noted between the central pyrrolyl unit and the N7 position of adenine groups. Overall, however, such $NH_{TPT} \dots Acceptor_{DNA}$ interactions do not appear to be dominant and structures with multiple such interactions are rare. A range of close contacts are evident between less polar sites on the $\{TPT\}_4$ oligomer and sites on the DNA that are largely maintained or shift between comparable sites throughout the simulation. Details are provided in the Supporting Information. These findings are consistent with the FTIR data, indicating the intimate interaction of the oligo-TPT primarily with the phosphate backbone and the bases of the DNA. A final point of interest is the fact that the $\{TPT\}_4$ molecule does not adopt a co-planar conformation over much of the trajectory (Figure 4b). Such a conformation is not optimal for effective charge transport.

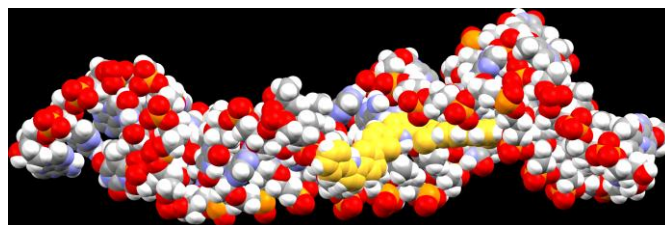
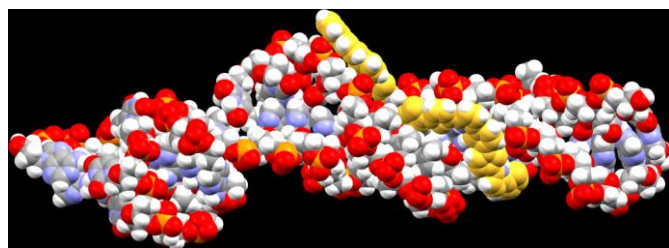


Figure 4. Selected structures from the 100 ps MD simulation of a 24-mer poly(dA)-poly(dT) duplex DNA with $[\{TPT\}_4]^{4+}$ (shown in yellow for clarity). (Top) Structure highlighting the interaction of the $\{TPT\}_4$ strand with both the upper and lower edges of the major groove of the duplex. (Bottom) Structure highlighting the lack of co-planarity of the $\{TPT\}_4$ as is observed over much of the trajectory. Atom colour code on DNA: O = red; P = orange; C = grey; H = white; N = purple; atom colour code on $\{TPT\}$ C = yellow; S = yellow; N = purple; H = white.

It is worth pointing out however that this model, with a 1:1 DNA: $\{\text{poly(TPT)}\}_n$ ratio, contains many fewer polyTPT strands than the prepared nanowires. An estimate of the number of poly(TPT) strands contained in an ~ 8 nm diameter structure can be made by assuming that the nanowire is cylindrical with a 2nm DNA duplex core. Filling the remainder of the cylinder volume with poly(TPT) as linear chains gives an estimate of *ca.* 240 strands. Incidentally, this is very many more strands than is required to charge balance the DNA which, based on a typical oxidation level of +1 per $\{TPT\}$ unit, requires only *ca.* 6 strands. Incorporation of additional anions, *e.g.* Cl^- , would then be expected, so as to balance the cationic charge; this is consistent with the XPS data.

DNA/polyTPT nanowire electrical properties

Initial, qualitative evaluation of the electronic properties of individual DNA/polyTPT nanowires was carried out using scanned conductance microscopy (SCM). This scanning probe microscopy (SPM) technique provides a convenient and rapid non-contact means of establishing the electrical behaviour of such 1D structures. In brief, samples are probed through monitoring changes in the phase angle of a vibrating AFM probe as it is scanned at a fixed height above the sample, whilst a direct current (dc) potential bias is simultaneously applied to it (Fig. 5a). The sign (+/-) of the resulting phase shifts associated with the nanostructures (relative to the substrate background) are known to be highly dependent upon the intrinsic electronic properties of the nanostructures themselves.^[56] Specifically, it has been shown that negative phase shifts can only be observed to be associated with such 1D structures if they are electrically conducting. Both the technical aspects and theory behind this SPM technique have previously been discussed at great length, and can be found in several earlier publications.^{[56] [57] [58] [17]}

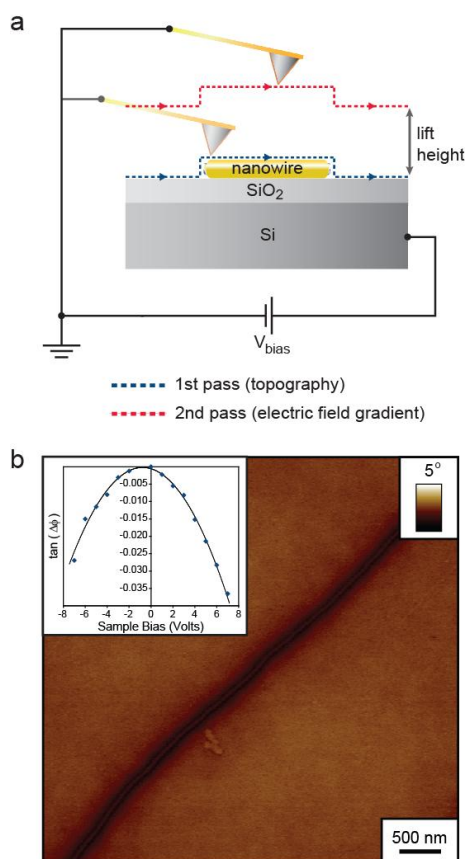
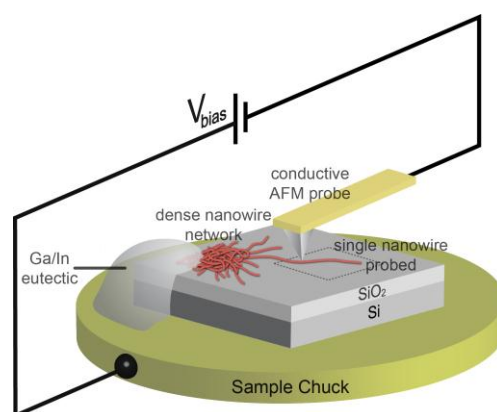


Fig 5. (a) Schematic representation outlining the principles of SCM operation, used to evaluate the electronic properties of one-dimensional nanostructures. (b) SCM phase image of a DNA/polyTPT nanowire supported upon a Si/200 nm SiO₂ substrate, modified with a TMS SAM. The dark line running diagonally across the image represents the negative phase shift which correlates to the position of the nanowire on the substrate surface. The inset shows a plot of the magnitude phase shifts as a function of the dc bias applied to the substrate during data acquisition.

SCM phase images of DNA/polyTPT nanowires supported on Si/200nm SiO₂ substrates show negative phase shifts consistent with the predicted observations for conductive objects (Fig. 5b). The magnitude of the phase shift associated with the DNA/polyTPT structures is found to be approximately proportional to the square of the applied bias (*i.e.* $\phi \propto V^2$), as is expected when the interaction of the conducting AFM probe with the electric field gradient above the sample is dominated by capacitance effects. This behaviour is clearly illustrated by the parabolic relationship shown when plotting the (tangent) phase shift against the dc bias applied to the substrate, (Fig. 5b, inset).

Conductive AFM (cAFM) was used to further probe the electrical properties of the DNA/polyTPT nanowires. For this, an experimental set-up we previously devised^[36] was used which allows for the required electrical contacts for probing an individual nanowire to be made in a relatively straightforward manner. Briefly,

this method involves applying a small volume of solution containing the nanowires onto the substrate support, to cover a region of *ca.* 5mm in diameter (Scheme 3). Subsequent evaporation of the solvent generally leaves a dense network of nanowires on the substrate, at the periphery of which individual nanowires can be found to extend out. The dense nanowire network can effectively be used as a macroscopic electrical contact to the nanowire under study. Electrical contact of the network to the metallic sample chuck can be made using a drop of Ga/In eutectic. The second electrical contact to the nanowire is made using the conductive metal-coated AFM probe itself.



Scheme 3 Experimental set-up for cAFM measurements carried out upon DNA/polyTPT nanowires. Measurements are recorded upon individual nanowires located at the periphery of a dense network of the nanowires deposited upon the substrate support.

Using this type of set-up, cAFM was performed to record the sample topography at the periphery of the dense nanowire network where individual DNA/polyTPT nanowires could be located. Whilst collecting the topographical data, detection of electrical currents passing through the sample was simultaneously carried out as a dc bias was applied to the sample. Fig. 6 shows an example of a contact mode AFM height image of a DNA/polyTPT nanowire, *ca.* 40nm in diameter, and the corresponding cAFM current image simultaneously recorded with a dc bias of +5V applied to the sample. It should be noted that the 40nm diameter of the DNA/polyTPT nanowire is significantly larger than the 7.0-8.0 nm modal size range revealed by the statistical study discussed previously. This is most likely due to the dense volume of material deposited on the substrate, leading to increased ropelike assemblies of nanowires.^[17] The bright contrast in the current image, which corresponds to the position of the nanowire on the substrate, indicates an electrical current in the order of nanoamps passing through the nanowire, thus confirming

its electrical conductivity. However, further studies of DNA/polyTPT nanowires of various sizes revealed that 40nm diameter represented the approximate lower limit of structure size from which electrical currents could be detected by the cAFM equipment. Though this findings appears to contradict the SCM studies, in which smaller nanowires (<10nm diameter) were shown to be electrically conductive, this simply highlights the extreme sensitivity of the SCM technique. SCM has been shown to allow for 1D structures (>400nm in length) with conductivities down to *ca.* 10^{-16}Scm^{-1} to be identified as conducting/semi-conducting materials,^[56] which far exceeds the sensitivity limits (nA) of the cAFM equipment.

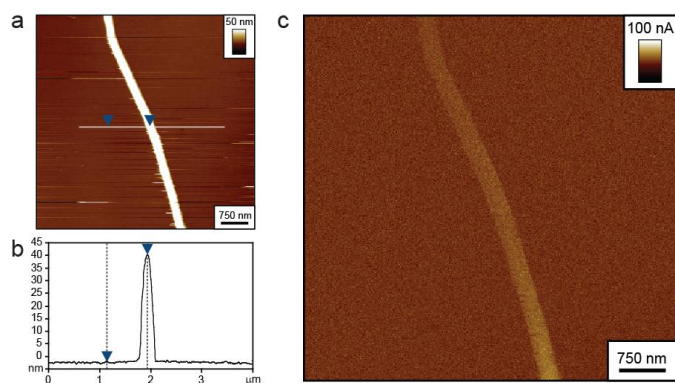


Fig 6. (a) Contact mode AFM height image of DNA/polyTPT nanowire. (b) Corresponding cross-section, showing nanowire height (*ca.* 40nm). (c) Corresponding cAFM current image of nanowire, acquired at a dc bias of +5V.

Quantitative information about the electrical behaviour of individual DNA/polyTPT nanowire structures was also gathered through fabrication of a bespoke two-terminal device. This device was constructed using Au electrode pairs, microfabricated using photolithography, embedded in a thermally grown insulating SiO₂ layer, on a silicon substrate. The Au electrodes were typically separated by a gap of 2–8μm, across which a DNA/polyTPT nanowire was aligned by molecular combing,^{[52] [53]} Fig. 7 shows a TappingMode™ mode AFM height image of the actual DNA/polyTPT nanowire device with a single nanowire, height 25nm, aligned across a ~2.5μm electrode gap.

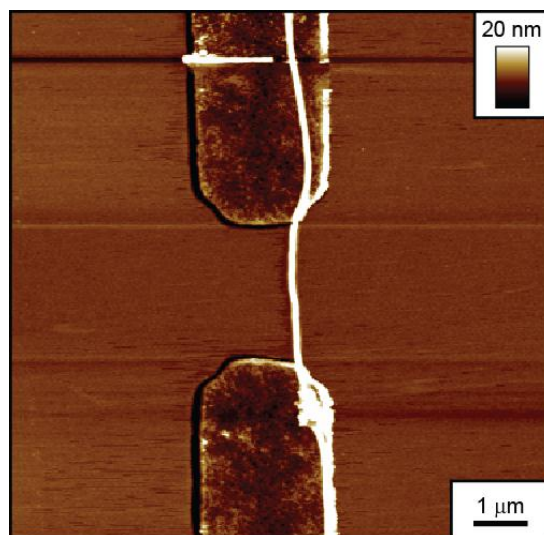


Fig. 7 (a) TappingMode™ AFM image of DNA/polyTPT nanowire aligned across a 2.5μm gap between two Au microelectrodes. The Au electrodes are embedded in a thermally grown, 200nm thick insulating SiO₂ layer on a Si substrate.

The resistance of the nanowire, determined from i-V measurements was found to be in the order of $10^{14}\Omega$. By evaluating the dimensions of the nanowire (see Supporting Information), a conductivity value was calculated to be $1.9 \times 10^{-7}\text{S cm}^{-1}$ at 303K. For comparison, we determined the conductivity of a bulk sample of polyTPT as lying in the range $1.0 \times 10^{-2} - 2.3 \times 10^{-2}\text{S cm}^{-1}$; an increase by several orders of magnitude compared to the nanowire.

Variable-temperature i-V studies over a temperature range of 293K–373K of the two-terminal nanowire device were also performed in order to elucidate details of the conduction mechanism. The conductivity of conjugated polymers is usually described by hopping models; the charge carriers are considered to be substantially localized and make thermally-assisted tunneling transitions, or hops, between sites. In general, several hops may be possible from a given site which differ with respect to the energy barrier or hopping distance. This situation is called variable range hopping because the thermal average over the different hops leads to a hopping range that is temperature-dependent. The typical functional form of the conductance-temperature relation is a stretched exponential:

$$G = G_0 \exp \left[- \left(\frac{T_0}{T} \right)^\beta \right] \quad (1)$$

where the exponent β depends on the dimensionality of the system. Other hopping models lead to similar stretched exponential forms,

e.g., the Efros-Shklovskii model^[59] which describes disordered materials with strong coulomb interactions. Experimental data on conjugated polymers typically shows behavior consistent with $\beta = 1/4$ for bulk samples^{[50] [60]} and, for thin films, $\beta = 1/2$ at low temperatures and $\beta = 1$ at high temperatures.^[61]

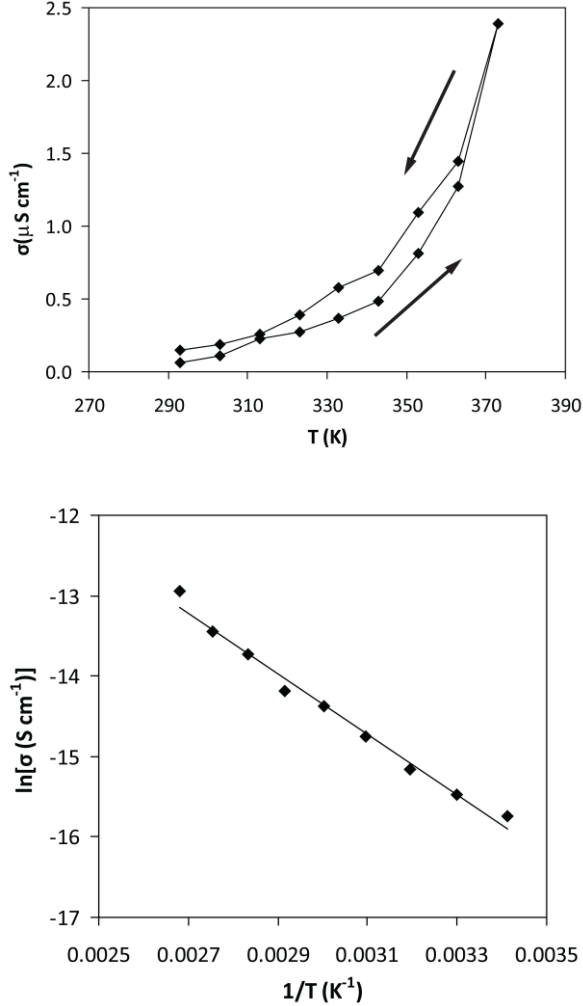


Fig. 8 (a) Variable temperature i-V measurements carried out upon a DNA/polyTPT nanowire aligned across two Au electrodes. (b) Arrhenius plot for the conductivity of a DNA/polyTPT nanowire.

The temperature dependence of the nanowire conductivity is shown in Fig. 8a with the conductivity values calculated from the gradient of the i-V plots around zero bias. The nanowire conductivity increases with increasing temperature. A small degree of hysteresis is also evident between the heating and cooling phases of the cycle, possibly due to the loss of residual water bound to the polymer during the heating of the sample. Figure 8b shows an Arrhenius plot of the conductance of DNA/polyTPT nanowires. The nanowires show a simple Arrhenius behavior, *i.e.*, $\beta \sim 1$ over a temperature range 293-373K. Such behavior has also been reported by us in

polyindole nanowires.^[36] The natural interpretation is that the hopping process in the nanowires is best described by a simple nearest-neighbour hopping model. This is consistent with hopping transport in one dimension where a given charge has only one possible hop. The activation energy for the hopping process obtained from the Arrhenius plot of Fig. 8b is $31.2 \pm 1.4 \text{ kJ mol}^{-1}$ which is similar to that for nanowires prepared from polyindole ($33.5 \pm 0.2 \text{ kJ mol}^{-1}$).^[36]

Figure 9 shows a typical current-voltage curve for the DNA/polyTPT device in Figure 7; the conductance discussed above was determined from the slope of the linear region around zero bias. The current-voltage curve shows significant non-linearity at large bias voltages. In principle, the metal/polymer nanowire/metal system can behave in a similar manner to a metal/semiconductor/metal system, although the nature of the charge transport in conductive polymers is very different compared to crystalline semiconductors. A metal/semiconductor junction typically has the IV characteristic of a diode:

$$I = J_0 \left[\exp\left(-\frac{eV}{k_b T}\right) - 1 \right] \quad (2)$$

where I is the current flowing through the system and V is the applied potential. In our metal/polymer/metal system, one of the contacts would always be reverse-biased and ought to limit the current at sufficiently high potentials, resulting in a sigmoidal IV characteristic. Field-induced breakdown can give rise to positive curvature in the i-V characteristics at large positive potentials, but this would only be consistent with a system in which the resistance along the length of the polymer does not dominate the contact (interfacial barrier) resistance.

Another way to view the metal/polymer nanowire/metal system is to consider the charge transport process in the same framework as that proposed for thin films of redox polymers.^{[62] [63] [64] [65] [66]} Redox polymers behave very differently to inorganic semiconductors because the 'doping level' is typically so high that one must account for the chemical potential of both occupied and unoccupied sites and therefore the transport is not described by the usual Nernst Planck equation.^{[62] [63]} The countercharge (anions in the case of a polycationic polymer) may also be mobile and their transport is coupled to that of the electrons. If the anions are mobile on the timescale of the experiment, they will collect near the positive

terminal and most of the applied potential will be dropped across the space charge layers at each electrode/polymer interface. In this case a sigmoidal i-V characteristic is obtained with a linear region around zero bias whose conductance is proportional to the electron self-exchange rate constant and the product of the occupied and unoccupied site densities.^[64] If the anions are immobile on the experimental timescale (typically the case for dry polymer films at low temperature), then the i-V characteristic shows positive curvature at high positive potentials. This case is typically described by an equation of the form:

$$I = \frac{n_p n F A \delta k_{ex}}{2D} \left[\exp\left(-\rho \alpha \frac{\delta eV}{L k_B T}\right) - \exp\left(-\rho(1-\alpha) \frac{\delta eV}{L k_B T}\right) \right] \quad (3)$$

where n and n_p are the densities of sites that are respectively empty or occupied by positive charges, δ is the site-site hopping distance, L is the length of the nanowire and k_{ex} is the electron self-exchange rate constant for site-site hopping at zero bias. D is the dimensionality of the system, α is a symmetry factor (about 0.5 in Marcus theory) and ρ is a non-ideality factor whose significance is explained below. F is the Faraday constant and A is the area of the cross-section of the wire.

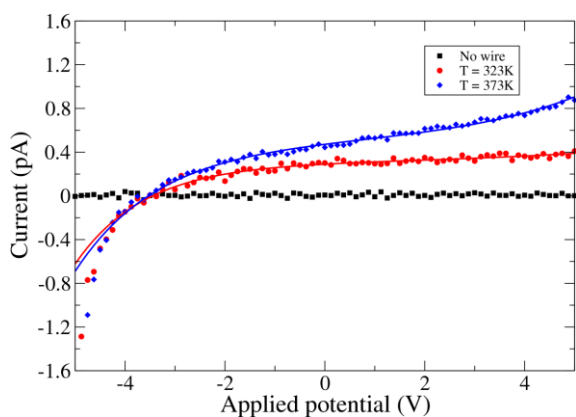


Figure 9. I/V curves for DNA/polyTPT nanowires at 323K and 373K. The black squares show the current in the absence of a nanowire where the noise floor is ~ 10 fA. Solid curves are fits of Eqn. (3) to the experimental data.

At low potentials a linear IV characteristic is still obtained, but the exponential terms give rise to an increasing differential conductance as the magnitude of the applied potential increases owing to non-linear aspects of the electron transfer rate process. The deviation from equation (3) observed in Fig. 9 at large negative potentials is likely to be due to some counteranion motion.^[65] The current offset at zero bias is a result of a combination of the presence of static charges on the substrate owing to the dry nitrogen atmosphere used

to avoid parasitic currents due to humidity and the low overall current levels. However, the fit of equation (3) to the data is satisfactory and allows us to estimate the effective site-site hopping distance, $\rho\delta$ as about 20 nm. This is clearly much larger than the expected hopping distance; in a conjugated polymer, the site-site distance might be expected to be the interchain distance or the distance between localised charges along the chain. However such effects (large values of ρ) are also commonly observed in redox polymers and have been explained in terms of clustering of the redox sites.^[65-66] Finally, it is worth noting that the redox hopping model also predicts an Arrhenius temperature dependence, whether the coupled ion motion occurs or not.^[64-66]

Conclusion

We have demonstrated that DNA-templating of the conducting polymer poly-(2,5-di(2-thienyl)-pyrrole) is effective in preparing nanowires despite the expected reduction in supramolecular interactions. The use of this monomer not only highlights the broad scope of the method but provides a route to pyrrole/thiophene-based copolymer materials with improved structural regularity compared to the alternative approach involving mixtures of the individual monomers. The resulting 1D DNA/poly(TPT) structures are shown to exhibit uniform, smooth morphologies, with a continuous polymer coating of the DNA template, whilst statistical analysis reveals a modal value of 7.0–8.0 nm for the nanowire diameters for the reaction conditions used. The use of FTIR and MD simulations provides some insight into the interactions between the CP and DNA template molecules, highlighting the nature of the supramolecular binding. Assessment of the electrical properties confirmed the DNA/polyTPT structures to be true nanowires, *i.e.* electrically conducting; however the conductivity was low. The dependence of the conductivity on the nanowire size was evident with cAFM experiments establishing a significant drop in conductivity as the diameter of the DNA/polyTPT structures is reduced < 40 nm. This was further supported by quantitative two-probe i-V studies carried out upon a DNA/polyTPT nanowire and bulk polyTPT material, in which the conductivity of the nanowire structure (10^{-7} S cm^{-1}) was determined to be several orders of magnitude lower than that of the bulk polyTPT material (10^{-2} S cm^{-1}).

Experimental Section

Materials. Lambda (λ) DNA (48502 base pairs in length, 500 $\mu\text{g mL}^{-1}$, 10mM Tris-HCl, 1mM EDTA, pH8 at 25°C) was purchased from New England Biolabs (cat no. N3011S, New England Biolabs UK Ltd. Hitchin, United Kingdom). DNA sodium salt from calf

thymus (Type I, highly polymerized, fibrous preparation, 16.7 A260 units mg^{-1} , 6% sodium), $\text{MgCl}_2 \cdot 6\text{H}_2\text{O}$ (99.0%), FeCl_3 (>97%), acetone ($\geq 99.8\%$), HF (48% in H_2O), and dodecyl sulfate sodium salt (99+%) were purchased from Sigma-Aldrich (Sigma-Aldrich Company Ltd., Dorset, United Kingdom). CH_3CN (99.6%) was purchased from Fisher Scientific (Fisher Scientific UK Ltd., Loughborough, United Kingdom). Si<p-100> wafers (3 inch diameter, boron doped, $525 \pm 50 \mu\text{m}$ thickness, single side polished, 1-10 Ωcm resistance) and Si<n-100> wafers (3 inch diameter, arsenic doped, $525 \pm 25 \mu\text{m}$ thickness, double side polished, $\leq 0.005 \Omega\text{cm}$ resistance, coated with a thermally grown SiO_2 layer, 200 nm $\pm 10\%$ thick) from Compart Technology Ltd, Peterborough, Cambridgeshire, U.K. NANOpure® deionized water (18 M Ω -cm resistivity) was supplied from a NANOpure® DIamond™ Life Science ultrapure water system equipped with a DIamond™ RO Reverse Osmosis System (Barnstead International). The 2,5-di(2-thienyl)-pyrrole (TPT) was prepared according to literature methods.¹⁶⁷¹

Formation of λ -DNA-templated polyTPT nanowires. 5 μL of aqueous MgCl_2 solution (0.5 mM) was added to 20 μL of an aqueous solution of λ -DNA (500 $\mu\text{g mL}^{-1}$), followed by 5 μL of TPT solution in CH_3CN (3 mM). 5 μL of a freshly prepared aqueous solution of FeCl_3 (3 mM) was then added to the DNA/TPT solution, and incubated for a period of 24 hours at room temperature to form the final DNA-templated polyTPT structures.

Formation of calf thymus DNA-templated polyTPT nanowires. Calf thymus DNA-templated polyTPT nanowires were prepared for use in FTIR studies. A solution of calf thymus DNA in NANOpure® water (0.5 mg mL^{-1}) was freshly prepared and left overnight to ensure the DNA is fully dissolved before use. 125 μL of Nanopure water and 125 μL of TPT solution in CH_3CN (3 mM) were successively added to 500 μL of the calf thymus DNA solution. 125 μL of a freshly prepared solution of FeCl_3 (3 mM) was then added to the DNA/TPT solution and incubated for a period of 24 hours at room temperature in order to form the final DNA-templated polyTPT structures.

Formation of bulk polyTPT. 2 mL of fresh FeCl_3 solution (0.3 M) was added to 2 mL of a DMF/water solution (1:4) of TPT (0.1 M) and left to stand for 24 hours, during which a black oil/precipitate formed in solution. After this period, the solution was centrifuged for 10 minutes (10,000 rpm) and the supernatant removed. The black oil/precipitate was rinsed 3 times with excess NANOpure® water with the sample centrifuged and the supernatant removed after each wash. The sample was subsequently dried in a vacuum oven (60°C) overnight.

Surface immobilization of λ -DNA-templated polyTPT nanowires for atomic force microscopy studies. Si<p-100> wafers were cut into ca. 1 x 1 cm^2 pieces with a diamond tip pen, swabbed with a cotton bud soaked in acetone ($\geq 99.8\%$) and washed in NANOpure® water. The wafers were then washed in a 0.1% (m/v) dodecyl sulfate sodium salt solution at ca. 70°C for 20 minutes, followed by thoroughly rinsing with NANOpure® water, and then sonicating (Transsonic T310, Camlab, Cambridge, United Kingdom) in NANOpure® water for 10 minutes. The wafers were cleaned further in 'piranha' solution (4:1 $\text{H}_2\text{SO}_4/\text{H}_2\text{O}_2$) at ca. 80°C for 45 minutes (*Caution! Piranha solution should be handled with extreme care; it is a strong oxidant and reacts violently with many organic materials. It also presents an explosion danger*), followed by rinsing thoroughly with NANOpure® water. Immediately before use, the wafers were blown dry in a stream of N_2 , and dried further in a clean oven for 10 minutes. Following these cleaning procedures, the Si substrates are highly "wetting", with static contact angles measured to typically be <20° (CAM 101, KSV Instruments Ltd., Helsinki, Finland), using 2 μL volumes of NANOpure® water as the probe liquid. The surface wetting of the cleaned Si substrates was subsequently modified through the formation of a trimethylsilane (TMS) self-assembled monolayer at the substrate surface. The Si substrate was positioned on top of specimen bottle containing 200 μL of chlorotrimethylsilane (Me_3SiCl) (polished side of the wafer facing upwards) and sealed inside a larger specimen bottle. The Si wafer was exposed to the vapour of the chlorotrimethylsilane in the specimen bottle for 10 minutes at room temperature. Static

contact angle measurements carried out upon the substrates following TMS modification were typically $71 \pm 1^\circ$.

Following incubation of the DNA/TPT/ FeCl_3 solution for 24 hours, the λ -DNA/polyTPT nanowires were aligned upon the TMS-modified Si substrate using molecular combing techniques.^{[52] [53] [33]} 5 μL of the DNA/TPT/ FeCl_3 solution was applied to the substrate surface and left for ca. 10 seconds before being withdrawn by micropipette. This procedure was repeated several times across the Si wafers' surface. This typically left a small residual amount of solution on the substrate surface (ca. <1 mm diameter), around which individually aligned DNA/polyTPT nanowires could be found.

Surface immobilization of λ -DNA-templated polyTPT nanowires for scanned conductance microscopy studies. Si<n-100> wafers, coated with a 200 nm SiO_2 layer, were cut into ca. 1 x 1 cm^2 pieces with a diamond tip pen, swabbed with a cotton bud soaked in acetone ($\geq 99.8\%$) and washed in NANOpure® water. The wafers were then washed in a 0.1% (m/v) dodecyl sulfate sodium salt solution at ca. 70°C for 20 minutes, followed by thoroughly rinsing with NANOpure® water, and then sonicating (Transsonic T310, Camlab, Cambridge, United Kingdom) in NANOpure® water for 10 minutes. The wafers were cleaned further in 'piranha' solution (4:1 $\text{H}_2\text{SO}_4/\text{H}_2\text{O}_2$), at ca. 80°C for 45 minutes, followed by thorough rinsing with NANOpure® water (*Caution! Piranha solution should be handled with extreme care; it is a strong oxidant and reacts violently with many organic materials. It also presents an explosion danger*). The SiO_2 layer was removed from one side of the wafer by applying a single drop of HF solution (48% in H_2O) onto the wafer surface. The HF solution was left on wafer for ca. 10–20 seconds until the surface wetting was observed to change from hydrophilic to hydrophobic, as evidenced by sudden beading of the HF solution. The HF solution was removed from the substrate surface and the wafer rinsed thoroughly with NANOpure® water. Complete removal of the SiO_2 layer was verified using a digital multimeter (Agilent Digit Multimeter, Agilent Technologies UK Ltd., Wokingham, United Kingdom). The wafers were subsequently cleaned for a second time in 'piranha' solution (4:1 $\text{H}_2\text{SO}_4/\text{H}_2\text{O}_2$), at ca. 80°C for 45 minutes, and thoroughly rinsed with NANOpure® water. Immediately prior to use the wafers were blown dry in a stream of N_2 , dried further in a clean oven for 10 minutes, and finally, modified with a TMS self-assembled monolayer at the substrate surface, as previously described. Alignment of the DNA/polyTPT nanowires upon the TMS-modified substrate surface was carried out through molecular combing, as described earlier.

Fourier transform infra-red spectroscopy. FTIR spectra (in the range 600–4000 cm^{-1}) were recorded in transmission mode with a Bio-Rad Excalibur FTS-40 spectrometer (Varian Inc., Palo Alto, CA, USA) equipped with a liquid nitrogen cooled deuterated triglycine sulfate (DTGS) detector, and were collected at 128 scans with 4 cm^{-1} resolution. The DNA used was calf thymus DNA and all samples were prepared through drop casting of solutions of the DNA (0.5 mg mL^{-1}) or DNA/polyTPT upon chemically oxidized Si<p-100> substrates. Data acquisition and analysis were carried out using Digilab Merlin version 3.1 software (Varian Inc.).

X-Ray Photoelectron Spectroscopy. XPS was carried out upon samples of λ -DNA/polyTPT nanowires, dropcast onto Au substrates. XPS measurements were carried out using a Thermo VG Escalab 250 instrument at Leeds EPSRC Nanoscience and Nanotechnology Research Equipment Facility (LENNF, Leeds University, Leeds, U.K.). A monochromated Al K_α X-ray source (1486.6 eV) was used, with pass energies of 150 eV and 20 eV employed for acquisition of survey and high resolution region scans, respectively. Measurements were recorded at a take-off angle of 90°, and all peaks were referenced to the bulk $\text{Au}4f_{7/2}$ peak at 84.0 eV. Data analysis was carried out using Winspec 2.06 software, with curve-fittings and carried out employing a Shirley-type background subtraction and fitted using Gaussian-Lorentzian functions.

Atomic force microscopy. Surface topography images were obtained by TappingMode™ AFM performed in air on both Multimode Nanoscope IIIa and

Dimension Nanoscope V systems (Veeco Instruments Inc., Metrology Group, Santa Barbara, CA, USA), using TESP7 probes (n-doped Si cantilevers, Veeco Instruments Inc., Metrology Group) with a resonant frequency of 234–287kHz, and a spring constant of 20–80Nm⁻¹. Tap300Al-G (Budget Sensors, Monolithic silicon cantilevers) with a resonance frequency of 100–400 kHz, and a spring constant of 20–75 Nm⁻¹ (Windsor Scientific, Sloughm Berks., U.K.). Data acquisition was carried out using Nanoscope version 5.12b36 software on the Multimode Nanoscope IIIa and Nanoscope version 7.00b19 software (Veeco Instruments Inc., Digital Instruments) on the Nanoscope Dimension V. For both AFM systems, vibrational noise was reduced with an isolation table/acoustic enclosure (Veeco Inc., Metrology Group).

Scanned conductance microscopy. SCM studies were carried out upon λ -DNA/polyTPT nanowires immobilised upon Si<n-100> substrates with a 200nm thick, SiO₂ layer, modified with a TMS self-assembled monolayer, as described above. All experiments were performed in air with a Dimension Nanoscope V system (Veeco Instruments Inc., Metrology Group), using MESP probes (n-doped Si cantilevers, with a Co/Cr coating, Veeco Instruments Inc., Metrology Group) with a resonant frequency of ca. 70kHz, a quality factor of 200–260, and a spring constant of 1–5Nm⁻¹. Acquisition and processing of SCM data was carried out using Nanoscope version 7.00b19 software (Veeco Instruments Inc., Digital Instruments). During SCM experiments, an independently controlled bias, typically set between -7V and +7V, was applied to the sample whilst the tip was kept grounded, and lift heights of 50–70nm were typically employed.

Conductive atomic force microscopy. cAFM studies were carried out upon λ -DNA/polyTPT nanowires supported upon Si<n-100> wafers bearing a 200nm thick, SiO₂ layer, modified with TMS self-assembled monolayer, as described above. All experiments were performed in air with a Dimension Nanoscope V system (Veeco Instruments Inc., Metrology Group), using MESP probes (n-doped Si cantilevers, with a Co/Cr coating, Veeco Instruments Inc., Metrology Group) with a spring constant of 1–5Nm⁻¹, and SCM-PIC probes (n-doped Si cantilevers, with a PtIr/Cr coating, Veeco Instruments Inc., Metrology Group) with a spring constant of 0.2Nm⁻¹. Acquisition and processing of SCM data was carried out using Nanoscope version 7.00b19 software (Veeco Instruments Inc., Digital Instruments). Ga/In eutectic was used to make an electrical contact between the DNA/ polyTPT material and the sample chuck.

Two-point probe current-voltage measurements. i-V measurements were carried out upon individual λ -DNA/polyTPT nanowires through the fabrication of tailor-made two-terminal nanowire devices, comprised of Au microelectrodes embedded in a thermally grown SiO₂ layer, supported on a Si substrate. Electrical measurements were made using a Probe Station (Cascade Microtech, Inc., Oregon, USA) and B1500A Semiconductor analyzer (Agilent Technologies UK Ltd., Edinburgh, United Kingdom), equipped with Agilent EasyEXPERT software. Prior to electrical testing, the two-terminal devices underwent a heating/cooling cycle between 293–373K, using a heating/cooling chuck (Model ETC-200L, ESPEC Corp., Osaka, Japan), under a N₂ atmosphere, to drive off any water bound to the nanowire. Subsequent i-V measurements were conducted under a N₂ atmosphere, without light illumination, and using a voltage range of -3 to +3V in steps of 0.05V. Variable temperature i-V measurements were carried out between a temperature range of 293–373K, at increments of 10K.

Electrical measurements of the bulk polyTPT were also recorded using the probe station, with the sample, supported on a Si<n-100>/200nm SiO₂ substrate, placed in the probe station chamber and purged with N₂ for 3 hours, prior to measurements being made. Measurements were repeated 4 times with the probes positioned at different locations on the bulk polyTPT material each time (though the distance between the probes was kept constant), from which an average conductivity was calculated. All measurements were taken at 303K, with an applied voltage range of -1 to +1V in steps of 0.05V.

Computational modelling. All starting geometries were built using the Spartan '04 programme.^[68] A B-form DNA 24-mer oligonucleotide duplex, {dA₂₄:dT₂₄} was built using the supplied oligonucleotide-builder complete with Na⁺ counter ions and this underwent equilibrium geometry calculations using MMFF with all the DNA atoms frozen to allow orientation of the sodium ions. The {TPT}₄ oligomer structure was geometry optimised similarly. Files for the {TPT}₄ and DNA duplex structures were exported to Accerlys Materials Studio and individually subjected to charge equilibrium calculations using Qeq with a convergence limit of 5.0x10⁻⁵e. Subsequent Forcite geometry optimization calculations were performed using Dreiding force field and the Smart algorithm with the tolerance for energy set at 2x10⁻⁵ Kcal/mol with both force and displacement disabled. These individual starting geometries were combined to form the Na:DNA:TPT complex with the {TPT}₄ placed in the major groove of the duplex and assigned a charge of +4; the overall charge of the complex was balanced by removal of sodium ions. This initial complex structure was geometry optimized prior to being placed in a box of water (1g cm⁻³). An initial 0.5 ps dynamic calculation was performed at medium quality using an NVE ensemble with a time step 0.1fs, energy deviation 5x10⁶ Kcal/mol and the temperature fixed at 298K. Finally, upon completion of this short dynamic calculation the time step was altered to 1.0fs and a final 100ps calculation was performed. Data was then extracted from the output files using the tools supplied within the program.

Acknowledgements

This work was financially supported by One North East, EU-FP7 Marie Curie IEF (MAG), EU-FP7 project LAMAND (Contract No. 245565), Newcastle University and EPSRC.Thanks to Dr. A. S. Walton of the Leeds EPSRC Nanoscience and Nanotechnology Research Equipment Facility (LENNF) for technical assistance with XPS measurements.

-
- [1] A. J. Heeger, *Angew. Chem. Int. Ed.* **2001**, *40*, 2591-2611.
 [2] T. A. Skotheim, R. L. Elsenbaumer, J. R. Reynolds, 2nd ed., M. Dekker, New York, **1998**.
 [3] A. G. MacDiarmid, *Angew. Chem. Int. Ed.* **2001**, *40*, 2581-2590.
 [4] A. B. Kaiser, *Rep. Prog. Phys.* **2001**, *64*, 1-49.
 [5] C. Li, H. Bai, G. Shi, *Chem. Soc. Rev.* **2009**, *38*, 2397-2409.
 [6] H. Xin, F. S. Kim, S. A. Jenekhe, *J. Am. Chem. Soc.* **2008**, *130*, 5424-5425.
 [7] T. Salim, S. Sun, L. H. Wong, L. Xi, Y. L. Foo, Y. M. Lam, *J. Phys. Chem. C* **2010**, *114*, 9459-9468.
 [8] Y. Liang, L. Yu, *Acc. Chem. Res.* **2010**, *43*, 1227-1236.
 [9] F. Cheng, W. Tang, C. Li, J. Chen, H. Liu, P. Shen, S. Dou, *Chem. Eur. J.* **2006**, *12*, 3082-3088.
 [10] A. L. Dyer, C. R. G. Grenier, J. R. Reynolds, *Adv. Funct. Mater.* **207**, *17*, 1480-1486.
 [11] Z. Bao, J. A. Rogers, H. E. Katz, *J. Mater. Chem.* **1999**, *9*, 1895-1904.
 [12] T. K. Tam, M. Pita, M. Motornov, I. Tokarev, S. Minko, E. Katz, *Adv. Mater.* **2010**, *22*, 1863-1866.
 [13] K. Wang, J. Huang, Z. Wei, *J. Phys. Chem. C* **2010**, *114*, 8062-8067.
 [14] F. Wang, H. Gu, T. M. Swager, *J. Am. Chem. Soc.* **2008**, *130*, 5392-5393.
 [15] C. M. Hangarter, M. Bangar, A. Mulchandani, N. V. Myung, *J. Mater. Chem.* **2010**, *20*, 3131-3140.
 [16] Y. Xia, P. Yang, Y. Sun, Y. Wu, B. Mayers, B. Gates, Y. Yin, F. Kim, H. Yan, *Adv. Mater.* **2003**, *15*, 353-389.
 [17] S. Pruneanu, S. A. F. Al-Said, L. Dong, T. A. Hollis, M. A. Galindo, N. G. Wright, A. Houlton, B. R. Horrocks, *Adv. Funct. Mater.* **2008**, *18*, 1-12.
 [18] H. D. Tran, D. Li, R. B. Kaner, *Adv. Mater.* **2009**, *21*, 1487-1499.
 [19] M. Hasegawa, M. Iyoda, *Chem. Soc. Rev.* **2010**, *39*, 2420-2427.
 [20] A. Houlton, S. M. D. Watson, *Annu. Rep. Prog. Chem. A* **2011**, *107*, 21-42.
 [21] Y. Berdichevsky, Y.-H. Lo, *Adv. Mater.* **2006**, *18*, 122-125.
 [22] M. G. Han, S. H. Foulger, *Chem. Commun.* **2005**, 3092-3094.
 [23] A. Drury, S. Chaire, M. Kröll, V. Nicolosi, N. Chaire, W. J. Blau, *Chem. Mater.* **2007**, *19*, 4252-4258.
 [24] C.-G. Wu, T. Bein, *Science* **1994**, *264*, 1757-1759.
 [25] C.-G. Wu, T. Bein, *Chem. Mater.* **1994**, *6*, 1109-1112.
 [26] J. Jang, B. Lim, J. Lee, T. Hyeon, *Chem. Commun.* **2001**, 83-84.
 [27] J. Jang, H. Yoon, *Chem. Commun.* **2003**, 720-721.
 [28] X. Zhang, J. Zhang, Z. Liu, C. Robinson, *Chem. Commun.* **2004**, 1852-1853.
 [29] J. Jang, H. Yoon, *Langmuir* **2005**, *21*, 11484-11489.
 [30] X. Zhang, J. Zhang, W. Song, Z. Liu, *J. Phys. Chem. B* **2006**, *110*, 1158-1165.
 [31] Y. Ma, J. Zhang, G. Zhang, H. He, *J. Am. Chem. Soc.* **2004**, *126*, 7097-7101.
 [32] P. Nickels, W. U. Dittmer, S. Beyer, J. P. Kotthaus, F. C. Simmel, *Nanotechnology* **2004**, *15*, 1524.

- [33] L. Dong, T. Hollis, S. Fishwick, B. A. Connolly, N. G. Wright, B. R. Horrocks, A. Houlton, *Chemistry Eur. J.* **2007**, *13*, 822-828.
- [34] S. A. F. Al-Said, R. Hassanien, J. Hannant, M. A. Galindo, S. Pruneanu, A. R. Pike, A. Houlton, B. R. Horrocks, *Electrochemistry Communications* **2009**, *11*, 550-553.
- [35] J. Hannant, J. H. Hedley, J. Pate, A. Walli, S. A. Farha Al-Said, M. A. Galindo, B. A. Connolly, B. R. Horrocks, A. Houlton, A. R. Pike, *Chem. Commun.* **2010**, *46*, 5870-5872.
- [36] R. Hassanien, M. Al-Hinai, S. A. Farha Al-Said, R. Little, L. Siller, N. G. Wright, A. Houlton, B. R. Horrocks, *ACS Nano* **2010**, *4*, 2149-2159.
- [37] E. Buhler, S. J. Candau, E. Kolomiets, J. M. Lehn, *Phys. Rev. E* **2007**, *76*, 061804.
- [38] A. Ciesielski, G. Schaeffer, A. Petitjean, J. M. Lehn, P. Samori, *Angew. Chem. Int. Ed.* **2009** *48* 2039-2043.
- [39] M. Ikeda, T. Nobori, M. Schmutz, J. M. Lehn, *Chemistry Eur. J.* **2005** *11*, 662-668.
- [40] N. Sreenivasachary, D. T. Hickman, D. Sarazin, J. M. Lehn, *Chemistry Eur. J.* **2006** *12* 8581-8588.
- [41] aM. Kofranek, T. Kovář, A. Karpfen, H. Lischka, *J. Phys. Chem.* **1992**, *96*, 4465; bR. Kostic, D. Raković, S. A. Stepanyan, I. E. Davidova, L. A. Gribov, *J. Chem. Phys.* **1995**, *102*, 3105.
- [42] G. I. Dovbeshko, N. Y. Gridina, E. B. Kruglova, O. P. Pashchuk, *Talanta* **2000**, *53*, 233-246.
- [43] V. Andrushchenko, J. H. Van de Sande, H. Wieser, *Biopolymers* **2003**, *72*, 374-390.
- [44] aA. A. Ouameur, H.-A. Tajmir-Riahi, *J. Bio. Chem.* **2004**, *279*, 42041-42054; bH. Arakawa, R. Ahmad, M. Naoui, H. Tajmir-Riahi, *J. Biol. Chem.* **2000**, *275*, 10150.
- [45] C. Briones, E. Mateo-Marti, C. Gómez-Navarro, V. Parro, E. Román, J. A. Martín-Gago, *Phys. Rev. Lett.* **2004**, *93*, 208103.
- [46] C.-Y. Lee, P. Gong, G. M. Harbers, D. W. Grainger, D. G. Castner, L. J. Gamble, *Anal. Chem.* **2006**, *78*, 3316-3325.
- [47] M. R. Vilar, A. M. Botelho do Rego, A. M. Ferraria, Y. Jugnet, C. Noguès, D. Peled, R. Naaman, *J. Phys. Chem. B* **2008**, *112*, 6957-6964.
- [48] P. Pfluger, G. B. Street, *J. Chem. Phys.* **1984**, *80*, 544-553.
- [49] L. Atanasoska, K. Naoi, W. H. Smyrl, *Chem. Mater.* **1992**, *4*, 988-994.
- [50] J. Joo, J. K. Lee, S. Y. Lee, K. S. Jang, E. J. Oh, A. J. Epstein, *Macromolecules* **2000**, *33*, 5131-5136.
- [51] F. Buckel, F. Effenberger, C. Yan, A. Götzhäuser, M. Grunze, *Adv. Mater.* **2000**, *12*, 901-905.
- [52] J. Li, C. Bai, C. Wang, C. Zhu, Z. Lin, Q. Li, E. Cao, *Nuc. Acids Res.* **1998**, *26*, 4785-4786.
- [53] Z. Deng, C. Mao, *Nano Lett.* **2003**, *3*, 1545-1548.
- [54] E. Braun, Y. Eichen, U. Sivan, G. Ben-Yoseph, *Nature* **1998**, *391*, 775-778.
- [55] J. Richter, M. Mertig, W. Pompe, I. Monch, H. K. Schackert, *Appl. Phys. Lett.* **2001**, *78*, 536-538.
- [56] M. Bockrath, N. Markovic, A. Shepard, M. Tinkham, L. Gurevich, L. P. Kouwenhoven, M. W. Wu, L. L. Sohn, *Nano Letters* **2002**, *2*, 187-190.
- [57] C. Staii, A. T. Johnson, N. J. Pinto, *Nano Letters* **2004**, *4*, 859-862.
- [58] T. S. Jespersen, J. Nygard, *Nano Lett.* **2005**, *5*, 1838-1841.
- [59] A. L. Efros, B. I. Shklovskii, *J. Phys. Chem. C* **1975**, *8*, L49-L51.
- [60] S. Chakrabarti, D. Banerjee, R. Bhattacharyya, *J. Phys. Chem. B*, **2002**, *106*, 3061-3064.
- [61] C. C. B. Bufon, T. Heinzel, *Phys. Rev. B* **2007**, *76*, 245206.
- [62] J.-M. Saveant, *J. Electroanal. Chem.* **1986**, *201* 211-213.
- [63] C. P. Andrieux, J.-M. Saveant, *J. Phys. Chem. B* **1988**, *92*, 6761-6767.
- [64] J. C. Jernigan, R. W. Murray, *J. Phys. Chem.* **1987**, *91*, 2030-2032.
- [65] R. H. Terrill, J. E. Hutchison, R. W. Murray, *J. Phys. Chem. B*, **1997**, *101*, 1535-1542.
- [66] E. F. Dalton, N. A. Surridge, J. C. Jernigan, K. O. Wilbourn, J. S. Facci, R. W. Murray, *Chem. Phys.* **1990**, *141* 143-157.
- [67] R. E. Niziurski-Mann, M. P. Cava, *Adv. Mater.* **1993**, *5*, 547-551.
- [68] Wavefunction Inc., Irvine, CA., **2004**.

[69] Accelrys, Inc, San Diego, CA 92121, USA

Received: ((will be filled in by the editorial staff))

Revised: ((will be filled in by the editorial staff))

Published online: ((will be filled in by the editorial staff))

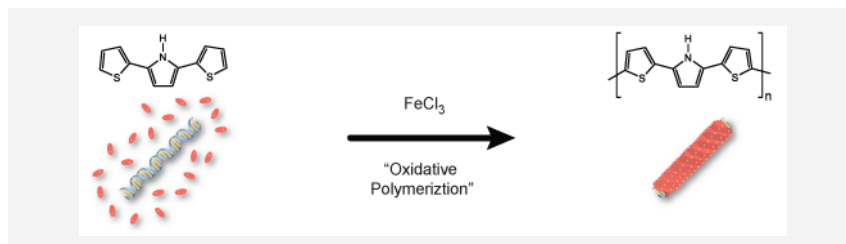
Supramolecular nanowires

*S. M. D. Watson, J. H. Hedley, M. A. Galindo, S. A. F. Al-Said, N. G. Wright, B. A. Connolly, B. R. Horrocks, A. Houlton**

Synthesis, characterization and electrical properties of supramolecular DNA-templated polymer nanowires of 2,5-(di-2-thienyl)-pyrrole

Title Text

*Author(s), Corresponding Author(s)** Page – Page



Duplex DNA molecules act as effective templates for the formation of nanowires of the conducting polymer, poly-(2,5-(di-2-thienyl)-pyrrole). The resulting supramolecular polymer strands are typically 6-8 nm in diameter and are shown to be electrically conducting by a variety of techniques including variable temperature conductivity measurements on a fabricated two-terminal device



Contents lists available at SciVerse ScienceDirect

Thin Solid Films

journal homepage: www.elsevier.com/locate/tsf

Formation of bismuth oxide nanowires by simultaneous templating and electrochemical adhesion of DNA on Si/SiO₂

Michael G. Hale ^a, Ross Little ^b, Mohamed Ali Salem ^b, Joseph H. Hedley ^a, Benjamin R. Horrocks ^a, Lidija Šiller ^{b,*}

^a School of Chemistry, Newcastle University, Newcastle upon Tyne, NE1 7RU, UK

^b School of Chemical Engineering and Advanced Materials, Newcastle University, Newcastle upon Tyne, NE1 7RU, UK

ARTICLE INFO

Article history:

Received 18 January 2012

Received in revised form 18 July 2012

Accepted 18 July 2012

Available online xxxx

Keywords:

DNA

Bismuth

Templating

Photoemission

Nanowires

ABSTRACT

Deoxyribonucleic acid (DNA)-templated growth of Bi/Bi₂O₃ nanowires attached to the Si surface was obtained by electrochemical reduction of Bi(III) at an n-type Si electrode in aqueous Bi(NO₃)₃/HNO₃ at pH 2.5 with calf thymus DNA. The nanowires had a mean diameter of 5 nm and a range of lengths from 1.4 μm to 6.1 μm. The composition and structure of the wires were determined by atomic force microscopy, Fourier transform infrared spectroscopy, Raman spectroscopy and X-ray photoemission spectroscopy. The dominant component of the material is Bi₂O₃ owing to the rapid re-oxidation of nanoscale Bi in the presence of air and water. Our method has the potential to construct complex architectures of Bi/Bi₂O₃ nanostructures on high quality Si substrates.

© 2012 Elsevier B.V. All rights reserved.

1. Introduction

Thin films of Bi₂O₃ exhibit many useful solid-state properties, including high refractive index, a large energy band gap, a high dielectric permittivity, a high oxygen conductivity and marked photoconductivity and photoluminescence [1]. Bi₂O₃ is therefore used for optical coatings, microelectronics and ceramic glass manufacturing [2]. Other applications can include photovoltaic cells, fuel cells, supercapacitors and photocatalysts [3–5].

Nanowires are potentially interesting as building blocks of nano-scale electronics and optoelectronics due to their unusual electron and exciton transport properties [6]. Although Bi nanowires readily oxidise when exposed to air at atmospheric pressure [7] recently it has been reported that when bismuth oxide nanowires are produced by co-sputtering of Al/Bi on SiO₂/Si substrate and post-annealing method, they become good gas sensors for detection of NO [8].

Bi nanostructures have been fabricated so far by pressure-injection of molten Bi into nano-sized pores of an alumina template [9], pulsed laser vaporization, [10], an oxidative metal vapour transport deposition technique [11] and by chemical reduction methods such as reduction of sodium bismuthate with ethylene glycol in the presence of poly(vinyl pyrrolidone) [12] and by a modified polyol process [13].

Electrochemical deposition is cost-effective, simple to operate and suited to substrates with complex geometry [14]. Electrochemically prepared Bi nanowires can be fabricated with different crystallinities, sizes and textures in a controlled way by properly choosing the

deposition parameters and the ability to fabricate multi-layered structures within nanowires has been demonstrated [15,16]. A comprehensive review of preparation techniques of bismuth nanostructures can be found elsewhere [17].

In the present paper, we report an electrochemical procedure for preparing Bi₂O₃ nanowires on Si surface utilizing the deoxyribonucleic acid (DNA) molecules as templates: this approach builds on previous work for metal- and polymer-templated DNA nanowires [18–20]. The use of DNA templates offers the potential to construct complex architectures by taking advantage of the self-assembly properties of DNA and programming the base sequence [21,22]. Our electrodeposition method not only allows the fabrication of high aspect ratio nanostructures, but also the process naturally leads to the adhesion of these structures at a high quality Si surface where they can be immediately examined by probe microscopy and photoemission spectroscopy or could be processed further.

2. Experimental details

All general reagents were obtained from Sigma-Aldrich at an analytical grade or equivalent. Calf thymus DNA was obtained from Sigma as type 1, highly polymerised, sodium salt. Bismuth nitrate pentahydrate was obtained as the ACS reagent from Sigma-Aldrich. All aqueous solutions were prepared with water from a Barnstead NANOPure water purification system with nominal resistivity of 18.2 MΩ cm.

Bi/Bi₂O₃/DNA nanowires were made by electrochemical reduction of Bi(III). Since Bi(III) is unstable at high pH and DNA is unstable at low pH, a compromise pH of 2.5 was obtained by the addition of 1 M NaOH to a solution of 0.5 mM Bi(NO₃)₃ in 1 M HNO₃ (aq). The

* Corresponding author. Tel.: +44 1912227858.

E-mail address: Lidija.Siller@ncl.ac.uk (L. Šiller).

solution was still slightly cloudy at this pH due to the presence of bismuth oxyhydroxides, therefore the solution was filtered and the filtrate was mixed with 2 parts calf thymus (sodium salt, Sigma) DNA solution ($500 \text{ ng } \mu\text{L}^{-1}$) to give 1.5 cm^3 of solution in total. The final DNA concentration was $1.6 \times 10^{-3} \text{ mold m}^{-3}$ (by phosphate) as determined by optical absorbance at 260 nm. Although DNA may be subject to depurination at a pH of 2.5, it is only necessary that the DNA retain its overall linear structure for the duration of the templating reaction reported. The electrochemical cell comprised a polytetrafluoroethylene body, a n-Si(111) working electrode, a tungsten wire counter electrode and a silver wire quasi reference electrode. The Bi(III) was reduced by constant potential electrolysis at -1.4 V vs Ag/QRE for 20 s. Cyclic voltammetric characterisation of the electrode reaction was carried out in the same cell and the potentiostat was a CH Instruments model 760B (Austin, TX, USA) in both types of experiment. After the electrolysis, the substrate was dried by blowing with dry N_2 .

TappingMode™ atomic force microscopy (AFM) imaging of surface topography was performed in air on a Multimode Nanoscope IIIa (Veeco Instruments Inc., Metrology Group, Santa Barbara, CA, USA) using TESP7 probes (n-doped Si cantilevers, Veeco Instruments Inc., Metrology Group).

X-ray photoemission spectroscopy (XPS) measurements were performed with a Kratos (Axis Ultra 165) XPS machine, using an ESCA 300 spectrometer and monochromatic Al $\text{K}\alpha$ radiation ($h\nu = 1486.6 \text{ eV}$). The measurements were carried out with an overall energy resolution of 0.35 eV at room temperature under a vacuum better than $2.7 \times 10^{-7} \text{ Pa}$. Gold foil was placed in electrical contact with each sample and the core level Au 4f spectrum was measured in order to calibrate the energy scale. A charge neutraliser was used to compensate for any charging effects.

Raman spectra were recorded with a confocal microscope (CRM200, Witec GmbH, Ulm, Germany) using the 488 nm line of an Argon ion laser for the excitation light. Three gratings were employed (1800, 600 and 150 lines/mm) to obtain high resolution spectra and also a broad spectra range.

3. Results and discussion

3.1. Electrochemical control of DNA adhesion at Si

Probe microscopic studies of DNA and DNA-templated materials require a means to immobilise the molecules on a high quality surface and this is usually achieved by adsorption of DNA on mica in the presence of Mg^{2+} [23]. The Mg^{2+} anchors DNA to the substrate because of the strong interaction of divalent cations with both the anionic

phosphate groups of DNA and the Si–O functionalities on the mica surface. The nature of this interaction is thought to be similar to a salt bridge in which a multivalent cation bridges two anions and is bound by mainly electrostatic forces.

It has also been shown that Si/SiO₂ wafers and Au-thiolate monolayers can serve as suitable substrates if negative charges can be introduced at the surface. In the case of p-Si wafers, the excitation with UV/visible light produces a negative surface photocharge and enhances the deposition of DNA [24]. In the case of metal electrodes (Au/thiolate self-assembled monolayers), the interface was charged simply by application of an external potential [25]. In this work, we have taken advantage of these observations to demonstrate the simultaneous templating and adhesion of DNA by Bi. Bi(III) acts both as the multivalent cation to enable DNA adhesion at a negatively polarised Si/SiO₂ electrode and as the source of Bi for the electrolytic templating. First, we demonstrate the adhesion of DNA to Si/SiO₂ surfaces using Mg^{2+} , which is not electrochemically active at these potentials and then we discuss the results obtained using Bi(III).

Fig. 1 shows 3 AFM images that illustrate the adhesion phenomenon and the role of multivalent cations. Image 1(a) is an n-Si(100) surface with native oxide that has been polarised at a potential of $+0.5 \text{ V}$ for 3 s in an aqueous solution of $0.5 \text{ mmol dm}^{-3} \text{ MgCl}_2$ /calf thymus-DNA, emersed from solution, rinsed with water and imaged after drying by N_2 . The surface shows some evidence of adsorbed material, but no clear evidence of DNA molecules. Our interpretation is that there are not enough negatively charged functionalities at the surface for Mg^{2+} to bind. Image 1(b) shows the corresponding result after polarisation at -0.5 V for 3 s; extensive adsorption of DNA has occurred as shown by the large deposits and the clear observation of long strands. Finally, image 1(c) shows the control for image 1(b) in the absence of Mg^{2+} : the surface is essentially clean. We note that in all cases, the solution in which the DNA is prepared contains Na^+ because calf-thymus DNA is supplied as the sodium salt, but, as expected, a monovalent cation alone is not capable of forming a salt bridge of the type required to adhere DNA to the surface. Next we describe the results of an experiment in which no Mg^{2+} is present, but the role of the multivalent cation is taken by Bi(III), which is also reduced to Bi metal at the electrode surface.

3.2. Simultaneous adhesion and templating of bismuth on DNA

Bi(III) is not conveniently reduced by simple chemical agents in aqueous solution, because of the low pH required to aid solubility and therefore electroless deposition of Bi on DNA was found to be

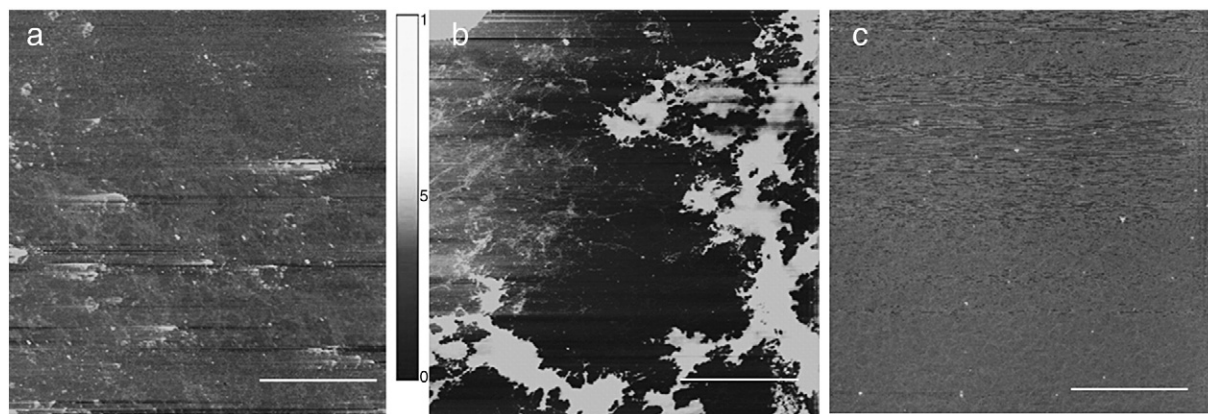


Fig. 1. AFM images of Si(100) surfaces after application of various potentials (with respect to Ag/AgCl/KCl (3 M)) in solutions of calf thymus DNA ($44 \mu\text{g mL}^{-1}$ in H_2O) with and without $0.5 \text{ mmol dm}^{-3} \text{ MgCl}_2$. Only (b) shows significant DNA deposits (white areas). (a) DNA with MgCl_2 on an n-Si(100) surface after application of a positive potential (0.5 V) for 3 s. The scale bar = $3 \mu\text{m}$, height scale is 10 nm and the common grayscale for (a)–(c) is shown on the right. (b) DNA with MgCl_2 on an n-Si(100) surface after application of a negative potential (-0.5 V) for 3 s. The scale bar = $3 \mu\text{m}$ and the height scale is 10 nm. (c) DNA without MgCl_2 on an n-Si(100) surface after application of a negative potential (-0.5 V) for 3 s. The scale bar = $3 \mu\text{m}$ and the height scale is 10 nm.

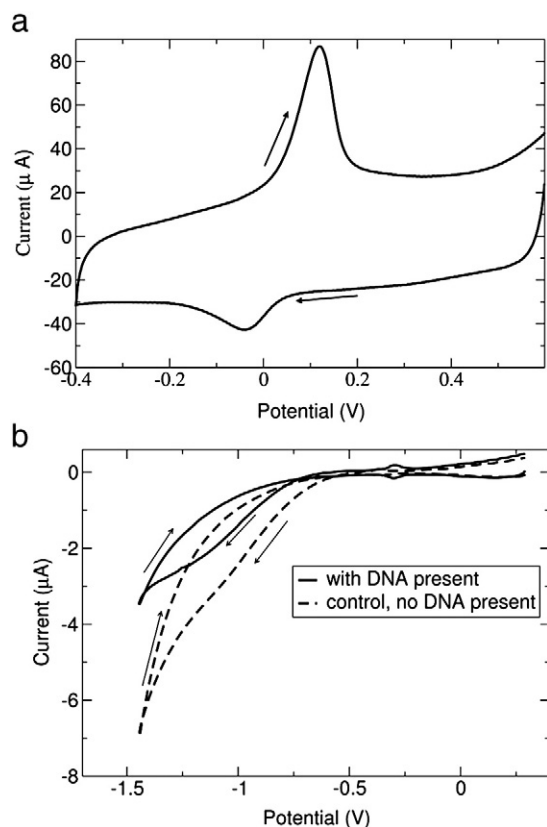


Fig. 2. (a) Cyclic voltammogram of 5 mM $\text{Bi}(\text{NO}_3)_3$ in 1 M HNO_3 at a 2 mm diameter Au disc electrode. Potentials are measured against an Ag quasi-reference electrode and the scan rate was 0.5 V s^{-1} . (b) Cyclic voltammograms at an n-Si(111) electrode in 0.5 mM $\text{Bi}(\text{NO}_3)_3$ at pH 2.5 in HNO_3/NaOH after filtration and in the presence and absence of calf thymus DNA ($1.6 \times 10^{-3} \text{ mol dm}^{-3}$ by phosphate). The wetted area of the Si was 0.79 cm^2 and the scan rate was 0.1 V s^{-1} . In both (a) and (b) the arrows denote forward and reverse scan directions.

difficult because the precipitated metal was rapidly dissolved. However Bi(III) can be reduced electrochemically. Fig. 2(a) shows a cyclic voltammogram of 5 mM $\text{Bi}(\text{NO}_3)_3$ in 1 M HNO_3 at a 2 mm diameter Au disc electrode. The reduction of Bi(III) to Bi metal is clearly evident in the cathodic peak at -0.05 V vs Ag Quasi-Reference electrode (QRE). It should be noted that the electrochemistry of bismuth is complex and dependent on halide ion concentrations as well as pH,

but the anodic peak is typical of the stripping of an electroplated metal and appears at $+0.1 \text{ V}$ in rough agreement with previous reports on Bi electrochemistry [26,27]. In order to deposit $\text{Bi}/\text{Bi}_2\text{O}_3$ on a suitable substrate for AFM and XPS characterisation, we employed n-Si(111) electrodes cut from phosphorus-doped wafer (Compart Technology, Cambridge, UK, miscut angle $<0.1^\circ$, resistivity $1\text{--}12 \Omega \text{ cm}$). Owing to the rectifying nature of the Si/electrolyte contact, Fig. 2(b) shows only the reduction wave for deposition of Bi on the electrode. There is a large apparent overpotential for the electrodeposition primarily determined by the flatband potential of the Si, which is substantially negative as expected for n-type material. Nucleation loops in which the reverse (anodic) scan crosses over the forward scan are visible at -0.56 V and -0.73 V in the absence and the presence of DNA. This feature indicates that there is also a substantial contribution to the overpotential arising from an unfavourable surface energy term for deposition of Bi(0) on Si. A comparison of the two curves in the presence and absence of calf thymus DNA shows that the cathodic electrodeposition current is decreased and the overpotential is increased slightly in the presence of DNA. The diminution of the current is caused by the relatively low diffusion coefficient of DNA compared to small inorganic molecules and therefore Bi(III) ions bound to the DNA produce a smaller transport-limited peak current. These effects demonstrate the strong binding of Bi(III) ions to the DNA, as expected for a trication. Finally, there is some anodic current at potentials $>0 \text{ V}$, but the Bi deposited in the forward scan is not completely stripped because of the rectifying nature of the Si/liquid interface.

3.3. Atomic force microscopy

Fig. 3 shows an atomic force microscopy image (AFM) of the $\text{Bi}/\text{Bi}_2\text{O}_3$ nanowires on the silicon electrode. Their lengths range from $1.4 \mu\text{m}$ to greater than $6.1 \mu\text{m}$. The wires are also thin, having an apparent mean diameter of 5 nm as determined by the height of the AFM images (see line profiles in Fig. 3). There was a significant variation in the diameter of the wires, with a range of $3\text{--}11 \text{ nm}$ and a standard deviation of $\pm 1.3 \text{ nm}$. The image also shows numerous particulates. The ratio of the volume of wires to the volume of particulates is 4:1 – on the assumption of cylindrical wires and spherical particulates. We also observe some clumping of particulates along the wires.

From Fig. 3 we see that the $\text{Bi}/\text{Bi}_2\text{O}_3$ is deposited mainly, though not exclusively on the DNA as evidenced by the presence of thick strands, thicker than bare DNA. However, there are a few small particles which are likely to be $\text{Bi}/\text{Bi}_2\text{O}_3$ deposited directly on the substrate.

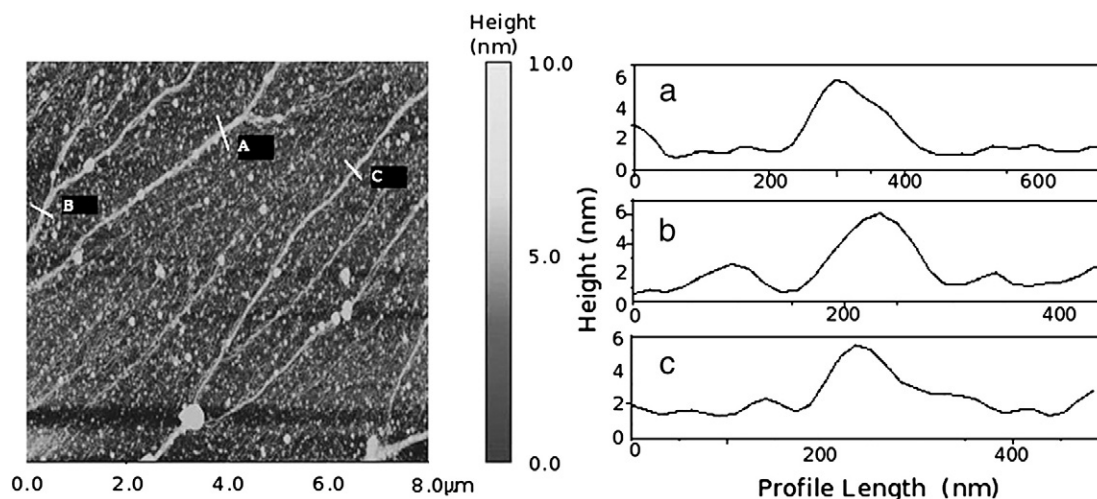


Fig. 3. An AFM image taken in air of the $\text{Bi}/\text{Bi}_2\text{O}_3$ nanowires on the n-Si(111) electrode after emersion from the electrolyte (0.5 mM $\text{Bi}(\text{NO}_3)_3$ at pH 2.5) and drying. On the right are line profiles across $\text{Bi}/\text{Bi}_2\text{O}_3$ nanowires obtained at positions marked A, B and C on the image.

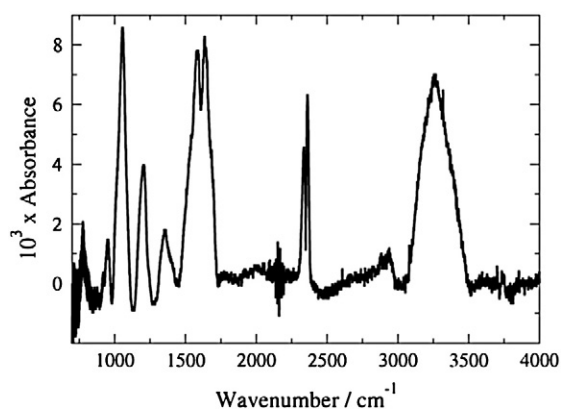


Fig. 4. Transmission FTIR spectrum of Bi/Bi₂O₃ nanowire sample formed by electrochemical templating from a λ -DNA solution. 32 scans were co-added and averaged. The resolution was 1 cm⁻¹.

3.4. FTIR and Raman spectroscopy

Fig. 4 shows a transmission FTIR spectrum of the Bi/Bi₂O₃ nanowires formed by templating on an n-Si(111) electrode. n-Si is a convenient substrate because it is transparent to mid-IR light and therefore can be used directly for spectroscopic characterisation with a bare n-Si chip as the background. **Table 1** represents FTIR spectral assignments for bismuth oxide/DNA nanowires. A comparison of the FTIR spectrum with literature precedents for bismuth nitrate solutions [28], solid nitrates [29], DNA [30–32] and α -Bi₂O₃ [33] shows that there are no peaks which can be attributed to bismuth, however the spectrum shows clearly the presence of DNA and some nitrate remaining from the electrolyte (assignments given in **Table 1**). The expected positions of the Bi₂O₃ bands (<544 cm⁻¹ [33]) are at wavenumbers too low for us to obtain good quality transmission FTIR data given the absorption of light by the substrate at low wavenumber. We have therefore employed Raman spectroscopy to demonstrate the presence of Bi₂O₃.

In order to obtain Raman spectra, we increased the time of electrolysis to 60 s in order to coat the substrate with a film of Bi/Bi₂O₃ nanowires and obtain a stronger signal-to-noise ratio as well as to reduce the contribution of the Raman spectrum from the underlying Si substrate. Each spectrum shown in **Fig. 5** comprises 30 individual spectra (100 for **Fig. 5c**) co-added and averaged and an integration time of 0.1 s. **Fig. 5** shows that there is a substantial luminescence background, this is not observed for DNA alone, which does not absorb light at wavelengths longer than about 300 nm; the observation of PL is therefore consistent with the presence of a semiconducting metal oxide such as Bi₂O₃. Although the spectrum is complex and not all the bands can be assigned, see **Table 2**, there are clear features due to α -Bi₂O₃, notably the Bi–O stretch at 444 cm⁻¹, which confirms the presence of the oxide [34–36]. We cannot rule out the presence of elemental bismuth on the basis of the Raman spectra because

Table 1
FTIR spectral assignments for bismuth oxide/DNA nanowires.

Wavenumber/cm ⁻¹	Assignment	Reference
780	DNA	
1056	Nitrate ν_1 . Close to and overlaps with DNA backbone and P–O symmetric str	[28,29] [30–32]
1205	–	
1356	Nitrate ν_3 antisymmetric stretch	[28,29]
1587	DNA bases	[30,32]
1635	Nitrate $2\nu_2$ overtone (out-of-plane deformation), also dT (C=O str)	[28,29] [30–32]
3300 (broad)	OH _{str} bound water/–OH	

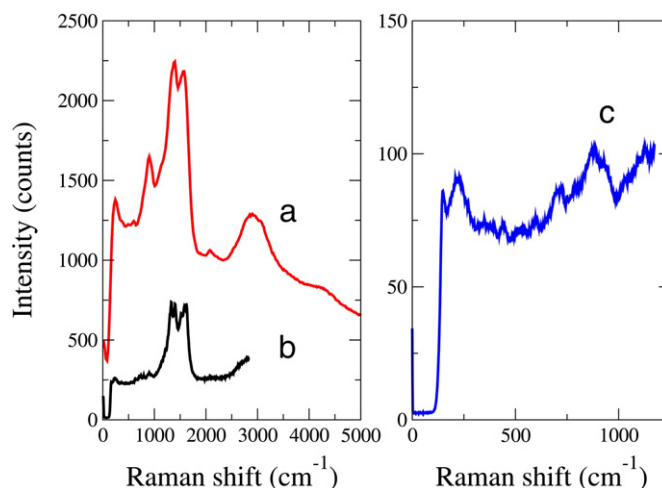


Fig. 5. Confocal Raman spectra of a film of Bi/Bi₂O₃ nanowires on n-Si(111). The excitation light was the 488 nm line of an argon ion laser and the integration time was 0.1 s. 30 scans were co-added and averaged for (a, b) and 100 scans for (c). The three spectra were obtained with successively higher resolution setting corresponding to (a) 150 lines/mm; (b) 600 lines/mm and (c) 1800 lines/mm diffraction gratings. The spectral resolution is about 0.07 cm⁻¹ for the highest resolution grating (c).

it shows no bands > 100 cm⁻¹ and our Raman filters block light shifted <200 cm⁻¹ from the laser line. However the photoemission work (see below) does show that the Bi is not present as the element. Finally, the Raman spectra show the major bands for DNA, as perturbed by bound metal ions, at 789 cm⁻¹ and 1587 cm⁻¹ [37–39]. Bands due to nitrate are also present, originating from the electrolyte.

In conclusion, the FTIR and Raman spectral data demonstrate the presence of Bi₂O₃, DNA and nitrate. The DNA bands are substantially perturbed in the manner expected upon interaction with a heavy metal ion and indicate a strong Bi–DNA interaction rather than a simple mixture.

3.5. X-ray photoemission spectroscopy

Fig. 6 shows an X-ray photoemission spectrum of the Bi 4f electron energy level of the Bi/Bi₂O₃ nanowires formed by templating on an n-Si(111) electrode. The data is fitted with one doublet, 3 Lorentzian singlets, experimental broadening and a Shirley background. The main peak position of the doublet is found at 158.7 eV with doublet separation of 5.24 eV. It has been reported that the Bi 4f_{7/2} in Bi₂O₃ with doublet separation of 5.2 eV is placed at 158.62 eV [14] and

Table 2
Raman spectral assignments for bismuth oxide/DNA nanowires.

Raman shift/ cm ⁻¹	Assignment	Reference
210, 226	210 cm ⁻¹ α -Bi ₂ O ₃	[34,35]
350	Broad. Band at 313 expected for α -Bi ₂ O ₃	[34,35]
444	Bi–O str	[34,35]
600	–	
704	Nitrate ν_4	[28,29]
726	–	
789	DNA backbone stretch.	[37–39]
870	–	
890	–	
930	Possible 2nd order Si band	
1337	dA dG intensity decrease upon transition metal binding	[37,38]
1407	Nitrate ν_3 antisymmetric stretch	[28,29]
1524	DNA band expected at 1490. Strongly suppressed by transition metals.	[38]
1587	DNA bases	[37–39]
1630	Bands in this region are an unresolved mixture of: nitrate $2\nu_2$ overtone (out-of-plane deformation), also dT (C=O str) and water bending modes.	[29,34]

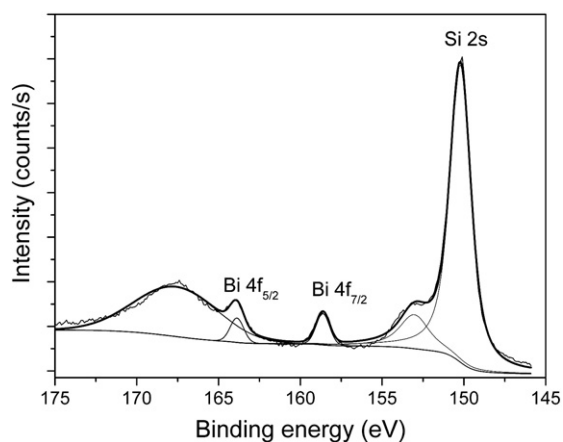


Fig. 6. X-ray photoemission spectrum of the Bi 4f and Si 2s energy levels of the Bi/Bi₂O₃ nanowires on the silicon electrode of Fig. 3. The bold curve is the fit to the experimental spectrum and the various components discussed in the text are shown as thinner grey lines.

158.7 eV [15]. The reported binding energy of Bi 4f_{7/2} in pure Bi metal is at 156.8 eV [16] which is ~1.9 eV lower than the observed peaks in this work; this rules out the presence of pure Bi nanowires.

It is likely that upon reaction of bismuth ions in an electrolytic solution with DNA, Bi nanowires are deposited on the slightly oxidised Si substrate (as seen from AFM images, see Fig. 3). When the electrolytic solution is evaporated in air, it is thought that the Bi nanowires reoxidise in air creating Bi₂O₃. Indeed, it has been observed that pure metallic Bi wires of 65 nm diameter gradually oxidise when exposed to air. Metallic Bi wires typically have an oxide layer ~1 nm thick after 4 h exposure to air. After 48 h exposure, the thickness of the oxide layer is ~4 nm [40]. High temperature hydrogen and ammonia environments were found to reduce the oxide without damaging the Bi metal after a sufficient amount of time, but the oxide was found to reform in less than 1 min of exposure to air [7]. Since the wires in our work are very thin (~5 nm), nearly complete oxidation across the wires is to be expected; we therefore assign the peaks at 158.7 and 163.9 eV to the Bi 4f_{7/2} and Bi 4f_{5/2} levels of Bi₂O₃ respectively.

Singlet peaks were used to account for the presence of the Si 2s peaks at 150.3 eV and 153.2 eV and the bulk plasmon loss at 167.3 eV as a satellite of the main Si 2s line (at 150.3 eV). Measurements of bulk plasmon dispersion in single crystal silicon at $q=0$ show a feature at 16.6 eV with a width of 3.3 eV [41], this is close to the measurements in this work (the plasmon loss peak is 167.3 eV – 150.3 eV = 17 eV and the width is ~3.6 eV) (Fig. 6). The observed peak at 153.2 eV is likely to originate from SiO_x or/and Bi and SiO_x bonding (possibly forming BiSiO₃). For example it has been observed for CaSiO₃ that the binding energy is 153.3 eV, for (Mg/Fe)SiO₃ it is 153.6 eV and for (Mg/Fe)₂SiO₄ it is 153 eV [42].

4. Conclusion

DNA-templated growth of Bi/Bi₂O₃ nanowires was obtained by electrochemical reduction of Bi(III) at an n-type Si electrode. The morphological characteristics as well as the electronic structure of the wires were determined by FTIR, Raman, AFM and XPS analysis;

the dominant component of the material is Bi₂O₃. This method has the potential to construct complex architectures.

Acknowledgements

MGH thanks Newcastle University for a summer studentship. We also thank One North East for the financial support.

References

- [1] H.T. Fan, X.M. Teng, S.S. Pan, C. Ye, G.H. Li, L.D. Zhang, *Appl. Phys. Lett.* 87 (2005) 231916.
- [2] H.W. Kim, J.W. Lee, S.H. Shim, M.A. Kebede, C. Lee, *Cryst. Res. Technol.* 43 (2008) 695.
- [3] K. Sardar, T.-T. Fang, T.-W. Yang, *J. Am. Ceram. Soc.* 90 (2007) 4033.
- [4] W.D. He, W. Qin, X.H. Wu, X.B. Ding, L. Chen, Z.H. Jiang, *Thin Solid Films* 515 (2007) 5362.
- [5] L. Zhou, W. Wang, H. Xu, S. Sun, M. Shang, *Chem. Eur. J.* 15 (2008) 1776.
- [6] X. Duan, Y. Huang, Y. Cui, J. Wang, C.M. Lieber, *Nature* 409 (2001) 66.
- [7] S.B. Cronin, Y.-M. Lin, P.L. Gai, O. Rabin, M.R. Black, G. Dresselhaus, M.S. Dresselhaus, *Mater. Res. Soc. Symp. Proc.* 635 (2000) C5.7.
- [8] Y.-W. Park, H.-J. Jung, S.-G. Yoon, *Sensors Actuators B* 156 (2011) 709.
- [9] Y. Hasegawa, M. Murata, D. Nakamura, T. Komine, T. Taguchi, S. Nakamura, *J. Electron. Mater.* 38 (2009) 944.
- [10] J. Reppert, R. Rao, M. Skove, J. He, M. Craps, T. Tritt, A.M. Rao, *Chem. Phys. Lett.* 442 (2007) 334.
- [11] Y.F. Qiu, D.F. Liu, J.H. Yang, S.H. Jang, *Adv. Mater.* 18 (2006) 2604.
- [12] J. Wang, X. Wang, Q. Peng, Y. Li, *Inorg. Chem.* 43 (2004) 7552.
- [13] Y. Wang, K.S. Kim, *Nanotechnol.* 19 (2008) 265303.
- [14] X.F. Wang, L.D. Zhang, J. Zhang, H.Z. Shi, X.S. Peng, M.J. Zheng, J. Fang, J.L. Chen, B.J. Gao, *J. Phys. D: Appl. Phys.* 34 (2001) 418.
- [15] T.W. Cornelius, J. Brötz, N. Chtanko, D. Dobrev, G. Mieke, R. Neumann, M.E.T. Molares, *Nanotechnol.* 16 (2005) S246.
- [16] L. Li, Y. Zhang, G. Li, L. Zhang, *Chem. Phys. Lett.* 378 (2003) 244.
- [17] O.V. Kharisova, B.I. Kharisov, *Synth. React. Inorg., Met.-Org., Nano-Met. Chem.* 38 (2008) 491.
- [18] L. Dong, T.A. Hollis, B.A. Connolly, N.G. Wright, B.R. Horrocks, A. Houlton, *Adv. Mater.* 19 (2007) 1748.
- [19] S. Pruneanu, S.A. Farha Al-Said, L. Dong, T.A. Hollis, M.A. Galindo, N.G. Wright, A. Houlton, B.R. Horrocks, *Adv. Funct. Mater.* 18 (2008) 2444.
- [20] L. Dong, T.A. Hollis, S. Fishwick, B.A. Connolly, N.G. Wright, B.R. Horrocks, A. Houlton, *Chem. Eur. J.* 13 (2007) 822.
- [21] B.G. Maiya, T. Ramasarma, *Curr. Sci.* 80 (2001) 1523.
- [22] M. Taniguchi, T. Kawai, *Phys. E* 33 (2006) 1.
- [23] J. Vesenska, M. Guthold, C.L. Tang, D. Keller, E. Delaine, C. Bustamante, *Ultramicroscopy* 42 (1992) 1243.
- [24] I.L. Volkov, N.V. Bazlov, A.S. Bondarenko, O.F. Vyvenko, N.A. Kas'yanenko, *J. Struct. Chem.* 50 (2009) 962.
- [25] M. Erdmann, R. David, A. Fornof, H.E. Gaub, *Nat. Nanotechnol.* 5 (2010) 154.
- [26] S.P.E. Smith, H.D. Abruña, *J. Phys. Chem. B* 102 (1998) 3506.
- [27] S. Komorsky-Lovric, M. Branica, *J. Electroanal. Chem.* 358 (1993) 213.
- [28] R.P. Oertel, R.A. Plane, *Inorg. Chem.* 7 (1968) 1192.
- [29] M.R. Waterland, D. Stockwell, A.M. Kelley, *J. Chem. Phys.* 114 (2001) 6249.
- [30] A.A. Ouameur, H.A. Tajmir-Riahi, *J. Biol. Chem.* 279 (2004) 42041.
- [31] S. Alex, P. Dupuis, *Inorg. Chim. Acta* 157 (1989) 271.
- [32] G.I. Dovbeshko, N.Y. Gridina, E.B. Kruglova, O.P. Pashchuk, *Talanta* 53 (2000) 233.
- [33] R. Irmawati, M.N. Noorfarizan Nasriah, Y.H. Taufiq-Yap, S.B. Abdul Hamid, *Catal. Today* 93–95 (2004) 701.
- [34] V.N. Denisov, A.N. Ivliiv, A.S. Lipin, B.N. Mavrin, V.G. Orlov, *J. Phys. Condens. Matter* 9 (1997) 4967.
- [35] K. Trentelman, *J. Raman Spectrosc.* 40 (2009) 585.
- [36] F.D. Hardcastle, I.E. Wachs, *J. Solid State Chem.* 97 (1992) 319.
- [37] H. Deng, V.A. Bloomfield, J.M. Benvenides, G.J. Thomas Jr., *Nucleic Acids Res.* 28 (2000) 3379.
- [38] J. Duguid, V.A. Bloomfield, J.M. Benevides, G.J. Thomas Jr., *Biophys. J.* 65 (1993) 1916.
- [39] L. Movileanu, J.M. Benevides, G.J. Thomas Jr., *Biopolymers* 63 (2002) 181.
- [40] Z. Zhang, D. Gekhtman, M.S. Dresselhaus, J.Y. Ying, *Chem. Mater.* 11 (1999) 1659.
- [41] C.H. Chen, A.E. Meixner, B.M. Kincaid, *Phys. Rev. Lett.* 44 (1980) 951.
- [42] H. Seyama, M. Soma, *Faraday Trans. 1* (81) (1985) 485.